

Synthesis and biological evaluation of 6-substituted coumaranone derivatives and related compounds as monoamine oxidase inhibitors

AS van Dyk
10791469

Dissertation submitted in fulfilment of the requirements for the degree *Magister Scientiae* in *Pharmaceutical Chemistry* at the Potchefstroom Campus of the North-West University

Supervisor: Dr LJ Legoabe
Co-Supervisor: Prof JP Petzer
Assistant Supervisor: Dr A Petzer

November 2014

INDEX

LIST OF FIGURES AND TABLES	IV
LIST OF ABBREVIATIONS	VII
ABSTRACT	1
UITTREKSEL	3
 CHAPTER 1: Introduction	 5
1.1 Brief background on Parkinson's disease	5
1.2 Monoamine oxidase inhibitors in PD	6
1.3 The rationale of this study	8
1.4 The hypothesis of this study	11
1.5 The objectives of this study	11
 CHAPTER 2: Literature overview	 13
2.1 Parkinson's disease	13
2.1.1 General background	13
2.1.2 Neurochemical and neuropathological features of PD	14
2.1.3 Aetiology and pathogenesis of PD	15
2.1.3.1 Oxidative stress and mitochondrial dysfunction	16
2.1.3.2 Protein aggregation and misfolding	16
2.1.3.3 Neuroinflammation	17
2.1.3.4 Excitotoxicity	17
2.1.3.5 Apoptosis	17
2.1.3.6 Loss of trophic factors	18
2.1.4 Genetics	18
2.1.5 Symptomatic treatment	19
2.2 Drugs for neuroprotection	25
2.2.1 MAO-B inhibitors	25
2.2.2 Dopaminergic drugs	27
2.2.3 Antioxidant drugs	27
2.2.4 Mitochondrial energy enhancers	28
2.2.5 Antiapoptotic drugs	29
2.2.6 NMDA antagonist and antiglutaminergic drugs	30
2.3 Monoamine oxidase	31
2.3.1 General background	31
2.3.2 The therapeutic role of MAO-A	32
2.3.3 The therapeutic role of MAO-B	33

INDEX

2.3.4	MAO inhibition	38
2.3.5	The three-dimensional structure of MAO	40
2.3.5.1	The three-dimensional structure of MAO-A	42
2.3.5.2	The three-dimensional structure of MAO-B	43
2.3.6	Mechanistic approach to MAO catalysis	46
2.4	Animal models of Parkinson's disease	49
2.4.1	MPTP models	49
2.4.2	6-Hydroxydopamine (6-OHDA)	51
2.4.3	Rotenone	52
2.4.4	Paraquat and maneb	52
2.5	The Measurement of MAO activity	54
2.5.1	Background	54
2.5.2	Radiometric assay	55
2.5.3	Luminometric assay	55
2.5.4	Fluorometric assay	55
2.5.5	Spectrophotometric assay	56
2.6	Conclusion	58
CHAPTER 3: Synthesis of 3-coumaranone derivatives		60
3.1	Introduction	60
3.2	Synthesis of target compounds	60
3.2.1	Literature method	60
3.2.1.1	Synthesis of 6-hydroxy-3-coumaranone	62
3.2.1.2	Literature approaches to the synthesis of 3-coumaranone derivatives	62
3.3	Materials and instrumentation	63
3.4	Synthesis of 3-coumaranone derivatives	64
3.5	Results - NMR spectra	65
3.6	Mass spectrometry	86
3.7	Interpretation of HPLC analysis	87
3.8	Conclusion	88
CHAPTER 4: Enzymology		89
4.1	Introduction	89
4.2	MAO activity measurements	89

INDEX

4.2.1	General background	89
4.2.2	Chemicals and instrumentation	90
4.2.3	Experimental method for determining IC ₅₀ values	90
4.2.4	Results - IC ₅₀ values	93
4.2.5	Experimental method for the determination of the reversibility of inhibition	98
4.2.6	Results - reversibility of inhibition	100
4.2.7	Experimental method for the construction of Lineweaver-Burk plots	102
4.2.8	Results - Lineweaver-Burk plots	105
4.3 Summary		106
CHAPTER 5: Conclusion		108
Bibliography		111
Appendix		116
Appendix	Section 1: List of ¹ H NMR and ¹³ C NMR spectra of the following compounds	116
Appendix	Section 2: List of mass spectra of the following compounds	117
Appendix	Section 3: List of HPLC traces of the following compounds	118
Acknowledgements		168

LIST OF FIGURES AND TABLES

Figure 1.1	Mechanistic representation of mitochondrial MAO-catalysed oxidative deamination	7
Figure 1.2	The structures of phthalide and 3-coumaranone	9
Figure 1.3	An overview of the 3-coumaranone derivatives that will be synthesised in this study	9
Table 1.1	The structures of compounds that will be synthesised in this study	10
Figure 1.4	An overview of the structural modifications that will be made to the 3-coumaranone moiety	12
Table 2.1	The motor and non motor symptoms of PD	14
Figure 2.1	A summary of the mechanisms involved in neurodegeneration in PD	18
Table 2.2	A summary of the genes associated to l-dopa responsive parkinsonism	19
Figure 2.2	The structures of selective MAO-B inhibitors, (R)-deprenyl, and rasagiline	20
Figure 2.3	The structure of levodopa	21
Figure 2.4	The structure of carbidopa	21
Figure 2.5	The structures of ergoline derivatives (dopamine agonist drugs)	22
Figure 2.6	The structures of non-ergoline derivatives (dopamine agonist drugs)	22
Figure 2.7	The structures of the anticholinergic drugs, trihexphenidyl and beztropine	23
Figure 2.8	The structures of the COMT inhibitors, entacapone and tolcapone	23
Figure 2.9	The structure of amantadine	24
Figure 2.10	The structure of istradefylline (KW-6002)	24
Table 2.3	Strategies that have been used for neuroprotection in PD	25
Figure 2.11	The structure of safinamide	26
Figure 2.12	The structure of lazabemide	27
Figure 2.13	The structure of pramipexole	27
Figure 2.14	The structure of α -tocopherol	28
Figure 2.15	The structure of ubiquinone	28
Figure 2.16	The structure of creatine	29
Figure 2.17	The structure of minocycline	29
Figure 2.18	The structure TCH 346	30
Figure 2.19	The structure of CEP-1347	30
Figure 2.20	The structure of riluzole	31
Figure 2.21	The structures of iproniazid, hydrazine, tranlycypromine, and pargyline	32
Figure 2.22	A schematic representation of the cheese reaction	33

LIST OF FIGURES AND TABLES

Figure 2.23	Schematic representation for the reaction pathway of MAO metabolism	34
Figure 2.24	Schematic representation of neurotoxicity induced by iron and hydrogen peroxide	35
Figure 2.25	Schematic representation of the Fenton reaction	36
Figure 2.26	A schematic representation of dopamine metabolism	37
Table 2.4	Categories and examples of MAO inhibitors	39
Figure 2.27	Examples of selective reversible MAO-A inhibitors	39
Figure 2.28	An example of a selective irreversible MAO-A inhibitor	40
Figure 2.29	Examples of non-selective MAO inhibitors	40
Figure 2.30	Ribbon diagram of human MAO-A, MAO-B, and rat MAO-A	41
Figure 2.31	The active sites of human and rat MAO-A	42
Figure 2.32	A ribbon diagram of human MAO-A	43
Figure 2.33	Comparison of the active site cavities of human MAO-A, and MAO-B	44
Figure 2.34	Ribbon diagram of human MAO-B	45
Figure 2.35	Schematic representation of the catalytic pathway of MAO	47
Figure 2.36	A representation of the SET mechanism of MAO catalysis	48
Figure 2.37	A representation of the polar nucleophilic mechanism of MAO catalysis	49
Figure 2.38	Schematic representation of MAO-B catalysed oxidation of MPTP to MPDP ⁺ and MPP ⁺ (pyridinium metabolite)	50
Figure 2.39	Structure comparison between 6-OHDA and dopamine	51
Figure 2.40	The oxidation reaction of 6-OHDA	51
Figure 2.41	The structure of rotenone	52
Figure 2.42	Schematic representation of the redox-cycling reaction of paraquat	53
Figure 2.43	Structure similarities between paraquat and MPP ⁺	53
Figure 2.44	The structure of maneb	54
Figure 2.45	The generalised reaction of oxidative deamination catalysed by MAO	54
Figure 2.46	Schematic representation of the oxidation of 5-amino-2,3-dihydro-1,4-phthalazinedione in the presence of hydrogen peroxide	55
Figure 2.47	Schematic representation of the oxidation of amplex red to produce a highly fluorescent product, resorufin	56
Figure 2.48	The use of 4-aminoantipyrine for the spectrophotometric determination of MAO activity	57
Figure 2.49	Kynuramine is oxidatively deaminated by MAO to yield 4-hydroxyquinoline	58

LIST OF FIGURES AND TABLES

Figure 2.50	The oxidation of benzylamine to yield benzaldehyde	58
Figure 3.1	The general synthetic route for the synthesis of the 6-hydroxy-3-coumaranone derivatives	60
Table 3.1	The structures of the 3-coumaranone derivatives 1(a-t) that were synthesised	61
Figure 3.2	A general reaction scheme to illustrate the synthesis of 6-(benzyloxy)-2 <i>H</i> -benzofuran-3-one	62
Figure 3.3	Illustration of experimental procedure for the synthesis of the 3-coumaranone derivatives 1a-t	64
Table 3.2	The mass spectrometric data for the 3-coumaranone derivatives, 1a-t .	87
Figure 4.1	Oxidative deamination of kynuramine by MAO-A and MAO-B to yield 4-hydroxyquinoline	89
Figure 4.2	Kynuramine is oxidatively deaminated by MAO to yield 4-hydroxyquinoline	90
Figure 4.3	Flow-diagram summarising the experimental method for IC ₅₀ determination	91
Figure 4.4	An example of the calibration curve routinely constructed in this study	92
Table 4.1	The IC ₅₀ values (provided in μ M) for the inhibition of human MAO-A and MAO-B by the 3-coumaranone derivatives 1a-t .	95
Figure 4.5	Flow-diagram summarising the experimental method for the determination of the reversibility of inhibition by dialysis	99
Figure 4.6	Histogram of the reversibility of MAO-B inhibition by compound 1g	101
Figure 4.7	Flow-diagram summarising the experimental method for constructing Lineweaver-Burk plots	103
Figure 4.8	Lineweaver -Burk plots for the inhibition of MAO-B by compound 1g	104
Figure 4.9	Graph of slopes of the Lineweaver-Burk plots versus the concentration of the inhibitor 1g	105

LIST OF ABBREVIATIONS

A

ADH Aldehyde dehydrogenase

C

CNS Central nervous system

COMT Catechol-O-methyl-transferase

D

DA Dopamine

DOPAC Dihydroxyphenylacetic acid

DMF N,N-dimethylformamide

E

E Enzyme

ES Enzyme-substrate

F

FAD Flavin adenine dinucleotide

FDA Food and drug administration

G

GPO Glutathione peroxidase

GSH Glutathione

H

HCl Hydrochloric acid

5-HIAA 5-Hydroxyindole acetic acid

5-HT Serotonin

HPLC High-pressure liquid chromatography

I

IC₅₀ Inhibitor concentration at 50% inhibition

LIST OF ABBREVIATIONS

K

K _d	Dissociation constant
K _i	Inhibitor constant
K _m	Michaelis constant

L

Lys	Lysine
-----	--------

M

MAO	Monoamine oxidase
MPP ⁺	1-Methyl-4-phenylpyridinium
MPTP	1-Methyl-4-phenyl-1,2,3,6-tetrahydropyridine
MS	Mass spectrometry

N

NA	Noradrenaline
NMDA	N-methyl-D-aspartate

P

PD	Parkinson's disease
----	---------------------

R

ROS	Reactive oxygen species
-----	-------------------------

S

SD	Standard deviation
SET	Single electron transfer
SNpc	Substantia nigra pars compacta
SN	Substantia nigra

U

UCH-L1	Ubiquitin C-terminal hydrolase L1
--------	-----------------------------------

V

VTA	Ventral tegmental area
-----	------------------------

ABSTRACT

Parkinson's disease (PD) is an age related neurodegenerative disorder that presents with both motor and non-motor symptoms. The most common pathological characteristic of PD is the loss of the pigmented dopaminergic neurons of the substantia nigra pars compacta (SNpc), with the appearance of intracellular inclusions known as Lewy bodies in the affected neurons. The loss of the SNpc neurons results in a deficiency of dopamine in the nigrostriatal pathway of the brain, and it is this deficiency that is responsible for the motor symptoms of PD.

Monoamine oxidase B (MAO-B) is predominantly found in the striatum and is responsible for the oxidative metabolism of dopamine. The first-line treatment of PD is dopamine replacement therapy with levodopa, the metabolic precursor of dopamine. Rapid metabolism of levodopa at central and peripheral level, however, hampers its therapeutic potential. MAO-B inhibition enhances striatal dopamine activity by means of inhibiting dopamine metabolism, and MAO-B inhibitors are thus used in the treatment of PD, particularly in combination with levodopa. The aim of this study was to design new potent, reversible MAO inhibitors with selectivity towards MAO-B for the symptomatic treatment of PD.

Recent studies have shown that C5-substituted phthalide derivatives are highly potent inhibitors of human MAO-B. Phthalide derivatives were also found to be potent inhibitors of human MAO-A. The structural similarity between phthalide and 3-coumaranone suggests that 3-coumaranone may be a useful scaffold for the design of reversible MAO-B inhibitors. In the present study, 3-coumaranone derivatives were thus synthesised and evaluated as potential MAO-A and MAO-B inhibitors.

By reacting 6-hydroxy-3-coumaranone with the appropriate alkylbromide in N,N-dimethylformamide in the presence of potassium carbonate, a series of twenty 3-coumaranone derivatives were synthesised. The structures of the compounds were verified with NMR spectroscopy and mass spectrometry. The purities of the compounds were determined by HPLC analyses.

To determine the inhibition potencies, the recombinant human MAO-A and MAO-B enzymes were used, and the inhibition potencies were expressed as IC_{50} values. The results indicated that the 3-coumaranone derivatives are highly potent MAO-B inhibitors. For example, 9 of the 3-coumaranone derivatives inhibited MAO-B with IC_{50} values $< 0.05 \mu\text{M}$, with the most potent inhibitor exhibiting an IC_{50} value of $0.004 \mu\text{M}$. Although the 3-coumaranone derivatives are selective MAO-B inhibitors, some compounds were also potent MAO-A inhibitors with the most potent inhibitor exhibiting an IC_{50} value of $0.586 \mu\text{M}$. The reversibility of MAO-B inhibition by a representative inhibitor was examined by measuring the degree to which the enzyme activity recovers after dialysis of the enzyme-inhibitor complex. Since MAO-B activity was almost completely recovered after dialysis, it may be concluded that the 3-coumaranone derivatives

ABSTRACT

bind reversibly to MAO-B. Lineweaver-Burk plots were constructed to show that the representative 3-coumaranone derivative is a competitive inhibitor of MAO-B.

To conclude, the 3-coumaranone derivatives are potent, selective, reversible and competitive inhibitors of MAO-B. These compounds may find application in the treatment of neurodegenerative disorders such as PD. Potent MAO-A inhibitors were also discovered, which suggests that 3-coumaranone derivatives may serve as leads for the design of drugs for the treatment of depression. In addition, 3-coumaranone derivatives which inhibited both MAO-A and MAO-B, may have potential application in the therapy of both PD and depressive illness.

Keywords: Parkinson's disease, Monoamine oxidase, Inhibitors, Reversible, 3-Coumaranone.

UITTREKSEL

Parkinson se siekte is 'n ouderdomsverwante, neurodegeneratiewe siekte wat gekarakteriseer word deur motoriese en nie-motoriese simptome. Die mees algemene eienskappe van Parkinson se siekte is die verlies van die gepigmenteerde dopamienergiese neurone van die substantia nigra pars compacta (SNpc) en die teenwoordigheid van intrasellulêre strukture bekend as Lewy-liggame in die aangetaste neurone. Die verlies aan SNpc neurone lei tot 'n tekort aan dopamien in die nigrostriatale baan van die brein, en hierdie tekort is verantwoordelik vir die motorsimptome van Parkinson se siekte.

Monoamienoksidase B (MAO-B) kom hoofsaaklik in die striatum van die brein voor, en is verantwoordelik vir die metabolisme van dopamien. Die eerste linie van die behandeling van Parkinson se siekte is dopamienvervanging met levodopa, die metaboliese voorloper van dopamien. Die metabolisme van levodopa in die sentrale en perifere weefsel verhoed egter die effektiewe werking van levodopa. Omdat MAO-B-inhibeerders die metabolisme van dopamien in die brein vertraag, word MAO-B-inhibeerders vir die behandeling van Parkinson se siekte aangewend, veral in kombinasie met levodopa. Die doel van hierdie studie was om nuwe potente, omkeerbare MAO-inhibeerders te ontwerp wat vir die behandeling van Parkinson se siekte aangewend kan word.

Onlangse studies het getoon dat C5-gesubstitueerde ftalied-derivate potente inhibeerders van menslike MAO-B is. Dit is bevind dat ftalied-derivate ook potente inhibeerders van menslike MAO-A is. Die strukturele ooreenkomste tussen ftalied en 3-kumaranoon dui daarop dat 3-kumaranoon 'n geskikte leidraadverbinding kan wees vir die ontwerp van omkeerbare MAO-B-inhibeerders. In die huidige studie is 3-kumaranoon-derivate dus gesintetiseer en geëvalueer as inhibeerders van MAO-A en MAO-B.

Deur 6-hidroksie-3-kumaranoon met 'n toepaslike alkielbromied in N,N-dimetielformamied in die teenwoordigheid van kaliumkarbonaat te reageer, is 'n reeks van twintig 3-kumaranoon-derivate gesintetiseer. Die strukture van die gesintetiseerde verbindings is bevestig met KMR-spektroskopie en massaspektrometrie. Die suiwerheid van die verbindings is bepaal deur hoëdrukvloeistofchromatografie (HDVC) analise.

Die potensies waarmee die 3-kumaranoon-derivate MAO inhibeer is gemeet deur van die menslike MAO-A en MAO-B ensieme gebruik te maak. Die potensies is as die IC_{50} -waardes uitgedruk. Die resultate toon dat die 3-kumaranoon-derivate potente MAO-B-inhibeerders is. Daar is gevind dat nege van die 3-kumaranoon-derivate MAO-B inhibeer met IC_{50} -waardes van $<0.05 \mu M$. Die mees potente inhibeerder het 'n IC_{50} -waarde van $0.004 \mu M$ getoon. Alhoewel die 3-kumaranoon-derivate selektiewe MAO-B-inhibeerders is, was sommige verbindings ook potente MAO-A-inhibeerders. Die mees potente MAO-A-inhibeerder het 'n IC_{50} -waarde van $0.586 \mu M$ getoon. Die omkeerbaarheid van MAO-B-inhibisie is met 'n

UITTREKSEL

verteenwoordigende inhibeerder ondersoek. Vir hierdie doel is daar bepaal of ensiemaktiwiteit herstel na dialise van die ensiem-inhibeerder kompleks. Aangesien MAO-B-aktiwiteit feitlik volkome herstel het na dialise, kan daar afgelei word dat die 3-kumaranoon-derivate omkeerbaar aan MAO-B bind. Lineweaver-Burk grafieke is opgestel om te wys dat die verteenwoordigende 3-kumaranoon-derivaat 'n kompeterende inhibeerder is van MAO-B.

Uit hierdie studie kan dus afgelei word dat 3-kumaranoon-derivate potente en selektiewe MAO-B-inhibeerders is, wat omkeerbaar aan die ensiem bind. Hierdie verbindings kan moontlik aangewend word vir die behandeling van neurodegeneratiewe siektes soos Parkinson se siekte. Potente MAO-A-inhibeerders is ook in hierdie studie ontdek, en 3-kumaranoon-derivate kan dus ook dien as behandeling vir depressie. Daarbenewens, kan 3-kumaranoon-derivate wat beide MAO-A en MAO-B inhibeer, moontlik vir die behandeling van Parkinson se siekte sowel as depressie aangewend word.

Sleutelwoorde: Parkinson se siekte, Monoamienoksidase, Inhibeerders, Omkeerbaar, 3-Kumaranoon.

CHAPTER 1

INTRODUCTION

1.1 Brief background on Parkinson's disease

Parkinson's disease (PD) is an incurable progressive neurodegenerative disorder. Neurodegenerative disorders are characterised by progressive and irreversible loss of neurons from specific regions of the brain. The symptoms of PD is caused by the loss of dopamine innervation in the striatum as a result of neurodegeneration of dopaminergic cells in the ventral midbrain (Romero-Ramos *et al.*, 2004; Hardman *et al.*, 2001). The neuronal cells of the ventral tegmental area (VTA) are dopamine cell groups with projections to the nucleus accumbens, the prefrontal cortex, septum olfactory turbucule and amygdala. Neuronal cells of the substantia nigra pars compacta (SNpc), in turn, project to the striatum. Neurodegeneration occurs in both cell groups, but due to severe cell death in the SNpc it is believed that this region is more involved in PD (Romero-Ramos *et al.*, 2004). The pathological hallmark of PD is the loss of the pigmented dopaminergic neurons of the SNpc with the manifestation of intracellular inclusions known as Lewy bodies. The loss of dopaminergic neurons is an attribute of normal aging, a risk factor for the development of PD. PD symptoms only appear after the loss of 70-80% of dopaminergic neurons (Gibb, 1992; Fearnley & Lees, 1994).

Previous studies suggested that more than 50,000 new PD cases develop each year in the United States alone. PD is a progressive disease that is associated with an increase in age and affect 17.4 persons in every 100 000 persons between the age of 50-59 years old, and 93.1 persons per 100 000 persons between the age of 70-79 years old. The average age of onset is 60 years, and a mean duration of the disease from diagnosis to death is 15 years (Lees *et al.*, 2009).

The aetiology of PD is complex and not well understood. It likely involves both genetic and environmental factors (Wirdefeldt *et al.*, 2011). Genetic contribution seems to be highly dependent with age of onset. Earlier age of onset is associated with a higher probability of having an affected relative. Studies indicate that if there is an affected sibling under the age of 45 years, the risk of developing PD is 6-fold higher. Some of the genes that are involved in the aetiology of PD are, α -synuclein, UCHL-1 and DJ-1. Even though they are responsible for a small percentage of PD cases, research into the involvement of these proteins in PD are invaluable for a better understanding of the pathophysiology of this disease (Romero-Ramos *et al.*, 2004). The idea that environmental factors may be involved in the aetiology of PD arose when a group of drug addicts developed PD in a short period of time. This was the result of exposure to 1-methyl-4-phenyl-1,2,3,6-tetrahydropyridine (MPTP), a contaminated by-product of the synthesis of a meperidine analogue..

Soon afterwards, other environmental toxins (such as rotenone and paraquat) have been found to induce PD-like neurodegeneration (Ballard *et al.*, 1985; Cummings *et al.*, 1998).

In idiopathic PD, early physical signs is usually overlooked, and more often ascribed to old age or rheumatism (Lees *et al.*, 2009). Clinical diagnosis is made based on specific signs and symptoms. The lack of dopamine in the nigrostriatal pathway results in motor dysfunction such as the appearance of bradykinesia, resting tremor, rigidity, postural instability and akinesia. A correct and complete diagnosis of PD can only be established when two of these symptoms are present, of which one must be tremors or bradykinesia (Romero-Ramos *et al.*, 2004).

Various treatment options exist, which incorporate non-pharmacological and pharmacological treatment. Non-pharmacological treatment includes exercise, physical therapy, speech therapy and occupational therapy. All of these play a major role in the patients' quality of life (Pedrosa & Timmerman, 2013). Progressive loss of dopaminergic neurons is the main cause of the motor features of PD, and the focus of current PD therapy is on the replacement of dopamine in the nigrostriatal pathway (Yacoubian & Standaert, 2009; Dauer & Przedborski, 2003). None of the current treatment options available today halt or retard the disease progression and dopaminergic neuron degeneration.

1.2 Monoamine oxidase inhibitors in PD

Monoamine oxidase (MAO) are flavin adenine dinucleotide (FAD) containing enzymes within the outer mitochondrial membrane. MAO plays a major role in the oxidation of monoamine neurotransmitters such as dopamine, and xenobiotic amines such as dietary tyramine (Youdim & Bakhle, 2006; Inoue *et al.*, 1999). MAO consist of two isoenzymes, MAO-A and MAO-B, they have different substrate and inhibitor specificities, pH optima and sensitivity to heat inactivation (Youdim *et al.*, 2006). The MAOs are considered to be drug targets for the treatment of various psychiatric and neurological disorders (Strydom *et al.*, 2013). Therapeutically, MAO-A inhibitors are used as antidepressant agents, while MAO-B inhibitors are used in the treatment of PD (Youdim & Bakhle, 2006; Youdim *et al.*, 2006).

MAO-A metabolises serotonin and norepinephrine in the brain. Since central deficiencies of these two monoamines have been implicated in depressive illness, inhibitors of MAO-A have been employed as antidepressant agents (Youdim & Bakhle, 2006). A substantial proportion of PD patients' exhibit signs of depression, and the antidepressant action of MAO-A inhibitors may thus be of value to these patients. MAO-B inhibitors, in turn, are used to reduce the MAO-B-catalysed metabolism of dopamine in the brain thus conserving the depleted dopamine and prolonging its action in the striatum. MAO-B inhibitors are also frequently combined with levodopa in PD therapy since MAO-B inhibitors, by reducing the oxidative metabolism of

dopamine, may further enhance dopamine levels derived from levodopa (Youdim & Bakhle, 2006).

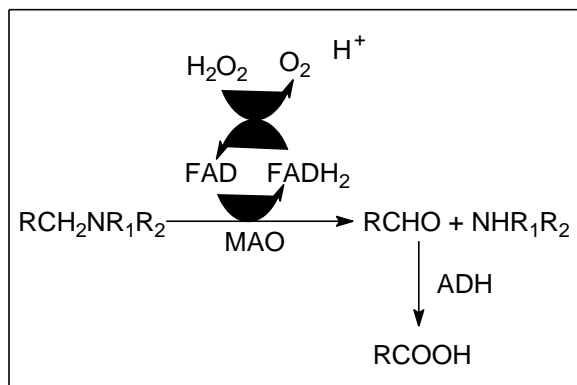


Figure 1.1 Mechanistic representation of mitochondrial MAO-catalysed oxidative deamination (Youdim & Bakhle, 2006).

It is clear that MAO-B inhibitors are useful therapeutic agents for PD. The first-line treatment of PD is however dopamine replacement therapy with levodopa. The rapid metabolism of levodopa at central and peripheral level, however, hampers its therapeutic potential. Levodopa is usually combined with aromatic amino acid decarboxylase inhibitors, reversible and selective catechol-O-methyltransferase (COMT) inhibitors and irreversible MAO-B inhibitors. The Food and Drug administration (FDA) approved only a few MAO inhibitors for the treatment of PD. The first to be approved was (R)-deprenyl (selegiline). This drug is approved for advanced patients with motor fluctuations. (R)-Deprenyl's symptomatic effects are dependent on the inhibition of MAO-B-catalysed metabolism of dopamine in the brain. This leads to enhanced central levels of dopamine and thus symptomatic relief in PD. Since it is metabolised to amphetamine, (R)-deprenyl may also produce an amphetamine effect by increasing dopamine release, which also may provide relief of the symptoms of PD. Rasagiline followed soon afterwards in 2006. Rasagiline is a second generation irreversible MAO inhibitor, and is selective towards MAO-B (Factor, 2008).

There are some disadvantages associated with the use of irreversible MAO-B inhibitors in PD. These include a loss of selectivity after long-term use, and enzyme recovery after drug withdrawal is dependent on the rate of enzyme synthesis. In contrast, the benefits of reversible inhibitors are the quick recovery of enzyme activity after drug withdrawal and the inhibitor is washed from the tissues, and due to the shorter duration of action, loss of selectivity is not frequently observed with reversible inhibitors (Tipton *et al.*, 2004). The prognosis of PD has been radically altered with the availability of effective pharmacological treatment. Some studies have suggested that MAO-B inhibitors may possess neuroprotective properties. This effect may be due to the reduction of harmful metabolic by-products of the MAO-B catalytic

cycle. The oxidative deamination reaction catalysed by MAO-B produces hydrogen peroxide, aldehyde and ammonia as by-products (figure 1.1). These by-products may be neurotoxic and accelerate neurodegeneration in PD.

The aim of this study is thus to design new potent, reversible MAO inhibitors with selectivity towards MAO-B for symptomatic treatment of PD. In addition, MAO-B inhibitors may also be neuroprotective in PD.

1.3 The rationale of this study

As mentioned above, the aim of this study is thus to design new potent, reversible MAO-B inhibitors. The lead compound for this study is phthalide. Previously phthalide has been used as a scaffold in the design of MAO inhibitors, but proved to be a weak MAO-B inhibitor (IC_{50} = 28.6 μ M). However, substitution at the C5 position of phthalide yielded highly potent reversible MAO-B inhibitors. For example, 5-benzyloxyphthalide was found to inhibit human MAO-B with an IC_{50} value of 0.024 μ M (Strydom *et al.*, 2010). Substituted phthalides were also found to be potent inhibitors of human MAO-A. For example, 5-(3-phenylpropoxy)phthalide was found to inhibit human MAO-A with an IC_{50} value of 0.096 μ M (Strydom *et al.*, 2010). In all cases, phthalide derivatives are, however, selective for the MAO-B over the MAO-A isoform. Based on these observations it was decided to further explore the MAO inhibition properties of phthalide derivatives, by focusing on the 3-coumaranone scaffold.

The structural similarity between phthalide and 3-coumaranone (Figure 1.2) is the principal reason to explore the possibility that 3-coumaranone may be a useful scaffold for the design of reversible MAO-B inhibitors. In the present study, 3-coumaranone derivatives will be synthesised and evaluated as potential MAO-A and MAO-B inhibitors. Since substitution at on the C5 position of phthalide yielded highly potent reversible MAO-B inhibition, a 3-coumaranone derivative, compound (table 1.1) **1a** containing the benzyloxy side chain on the C6 position was designed as the first member of the series of 3-coumaranone derivatives. To explore chemical space and to create an appropriate series of 3-coumaranone derivatives for establishment of structure-activity relationships, a total of twenty derivatives will be synthesised. Firstly, the benzyloxy-substituted derivative **1a** will be substituted on the *meta* and *para* positions of the phenyl ring with halogens (F, Cl, Br, I) and alkyl groups (CN, CH₃, CF₃) to yield thirteen derivatives, compounds **1b-n**. The current study will also attempt to synthesise novel derivatives which contain the phenylethoxy, phenylpropoxy and phenoxyethoxy substituents on the C6 position of the 3-coumaranone moiety to yield an additional six derivatives, compounds **1o-t**. The phenylethoxy-substituted derivative **1o** will be substituted on the phenyl ring with bromine and the methyl group.

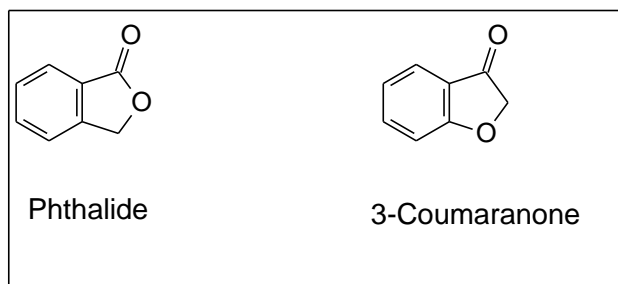


Figure 1.2 The structures of phthalide and 3-coumaranone.

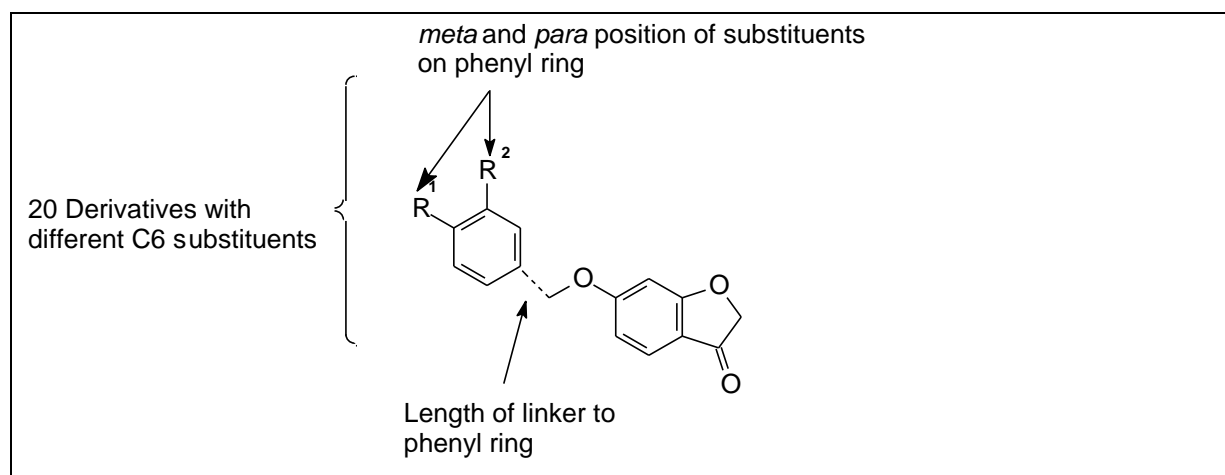
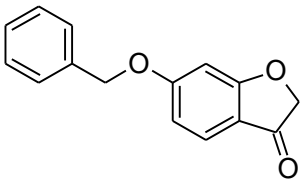
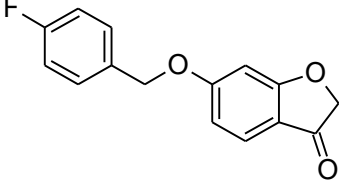
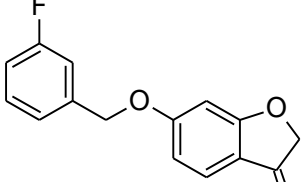
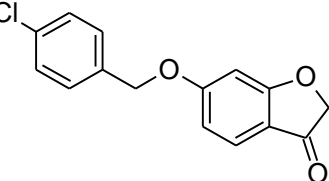
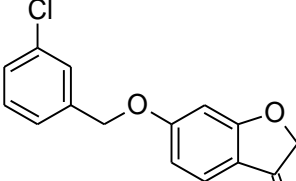
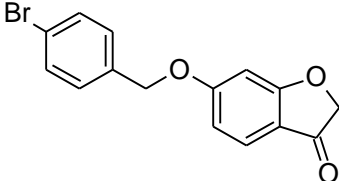
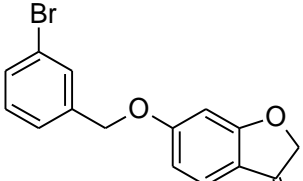
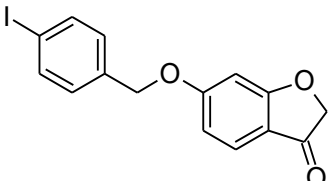
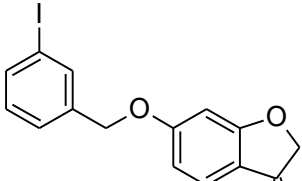
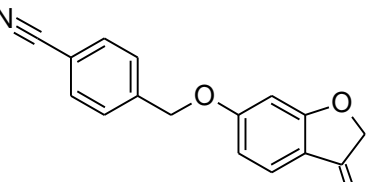
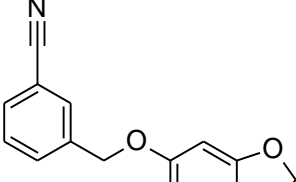
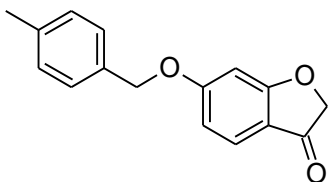
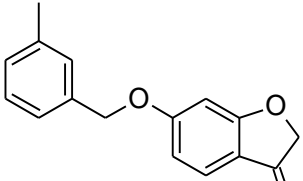
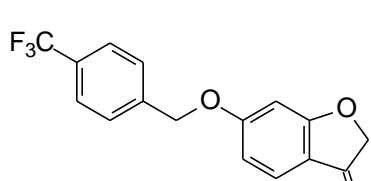
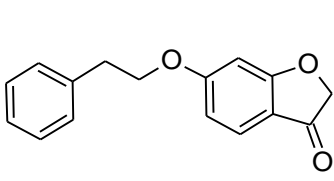
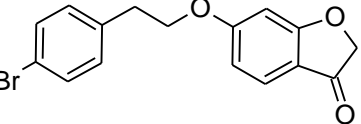
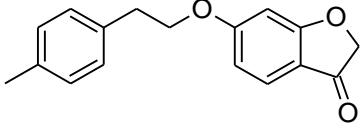
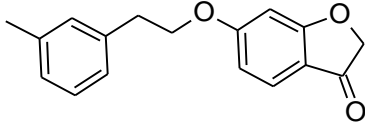
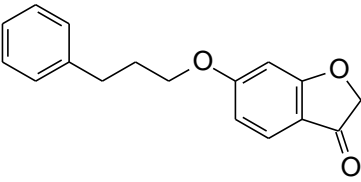
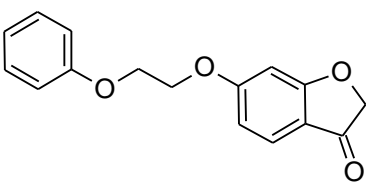


Figure 1.3 An overview of the 3-coumaranone derivatives that will be synthesised in this study

Table 1.1 The structures of compounds that will be synthesised in the study

 1a	 1b	 1c
 1d	 1e	 1f
 1g	 1h	 1i
 1j	 1k	 1l
 1m	 1n	 1o
 1p	 1q	 1r
 1s	 1t	

1.4 The hypothesis of this study

Based on a recent study which has reported that substituted phthalide derivatives are highly potent inhibitors of human MAO-B, it is postulated that substituted 3-coumaranone derivatives will also act as potent MAO-B inhibitors. This hypothesis is based on the observation that the phthalide and 3-coumaranone moieties are similar in structure, and substituted derivatives of phthalide and 3-coumaranone may thus exhibit similar properties with respect to binding to the MAO-B enzyme. In addition, certain substituted phthalide derivatives are also reported to be potent MAO-A inhibitors. We thus postulate that substituted 3-coumaranone derivatives may also inhibit the MAO-A isoform (Strydom *et al.*, 2011; Strydom *et al.*, 2010).

We will thus explore the possibility that 3-coumaranone derivatives act as MAO-A and MAO-B inhibitors. As shown in figure 1.4 substitution will occur at the C6 position of the 3-coumaranone moiety. We will attempt to determine the optimal length of the linker between the 3-coumaranone ring system and the terminal C6 phenyl ring, and determine the effect of halogen (F, Cl, Br, I) and alkyl group (CN, CH₃, CF₃) substitution on the side chain phenyl ring.

1.5 The objectives of this study

- A series of twenty 3-coumaranone derivatives (table 1.1) will be synthesised. For the purpose of this study, the 3-coumaranone derivatives will contain the benzyloxy, phenylethoxy, phenylpropoxy and phenoxyethoxy substituents on the C6 position of the 3-coumaranone moiety. In addition, substitution on the *meta* and *para* positions of the phenyl ring with halogens (F, Cl, Br, I) and alkyl groups (CN, CH₃, CF₃) will also be investigated as shown in table 1.1.
- For a selected 3-coumaranone derivative in the series, the reversibility of MAO-B inhibition will be determined. For the purpose of reversibility studies, the recovery of the enzymatic activity after dialysis of enzyme-inhibitor complexes will be evaluated.
- Lineweaver Burk plots will be used to determine if a selected 3-coumaranone derivative displays competitive inhibition of MAO-B.

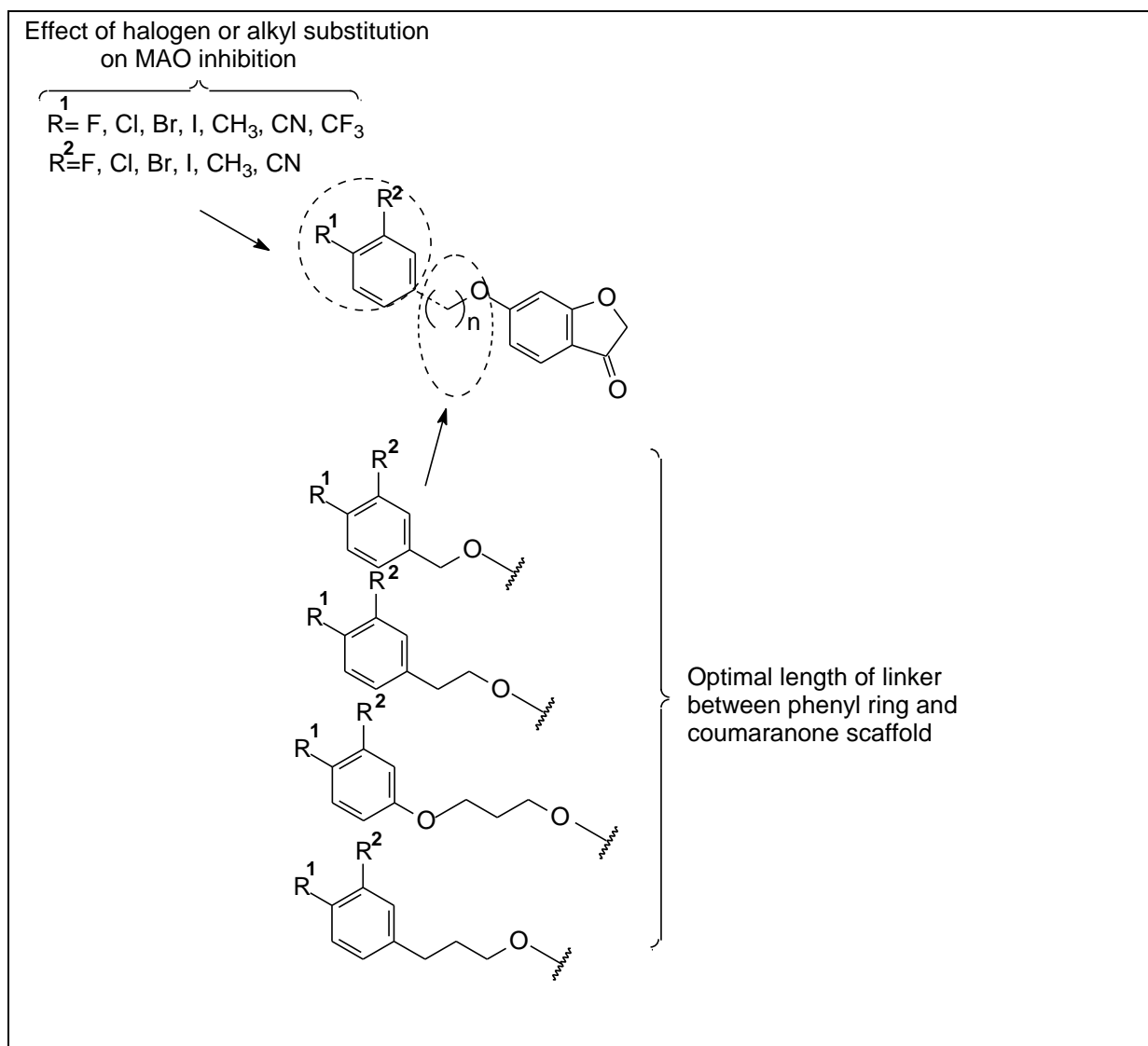


Figure 1.4 An overview of the structural modifications that will be made to the 3-coumaranone moiety.

CHAPTER 2

LITERATURE OVERVIEW

2.1 Parkinson's disease

2.1.1 General background

In the past 200 years, since the publication of the essay “Shaking Palsy” by James Parkinson in 1817, remarkable progress has been made in the treatment of PD. The aetiology of PD is complex and not well understood, and likely involves both genetic and environmental factors (Wirdefeldt *et al.*, 2011). Genetic contribution seems to be highly dependent on age of onset. PD is a slow progressive neurodegenerative disorder which results mainly from the death of the dopaminergic neurons projecting from the SNpc to the striatum, and the appearance of intracellular inclusions called Lewy bodies. Lewy bodies were first discovered by Fredrich Heinrich in 1912. The death of the nigrostriatal dopaminergic neurons results in the decrease of dopamine concentration in the striatum of the brain (Hoy & Keating, 2012). The reduced dopamine concentration in the striatum is responsible for the motor symptoms of PD (table 2.1). PD was once seen as a pure motor disorder, but in recent years researchers have focused, not only on the motor symptoms of this disease, but also the non-motor symptoms (table 2.1). The link between PD and dopamine was made by Carlsson and colleagues, who discovered that most dopamine in the brain is found in the basal ganglia. This discovery led to the understanding that the loss of dopamine causes the majority of motor symptoms of PD, and that the metabolic precursor of dopamine, levodopa, may serve as treatment of PD since it increases dopamine levels in the brain (Carlsson *et al.*, 1958). By increasing the dopamine levels, most of the symptoms associated with PD may be alleviated (Carlsson *et al.*, 1958; Bretler & Rossengren, 1959; Dauer & Przedborski, 2003).

As mentioned, both genetic and environmental factors contribute to the aetiology of PD. Genes that contribute to the genetic factors are, α -synuclein, UCHL-1, DJ-1, and Parkin (Romero-Ramos *et al.*, 2004). Environmental factors in the aetiology of PD include toxins such as MPTP and environmental toxins (rotenone, paraquat, and maneb), which have been found to induce PD-like neurodegeneration (Ballard *et al.*, 1985; Cummings *et al.*, 1998). Various treatment options exist, which include non-pharmacological and pharmacological treatment. Non-pharmacological treatment plays a major role in the patient's quality of life (Pedrosa & Timmerman, 2013). Progressive loss of dopaminergic neurons is the main cause of motor features, and the focus of current PD therapy, which has been on the replacement of dopamine (Yacoubian & Standaert, 2009; Dauer & Przedborski, 2003). PD treatment can be divided into 3 categories namely protective or preventative, symptomatic and regenerative.

Table 2.1 The motor and non-motor symptoms of PD.

Motor symptoms	Description	
Bradykinesia	Slowness of movement, arrest in on-going movement, decreased eye blinking, excessive swallowing, arm swinging (early onset).	
Tremor	Rhythmic sinusoidal movement of a body part, regular contractions of innervated muscles occurs at rest (early onset).	
Muscle rigidity	Increased resistance to passive movements, stiffness of joints but no major source of disability (early onset).	
Postural change	Flexed posture, instability of posture, falling (late onset).	
Gait disorder	Shuffling, lack of arm swing, walking-running, freezing (late onset).	
Non-motor symptoms		
Depression	Psychosis	Confusion
Apathy	Anxiety	Urinary difficulties
Dementia	Fatigue	Sleep disorders

2.1.2 Neurochemical and neuropathological features of PD

The presence of Lewy bodies and the loss of dopaminergic neurons from the substantia nigra are the two most well-known pathological hallmarks of PD (Yacoubian & Standaert, 2009). Dopaminergic neuron cell bodies are mostly situated in the SNpc. The projections of these dopaminergic neurons, the axons and nerve terminals, are primarily found in the putamen, a structure of the striatum. These neurons are known as the nigrostriatal neurons and contain large amounts of neuromelanin, particularly in the neuronal cell bodies in the substantia nigra. In PD these neurons are lost, which leads to the depigmentation of the substantia nigra. In PD, the dorsolateral putamen has very low levels of dopamine. It has been found that 80% of the putamenal dopamine and 60% of the substantia nigra dopaminergic neurons are lost at the onset of the symptoms in PD. Dopamine depletion in the mesolimbic region is far less and the neurons that reside here are much less affected in PD. Studies have shown that, in patients with PD, cell loss is concentrated in the ventrolateral and caudal portions of the substantia nigra, whereas the dorsal medial aspect of the substantia nigra is affected in normal aging. It has also been suggested that neuronal degeneration occurs with terminal loss in the

striatum, which may suggest that striatal dopaminergic nerve terminals are the primary target of the degenerative process (Yacoubian & Standaert, 2009).

2.1.3 Aetiology and pathogenesis of PD

PD is a sporadic and progressive disease. The mean age of onset of PD is 55 years, and the incidence rises dramatically with age, from 20 patients in a 100 000 overall, to 120 patients at the age of 70 years. In the case of sporadic PD (affecting \pm 95% of PD patients) there is no apparent genetic linkage, while for the other 5% of patients PD is inherited (Dauer & Przedborski, 2003). Even though PD is regarded as a sporadic disorder, a few environmental triggers have been identified. Although only 10% of people with the disease are younger than 45 years of age, aging is seen as the major risk factor. The role of the environmental and genetic factors in PD remain indefinable. Recent studies identified that non-smokers are twice as likely to develop PD than smokers, due to the fact that MAO (an enzyme that accelerates neurodegeneration due to an increase in oxidative stress) are inhibited in the brain tissue of smokers. Men and postmenopausal women, not on hormone replacement therapy, who consume very low quantities of caffeine have a 25% higher risk for developing PD. It has been suggested that caffeine, by acting as an adenosine A_{2A} receptor antagonist, may protect against the neurodegenerative processes in PD. Other weak associations with the cause of PD are head injuries, rural living, middle-age obesity, lack of exercise, occupation, drugs and alcohol. Furthermore the chronic exposure to environmental toxins, such as cyanide, carbon disulfide and toluene, can initiate neurodegeneration that is similar but not identical to that of PD (Lees *et al.*, 2009). Endogenous toxins such as reactive oxygen species (ROS) generated from the normal metabolism of dopamine may be another cause of PD, and the formation of these toxins are linked to the distortions of the normal metabolic pathways that may lead to neurodegeneration (Dauer & Przedborski, 2003). Some medications such as dopamine antagonists, calcium channel blockers and herbal remedies can also cause drug-induced parkinsonism. Oxidative stress and mitochondrial dysfunction, protein aggregation and misfolding, neuroinflammation, excitotoxicity, apoptosis, the loss of trophic factors, and some genetic factors are just a few of the pathological mechanisms involved in neurodegeneration in PD (Figure 2.1). These mechanisms act synergistically through complex interactions to promote neurodegeneration (Dauer & Przedborski, 2003).

2.1.3.1 Oxidative stress and mitochondrial dysfunction

Laboratory evidence suggests that the overabundance of ROS is a potential mechanism of neurodegeneration in PD. Both overproduction of ROS and failure of cellular protective mechanisms are active in PD. Oxidative damage to proteins, lipids, and nucleic acids have been found in patients with PD. Dopamine metabolism is another source of oxidative stress, through the production of quinones, peroxides and other ROS. Another source of the production of ROS is mitochondrial dysfunction, which further damages the mitochondria (Yacoubian & Standaert, 2009). Mitochondria related energy failure disrupts vesicular dopamine storage, causing the increase of cytosolic dopamine concentration, which in turn, leads to the damage of cellular macromolecules (Dauer & Przedborski, 2003). Decreased activity of complex I is found in the substantia nigra of PD patients, and in animal models a parkinsonian syndrome is initiated by complex I inhibitors such as MPP⁺ and rotenone. Even though the mechanism is not fully understood, evidence shows that decreased levels of glutathione in postmortem PD nigra exist. Data show that several of the genes linked to familial forms of PD appear to be involved in the protection against oxidative stress. Thus, any mutation on these genes [PTEN-induced putative kinase [PINK1], and DJ-1] may lead to PD (Yacoubian & Standaert, 2009).

2.1.3.2 Protein aggregation and misfolding

Protein aggregation and misfolding have been recognized as important mechanisms in neurodegenerative disorders. Localization of protein aggregates is disease specific, but in all the cases protein aggregation is toxic to neurons (Dauer & Przedborski, 2003). As in Alzheimer's and Huntington's disease, the primary aggregating protein is α -synuclein, whose link was discovered in familial autosomal dominant PD due to the mutation in this protein (Yacoubian & Standaert, 2009). There are only a few cases of inherited PD that are linked to mutations in α -synuclein, whereas in sporadic PD α -synuclein is the major component of Lewy bodies. The aggregation of misfolded proteins is toxic through numerous mechanisms; it could cause direct damage by deforming the cell or by interfering with intracellular trafficking in neurons. Gene duplication of the α -synuclein locus, point mutations, overexpression and oxidative damage have been implicated in self-aggregation. Recent studies implicating parkin and ubiquitin carboxyl-terminal hydrolase L1 (UCH-L1) in the genetic forms of PD reinforce the connection between protein aggregation and PD pathogenesis. Parkin, an E₃ ubiquitin ligase, is involved in the mechanism which identifies and targets misfolded proteins for degradation. Mutations disrupt the E₃ ubiquitin ligase activity. UCH-L1 acts as an ubiquitin recycling enzyme, and mutations may lead to the aggregation of damaged proteins. Thus, the

overproduction or impaired clearance of α -synuclein may contribute to aggregation (Yacoubian & Standaert, 2009).

2.1.3.3 Neuroinflammation

The presence of inflammatory mediators (interleukins and TNF- α) has been identified in PD. Increased levels of these mediators stimulate microglial cell activation and nitric oxide production, which directly triggers the production of cytotoxic factors that cause oxidative stress and intensify cell damage. The mechanism involved with the activation of microglia is not fully understood, but cytokines and α -synuclein aggregation can lead to microglia activation (Yacoubian & Standaert, 2009).

2.1.3.4 Excitotoxicity

Excitotoxicity has been implicated as a pathogenic mechanism in several neurodegenerative diseases. Glutamate is the primary excitatory transmitter and driver of the excitotoxicity process in the central nervous system. Glutamate receptors are found in dopaminergic neurons in the substantia nigra, which receive glutamatergic innervations from the subthalamic nucleus and cortex. Increased N-methyl-D-aspartate (NMDA) receptor activation by glutamate causes an influx of calcium, which may lead to the activation of apoptosis pathways. In addition to apoptosis activation, this process also promotes peroxynitrite production through nitric oxide synthase. High levels of 3-nitrotyrosine, a marker of peroxynitrite formation, are seen in the postmortem substantia nigra of PD patients (Yacoubian & Standaert, 2009).

2.1.3.5 Apoptosis

Programmed cell death is a mechanism that participates in neural development and in some forms of neural injury (Yacoubian & Standaert, 2009). In apoptosis, intracellular signalling pathways are activated to cause cell death. Even though programmed cell death is part of normal development, the deregulation of this mechanism in the brain may contribute to neurodegeneration (Dauer & Przedborski, 2003). Several studies implicate apoptotic and autophagic cell death in the substantia nigra of PD patients. The alterations in cell death pathways are unlikely to be the primary cause of PD. Activation of both apoptotic and autophagic cell death pathways occurs through oxidative stress, protein aggregation, excitotoxicity or inflammation (Yacoubian & Standaert, 2009).

2.1.3.6 Loss of trophic factors

A potential contributor to cell death in PD is the loss of trophic factors. Decreased levels of brain-derived neurotrophic factor, glial-derived neurotrophic factor, and nerve-derived trophic factor have been found in the SN of PD patients (Yacoubian & Standaert, 2009).

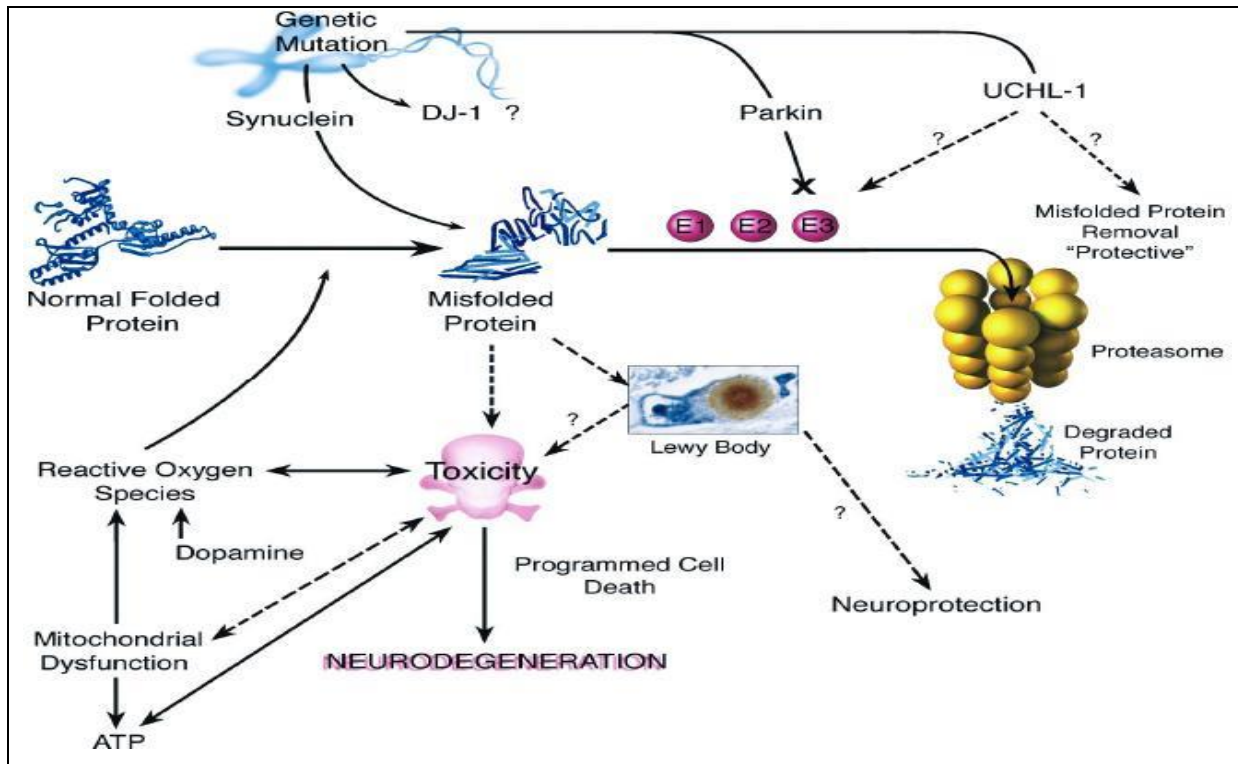


Figure 2.1 A summary of the mechanisms involved in neurodegeneration in PD (Dauer & Przedborski, 2003).

2.1.4 Genetics

As mentioned, mutations in seven genes are linked to L-dopa-responsive parkinsonism. Six of the pathogenic mutations are found in leucine rich repeat kinase 2 (LRRK-2) and the most common of these is the Gly2019Ser mutation. In sporadic cases this mutation has a frequency of 1%, and in hereditary parkinsonism a frequency of 4%. With this mutation, there is a risk of 28% for developing parkinsonism when younger than 60 years, with the incidence rising to 74% at the age of 79 years (Lees *et al.*, 2009). Recessive early onset parkinsonism with an age of onset of younger than 40 years is caused by mutations in four genes; parkin, DJ-1, PINK1, and ATP13A2. Parkin mutations are common, whereas mutations in the other three genes are rare (Lees, 2005). Generally, parkin mutations occur in patients younger than 30 years, especially those with a family history of recessive inheritance of PD. This form of PD is characterised by loss of dopaminergic neurons from the substantia-nigra, but is not associated with Lewy bodies (Dauer & Przedborski, 2003).

Mutations of α -synuclein are much rarer than the LRRK-2 Gly2019Ser mutation, but cause a syndrome indistinguishable from PD. The cause of α -synuclein's neurotoxicity may be due to the misfolding and formation of amyloid fibrils and nonfibrillary oligomers (Dauer & Przedborski, 2003). There is a fivefold increase in the risk of developing PD with heterozygous loss of function of glucocerebrosidase (GBA) (Lees *et al.*, 2009). This mutation is common among Ashkenazi Jews, but the relationship between GBA mutations and PD is still unclear.

Table 2.2 Summary of the genes associated to L-dopa responsive parkinsonism (Lees *et al.*, 2009).

Parkinsonism	Pathological aggregates	Onset
Parkin	SN degeneration with no Lewy bodies	Recessive young onset
PINK1	No pathology reported	Recessive young onset
DJ-1	No pathology reported	Recessive young onset
ATP13A2	No pathology reported	Recessive young onset
Parkinson's disease		
α -synuclein	Lewy bodies	Dominant point mutations and duplications. Genetic variability contributes to the disease
LRRK-2	Lewy bodies are unusual	Dominant mutations
GBA	Lewy bodies	Dominant loss of function mutations increase risk

2.1.5 Symptomatic treatment

As previously stated, PD is an incurable, progressive, neurodegenerative disease. Treatment focuses solely on the management of the disease symptoms by improving the quality of life and improving the functional capacity of the patient. PD is characterised by primary and secondary motor symptoms as well as non-motor symptoms. Primary motor symptoms include rigidity, resting tremor, bradykinesia and postural instability. These symptoms affect the majority of PD patients. Secondary motor symptoms do not affect the majority of patients and include stooped posture, dystonia, fatigue, impaired fine motor movement, sexual dysfunction, loss of facial expression, drooling, muscle cramps, akathisia and speech impairment. Non-

motor symptoms include memory impairment, dementia, constipation, anxiety, confusion, urinary difficulties and sleep disorders. Pharmacological treatment focuses on the management of disease symptoms (Pedrosa & Timmermann, 2013).

PD is a neurodegenerative disease for which there is no cure, and as mentioned, is characterised by a loss of dopaminergic neurons in the SN (Heisters & Bains, 2012). Pharmacological therapy is key to the management of PD. Current treatment includes a variety of drugs from different pharmacological classes. The majority of these drugs aim to alleviate the motor symptoms and complications by restoring striatal dopamine action (Heisters, 2011). This is accomplished by either increasing dopamine supply with a prodrug precursor (levodopa), directly stimulating dopamine receptors with dopamine agonists or through inhibiting the reuptake and metabolism of dopamine (Cranwell-Bruce, 2010). However, the primary goal is neuroprotection and slowing down the progression of the disease by protecting or salvaging neurons, even though there is no concrete evidence that current drugs used today provide neuroprotection (Fernandez & Chen, 2007).

MAO-B inhibitors: MAO-B inhibitors can be used as monotherapy or as combination therapy in PD. MAO-B inhibitors enhance dopaminergic activity by inhibiting dopamine metabolism, and they may also modify disease progression by acting as neuroprotective agents (Fernandez & Chen, 2007). Selective MAO-B inhibitors increase synaptic dopamine concentrations without affecting MAO-A activity (LeWitt & Taylor, 2008). (R)-Deprenyl and rasagiline, irreversible MAO-B inhibitors, delay the initiation of dopaminergic treatment, decrease dopamine catabolism and antagonise the cellular processes that are involved in apoptosis (LeWitt & Taylor, 2008).

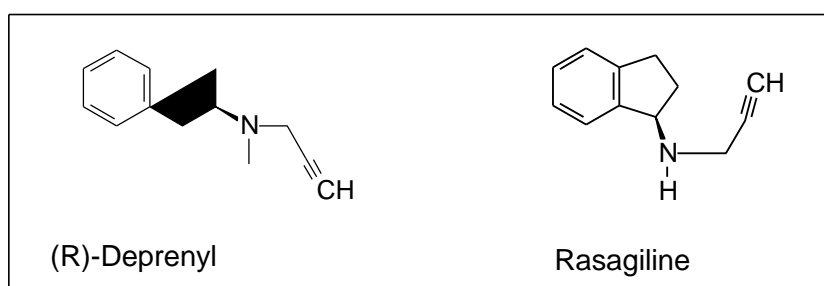


Figure 2.2 The structures of selective MAO-B inhibitors, (R)-deprenyl and rasagiline.

Levodopa: Levodopa has been used for 40 years and is still considered to be the gold standard therapy in the treatment of PD. Levodopa is the metabolic precursor of dopamine and replaces the dopamine lost in PD by momentarily restoring striatal dopaminergic neurotransmission. Whatever the age of the patient, levodopa in combination with benserazide or carbidopa (peripheral dopa decarboxylase inhibitors) should be considered. Levodopa is the most

effective agent for symptomatic treatment of PD, offering benefit to all treated patients. Non-motor symptoms (such as dementia) are not improved by levodopa and patients may develop motor complications (dyskinesia), motor fluctuations (on-off periods) and delayed-on episodes after long-term treatment. As the disease progresses the dose of levodopa needs to be increased to maintain a therapeutic effect, and the development of levodopa-induced dyskinesia with motor fluctuations is thus more frequently encountered. During the off period the voluntary movements are impaired, and during the on period dyskinesia usually develop (Lees *et al.*, 2009).

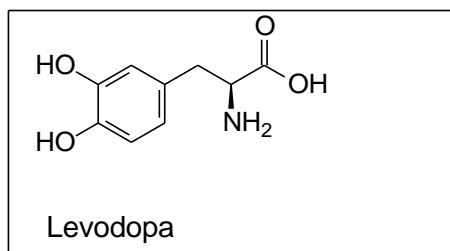


Figure 2.3 The structure of levodopa.

Carbidopa: Levodopa is usually combined with carbidopa in PD therapy. The combination of levodopa and a dopa decarboxylase inhibitor is usually used as initial therapy for patients of all ages. Carbidopa, a dopa decarboxylase inhibitor, prevents the conversion of levodopa to dopamine in the peripheral nervous system (Lees *et al.*, 2009; Cranwell-Bruce, 2010). Treatment with this combination results in an improvement of 20-70% of the motor symptoms within 7-14 days from the onset of the treatment. Fatigue, rigidity and bradykinesia also improve over a period of 3 months. Motor complications, however, tend to develop within a period of 4-6 years after the treatment with levodopa, and are not prevented by combination with carbidopa (Lees *et al.*, 2009).

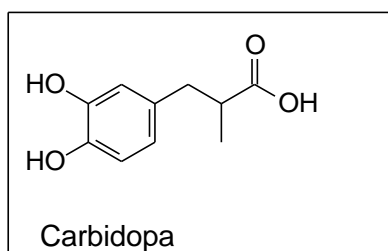


Figure 2.4 The structure of carbidopa.

Dopamine agonists: Dopamine agonists act at striatal dopamine receptors which may hold several advantages. They may be more effective than levodopa since their action is not dependent on the functional capacity of nigrostriatal neurons (Hardman *et al.*, 2001), and dopamine agonists may delay the motor complications induced by levodopa therapy. All

dopamine agonists act on D₂-receptors. Even though the mechanism of action is not fully understood, it is suggested that presynaptic D₂-receptor stimulation leads to antiparkinsonian activity, whereas postsynaptic stimulation may lead to the neuroprotective properties of dopamine agonists (Lees, 2005). Dopamine agonist drugs are divided into 2 categories, ergoline derivatives (bromocriptine, cabergoline, lisuride and pergolide), which have severe side effects, and the non-ergoline derivatives (pramipexole, ropinirole, rotigotine, piribedil and apomorphine). The non-ergoline derivatives are well accepted first-line treatment in patients younger than 55 years (Lees, 2005; Lees *et al.*, 2009). These drugs do not cause dyskinesia when used as monotherapy. Levodopa therapy is, however, needed within 3 years of diagnosis (Pedrosa & Timmermann, 2013).

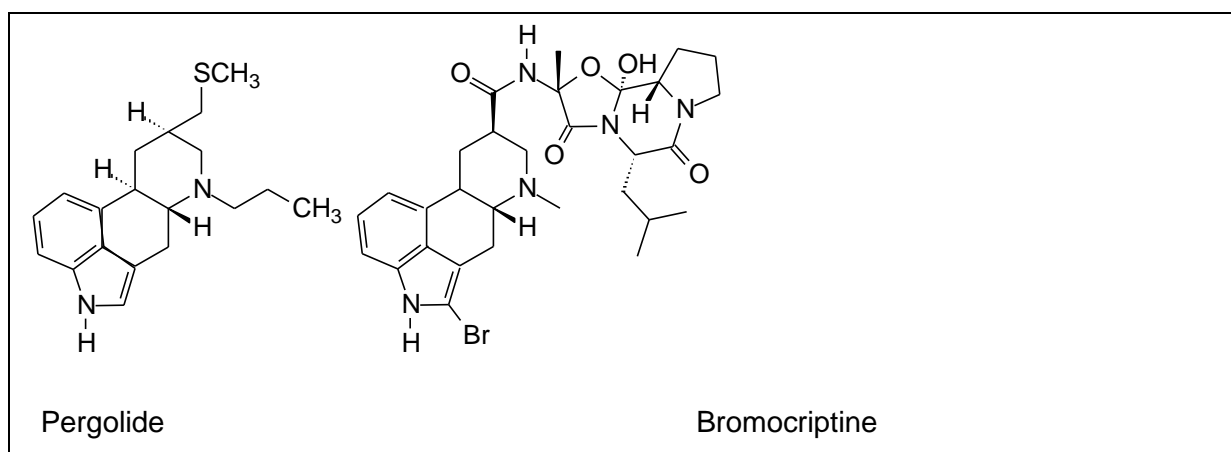


Figure 2.5 The structures of ergoline derivatives (dopamine agonist drugs).

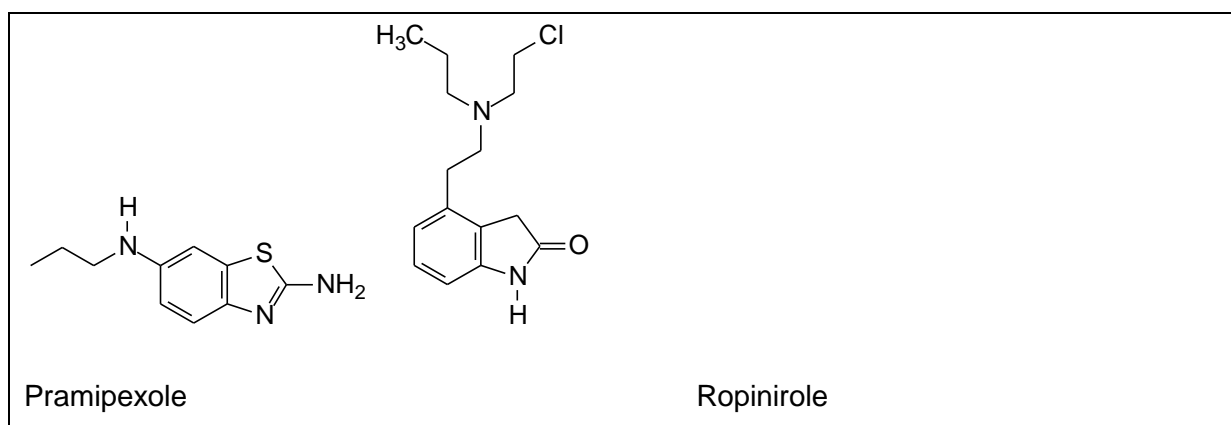


Figure 2.6 The structures of non-ergoline derivatives (dopamine agonist drugs).

Anticholinergic drugs: Anticholinergic drugs such as benztropine and trihexphenidyl, restores the imbalance between cholinergic and dopaminergic function in the brains of PD patients. Anticholinergic drugs are mainly used to treat mild early resting tremors (Lees, 2005). These

agents are often used as monotherapy for symptomatic relief or in combination with other drugs (Lees, 2005; Hardman *et al.*, 2001).

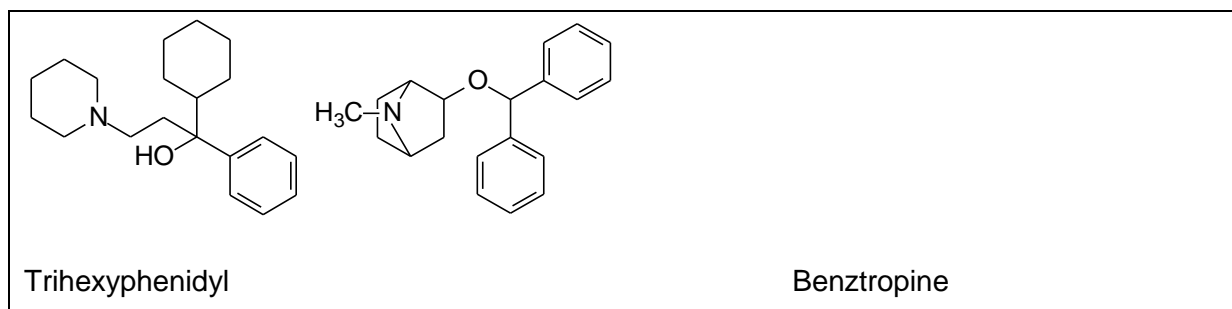


Figure 2.7 The structures of the anticholinergic drugs, trihexphenidyl and benztropine.

COMT inhibitors: Another combination therapy used in PD is that of levodopa in combination with catechol-O-methyltransferase (COMT) inhibitors. COMT inhibitors block the metabolism of levodopa and therefore allows for a reduction of the levodopa dose required for a therapeutic effect. The main benefit of this combination is that it improves motor fluctuations. The COMT inhibitors, tolcapone (which is hepatotoxic) and entacapone, improve activities of daily living and reduce the “off” time in fluctuating patients (Pedrosa & Timmermann, 2013).

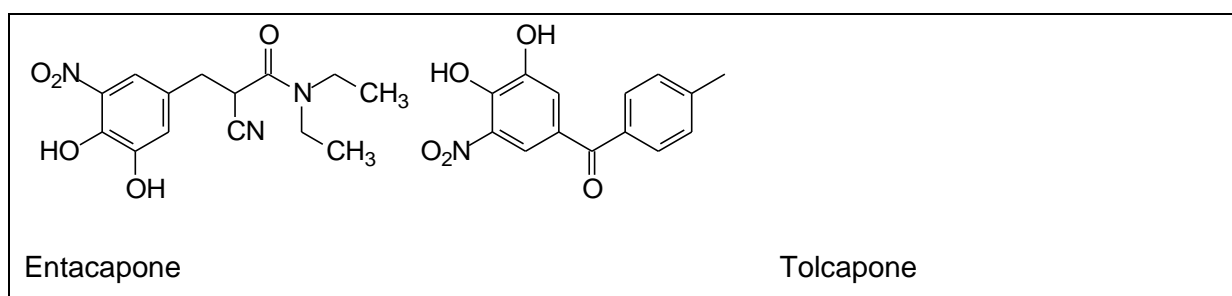


Figure 2.8 The structures of the COMT inhibitors, entacapone and tolcapone.

Anti-viral agents: Amantadine is an anti-viral drug and is used in PD as initial treatment for patients who experience muscle rigidity and tremors. Amantadine has 3 mechanisms of action that may be valuable in PD. It enhances dopamine release and block dopamine reuptake, it has mild antimuscarinic effects and it is a non-competitive inhibitor of NMDA glutamate receptors. Amantadine is well tolerated, and when combined with levodopa, it may prolong the “on” time and decrease tremors, dyskinesia and muscle fatigue (Snyder & Adler, 2007). Amantadine is used for symptomatic relief as monotherapy or in combination with other drugs such as anticholinergic drugs or dopamine agonists. The fact that it blocks NMDA glutamate

receptors suggests that amantadine may limit excitotoxic reactions due to excess glutaminergic stimulation and therefore this drug may be neuroprotective (Lees, 2005).

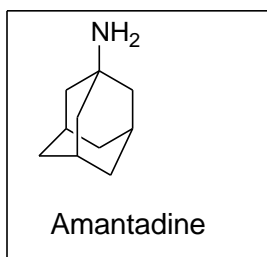


Figure 2.9 The structure of amantadine.

Adenosine A_{2A} antagonists: In the central nervous system, adenosine is an endogenous purine nucleoside, which modulates a variety of physiological processes. It acts as a homeostatic modulator by means of its post synaptic neuronal responses (Cunha, 2005). The action of striatal A_{2A} receptor antagonists could provide a new therapeutic role in the treatment of PD. A_{2A} receptor antagonists act by two mechanisms: A_{2A} receptor blockade results in a strong A_{2A} - D_2 receptor interaction which potentiates the effects of dopamine. Secondly, A_{2A} receptor blockade decreases glutamate-dependent excitation of GABAergic neurons, thus providing a neuroprotective effect. According to Schwarzschild *et al.* (2006), A_{2A} receptor antagonism reduces postsynaptic dopamine depletion, which in turn reduces the motor complications of PD. Studies showed that the combination of a reduced dose of levodopa with a xanthine-based A_{2A} antagonist, istradefylline (KW-6002), produces the same symptomatic relief as an optimal dose of levodopa as monotherapy. Another advantage of KW-6002 is that it reduces levodopa associated dyskinesia (Bara-Jimenez *et al.*, 2003; Cunha, 2005).

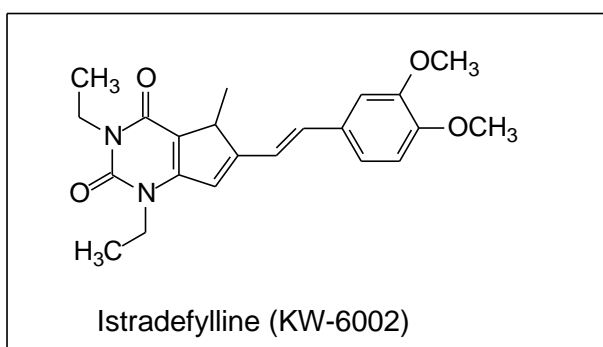


Figure 2.10 The structure of istradefylline (KW-6002).

2.2 Drugs for neuroprotection

Table 2.3 Strategies that have been used for neuroprotection in PD.

Mechanism	Targets	Drugs with possible neuroprotective properties
Oxidative stress & mitochondrial dysfunction	Electron transfer enhancers, antioxidants	Pramipexole, (<i>R</i>)-deprenyl, rasagiline, lazabemide, α -tocopherol (Vit E), co-enzyme Q10 (Co-Q10), creatine, and selenium
Apoptosis	Antiapoptotic agents	Minocycline, TCH 346, CEP-1347
Excitotoxicity	NMDA receptor antagonists	riluzole

2.2.1 MAO-B inhibitors

(*R*)-deprenyl is an irreversible MAO-B inhibitor and delays the initiation of dopaminergic treatment in PD. (*R*)-deprenyl is a propargyl amphetamine derivative, which undergoes extensive first-pass metabolism to three metabolites: desmethylselegiline, L-methamphetamine, and L-amphetamine. Patients receiving (*R*)-deprenyl are less likely to experience the "on-off phenomenon" or freezing gait and are significantly less likely to experience dyskinesia. In addition to its symptomatic effects, (*R*)-deprenyl has been shown to be neuroprotective in two studies. In MPTP treated rodents and nonhuman primates pre-treatment with (*R*)-deprenyl prevents neurodegeneration. *In vitro*, (*R*)-deprenyl reduces oxidative stress associated with MAO-B mediated dopamine metabolism, and it preserves mitochondrial integrity during oxidative stress by altering gene expressions for pro- and anti-apoptotic proteins (Fernandez & Chen, 2007).

Rasagiline, a second generation MAO-B inhibitor is a nonamphetamine derivative with no amphetamine metabolites. Rasagiline increases dopamine release, decreases dopamine catabolism and antagonises the cellular processes that are involved in apoptosis (LeWitt & Taylor, 2008). In addition to its symptomatic benefits, rasagiline was shown to be neuroprotective. Pre-treatment with rasagiline inhibits dopaminergic nigral cell degeneration in animal models of MPTP-induced Parkinsonism. The mechanism of this neuroprotective action appears to be multifactorial. Antioxidant and antiapoptotic mechanisms play a central role in this multifactorial mechanism. During mitochondrion-induced apoptosis, rasagiline prevents apoptosis by preserving the integrity of the mitochondrial membrane. A neurotoxic challenge alters mitochondrial membrane permeability to open the mitochondrial permeability

transition pore complex. Rasagiline binds to this complex and thereby prevents the induction of proapoptotic catalysts [caspase 3, glyceraldehyde-3-phosphate dehydrogenase, cytochrome C, and poly(adenosine-5'-diphosphate-ribose) polymerase]. Rasagiline also activates antiapoptotic proteins such as Bcl-2, Bcl-XL and protein kinase C. Rasagiline down-regulates proapoptotic proteins (Bad, and Bax). In addition to these neuroprotective properties, rasagiline also increases the glial cell line derived neurotrophic factor, which promotes dopaminergic neuron survival, and increases the expression of antioxidant enzymes such as superoxide dismutase, which in turn leads to the suppression of oxidative stress in dopaminergic neurons (Fernandez & Chen, 2007).

Safinamide: Safinamide is an amide derivative which combines MAO-B inhibition with dopamine reuptake inhibition. Currently in phase III development, the addition of safinamide to patients on a stable dose of dopamine agonist provided significant improvement. Compared to dopamine agonist monotherapy, safinamide addition is associated with improvements in measures of cognitive function, working memory and strategic target detection. Safinamide may represent an alternative to current therapies and will probably be used in combination with levodopa or dopamine agonists (Fernandez & Chen, 2007).

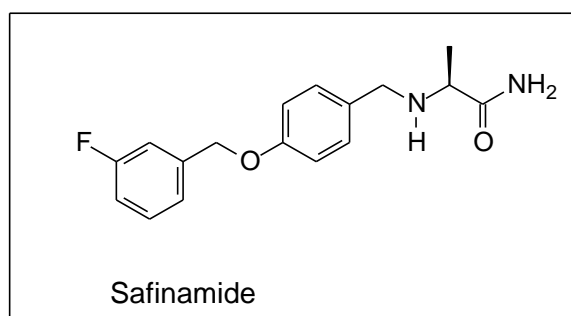


Figure 2.11 The structure of safinamide.

Lazabemide: Lazabemide is another well-known MAO-B inhibitor. Lazabemide differs from (R)-deprenyl and rasagiline in several ways. It has greater MAO-B selectivity, it is a reversible inhibitor, and it does not have a propargylamine moiety (Chen & Swope, 2007).

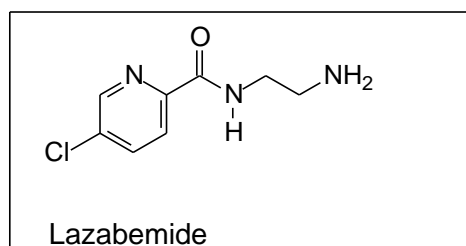


Figure 2.12 The structure of lazabemide.

2.2.2 Dopaminergic drugs

Dopamine agonist drugs not only play a role in the reduction of the symptoms of PD, but some of these drugs may display neuroprotective properties as well. These neuroprotective properties are due to the activation of D₂ and D₃ receptors, and possibly by blocking the apoptosis cascade. Dopamine agonists also suppress dopamine release and therefore reduce oxidative stress. Animal and *in vitro* studies also indicate the reduction of dopaminergic cell death as a result of dopamine agonist treatment. Pramipexole has been shown to have antioxidant activity, and is therefore relevant in neuroprotection in PD (Deleu *et al.*, 2002).

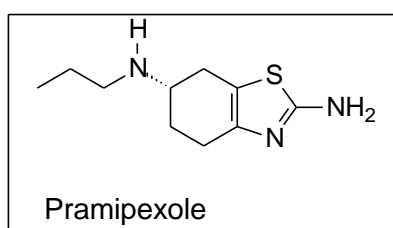


Figure 2.13 The structure of pramipexole.

2.2.3 Antioxidant drugs

Even though no conclusion as to the effectiveness of their neuroprotective properties have been made, antioxidant drugs such as α -tocopherol (vitamin E) play an important role in the defence against free radicals. In addition to their effects on mitochondrial complex 1 activity, vitamin E is a chain breaking antioxidant which acts by quenching oxyradical species. No evidence exists of vitamin E deficiency in PD, and severe deficiency states do not lead to Parkinsonism. However, this natural occurring antioxidant offers a safe and promising option for reducing oxidative stress in the pathogenesis of PD (LeWitt & Taylor, 2008).

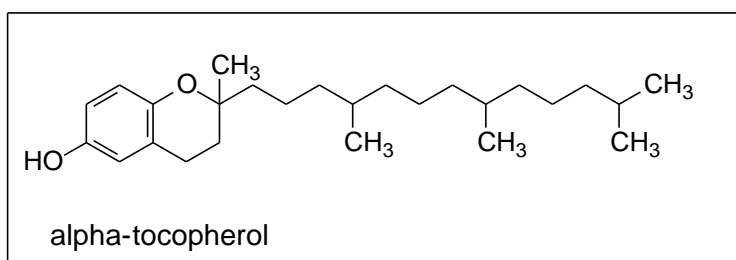


Figure 2.14 The structure of α -tocopherol.

2.2.4 Mitochondrial energy enhancers

Ubiquinone (Co-enzyme Q10) is an essential co-factor and acts as an electron acceptor for mitochondrial complex 1 of the electron transport chain. It has been shown to reduce neurodegeneration in mouse models of PD. Ubiquinone is a potent antioxidant in lipid membranes and the mitochondria. Several studies indicated the advantage of taking ubiquinone as supplement to the diet, and it is suggested that ubiquinone enhances mitochondrial electron transport and decreases the rate of PD progression (Chao *et al.*, 2012).

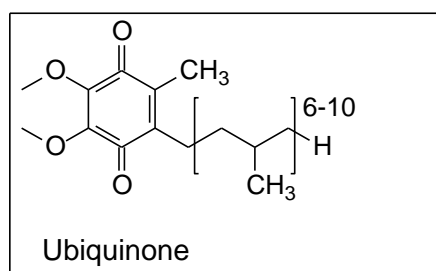


Figure 2.15 The structure of ubiquinone.

Creatine acts as a precursor for phosphocreatine, which transfer phosphoryl groups for ATP synthesis. The hypothesis is that an increase in creatine concentrations will lead to an increase of phosphocreatine formation, ultimately resulting in the decrease of oxidative stress through the stabilization of mitochondrial creatine kinase. Creatine kinase inhibit mitochondrial transition pore opening, the mechanism involved in the initiation of apoptosis. Creatine thus may lead to improved mitochondrial metabolism and a decrease in the neurodegeneration process in PD (Yacoubian & Standaert, 2009).

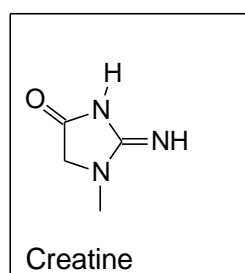


Figure 2.16 The structure of creatine.

2.2.5 Antiapoptotic drugs.

Antiapoptotic drugs such as minocycline, TCH 346 and CEP-1347 may protect against neurodegeneration in PD. Studies with neurotoxins have shown that minocycline protects against the neurodegeneration of dopaminergic neurons in the substantia nigra. Minocycline inhibits microglia activation, which plays a prominent role in neurodegeneration. In addition, minocycline acts to lessen factors that mediate apoptosis such as caspase-I. However,

preclinical results have been inconsistent for its application as a neuroprotective drug (LeWitt & Taylor, 2008).

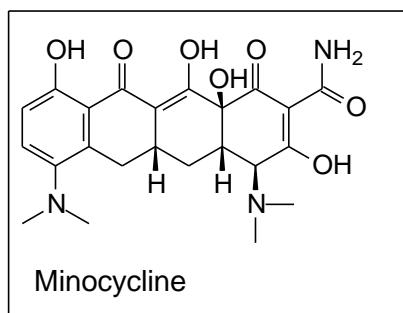


Figure 2.17 The structure of minocycline.

TCH 346 is structurally similar to (R)-deprenyl. This compound inhibits neuronal apoptosis by binding to glyceraldehyde-3-phosphate dehydrogenase. As mentioned above, apoptosis is thought to play a role in neurodegeneration. In addition to the role it plays in apoptosis, in rhesus monkeys exposed to MPTP, administration of TCH 346 provided almost near complete protection against the development of motor impairment, and histological analysis showed a sparing of the usual loss caused by MPTP in dopaminergic substantia nigra neurons and projections to the striatum (Yacoubian & Standaert, 2009).

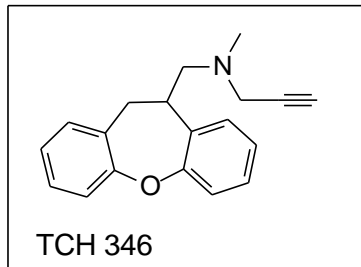


Figure 2.18 The structure of TCH 346.

The role of CEP-1347 in neuroprotection stems from its inhibition of mixed lineage kinase-3. This enzyme forms part of the transcription factor c-Jun-mediated terminal kinase signalling pathway, and is involved in apoptotic neuron death. In animal models, CEP-1347 mediated the enhanced survival of substantia nigra neurons. The ability of antiapoptotic drugs to act as neuroprotective agents have, however, not yet been established in a clinical setting (LeWitt & Taylor, 2008).

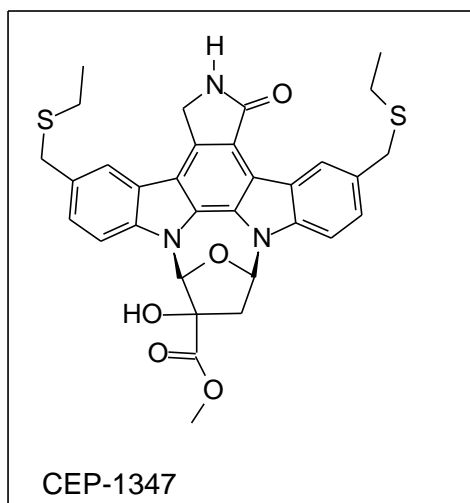


Figure 2.19 The structure of CEP-1347.

2.2.6 NMDA antagonist and antiglutaminergic drugs

Studies with experimental animals have suggested that glutamate can cause excitotoxic damage by acting on NMDA receptors. Riluzole, a NMDA antagonist, block the pre-synaptic release of glutamate and thus inhibits NMDA receptor action. Riluzole is a FDA approved drug for its effectiveness in decreasing the rate of deterioration of amyotrophic lateral sclerosis, and therefore may possess potential as a neuroprotective drug in PD (LeWitt & Taylor, 2008).

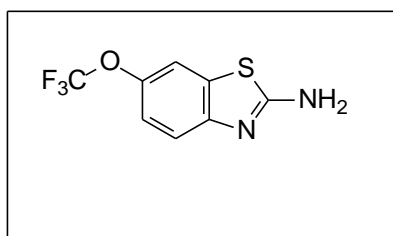


Figure 2.20 The structure of riluzole.

2.3 Monoamine oxidase

2.3.1 General background

Tyramine oxidase was discovered by Mary Hare-Bernheim in 1928, when she noticed it catalysed the oxidative deamination of tyramine. It was Hugh Blaschko who realized that tyramine oxidase, noradrenaline oxidase and aliphatic amine oxidase were in fact one enzyme, which is capable of metabolising primary, secondary and tertiary amines. The enzyme was subsequently renamed as mitochondrial monoamine oxidase (Schnaitman *et al.*,

1967). MAO is a membrane bound enzyme, and the membrane environment is an important factor to consider for enzyme activity. MAO exists as two isoforms, MAO-type A (MAO-A), and MAO-type B (MAO-B). These two isoforms are 70% identical, are encoded by different genes, have different pH optima, sensitivity to heat inactivation and have different substrate and inhibitor specificities (Youdim & Weinstock, 2004). Substrates such as dopamine, tyramine, and tryptamine are oxidised by both isoforms (Fernandez & Chen, 2007). Located in the outer mitochondrial membrane, the MAOs are flavo-proteins with flavin adenine dinucleotide (FAD) as cofactor. It was found that MAO-A is inhibited by clorgyline and its preferred substrates are noradrenalin and serotonin. MAO-A is found primarily in the intestinal tract. MAO-A metabolises catecholamines and dietary vasopressors such as tyramine and also catalyses the breakdown of neurotransmitters in the brain. MAO-B on the other hand is resistant to clorgyline inactivation and prefers benzylamine as substrate. MAO-B take part in the degradation of dopamine in the brain (Youdim *et al.*, 1988; Grimsby *et al.*, 1990). The two MAO isoforms are distributed differently in the mammalian brain, which opens up the possibility for the development of treatments based on the inhibition of MAO, especially the treatment of depression and other neuropsychiatric diseases (Youdim *et al.*, 2006). The first therapeutically used MAO inhibitor, iproniazid, has a hydrazine structure. Other non-hydrazine MAO inhibitors followed, such as tranylcypromine and pargyline. The therapeutic use of these was short lived, due to the severe side effects such as liver toxicity due to iproniazid's hydrazine structure. Unfortunately the non-hydrazine MAO inhibitors, tranylcypromine and pargyline, lead to well-known serious adverse effects, the cheese reaction and serotonin syndrome (Youdim *et al.*, 2006). Neurotransmitter concentrations in the brain play an intricate role in movement, emotion, and cognition, and thus it is associated with depression and other neurodegenerative disorders such as PD (Nagatsu, 2004).

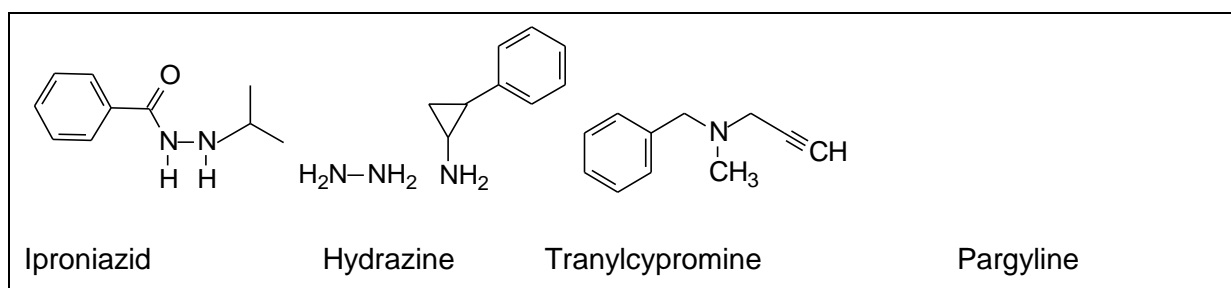


Figure 2.21 The structures of iproniazid, hydrazine, tranylcypromine, and pargyline.

2.3.2 The therapeutic role of MAO-A

Isoniazid is a drug that has been used to treat tuberculosis and was later found to act as a potent MAO inhibitor. Iproniazid, a related compound to isoniazid, became the first MAO inhibitor to treat depression successfully. Due to the severity of the adverse effects, the success and clinical use of this drug was short lived. Liver toxicity is caused by the hydrazine structure of iproniazid. This side effect was overcome by the development of non-hydrazine MAO inhibitors, however, as mentioned above these inhibitors presented with another serious side effect known as the cheese reaction (Youdim & Bakhle, 2006).

The cheese reaction occurs when tyramine and other indirect sympathomimetic amines enter the circulatory system. Normally these amines are metabolised by MAO-A in the gut and liver, which prevents them from entering the circulatory system. However, with inhibition of MAO-A, tyramine enters the circulatory system which leads to the release of noradrenaline. The consequence of noradrenaline release is severe hypertension, which may even be fatal. The cheese reaction is mostly observed with irreversible MAO-A inhibitors. The reversible MAO-A inhibitor, moclobemide, does not cause the cheese reaction because reversible inhibitors allow competition and therefore is displaced by tyramine and other dietary amines (Youdim *et al.*, 2006; Finberg & Tenne, 1982).

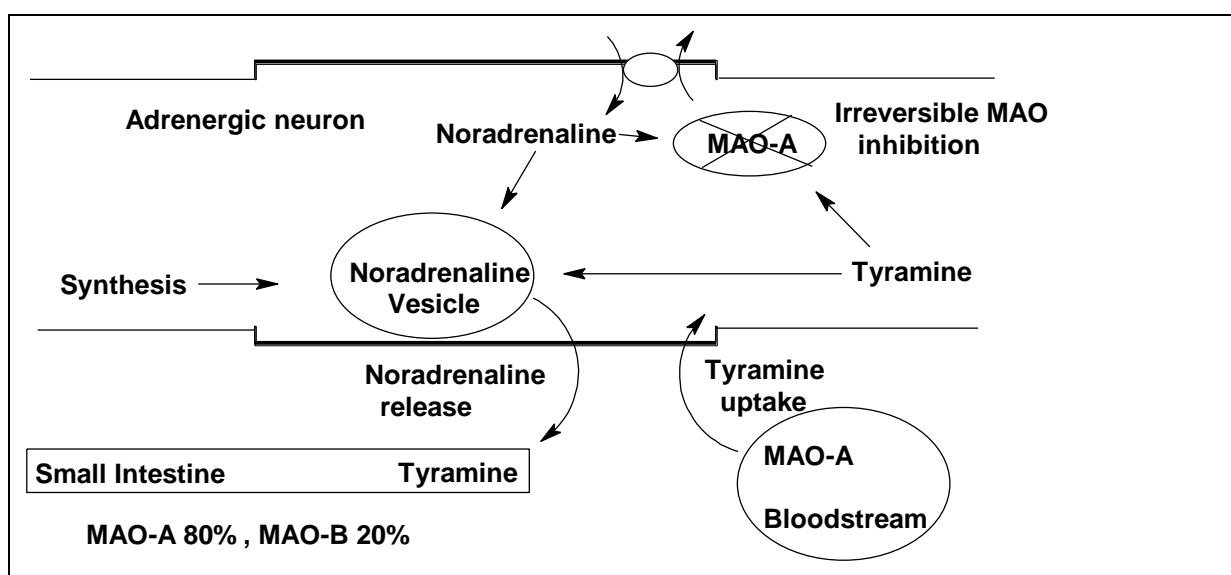


Figure 2.22 A schematic representation of the cheese reaction (Youdim & Weinstock 2004).

Serotonin syndrome is yet another severe adverse reaction of MAO-A inhibitors. This side effect is based on the fact that serotonin is metabolised by MAO-A in the brain. When a MAO-A inhibitor and tricyclic antidepressant or a selective serotonin reuptake inhibitor are used together, extensive stimulation of the postsynaptic serotonin receptors in the brain may occur.

This leads to hallucinations, increased heartbeat, increased blood pressure, elevated body temperature, nausea, vomiting and diarrhoea (Riederer & Youdim, 1986; Finberg & Tenne, 1982).

Although MAO-B inhibitors are frequently used in the therapy of PD, MAO-A inhibitors also may have a role. Non-selective irreversible inhibitors such as phenelzine, and reversible MAO-A inhibitors such as moclobemide are still used in the therapy of depression and anxiety. MAO-A inhibitors may be beneficial in PD since they alleviate the symptoms of depression and improve alertness and long-term memory in patients who experience the secondary symptoms of PD (Bonnet, 2003).

2.3.3 The therapeutic role of MAO-B

MAO-B and neurodegeneration: Dopaminergic neurons decline gradually in PD, however MAO-B levels increase with age. Fowler *et al.* (1997) has found with positron emission tomography (PET) that MAO-B density increases in the human brain with ageing. This strengthens the notion that MAO-B levels increase with neural cell death. Studies have shown that the increase of MAO-B with age is consistent with its localization within the serotonergic neurons and glial cells, and that glial cells increase in the brain with age due to neurodegeneration. Therefore MAO-B activity and density increase due to its localization in the glial cells. A further point of interest is that monoamine metabolism by MAO-B (Figure 2.23) produces toxic metabolites such as aldehydes (from dopamine metabolism) and hydrogen peroxide (in the MAO catalytic cycle) (Fowler *et al.*, 1997). Based on the above analysis it may be argued that the higher activity of MAO-B in the aged parkinsonian brain may produce increased amounts of toxic metabolites, and thus accelerate neurodegeneration.

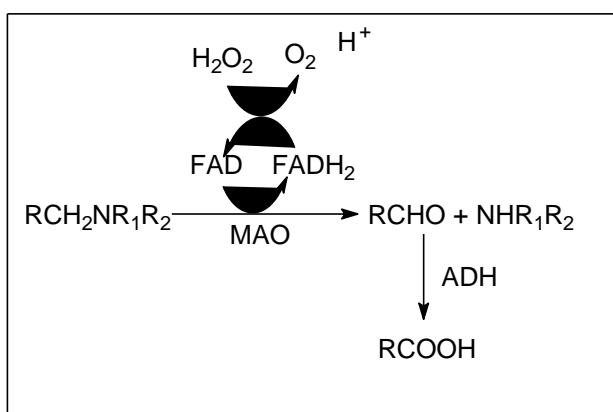


Figure 2.23 Schematic representation of the reaction pathway of MAO metabolism (Youdim & Bakhle, 2006).

The hydroxyl radical generated from hydrogen peroxide by iron in the Fenton reaction (Figure 2.25) is a highly active free radical. Proteins and DNA run the risk of damage when cellular anti-oxidants are depleted leaving them vulnerable to the hydroxyl radical. Due to the increase in brain iron and MAO-B activity, one may conclude that an increase of age will result in the increase of hydroxyl radical generation (Youdim & Bakhle, 2006). Thus, MAO-B may contribute to neurodegeneration by producing hydrogen peroxide which is converted to toxic oxygen free radicals. As already discussed, toxic oxygen free radicals and oxidative stress are integral parts of neurodegeneration in PD.

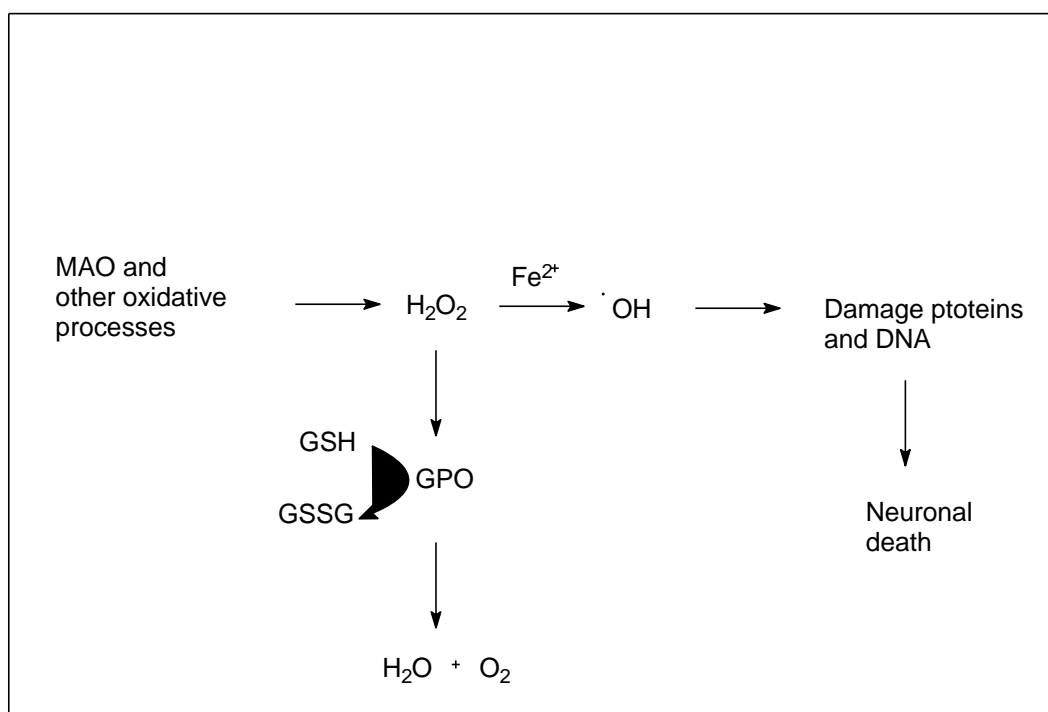


Figure 2.24 Schematic representation of neurotoxicity induced by iron and hydrogen peroxide (Youdim & Bakhle, 2006).

The other product of amine oxidation by MAO is an aldehyde. Aldehydes may become neurotoxic when they are not rapidly metabolised to yield acidic metabolites. Aldehyde dehydrogenase (ADH), an enzyme responsible for the rapid metabolism of aldehydes, may be reduced in PD. Similarly, glutathione peroxidase activity (GPO) is also affected in PD due to low GSH levels (Figure 2.24). This causes oxidative stress as a result of the accumulation of hydrogen peroxide (Riederer *et al.*, 1989).

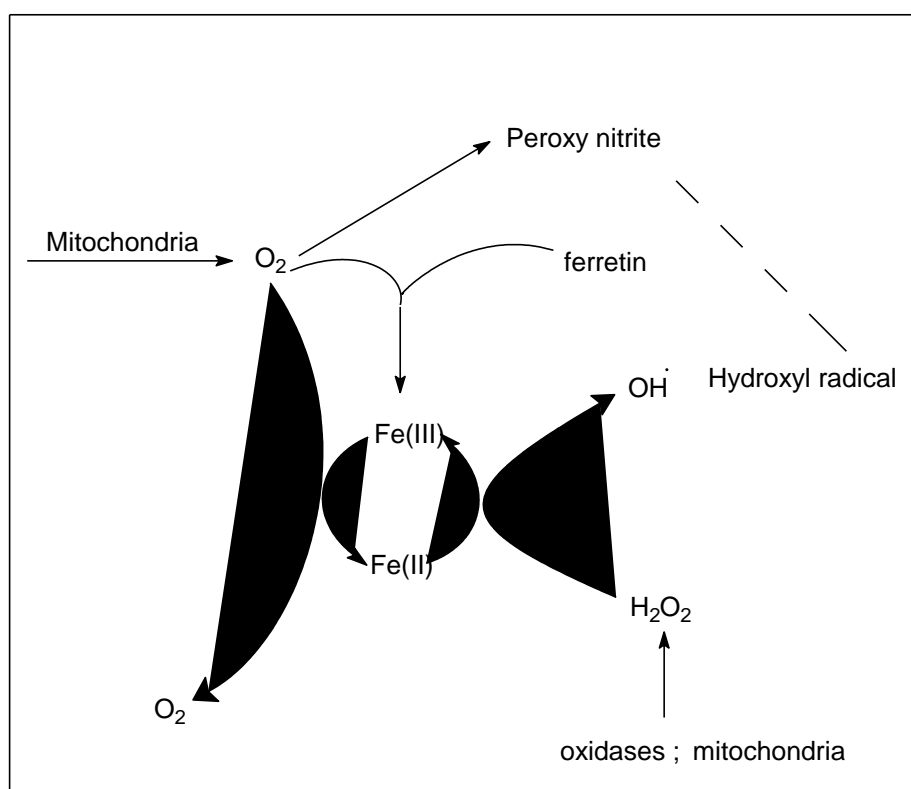


Figure 2.25 Schematic representation of the Fenton reaction(Youdim & Bakhle, 2006).

MAO-B inhibition: Inhibitors of MAO-B improve the motor symptoms of PD in several ways (Karunapuzha, 2010). MAO-B inhibitors can be used in early stage PD since they delay the need for levodopa therapy by conserving the available dopamine in the brain. In late stage PD, MAO-B inhibitors are used in conjunction with levodopa to enhance dopamine levels that are derived from levodopa therapy (Cranwell-Bruce, 2010). MAO-B inhibitors thus prevent dopamine breakdown in the brain, and subsequently decrease the amount of levodopa required for effective treatment. Dopamine is synthesised in the brain from the amino acid,

tyrosine. In this biosynthetic route, tyrosine is converted to dihydroxyphenylalanine (levodopa) by tyrosine hydroxylase (Figure 2.26). Aromatic amino acid decarboxylase metabolise levodopa to dopamine. Since MAO-B and COMT inhibitors metabolise dopamine, by inhibiting one of these or even both of these enzymes, dopamine levels in the brain will be enhanced (Pahwa *et al.*, 2006).

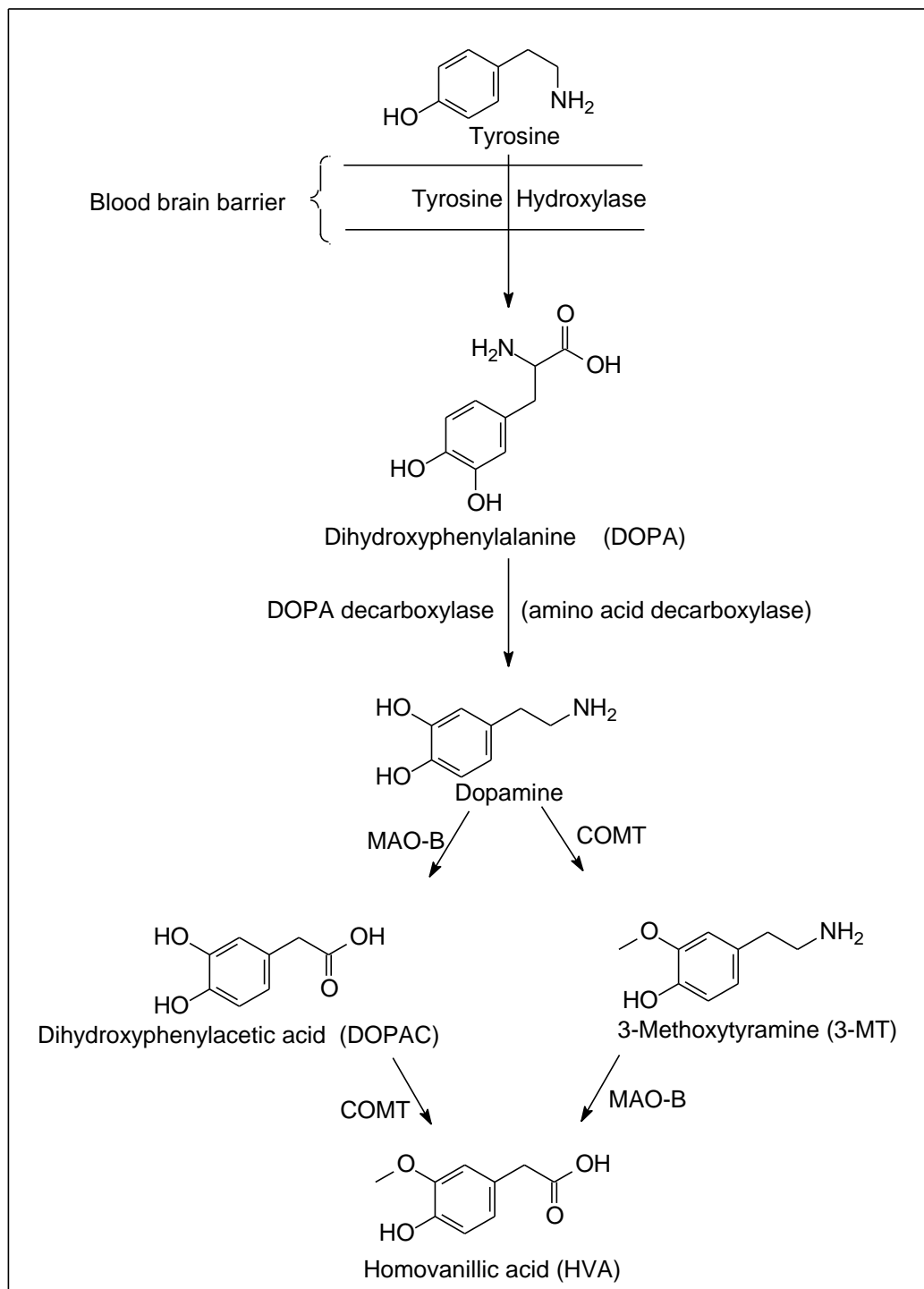


Figure 2.26 A schematic representation of dopamine metabolism (Pahwa *et al.*, 2006).

Other advantages of MAO-B inhibitors are that they may possess neuroprotective properties by limiting the formation of toxic oxygen radicals, which may be derived from the MAO catalytic cycle. The contribution of these toxic species to PD has been discussed in the previous section. MAO-B inhibitors also inhibit the oxidation of 1-methyl-4-phenyl-1,2,3,6-tetrahydropyridine (MPTP) to its toxic metabolite 1-methyl-4-phenylpyridinium MPP^+ , which suggests that MAO-B inhibitors may prevent the oxidation of other neuron damaging toxins. (R)-Deprenyl is the MAO-B inhibitor that is most commonly used in PD therapy. (R)-Deprenyl has several purposes: it blocks oxidative stress that is associated with MAO-B oxidation of dopamine, and preserve the residual dopamine in the brain. (R)-Deprenyl also enhances dopamine levels after treatment with levodopa. Treatment with (R)-deprenyl as monotherapy or in combination therapy with levodopa results in a decrease in the progression and signs of PD. (R)-Deprenyl and rasagiline, another clinically used MAO-B inhibitor, exhibits neuroprotective properties which has been linked to the propargyl moieties present in the molecular structures of these compounds (Lees, 2005; Pahwa *et al.*, 2006).

2.3.4 MAO inhibition

Iproniazid was initially developed as an anti-tuberculosis drug. Although unsuccessful as an anti-tuberculosis drug, iproniazid was shown to be a potent MAO inhibitor, a discovery which led to the first MAO inhibitor to be used for depression. The development of other hydrazine MAO derivatives, for example phenelzine, followed shortly. The therapeutic use of the hydrazine derivatives was short lived due to the severe side effects they caused, which include liver toxicity, hypertensive crisis, and severe haemorrhage. Non-hydrazine derivatives such as tranylcypromine and pargyline were developed to overcome the problems of liver toxicity, but hypertensive crisis was still associated with these drugs (Knoll, 1992; Youdim & Weinstock, 2004). A new era dawned with the development of selective MAO-B inhibitors [such as (R)-deprenyl and lazabemide] and reversible MAO-A inhibitors (such as moclobemide), which do not elicit hypertensive crisis as a result of the cheese reaction. Nowadays MAO inhibition can be categorised into two groups: reversible and irreversible MAO-A and MAO-B inhibitors, which may be further divided into selective and non-selective MAO inhibitors. Listed in table 2.4 are examples of MAO inhibitors. Reversible inhibitors bind non-covalently to the active site, causing inhibition. Enzyme activity can thus be restored by increasing substrate concentration. Irreversible inhibitors, on the other hand, firstly bind reversibly to the enzyme, where it is oxidised to yield the active inhibitor that binds covalently to the active site via the FAD co-factor.

Table 2.4 Categories and example of MAO inhibitors.

Selective reversible MAO-A	Selective reversible MAO-B	Selective irreversible MAO-A	Selective irreversible MAO-B	Non-selective irreversible MAO inhibitors
Befloxatone	Lazabemide	Clorgyline	(R)-Deprenyl	Iproniazid
Brofaromine	Safinamide		Rasagiline	Isocarboxazid
Moclobemide				Ladostigil
Toloxatone				Phenelzine
				Tranylcypromine

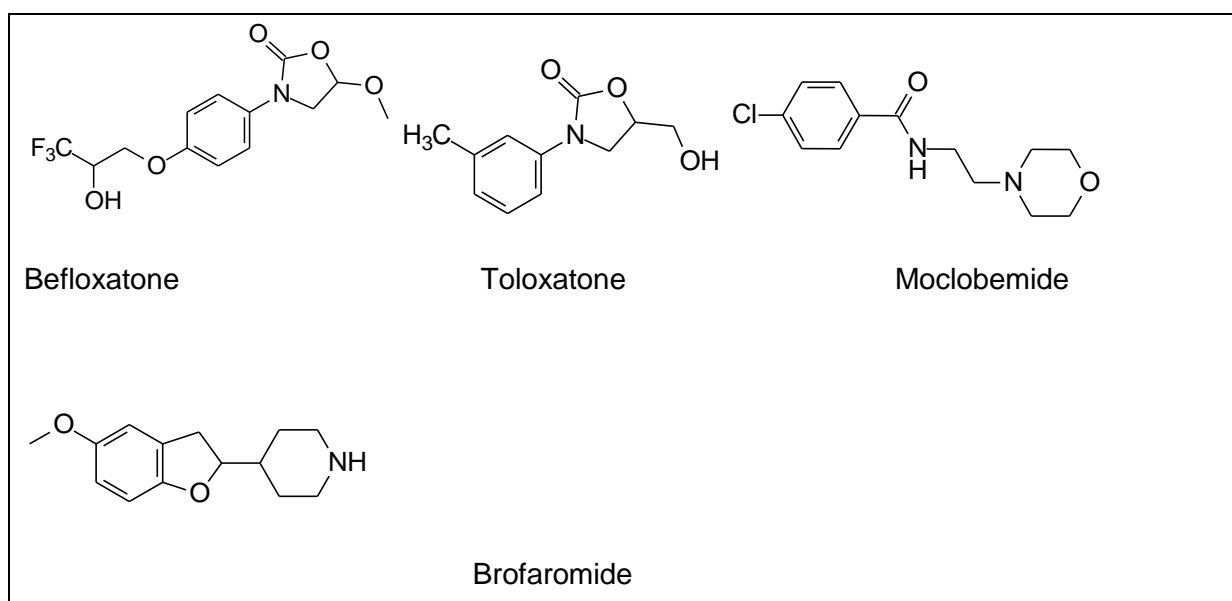
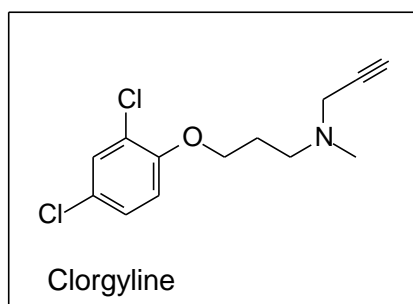
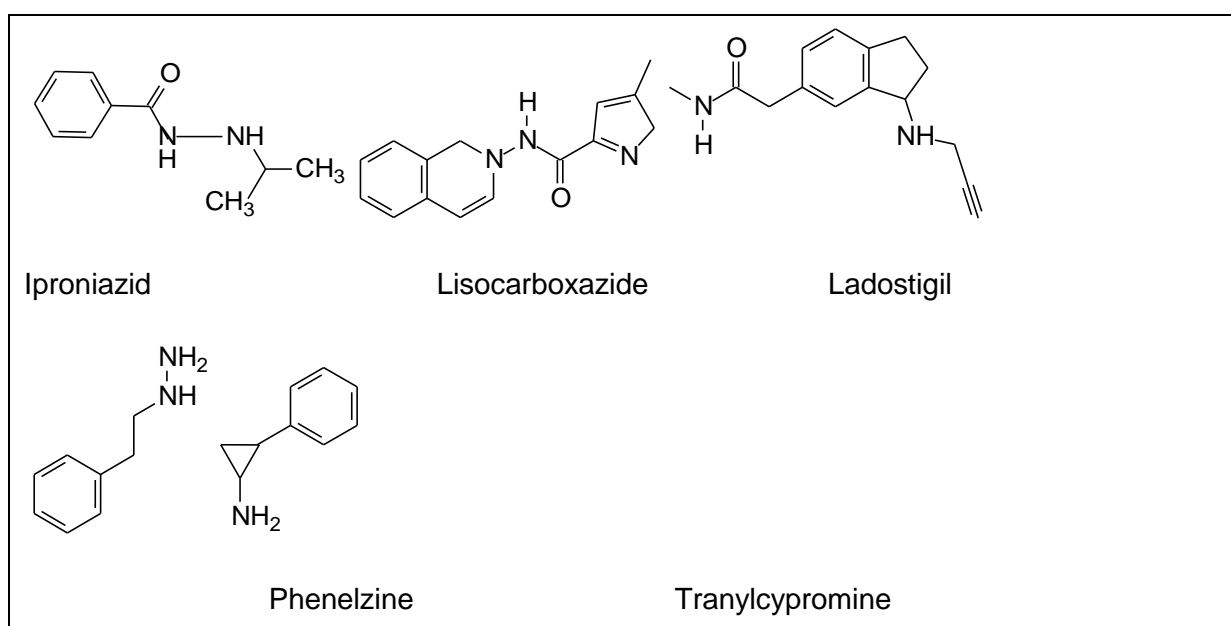


Figure 2.27 Examples of selective reversible MAO-A inhibitors.**Figure 2.28** An example of a selective irreversible MAO-A inhibitor.**Figure 2.29** Examples of non-selective MAO inhibitors.

2.3.5 The three-dimensional structure of MAO

For structural studies of the two MAO isoforms reliable expression systems have been developed. Differences and similarities are depicted in figure 2.30. The cloning and sequencing of the respective genes for these two enzymes demonstrated that MAO-A and MAO-B are two separate enzymes and share similar properties: they are 70% identical with respect to their amino acid sequences, both consist of 15 exons with identical intron-exon organization, the FAD coenzyme binds covalently to a cysteine residue in each MAO isoform, and both isoforms contain hydrophobic aromatic cages in front of the flavin co-factor, opposite the entrance cavity. Regardless of these similarities MAO-A and MAO-B have separate but overlapping biological functions. A detailed understanding of the structures and mechanisms

of both these isoenzymes is required for developing inhibitors that would exhibit a high level of specificity with little or no side effects (Edmondson *et al.*, 2004a, Edmondson *et al.*, 2004b).

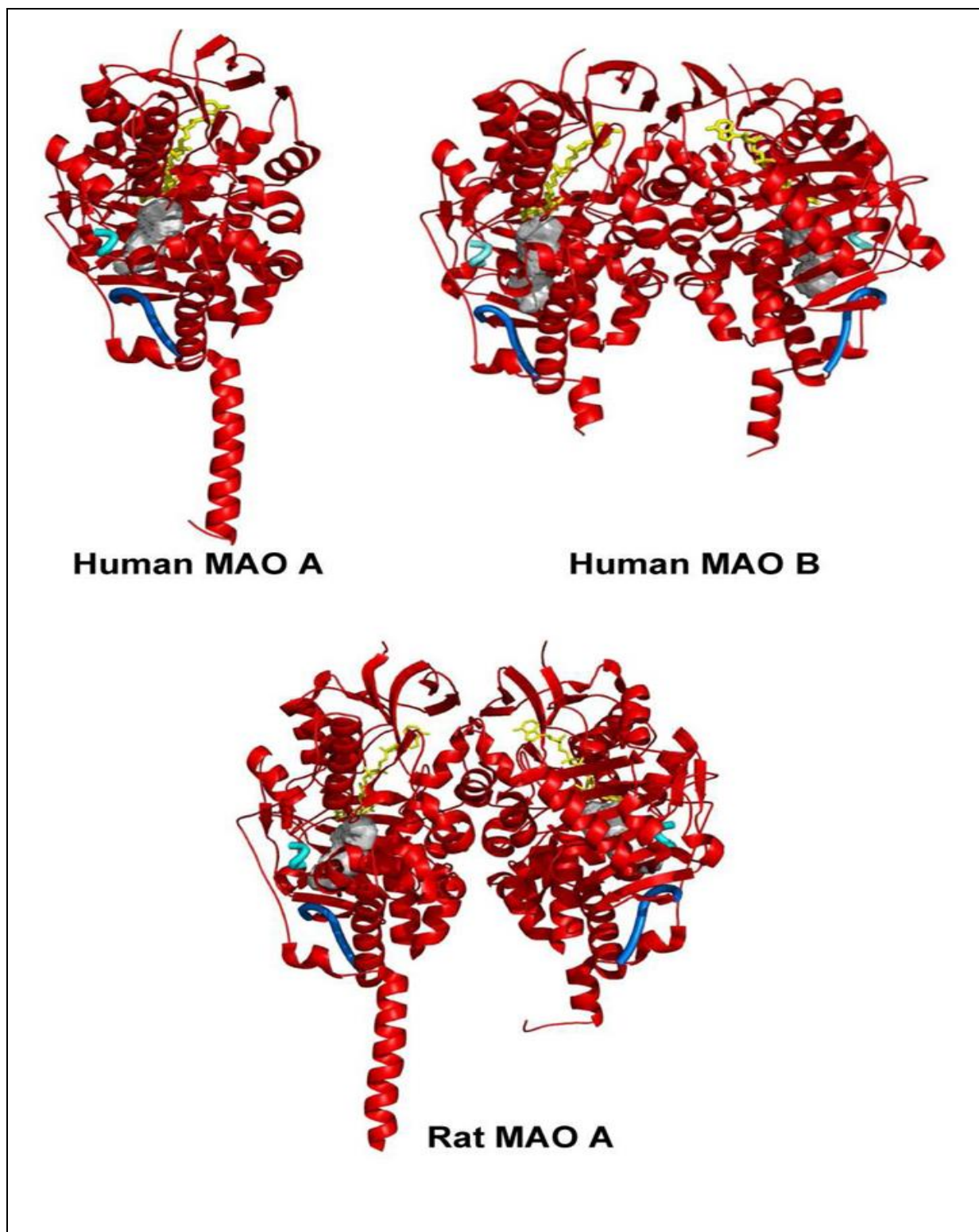


Figure 2.30 Ribbon diagram of human MAO-A, MAO-B, and rat MAO-A(Edmondson *et al.*, 2009).

2.3.5.1 The three-dimensional structure of MAO-A

Rat MAO-A crystals only diffracted to 3.2 Å resolutions, which provided a limited amount of detail about the molecular structure of its binding site. More recently human MAO-A in complex with clorgyline has been solved providing detailed information regarding the molecular structure of the active site of MAO-A (Youdim *et al.*, 2006). MAO-A consists of 527 amino acids, and contains covalently bound FAD as redox cofactor that is required for catalysis. The site of covalent attachment of the flavin to the enzyme is through a thioether linkage between a cysteinyl residue, Cys 406, and the 8 α -methylene of the FAD isoalloxazine ring, and the site of linkage is towards the C-terminal portion of the molecule. Rat MAO-A crystallises as a dimer with monomer-monomer interactions. The entire C-terminal can be elucidated from this diffraction whereas human MAO-A crystallise as a monomer. This is due to the amino-acid differences at position 151, human MAO-A possessing a lysine and rat MAO-A a glutamic acid (Edmondson *et al.*, 2007) at this position. The C-terminal region of rat MAO-A forms a transmembrane α -helix and acts as an anchor between the enzyme and the outer membrane of the mitochondria. The rest of the protein is exposed to the cytoplasm. In rat MAO-A and human MAO-A the active sites are hydrophobic cavities of 550 Å³ and 450 Å³, respectively. Together the FAD and two tyrosine residues, Tyr407 and Tyr444, form the aromatic cage, wherein the amine moieties of substrates bind (Edmondson *et al.*, 2007). In human MAO-A the shape of the substrate binding site appears to be more elongated than in rat MAO-A. For MAO-A, the residue pair Phe208/Ile335, located in the active site, appear to be major determinants in substrate/inhibitor specificity.

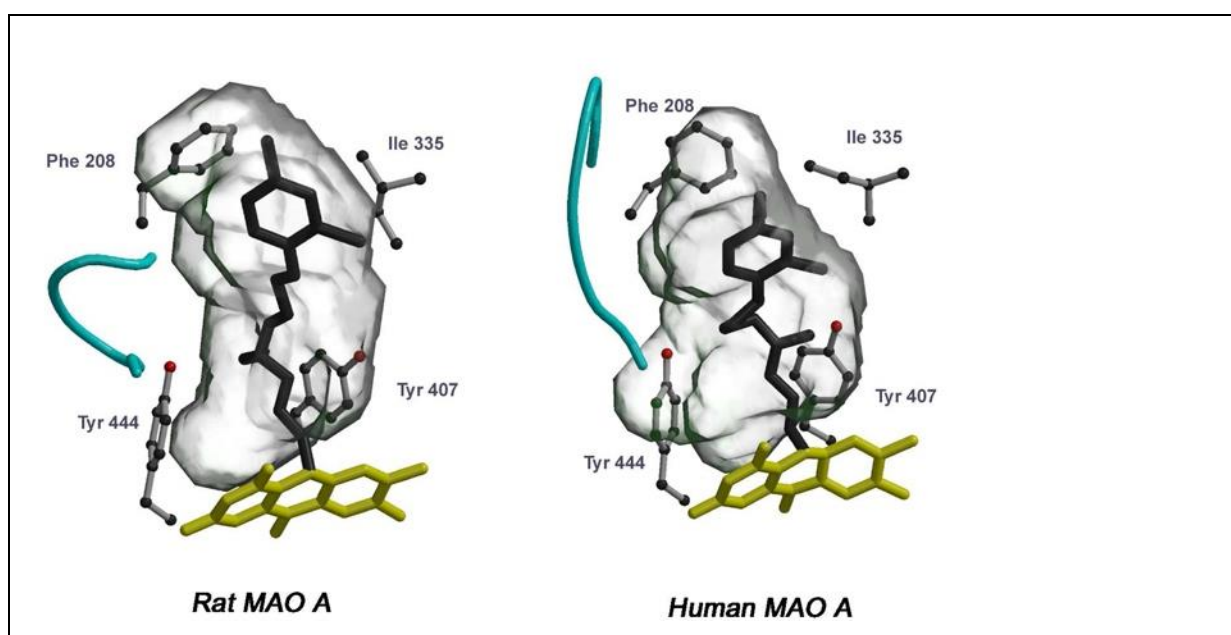


Figure 2.31 The active sites of human and rat MAO-A (Edmondson *et al.*, 2007).

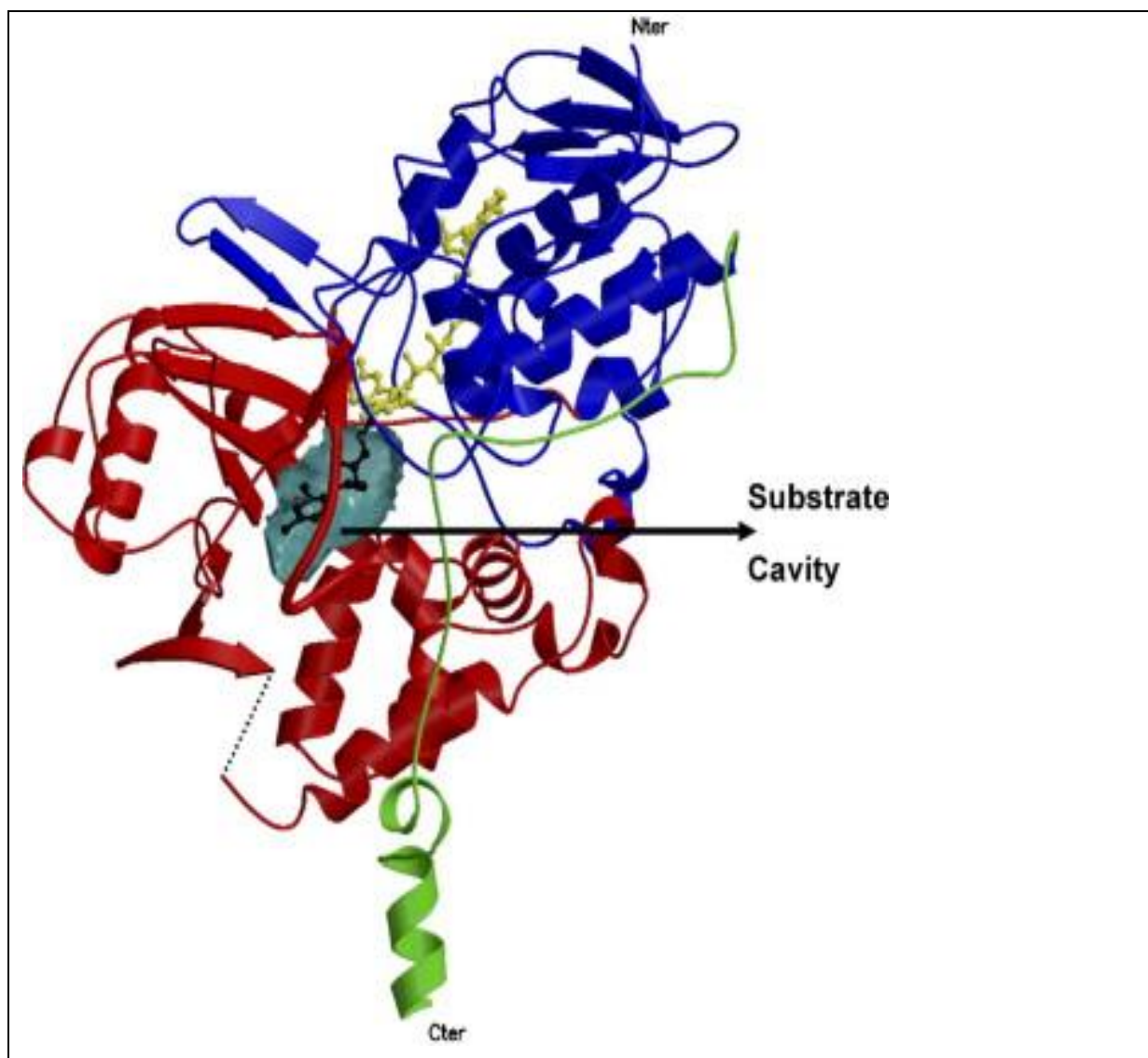


Figure 2.32 A ribbon diagram of human MAO-A (Edmondson *et al.*, 2007).

2.3.5.2 The three dimensional structure of MAO-B

For structural studies of the two MAO isoforms, reliable expression systems have been developed. In previous preparations of human MAO-B, crystals diffracted with a resolution of 3.0 Å, but with recent advances a 1.65 Å structure is now available. MAO-B consists of 520 amino acids and crystallises as a dimer with extensive monomer-monomer interactions. The C-terminal is a transmembrane α -helix and anchors the enzymes to the mitochondrial outer membrane, which leaves the rest of the protein exposed in the cytoplasm (Youdim *et al.*, 2006). The MAO-B active site is divided into a substrate and entrance cavity, with substrate entry occurring near the intersection between the enzyme and mitochondrial outer membrane. A protein loop at residues 99-112 in MAO-B covers the entrance cavity. Tyr326, Ile199, leu171 and Phe168 are located between the entrance and substrate cavities of MAO-B and act as a gating switch. Together with the FAD, two tyrosine residues, Tyr398 and Tyr435, form the

aromatic cage (Edmondson *et al.*, 2007). The substrate cavity is hydrophobic and flat with a volume of 490 Å³, which leaves less freedom of rotation for the substrate compared to MAO-A (Edmondson *et al.*, 2007). Irreversible MAO-B inhibitors bind covalently to the N(5) position of the flavin moiety between the two tyrosine residues (Tyr 398 and Tyr 435) and perpendicular to the flavin ring. A covalent thioether linkage is formed between the adjacent Cys397 and the 8α position on the flavin ring. The structure of the adduct of MAO-B with rasagiline, a selective irreversible inhibitor, and pargyline a non-selective inhibitor of MAO-B, provided new structural information. Both inhibitors form covalent N(5)-flavocyanine complexes with MAO-B. The *R*- and *S*-isomers of rasagiline bind covalently and in the same manner, but only the *R*-isomer is pharmacologically active. Interestingly for both isomers, the aminoindan rings partially extend into the entrance cavity. The Ile199 side chain acts as a gate between the entrance and substrate cavities since its side chain can exist in either an open or closed conformation (Youdim *et al.*, 2006). In bovine MAO-B and all MAO-A sequences, mutation of Ile199 to phenylalanine results in an enzyme that binds to rasagiline, and other irreversible inhibitors, but is unable to bind to the selective reversible MAO-B inhibitors such as 1,4-diphenyl-2-butene, (E)-8-(3-chlorostyryl)caffeine and farnesol. Studies indicate that these larger inhibitors occupy both the entrance and substrate cavities when bound to MAO-B, a binding mode which requires the Ile199 residue to exist in the open conformation. These structural insights are valuable in the search of selective MAO-B inhibitors that possess neuroprotective properties

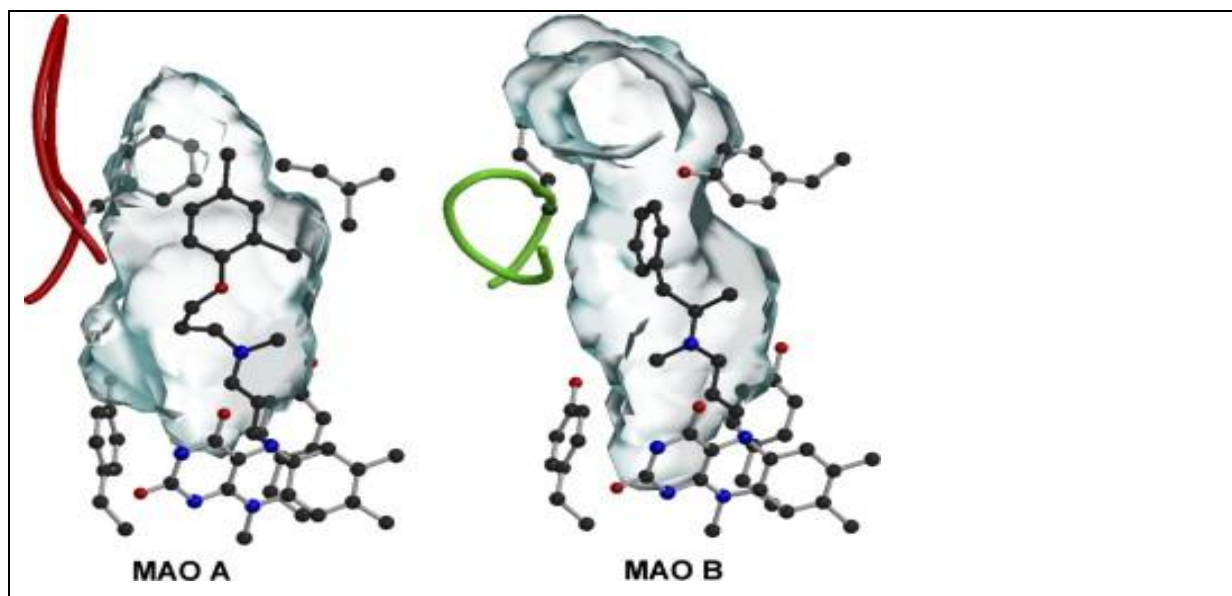


Figure 2.33 Comparison of the active site cavities of human MAO A (left) and human MAO B (right). Clorgyline is in the active site of MAO A and (R)-deprenyl is in the active site of MAO B. Both of these inhibitors form covalent N(5) flavocyanine adducts with the respective flavin co-factors (Edmondson *et al.*, 2007).

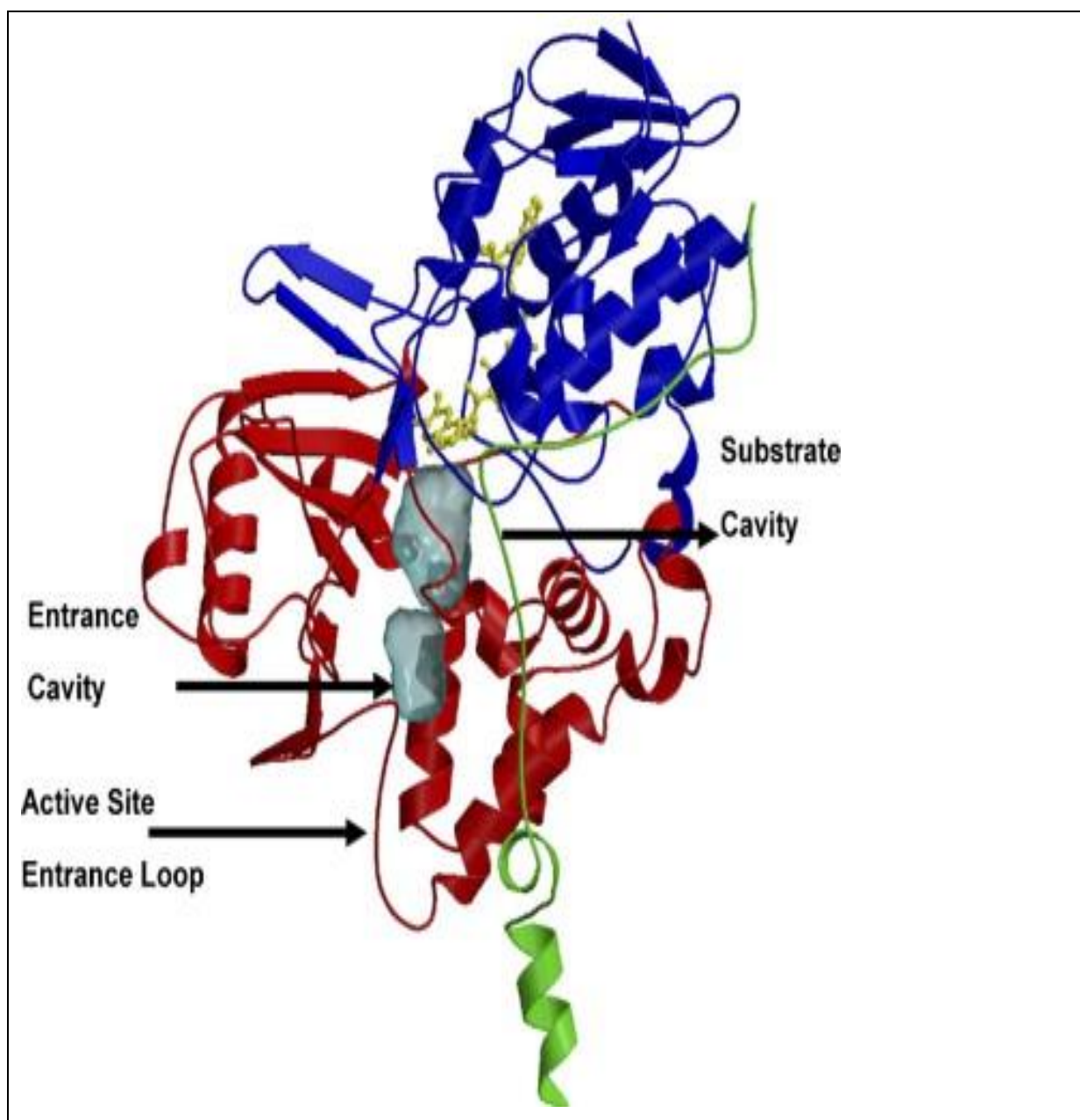


Figure 2.34 Ribbon diagram of human MAO-B (Edmondson *et al.*, 2007).

2.3.6 Mechanistic approach to MAO catalysis

Mechanism-based enzyme inactivators play a large role in the study of enzyme mechanisms and the development of innovative prospective drugs. Enzyme inactivators are custom-made substrates for specific target enzymes. Once inside the active site of the target enzyme mechanism-based inactivators change to products that inactivate the enzyme. The mechanisms by which mechanism-based inactivators function provide much information on the catalytic mechanism of the enzyme. This is especially true for the MAOs. The MAOs catalyses the oxidative deamination of various neurotransmitters to imines which, in turn, are hydrolysed to yield aldehydes. MAO-A and MAO-B both contain FAD as their only redox co-factor which is absolutely crucial for catalysis (Edmondson *et al.*, 2004). The FAD co-factor participates in this reaction that consists of three steps namely, FAD reduction, deamination, and FAD re-oxidation. Molecular oxygen is required for the re-oxidation step, which produces aldehydes and hydrogen peroxide. From the mechanism, it is evident that substrate oxidation by MAO may lead to excessive hydrogen peroxide formation. This in turn leads to oxidative stress and neural cell death.

The catalytic pathway of MAO consists firstly of a reductive half reaction, which involves cleaving of the amine C α -H bond, and a two electron transfer to the flavin to generate an imine and flavin hydroquinone. Data suggest that, for interaction with the flavin to occur, the amine substrate needs to be in a deprotonated form. The deprotonated amine moiety on the substrate bind to the active site of the MAO enzyme where it is oxidised to a protonated imine and the FAD co-factor is reduced to its hydroquinone form. An oxidised flavin and hydrogen peroxide is produced when the reduced FAD co-factor reacts with molecular O₂. The enzyme releases the protonated imine, where it undergoes a noncatalysed hydrolysis to generate NH₄⁺ and the corresponding aldehyde (Figure 2.35) (Edmondson *et al.*, 2007).

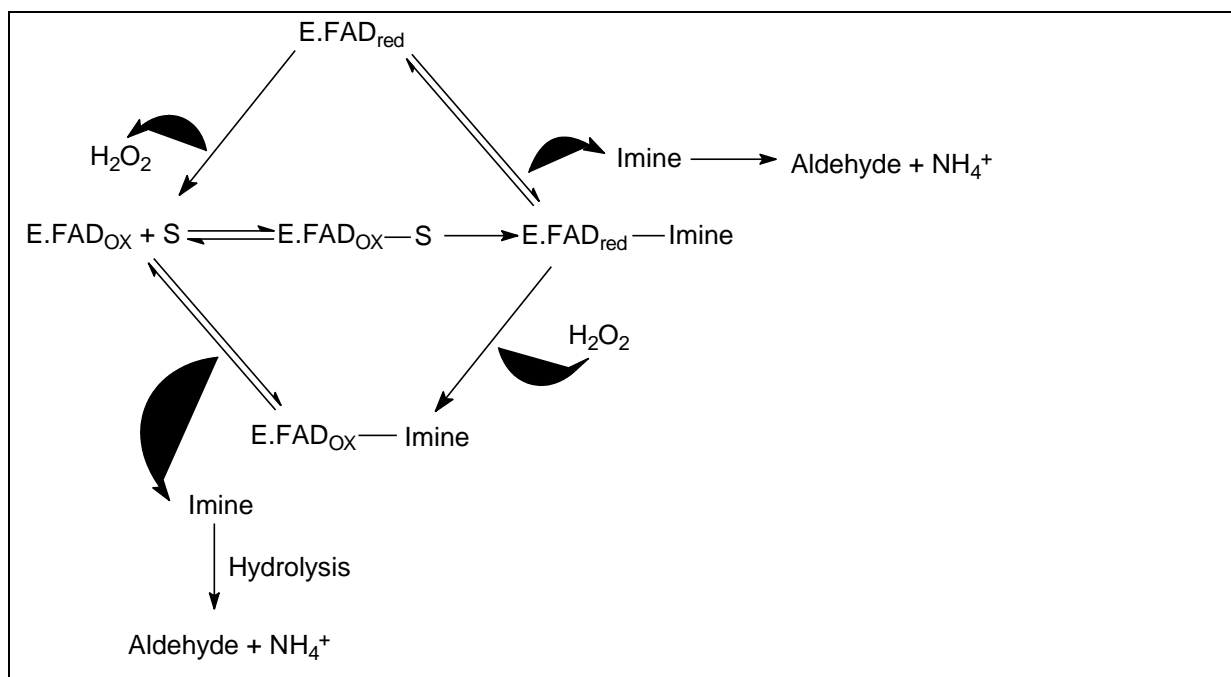


Figure 2.35 Schematic representation of the catalytic pathway of MAO (Edmondson *et al.*, 2007).

The mechanisms of enzyme catalysed oxidation can be described by the single electron transfer (SET) pathway and by the polar nucleophilic pathway. Silverman (1980) proposed that the mechanism for MAO catalysed α -carbon oxidation of amines proceeds with a single SET step, from the lone pair electrons on the nitrogen of the amine substrate to an oxidised flavin, resulting in the formation of an amine radical and the flavin semiquinone. Deprotonation of the α -carbon produces an α -amino radical, which proceeds with a second SET step to the semiquinone producing an iminium ion and a reduced flavin.

Evidence against the SET pathway lies in the fact that spectral data failed to observe any intermediates such as flavin semiquinones or amine radicals during MAO-B flavin reduction. Also energy calculations proved that the SET transfer of the lone pair electrons of the amine to the flavin semiquinone radical is unfavourable (Yu, 1998).

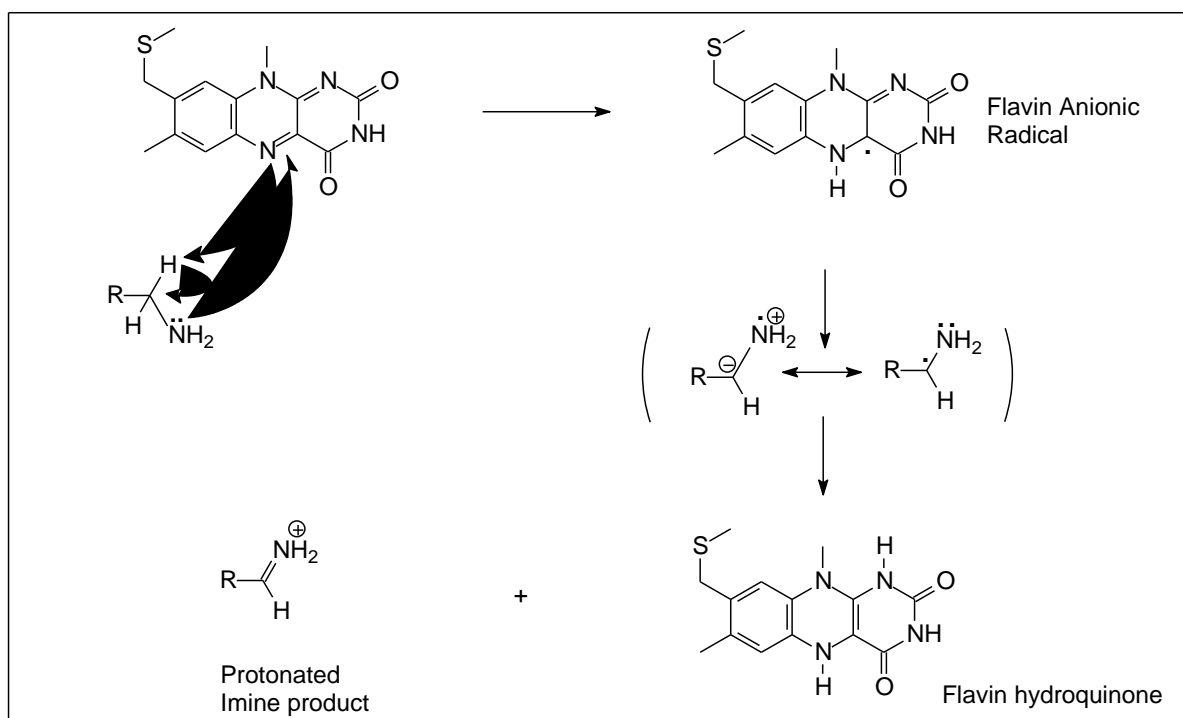


Figure 2.36 A representation of the SET mechanism of MAO catalysis(Edmondson *et al.*, 2004).

The proposed polar nucleophilic pathway is based, in part, on chemical model studies of the reactions of primary and secondary amines with flavin derivatives. These models show that, under certain conditions, benzylamine is reduced to benzaldehyde in the presence of 3-methylflavin. These models also show that primary amines and hydrazines undergo oxidation by the nucleophilic pathway in the presence of 3-methyl-5-ethylflavinium perchlorate. During the polar nucleophilic pathway the amine substrate forms an adduct with FAD. Cleavage of the adduct produces the iminium metabolite and FADH₂ (Yu, 1998). The proposed polar nucleophilic mechanism occurs with the abstraction of a proton from the pro-R α -CH. For abstraction to take place, the flavin must be activated to become a strong base. The initial step in catalysis via the polar nucleophilic mechanism proceeds where the deprotonated amine facilitates a nucleophilic attack to the flavin on the C4 position, resulting in the formation of flavin C4 nucleophilic adducts. Due to the formation of the flavin C4 adducts the N-5 position of the flavin becomes a strong base with enough basicity to abstract the α -pro-R proton from the substrate (Edmondson *et al.*, 2004).

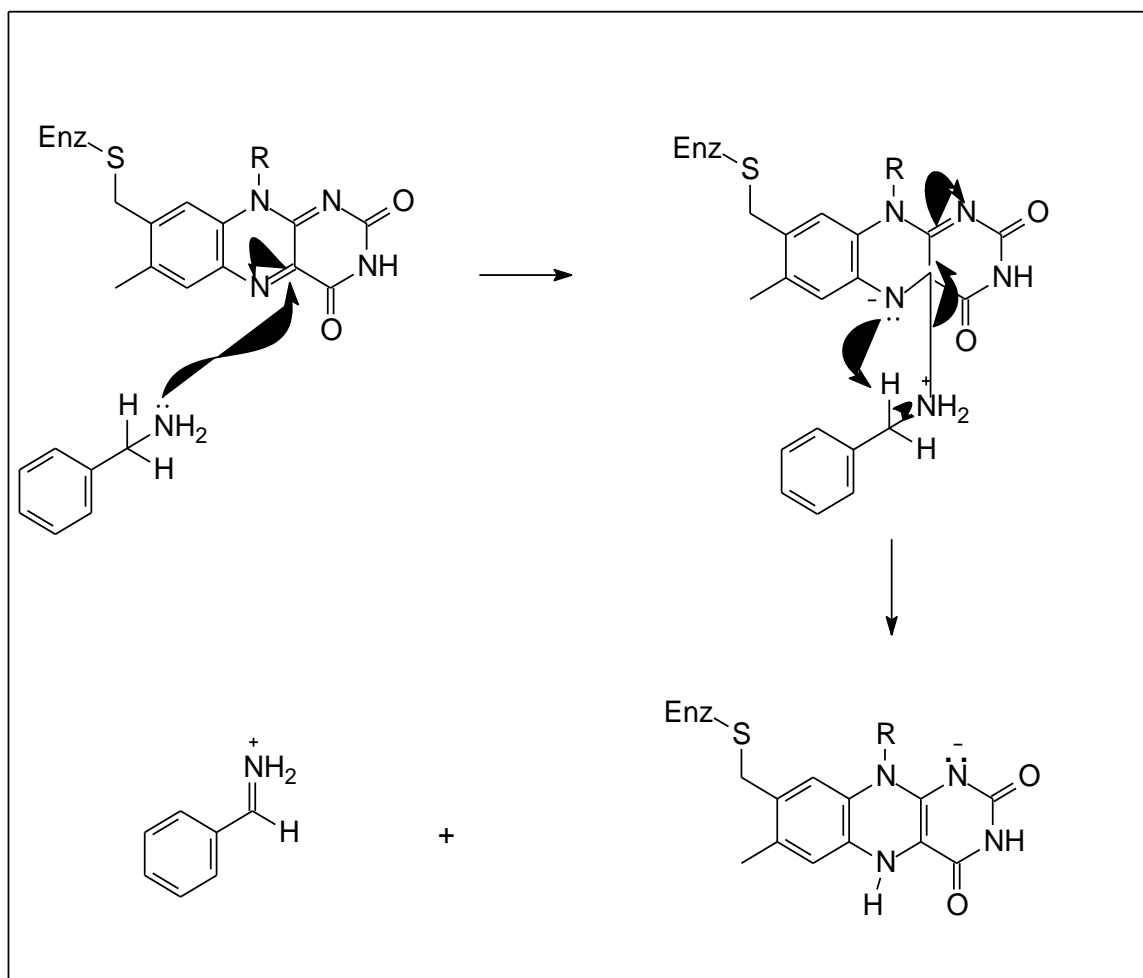


Figure 2.37 A representation of the polar nucleophilic mechanism of MAO catalysis (Edmondson *et al.*, 2004).

2.4 Animal models of Parkinson's disease

2.4.1 MPTP models

In 1982 Dr. Langston and colleagues were the first to propose that MPTP causes a parkinsonian syndrome, when they treated a handful of drug addicts injected with a synthetic version of mepiridine that was contaminated by its by-product, MPTP. These patients developed bradykinesia which were successfully treated with levodopa. Since then this neurotoxin has been used extensively to produce models of PD (Hisahara & Shimohama, 2010).

As mentioned above, MPTP was first identified as a strong neurotoxin when heroin addicts administered MPTP by mistake and developed an acute form of Parkinsonism. The tragic outcome of MPTP poisoning in the heroin addicts led to the development of MPTP rodent and

primate animal models. A neuropathological study of MPTP-induced Parkinsonism revealed neuronal degeneration in the SN and the absence of Lewy bodies. Primates exposed to MPTP responded well to therapy with levodopa and dopamine receptor agonists. Rats and mice on the other hand, were relatively insensitive to MPTP neurotoxicity. In these animals, neurodegeneration occur only at high doses (Hisahara & Shimohama, 2010).

MPTP metabolism consists of a multi-step process (Fig 2.38). MPTP is highly lipophilic, which allows it to cross the blood-brain barrier. MAO-B metabolise MPTP in the brain to yield 1-methyl-4-phenyl-2,3-dihydropyridinium (MPDP⁺). Once in this form, it is oxidised to yield 1-methyl-4-phenylpyridium (MPP⁺), the active toxic compound. MPP⁺ is taken up by the dopamine transporter system into dopaminergic cells. Once in the dopaminergic cells, MPP⁺ can follow various routes: i) bind to vesicular monoamine transporter (VMAT), ii) concentrate by an active process within the mitochondria and iii) remain in the cytosol and interact with cytosolic enzymes. When concentrated by an active process in the mitochondria, MPP⁺ inhibits complex 1 of the electron transport chain and thus inhibits mitochondrial respiration, which subsequently leads to a decrease of ATP formation. Inhibition of complex 1 also causes the production of toxic oxygen species, which may lead to neuronal cell death. MPP⁺ also may cause the up-regulation of TNF α , interleukin-1 β and interleukin-6, which in turn cause the up-regulation of inducible nitric oxide synthase (i-NOS). i-NOS produces large amounts of uncharged nitric oxide (NO), which can move freely through membranes. Neurons in the direct vicinity of NO molecules are at risk for possible attack by glial-derived reactive nitrogen related species (Jalkanen & Salmi, 2001).

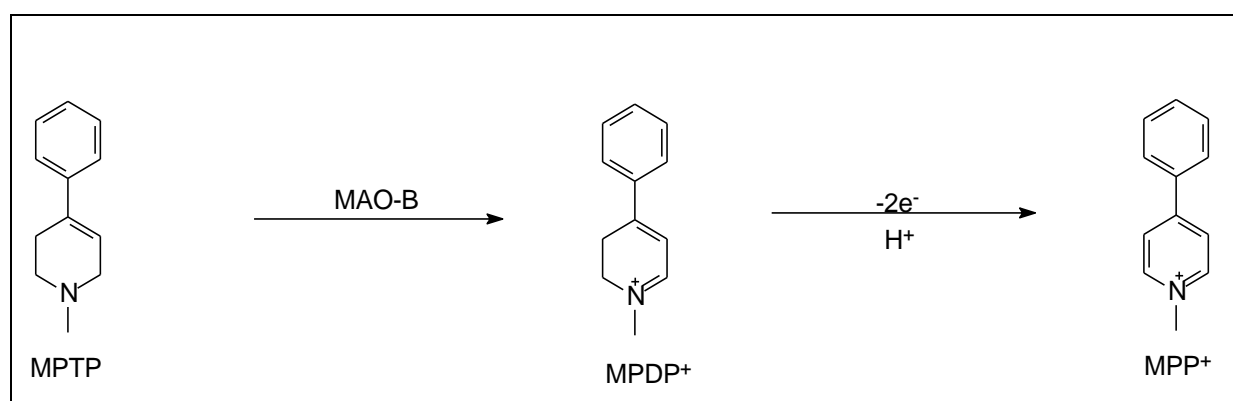


Figure 2.38 Schematic representation of MAO-B catalysed oxidation of MPTP to MPDP⁺ and MPP⁺ (pyridinium metabolite) (Yu, 1998).

2.4.2 6-Hydroxydopamine (6-OHDA).

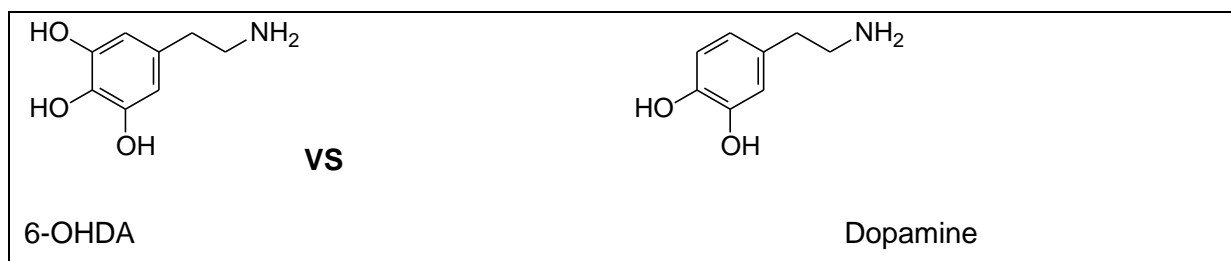


Figure 2.39 Structure comparison between 6-OHDA and dopamine (Bove' *et al.*, 2005).

Similar to MPTP, 6-OHDA also is a neurotoxin that has been used to produce animal models of PD. Classified as a catecholaminergic neurotoxin with similar structure to noradrenaline and dopamine, 6-OHDA cannot cross the blood-brain barrier. However, 6-OHDA has a high affinity for several catecholaminergic plasma membrane transporters such as DAT and norepinephrine transporters. Intrastriatal injection of 6-OHDA cause retrograde neuronal degeneration in the SN and ventral tegmental complex. 6-OHDA causes dopaminergic neuron death, while non-dopaminergic neurons are preserved. Interestingly, Lewy bodies are not observed with 6-OHDA treatment. The pathological mechanism by which 6-OHDA causes neuronal death includes the effects of ROS and quinones. In an aerobic medium 6-OHDA is oxidised to yield hydrogen peroxide and para-quinone(Bove' *et al.*, 2005).The toxicity associated with 6-OHDA is thus due to oxidative stress (Figure 2.40).

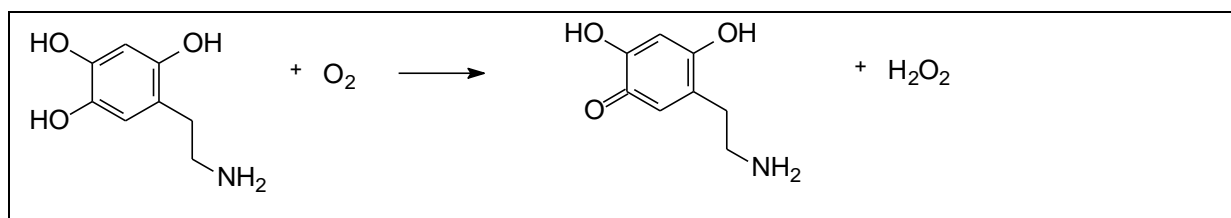


Figure 2.40 The oxidation reaction of 6-OHDA (Bove' *et al.*, 2005).

2.4.3 Rotenone

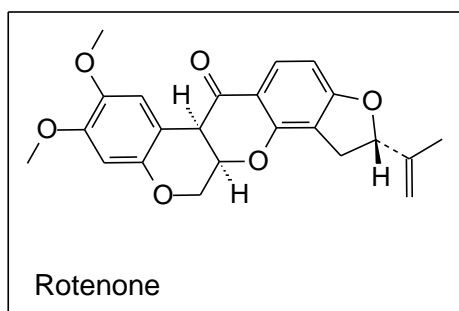


Figure 2.41 The structure of rotenone.

Derived from the roots of *Lanchocarpus* species, rotenone is a naturally occurring complex ketone pesticide. It is a strong complex I inhibitor and crosses cellular membranes and the blood-brain barrier without the aid of transporters. Chronic systemic exposure to rotenone causes many features of PD, including nigrostriatal dopaminergic degeneration. Betarbet *et al.* (2002) showed that the pathological features seen in rotenone toxicity match those of PD. They observed intracellular inclusions in the degenerating neurons that are morphological similar to Lewy bodies. These intracellular inclusions display the same characteristics of true Lewy bodies. For example, they show immuno reactivity for α -synuclein and ubiquitin. In addition rotenone administration to animals produces all the behavioural and pathological features seen in PD (Hisahara & Shimohama, 2010).

2.4.4 Paraquat and maneb

Exposure to 1,1'-dimethyl-4,4'-bipyridinium (paraquat), a herbicide, has been suggested as a possible risk factor for PD, due to the structural similarity with MPP⁺. Paraquat's toxicity is mediated by redox cycling with a cellular diaphorase such as nitric oxide synthase. This results in the generation of ROS. The mechanism of the redox-cycling reaction is depicted in figure 2.42.

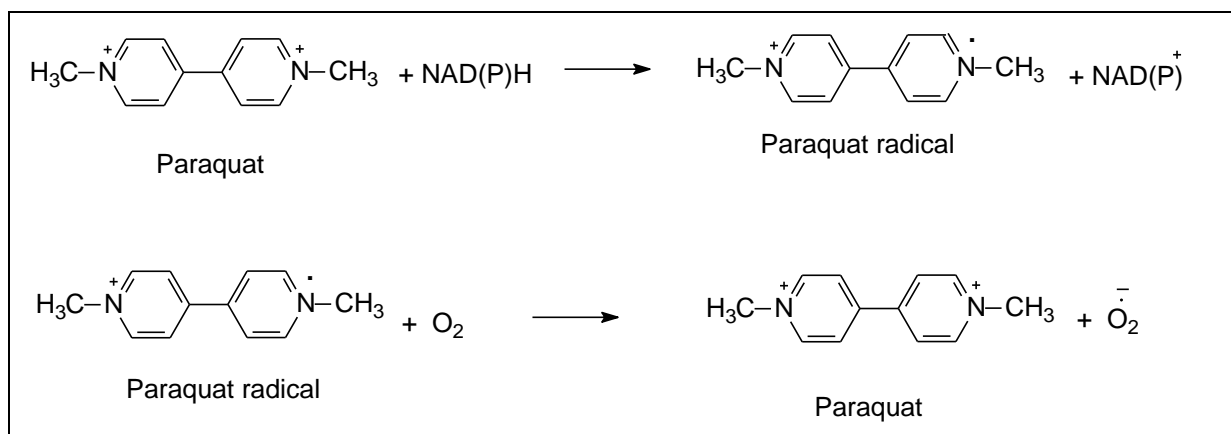


Figure 2.42 Schematic representation of the redox-cycling reaction of paraquat (Bove' *et al.*, 2005).

In animal models, systemic administration of paraquat leads to a decrease in substantia nigra dopaminergic neurons, decrease in striatal dopamine nerve terminal density, and neurobehavioral syndrome characterised by reduced motor activity. Like MPP⁺, paraquat crosses the blood-brain barrier and damages the dopaminergic neurons in the SN. Prolonged exposure causes α-synuclein-like aggregate formation in the substantia nigra.

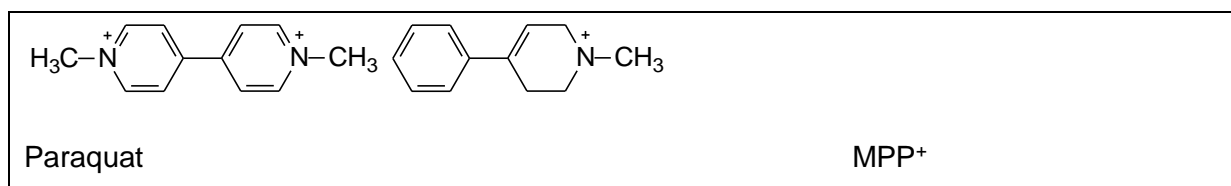


Figure 2.43 Structure similarities between paraquat and MPP⁺(Hisahara & Shimohama, 2010).

Manganese ethylenebis(dithiocarbamate) (Maneb) is a organomanganese fungicide used in agriculture and is a putative causative agent for PD. Studies have found that the neurotoxic effect of paraquat on the nigrostriatal dopaminergic system in mice is synergistically potentiated by Maneb. When Maneb is directly administered to the lateral ventricles, it causes selective dopaminergic neurodegeneration. The mechanism of toxicity possibly involves the inhibition of mitochondrial complex III (Hisahara & Shimohama, 2010).

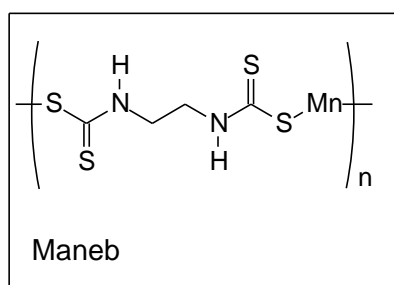


Figure 2.44 The structure of Maneb.

2.5 The measurement of MAO activity

2.5.1 Background

The determination of MAO activity is performed for the purpose of identification of novel endogenous and exogenous substances that behave as substrates or inhibitors of MAO. As shown in figure 2.45, for most MAO substrates the first step in the oxidative deamination reaction is the conversion of the amine substrate into the imine, which is then hydrolysed to form an aldehyde and ammonia. Due to the reoxidation of the FAD co-factor hydrogen peroxide is formed as by-product. The aldehyde product may be further metabolised forming an acid or alcohol. Thus, the activity of MAO can be measured through the disappearance of the amine substrate, oxygen consumption, and aldehyde, ammonia and hydrogen peroxide formation.

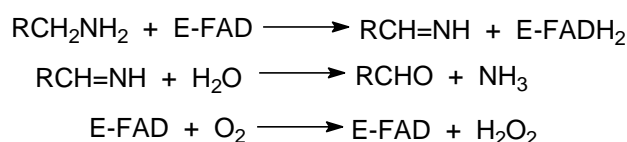


Figure 2.45 The generalized reaction of oxidative deamination catalysed by MAO (Yu.,1998).

Numerous methods have been developed to determine MAO activity and are based on measuring the disappearance of the reagent species, or the formation of the reaction products. The methods that have been used to measure MAO activity include radiometric, fluorometric, spectrophotometric, polarographic, chromatographic and luminometric assays (Nicotra & Parvez, 1999).

2.5.2 Radiometric assay

When ^{14}C -labelled substrates (dopamine and tyramine) are used, the labelled products of the enzymatic degradation may be separated by high performance liquid chromatography (HPLC) and measured by using a radiochemical detector. Due to its sensitivity and specificity, this is a very accurate method (Nicotra & Parvez, 1999). Under certain conditions, the labelled products may also be separated from the substrates by extraction, and may subsequently be counted with a scintillation counter.

2.5.3 Luminometric assay

A useful approach to determine MAO activity is to measure the hydrogen peroxide that is produced by MAO activity. Light is produced during the oxidation of 5-amino-2,3-dihydro-1,4-phthalazinedione in the presence of hydrogen peroxide and peroxidase (POD). The quantity of light produced is used to determine the quantity of hydrogen peroxide produced by MAO activity. Advantages of this method are that a wider range of substrates can be used. Disadvantages are that this approach is time-consuming and not applicable to all substrates, among these are 5-hydroxytryptamine, adrenaline and noradrenalin (Nicotra & Parvez, 1999).

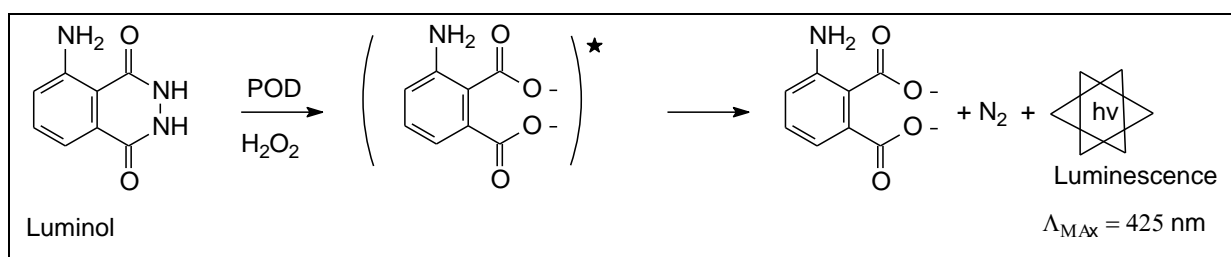


Figure 2.46 Schematic representation of the oxidation of 5-amino-2,3-dihydro-1,4-phthalazinedione in the presence of hydrogen peroxide (Nicotra & Parvez, 1999).

2.5.4 Fluorometric assay

Another approach to determine MAO activity is to measure hydrogen peroxide in a horseradish peroxidase (HRP) coupled reaction. This is a one-step indirect method which allows endpoint measurement and kinetic experiments. Amplex red (N-acetyl-3,7-dihydroxyphenoxazine) is used as fluorogenic substrate for hydrogen peroxide. In the presence of hydrogen peroxide, horseradish peroxidase catalyses the oxidation of amplex red to produce a highly fluorescent product, resorufin. Resorufin is characterised by good stability and high extinction coefficient ($54,000 \text{ cm}^{-1} \cdot \text{M}^{-1}$). Resorufin has an excitation and emission maximum at 560 nm and 590 nm, respectively. Advantages of this method are that it is 5-20-fold more sensitive than the current

spectrophotometric assays, requires a small sample size and can analyse numerous samples can be analysed at the same time (Nicotra & Parvez, 1999)

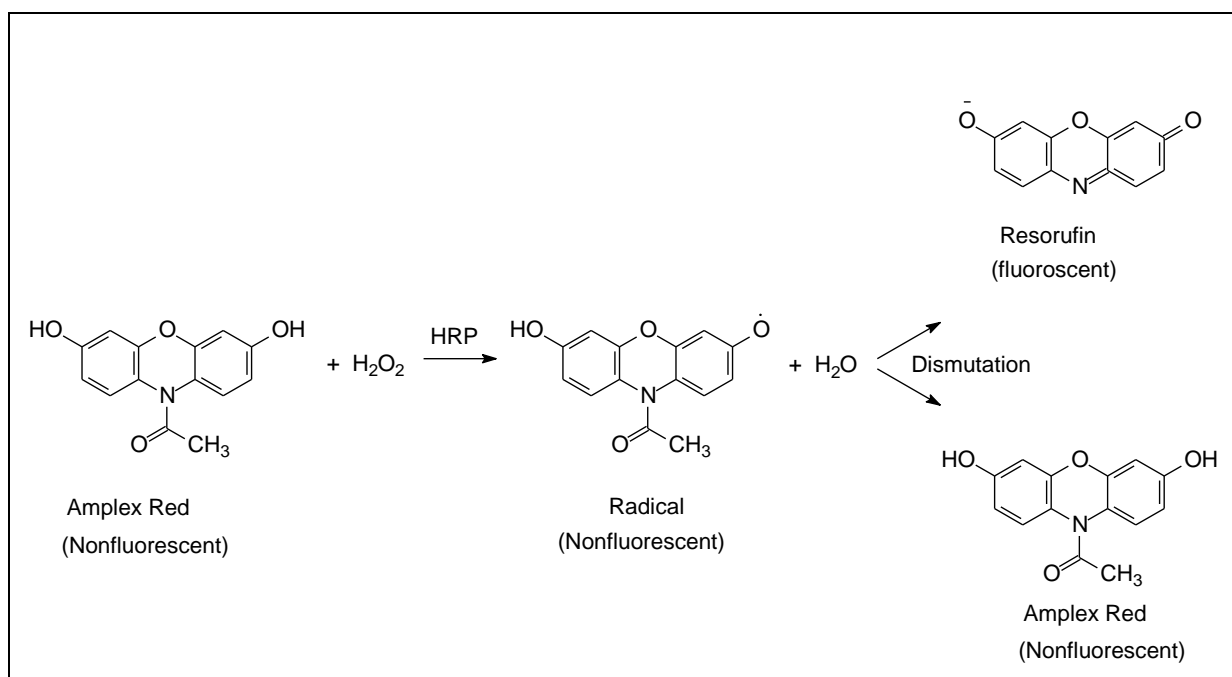


Figure 2.47 Schematic representation of the oxidation of amplex red to produce a highly fluorescent product, resorufin (Nicotra & Parvez, 1999).

2.5.5 Spectrophotometric assay

A frequently used spectrophotometric method for measuring MAO activity employs 4-aminoantipyrine. This compound is firstly oxidised by hydrogen peroxide in a peroxidase-coupled reaction, and the oxidised product subsequently condenses with 4-hydroxy-3-methoxybenzoic acid (vanillic acid) to produce a red quinoneimine dye, which absorbs light at a wavelength maxima of 498 nm. The quantity of hydrogen peroxide produced by MAO activity is directly proportional to the absorbance measured at 498 nm. Advantages of this approach is that it is an inexpensive and fast method, and can be used with all amine oxidase substrates which has a higher oxidation-reduction potential than 4-aminoantipyrine. Disadvantages of this method are that it is less sensitive than radiochemical or fluorometric assays (Nicotra & Parvez, 1999).

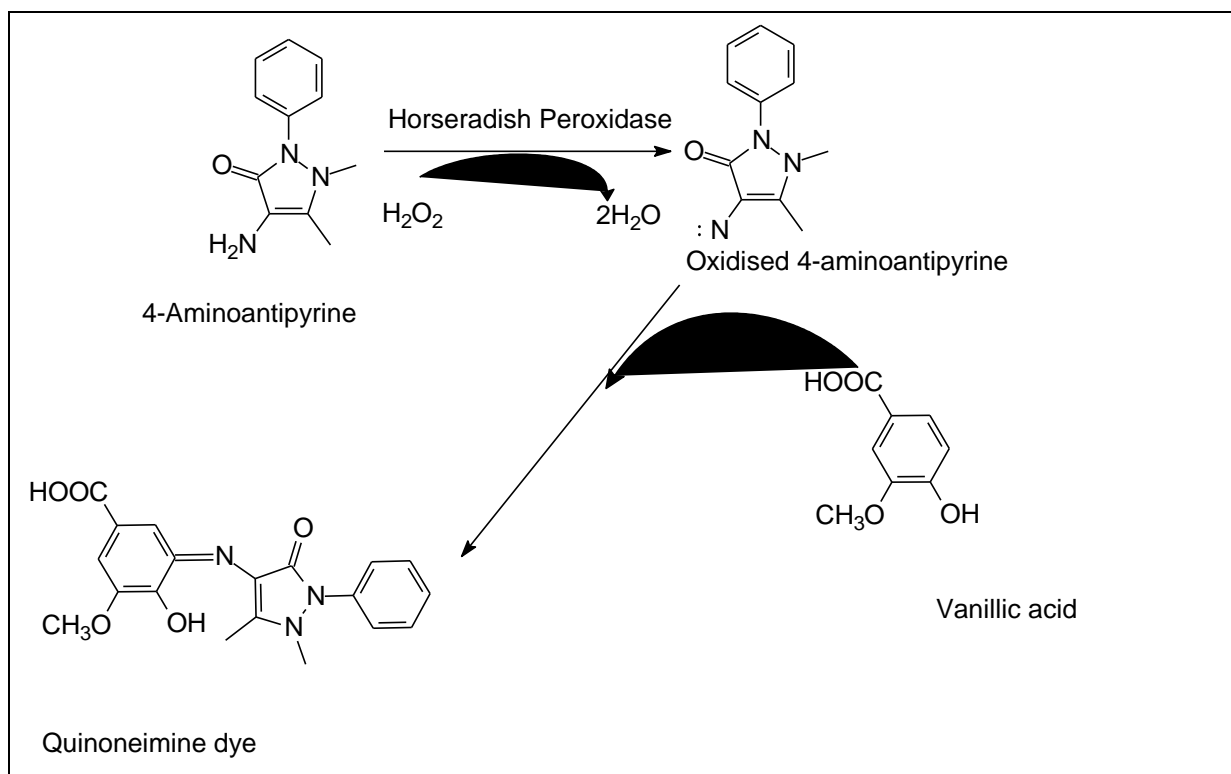


Figure 2.48 The use of 4-aminoantipyrine for the spectrophotometric determination of MAO activity (Nicotra & Parvez, 1999).

A second spectrophotometric assay employs the substrate, kynuramine, which is a non-specific substrate of both MAO-A and MAO-B. Kynuramine has a distinguishing ultraviolet light absorption spectrum with a maximum at 366 nm. Through enzymatic degradation an aldehyde is produced, which subsequently undergoes ring-closure to form 4-hydroxyquinoline. 4-Hydroxyquinoline exhibits no absorption at 366 nm, but absorbs light at a wavelength of 314 nm. MAO activity may thus be monitored spectrophotometrically by the disappearance of kynuramine (366 nm) or the appearance of 4-hydroxyquinoline (314 nm). Alternatively, 4-hydroxyquinoline may be measured by fluorescence spectrophotometry since this metabolite fluoresces ($\lambda_{ex} = 310$ nm; $\lambda_{em} = 400$ nm) in alkaline media. Kynuramine, on the other hand, does not fluoresce. As shown in fig. 2.49, aminoaldehyde condensation (to yield 4-hydroxyquinoline) appears to be faster than the further oxidation of the aldehyde to an acid, which would lead to the formation of the lactam (Nicotra & Parvez, 1999).

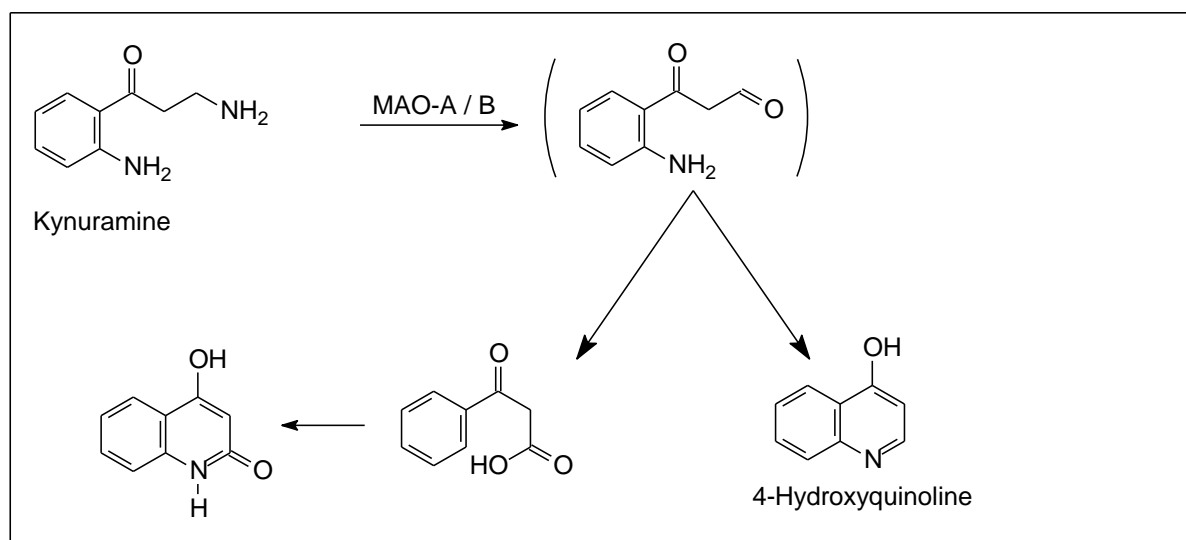


Figure 2.49 Kynuramine is oxidatively deaminated by MAO to yield 4-hydroxyquinoline (Nicotra & Parvez, 1999).

The MAO-B selective substrate, benzylamine, has also been used extensively to measure MAO-B activity. MAO-B oxidises benzylamine to yield benzaldehyde. The formation of benzaldehyde may be measured by spectrophotometry since this compound absorbs maximally at 250 nm. Background interference from crude MAO preparations, however, often prevents spectrophotometric analysis at such low wavelengths (Petzer *et al.*, 2003).

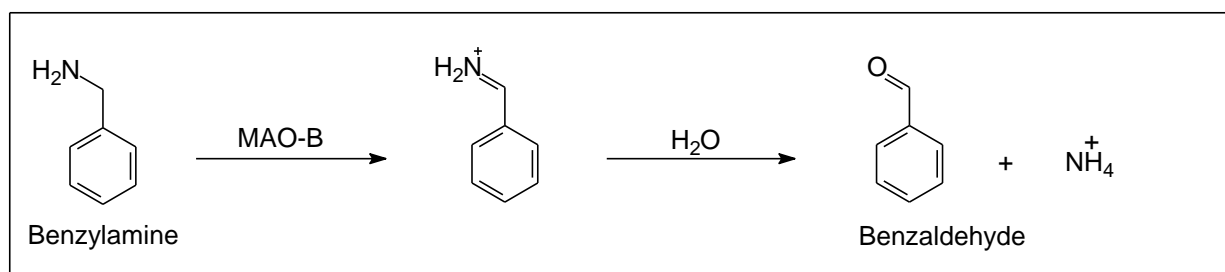


Figure 2.50 The oxidation of benzylamine to yield benzaldehyde (Petzer *et al.*, 2003).

2.6 Conclusion

In this chapter PD was discussed, as an incurable neurodegenerative disease. Particular attention was given to the neurochemical and neuropathological features of PD and possible causes were discussed. An overview of the current PD treatment was also given. It is evident that the available pharmacotherapies address only the symptoms of the disease, and while several neuroprotective therapies have been proposed, no definite evidence for neuroprotection exists. This chapter further shows that MAO inhibitors have a prominent role in PD therapy. MAO inhibitors are mainly used for the symptomatic therapy of PD as they

preserve dopamine in the brain. In this respect, the biochemistry and pharmacology of MAO have been extensively discussed in this chapter. This provides the necessary background for the theme of this dissertation, namely the design of novel MAO inhibitors for PD therapy. The chapter concluded with a brief discussion of animal models of PD, where MAO-B plays an important role in the bioactivation of certain proneurotoxins. The chapter also discusses potential methods for measuring MAO activity. These methods are typically used to evaluate the inhibition potencies of potential MAO inhibitors, as will be done in Chapter 4.

CHAPTER 3

SYNTHESIS OF 3-COUMARONONE DERIVATIVES

3.1 Introduction

In this study a series of 3-coumaronone derivatives were synthesised and investigated as potential lead compounds for the development of reversible MAO-A and MAO-B inhibitors. In total, twenty compounds were synthesised and all compounds contained a substituent on the C6 position of the 3-coumaronone moiety. For this purpose, the benzyloxy, phenylethoxy and phenylpropoxy substituents were selected to yield compounds **1a**, **1o** and **1s**. To further explore chemical space, the benzyloxy-substituted homologue (**1a**), was substituted on the benzyloxy phenyl ring with halogens (F, Cl, Br, I) and alkyl groups (CH₃, CN, CF₃). The phenylethoxy-substituted homologue (**1o**), was similarly substituted on the phenyl ring with chlorine and the methyl group. Finally, a homologue (**1t**) containing the phenoxyethoxy side chain on the C6 position of the 3-coumaronone moiety was also synthesised. With this series, the effect of the size of the substituent on C6 of the 3-coumaronone moiety on MAO-A and MAO-B inhibition activity may be evaluated (**1a** vs. **1o** vs. **1s**). In addition, the effect of the different groups on the phenyl rings of the C6 substituents may be evaluated. In certain instances, the effect of the position of the different groups on the phenyl rings (*meta* vs. *para*) on MAO-A and MAO-B inhibition activity may be also be evaluated. However the main goal of this study is to discover new highly potent inhibitors of human MAO-A and MAO-B.

3.2 Synthesis of target compounds

3.2.1 Literature method

In this study, a modified version of the literature method was used. 6-Hydroxy-3-coumaronone was reacted with an appropriately substituted alkyl bromide. For this purpose N,N-dimethylformamide (DMF) served as solvent and potassium carbonate as base (Laczkowski *et al.*, 2008).

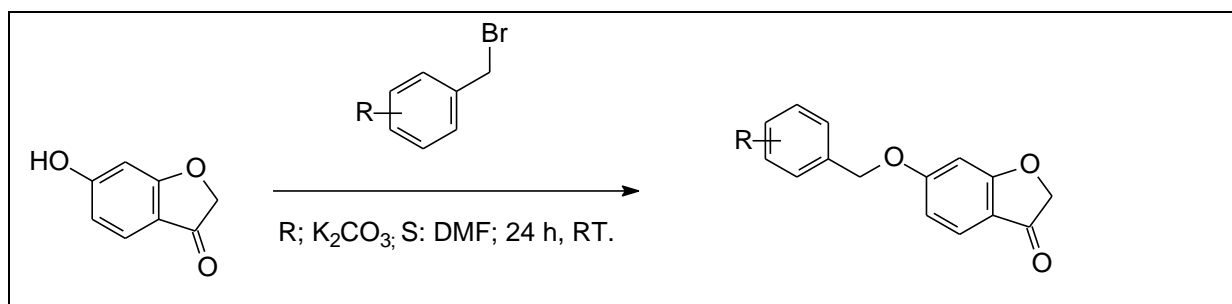
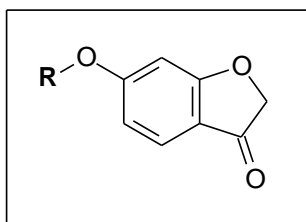
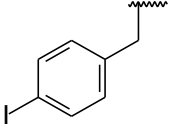
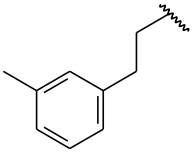
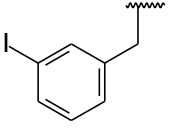
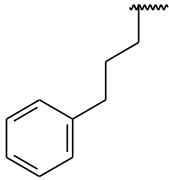
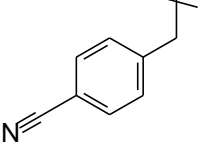
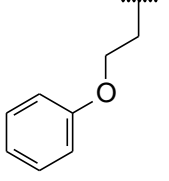


Figure 3.1 The general synthetic route for the synthesis of the 6-substituted-3-coumaronone derivatives (Laczkowski *et al.*, 2008).

Table 3.1 The structures of the 3-coumaranone derivatives (**1a-t**) that were synthesised in this study.

COMPOUND	R	COMPOUND	R
1a		1k	
1b		1l	
1c		1m	
1d		1n	
1e		1o	
1f		1p	
1g		1q	

1h		1r	
1i		1s	
1j		1t	

3.2.1.1 The synthesis of 6-hydroxy-3-coumaranone

The synthesis of 6-hydroxy-3-coumaranone has previously been reported by Lantos *et al.* (1997). In this procedure, 6-hydroxy-3-coumaranone is synthesised from the reaction of resorcinol and chloroacetonitrile in the presence of potassium carbonate. This method was, however, not employed in the study because 6-hydroxy-3-coumaranone was commercially available (Sigma-Aldrich).

3.2.1.2 Literature approaches to the synthesis of 3-coumaranone derivatives

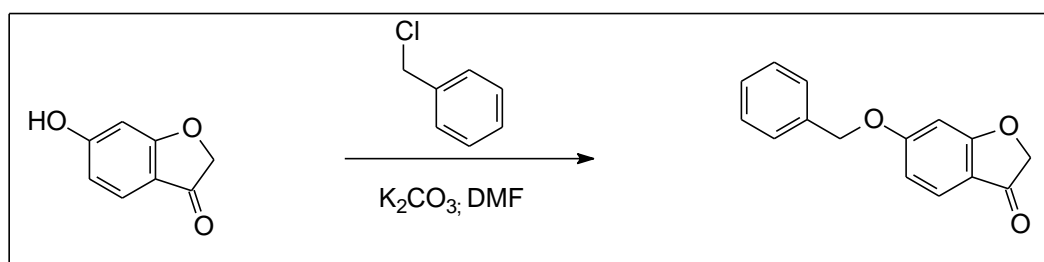


Figure 3.2 A general reaction scheme to illustrate the synthesis of 6-(benzyloxy)-2H-benzofuran-3-one.

The synthesis of the 3-coumaranone derivative, 6-(benzyloxy)-2H-benzofuran-3-one (**1a**) has previously been reported by Laczkowski *et al.* (2008). As mentioned above, in this method 6-hydroxy-3-coumaranone was reacted with an appropriately substituted alkyl bromide or alkyl chloride, with DMF serving as solvent, and potassium carbonate as base (Laczkowski *et al.* 2008). The following is a detailed account of the procedure:

To a stirred mixture of 6-hydroxy-2,3-dihydrobenzofuran-3-one (3.00 g, 20 mmol), DMF (50 ml) and anhydrous potassium carbonate, benzyl chloride (3.90 g, 31 mmol) was added dropwise over 30 min. The mixture was stirred for 24 h at room temperature and water (75 ml) was added. The reaction mixture was kept incubated at 4 °C for 3 h. The precipitate which formed was collected by filtration and dried. After treatment with activated charcoal, the product was recrystallised from cyclohexane. This method gave the product in a yield of 87%.

3.3 Materials and instrumentation

Materials: Sigma-Aldrich supplied all starting materials and solvents, and these were used without further purification.

Nuclear magnetic resonance (NMR): A Bruker Avance III 600 spectrometer was used to record the proton (^1H) and carbon (^{13}C) NMR spectra at frequencies of 600 MHz and 150 MHz, respectively, with chloroform-d as NMR solvent. All chemical shifts are reported in parts per million (δ) downfield from the signal of $\text{Si}(\text{CH}_3)_4$. Spin multiplicities are given as s (singlet), d (doublet), dd (doublet of doublets), t (triplet), qn (quintet) or m (multiplet).

High resolution mass spectra (HRMRS): The mass spectra were recorded with a Bruker micrOTOF-Q II mass spectrometer in atmospheric-pressure chemical ionization (APCI) mode.

Melting points: A Buchi M-545 melting point apparatus was used to record the melting points of the synthesised compounds. The melting points are given in degrees Celsius and are uncorrected

Thin layer chromatography (TLC): TLC was used to establish whether a reaction proceeded to completion. The TLC sheets were developed in a mobile phase consisting of 1 parts ethyl acetate and 4 parts petroleum ether. The developed sheets were subsequently examined at a wavelength of 254 nm under an ultraviolet lamp.

High pressure liquid chromatography (HPLC): HPLC was used to verify the purities of the synthesised compounds. The analyses were conducted with an Agilent 1100 HPLC system equipped with a quaternary pump and a diode array detector. HPLC grade acetonitrile (Merck) and milli-Q water (Millipore) were employed for the chromatography. A Venusil XBP C18 column (4.60 x 150 mm, 5 μm) was used for the separation. At the start of each run, the mobile

phase consisted of 30% acetonitrile and 70% MilliQ water with a flow rate of 1 ml/min. During every run the mobile phase composition was linearly adjusted to 85% acetonitrile over a period of 5 min. Each run lasted 15 min and a time period of 5 min was allowed for equilibration between runs. A volume of 20 μ l of solutions of the test compounds in acetonitrile (1 mM) was injected into the HPLC system and the eluent was monitored at wavelength of 254 nm or at 210 nm. All the test compounds were dissolved in acetonitrile.

3.4 Synthesis of 3-coumaranone derivatives

The following is an account of the method used for the synthesis of the 3-coumaranone analogues **1a-t**. Figure 3.1 depicts the general synthetic route, and figure 3.3 illustrates the experimental setup.

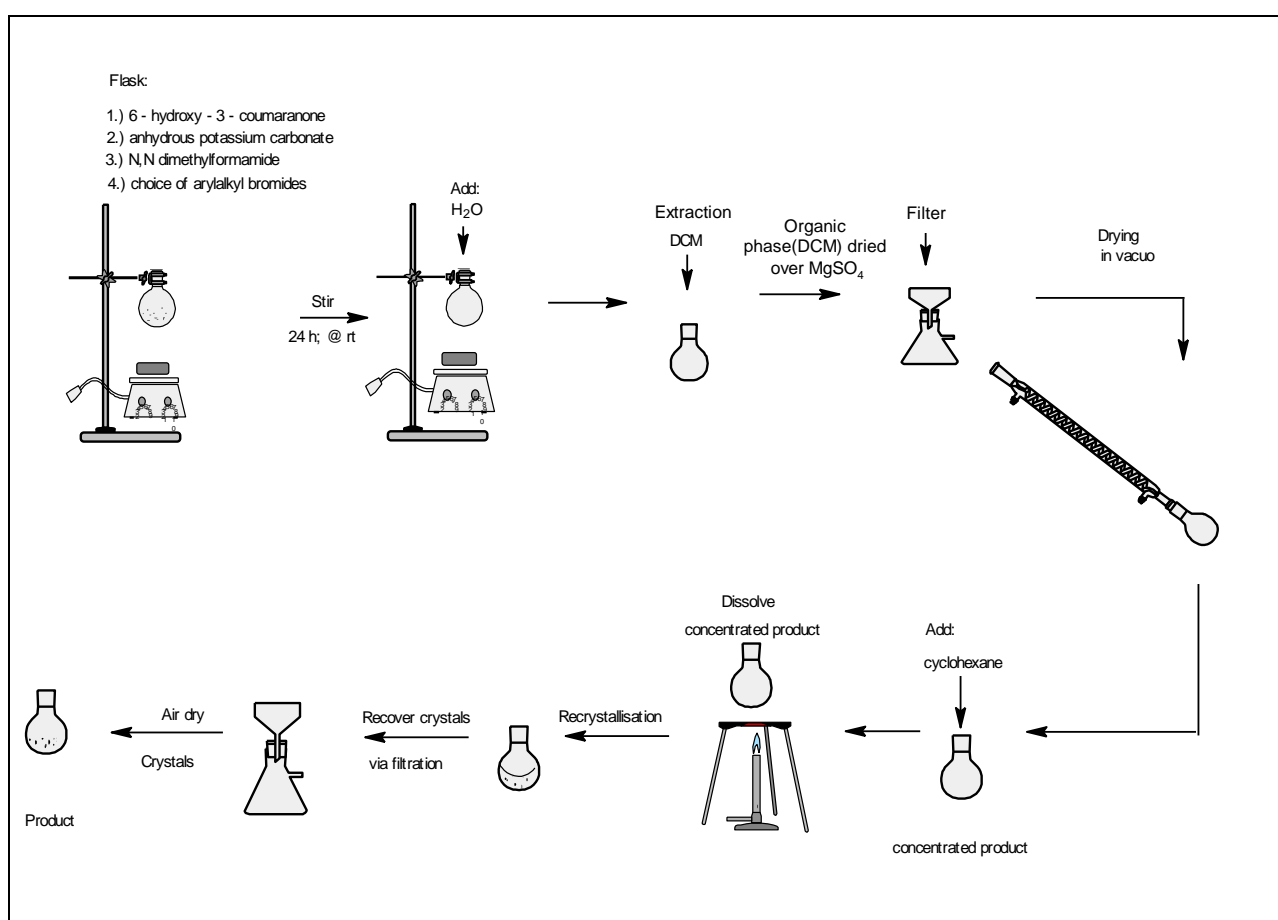


Figure 3.3. Illustration of experimental procedure for the synthesis of the 3-coumaranone derivatives **1a-t**.

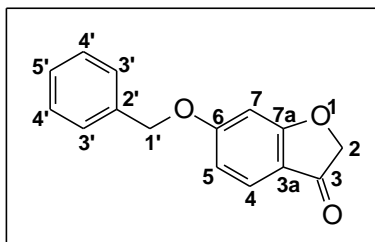
The protocol used in this study is as follows:

To commercially available 6-hydroxy-3-coumaranone (300 mg; 1.998 mmol) in a 100 ml round bottom flask, was added 3 ml DMF and anhydrous potassium carbonate (552 mg; 3.996 mmol). The appropriate alkyl bromide (2.197 mmol) was added to the reaction, and the mixture was stirred for 24 h at room temperature. TLC was performed to determine the completion of the reaction. Upon completion, water (8 mL) was added to the reaction and the resulting mixture was filtered. The reaction was extracted to dichloromethane (DCM; 3 × 20 ml), and the organic phase was dried over anhydrous MgSO₄, filtered and concentrated in vacuo. After crystallisation from cyclohexane, the product was collected via filtration, and the crystals were air dried.

3.5 Results - NMR spectra

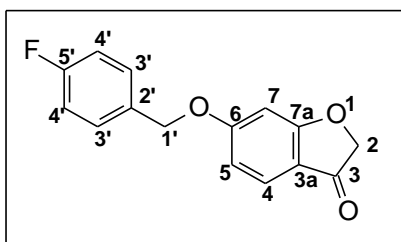
The NMR spectra of the synthesised 3-coumaranone derivatives are given in appendix A. Below, the structures of the synthesised derivatives are given and correlated with the ¹H NMR and ¹³C NMR data. As shown by the correlations, the appropriate signals were observed for each compound, which include the singlets for the benzylic CH₂ protons of compounds **1a-1n**, and the appropriate signals for the CH₂CH₂ and (CH₂)₃ groups of phenylethoxy- and phenylpropoxy-and phenoxyethoxy-substituted compounds, **1o-t**. For all compounds, the expected singlets for the coumaranone CH₂ protons were observed. In addition, the appropriate signals for the phenyl protons were also present. In this respect, the appropriate integration values and chemical shifts were observed for all signals. The ¹³C NMR data corresponded to the target structures. In particular, the signal of the carbonyl carbon was present at ~197 ppm. For the ¹³C NMR spectra, the number of signals as well as the chemical shifts were as expected for the synthesised compounds. Based on the NMR data, it may thus be concluded that the structures of these derivatives are those proposed in this dissertation.

1a: 6-(Benzyloxy)-2H-1-benzofuran-3-one



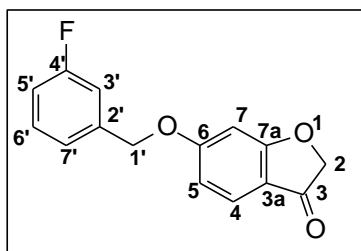
The title compound was prepared in a yield of 56%. mp 91.4–96.6 °C. ^1H NMR (600 MHz, CDCl_3) δ 7.56 (d, J = 8.6 Hz, 1H), 7.40 (m, 4H), 7.35 (m, 1H), 6.71 (dd, J = 8.6, 2.1 Hz, 1H), 6.60 (d, J = 2.0 Hz, 1H), 5.11 (s, 2H), 4.60 (s, 2H). ^{13}C NMR (151 MHz, CDCl_3) δ 70.6, 75.5, 97.4, 112.2, 114.5, 125.2, 127.5, 128.4, 128.8, 135.5, 167.2, 176.4, 197.5. APCI-HRMS m/z : calcd for $\text{C}_{15}\text{H}_{13}\text{O}_3$ (MH^+), 241.0859, found 241.0852. Purity (HPLC): 100%.

^1H NMR	^{13}C NMR
<ul style="list-style-type: none"> The singlet at 4.60 ppm (2H) corresponds to the benzylic CH_2 protons at C1'. The singlet at 5.11 ppm (2H) corresponds to the coumaranone CH_2 protons at C2. The multiplet at 7.35 ppm (1H) and the multiplet at 7.40 ppm (4H) correspond to the phenyl protons at C5' and C3' and C4'. The doublet at 7.56 ppm (1H) corresponds to the coumaranone CH proton at C4. The small coupling constant indicates that the doublet at 6.60 ppm (1H) corresponds to the coumaranone CH proton at C7. The doublet of doublets at 6.71 ppm (1H) corresponds to the coumaranone CH proton at C5. 	<ul style="list-style-type: none"> The signals at 70.5 ppm and 75.5 ppm represent the aliphatic carbons C1' and C2, respectively. The signal at 197.5 ppm represents the carbonyl carbon C3. The signals at 167.2 ppm and 176.4 ppm most likely represent the carbons C6 and C7a. The other aromatic carbons are represented by the signals at 97.4, 112.2, 114.5, 125.2, 127.5, 128.4, 128.8, 135.5 ppm.

1b: 6-(4-Fluorobenzyloxy)-2H-1-benzofuran-3-one

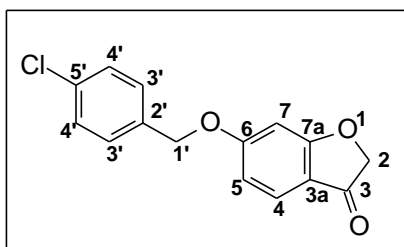
The title compound was prepared in a yield of 55%. mp 121.6–126.5 °C. ^1H NMR (600 MHz, CDCl_3) δ 7.56 (d, J = 8.6 Hz, 1H), 7.41–7.35 (m, 2H), 7.08 (t, J = 8.7 Hz, 2H), 6.69 (dd, J = 8.6, 2.1 Hz, 1H), 6.58 (d, J = 2.1 Hz, 1H), 5.06 (s, 2H), 4.60 (s, 2H). ^{13}C NMR (151 MHz, CDCl_3) δ 69.9, 75.5, 97.3, 112.1, 114.6, 115.8, 125.2, 129.4, 131.3, 161.9, 163.5, 166.9, 176.3, 197.5. APCI-HRMS m/z : calcd for $\text{C}_{15}\text{H}_{12}\text{FO}_3$ (MH^+), 259.0765, found 259.0764. Purity (HPLC): 82%.

^1H NMR	^{13}C NMR
<ul style="list-style-type: none"> The singlet at 5.06 ppm (2H) corresponds to the benzylic CH_2 protons at C1'. The singlet at 4.60 ppm (2H) corresponds to the coumaranone CH_2 protons at C2. The signal at 7.08 ppm (2H) and at 7.41 ppm - 7.35 ppm (2H) correspond to the phenyl protons at C3' and C4'. The doublet at 7.56 ppm (1H) corresponds to the coumaranone CH proton at C4. The small coupling constant indicates that the doublet at 6.58 (1H) corresponds to the coumaranone CH proton at C7. The doublet of doublets at 6.69 (1H) corresponds to the coumaranone CH proton at C5. 	<ul style="list-style-type: none"> The signals at 69.9 ppm and 75.5 ppm represent the aliphatic carbons C1' and C2, respectively. The signal at 197.5 ppm represents the carbonyl carbon C3. The signals at 166.9 ppm and 176.3 ppm most likely represent the carbons C6 and C7a. The other aromatic carbons are represented by the signals at, 97.3, 99.9, 112.1, 114.6, 115.8, 125.2, 129.4, 131.3, 161.9, 163.5 ppm.

1c: 6-(3-Fluorobenzyloxy)-2H-1-benzofuran-3-one

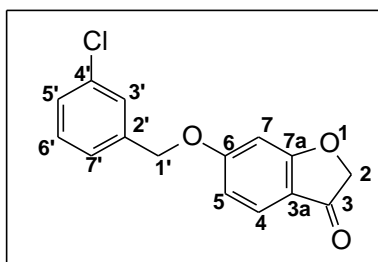
The title compound was prepared in a yield of 58%. mp 56.2–56.3 °C. ^1H NMR (600 MHz, CDCl_3) δ 7.57 (d, J = 8.6 Hz, 1H), 7.35 (td, J = 7.9, 5.8 Hz, 1H), 7.17 (d, J = 8.1 Hz, 1H), 7.12 (d, J = 9.4 Hz, 1H), 7.03 (td, J = 8.4, 2.2 Hz, 1H), 6.71 (dd, J = 8.6, 2.1 Hz, 1H), 6.58 (d, J = 2.0 Hz, 1H), 5.11 (s, 2H), 4.61 (s, 2H). ^{13}C NMR (151 MHz, CDCl_3) δ 69.7, 75.5, 97.4, 112.1, 114.2, 114.8, 115.4, 122.7, 125.3, 130.3, 138.1, 162.2, 166.8, 176.3, 197.5. APCI-HRMS m/z : calcd for $\text{C}_{15}\text{H}_{12}\text{FO}_3$ (MH^+), 259.0765, found 259.0752. Purity (HPLC): 100%.

^1H NMR	^{13}C NMR
<ul style="list-style-type: none"> The singlet at 5.11 ppm (2H) corresponds to the benzylic CH_2 protons at C1'. The singlet at 4.61 ppm (2H) corresponds to the coumaranone CH_2 protons at C2. The signals at 7.03 ppm (1H), and the doublets at 7.12 ppm (1H), 7.17 ppm (1H), and 7.35 ppm (1H) correspond to the phenyl protons at, C6', C3', and C5'. The doublet at 7.57 ppm (1H) corresponds to the coumaranone CH proton at C4. The small coupling constant indicates that the doublet at 6.58 ppm (1H) corresponds to the coumaranone CH proton at C7. The doublet of doublets at 6.71 ppm (1H) corresponds to the coumaranone CH proton at C5. 	<ul style="list-style-type: none"> The signals at 69.7 ppm and 75.5 ppm represent the aliphatic carbons C1' and C2, respectively. The signal at 197.5 ppm represents the carbonyl carbon C3. The signals at 166.8 ppm and 176.3 ppm most likely represent the carbons C6 and C7a. The other aromatic carbons are represented by the signals at 97.4, 112.1, 114.2, 114.8, 115.4, 122.7, 125.3, 130.3, 138.1, 162.2 ppm.

1d: 6-(4-Chlorobenzoyloxy)-2H-1-benzofuran-3-one

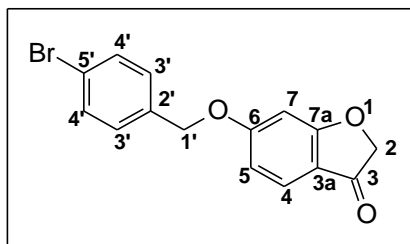
The title compound was prepared in a yield of 51%. mp 137.5–141.7°C. ^1H NMR (600 MHz, CDCl_3) δ 7.56 (d, J = 8.6 Hz, 1H), 7.37 – 7.33 (m, 4H), 6.69 (dd, J = 8.6, 2.1 Hz, 1H), 6.57 (d, J = 2.1 Hz, 1H), 5.07 (s, 2H), 4.60 (s, 2H). ^{13}C NMR (151 MHz, CDCl_3) δ 69.7, 75.5, 97.4, 112.1, 114.7, 125.2, 128.8, 128.9, 134.0, 134.3, 166.9, 176.3, 197.5. APCI-HRMS m/z : calcd for $\text{C}_{15}\text{H}_{12}\text{ClO}_3$ (MH^+), 275.0469, found 275.0452. Purity (HPLC): 100%.

^1H NMR	^{13}C NMR
<ul style="list-style-type: none"> The singlet at 5.07 ppm (2H) corresponds to the benzylic CH_2 protons at C1'. The singlet at 4.60 ppm (2H) corresponds to the coumaranone CH_2 protons at C2. The signal at 7.37 ppm - 7.33 ppm (4H) correspond to the phenyl protons at C3' and C4'. The doublet at 7.56 ppm (1H) corresponds to the coumaranone CH proton at C4. The small coupling constant indicates that the doublet at 6.57 ppm (1H) corresponds to the coumaranone CH proton at C7. The doublet of doublets at 6.69 ppm (1H) corresponds to the coumaranone CH proton at C5. 	<ul style="list-style-type: none"> The signals at 69.7 ppm and 75.5 ppm represent the aliphatic carbons C1' and C2, respectively. The signal at 197.5 ppm represents the carbonyl carbon C3. The signals at 166.9 ppm and 176.3 ppm most likely represent the carbons C6 and C7a. The other aromatic carbons are represented by the signals at 97.4, 112.1, 114.7, 125.2, 128.8, 128.9, 134.0, 134.3 ppm.

1e: 6-(3-Chlorobenzoyloxy)-2H-1-benzofuran-3-one

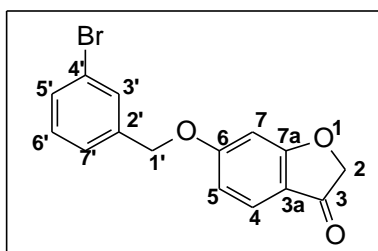
The title compound was prepared in a yield of 57%. mp 108.7–112.3 °C. ^1H NMR (600 MHz, CDCl_3) δ 7.47 (d, J = 8.6 Hz, 1H), 7.31 (s, 1H), 7.24 – 7.17 (m, 3H), 6.61 (dd, J = 8.6, 2.0 Hz, 1H), 6.48 (d, J = 2.0 Hz, 1H), 4.98 (s, 2H), 4.51 (s, 2H). ^{13}C NMR (151 MHz, CDCl_3) δ 69.6, 75.5, 97.4, 112.0, 114.8, 125.2, 125.3, 127.4, 128.5, 130.0, 134.7, 137.5, 166.8, 176.3, 197.5. APCI-HRMS m/z : calcd for $\text{C}_{15}\text{H}_{12}\text{ClO}_3$ (MH^+), 275.0469, found 275.0453. Purity (HPLC): 85%.

^1H NMR	^{13}C NMR
<ul style="list-style-type: none"> The singlet at 4.51 ppm (2H) corresponds to the benzylic CH_2 protons at C1'. The singlet at 4.98 ppm (2H) corresponds to the coumaranone CH_2 protons at C2. The signals at 7.31 ppm (1H) and 7.24 ppm - 7.17 ppm (3H) correspond to the phenyl protons at C3', C6', C5' and C7'. The doublet at 7.47 ppm (1H) corresponds to the coumaranone CH proton at C4. The small coupling constant indicates that the doublet at 6.48 ppm (1H) corresponds to the coumaranone CH proton at C7. The doublet of doublets at 6.61 ppm (1H) corresponds to the coumaranone CH proton at C5. 	<ul style="list-style-type: none"> The signals at 69.6 ppm and 75.5 ppm represent the aliphatic carbons C1' and C2, respectively. The signal at 197.5 ppm represents the carbonyl carbon C3. The signals at 166.8 ppm and 176.3 ppm most likely represent the carbons C6 and C7a. The other aromatic carbons are represented by the signals at, 97.4, 112.0, 114.8, 125.2, 125.3, 127.4, 128.5, 130.0, 134.7, 137.5 ppm.

1f: 6-(4-Bromobenzyloxy)-2H-1-benzofuran-3-one

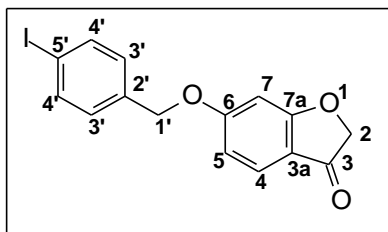
The title compound was prepared in a yield of 51%. mp 140.0–142.1 °C. ^1H NMR (600 MHz, CDCl_3) δ 7.56 (d, $J = 8.6$ Hz, 1H), 7.52 (d, $J = 8.4$ Hz, 2H), 7.28 (d, $J = 8.4$ Hz, 2H), 6.69 (dd, $J = 8.6, 2.1$ Hz, 1H), 6.57 (d, $J = 2.0$ Hz, 1H), 5.06 (s, 2H), 4.60 (s, 2H). ^{13}C NMR (151 MHz, CDCl_3) δ 69.8, 75.5, 97.4, 112.1, 114.7, 122.4, 125.2, 129.1, 131.9, 134.5, 166.8, 176.3, 197.5. APCI-HRMS m/z : calcd for $\text{C}_{15}\text{H}_{12}\text{BrO}_3$ (MH^+), 318.9964, found 318.9963. Purity (HPLC): 92%.

^1H NMR	^{13}C NMR
<ul style="list-style-type: none"> The singlet at 4.60 ppm (2H) corresponds to the benzylic CH_2 protons at C1'. The singlet at 5.06 ppm (2H) corresponds to the coumaranone CH_2 protons at C2. The doublets at 7.52 ppm (2H) and 7.28 ppm (2H) correspond to the phenyl protons at C3' and C4'. The doublet at 7.56 (1H) corresponds to the coumaranone CH proton at C4. The small coupling constant indicates that the doublet at 6.57 (1H) corresponds to the coumaranone CH proton at C7. The doublet of doublets at 6.69 (1H) corresponds to the coumaranone CH proton at C5. 	<ul style="list-style-type: none"> The signals at 69.8 ppm and 75.5 ppm represent the aliphatic carbons C1' and C2, respectively. The signal at 197.5 ppm represents the carbonyl carbon C3. The signals at 166.8 ppm and 176.3 ppm most likely represent the carbons C6 and C7a. The other aromatic carbons are represented by the signals at , 97.4, 112.1, 114.7, 122.4, 125.2, 129.1, 131.9, 134.5 ppm.

1g: 6-(3-Bromobenzyloxy)-2H-1-benzofuran-3-one

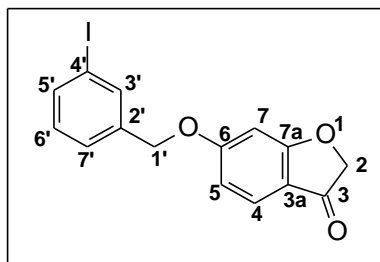
The title compound was prepared in a yield of 50%. mp 120.0–122.6 °C. ^1H NMR (600 MHz, CDCl_3) δ 7.59–7.54 (m, 2H), 7.47 (d, J = 7.9 Hz, 1H), 7.32 (d, J = 7.7 Hz, 1H), 7.26 (d, J = 7.8 Hz, 1H), 6.70 (dd, J = 8.6, 2.1 Hz, 1H), 6.57 (d, J = 2.1 Hz, 1H), 5.07 (s, 2H), 4.61 (s, 2H). ^{13}C NMR (151 MHz, CDCl_3) δ 69.5, 75.5, 97.4, 112.0, 114.8, 122.8, 125.3, 125.8, 130.3, 130.3, 131.5, 137.8, 166.8, 176.3, 197.5. APCI-HRMS m/z : calcd for $\text{C}_{15}\text{H}_{12}\text{BrO}_3$ (MH^+), 318.9964, found 318.9955. Purity (HPLC): 100%.

^1H NMR	^{13}C NMR
<ul style="list-style-type: none"> The singlet at 4.61 ppm (2H) corresponds to the benzylic CH_2 protons at C1'. The singlet at 5.07 ppm (2H) corresponds to the coumaranone CH_2 protons at C2. The signals at 7.59 ppm - 7.54 ppm (2H), 7.32 ppm (1H), and 7.26 ppm (1H) correspond to the phenyl protons at C3', C5', C6', and C7'. The doublet at 7.47 ppm (1H) corresponds to the coumaranone CH proton at C4, although this may be a phenyl proton, with the CH at C4 being part of the multiplet at 7.59 ppm - 7.54 ppm. The small coupling constant indicates that the doublet at 6.57 ppm (1H) corresponds to the coumaranone CH proton at C7. The doublet of doublets at 6.70 ppm (1H) corresponds to the coumaranone CH proton at C5. 	<ul style="list-style-type: none"> The signals at 69.5 ppm and 75.5 ppm represent the aliphatic carbons C1' and C2, respectively. The signal at 197.5 ppm represents the carbonyl carbon C3. The signals at 166.8 ppm and 176.3 ppm most likely represent the carbons C6 and C7a. The other aromatic carbons are represented by the signals at 97.4, 112.0, 114.8, 122.8, 125.3, 125.8, 130.3, 130.3, 131.5, 137.8 ppm.

1h: 6-(4-Iodobenzyloxy)-2H-1-benzofuran-3-one

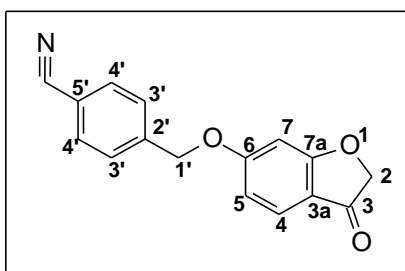
The title compound was prepared in a yield of 52%. mp 136.0–138.5 °C. ^1H NMR (600 MHz, CDCl_3) δ 7.72 (d, J = 8.1 Hz, 2H), 7.56 (d, J = 8.6 Hz, 1H), 7.15 (d, J = 8.1 Hz, 2H), 6.68 (dd, J = 8.6, 1.5 Hz, 1H), 6.56 (d, J = 1.6 Hz, 1H), 5.05 (s, 2H), 4.60 (s, 2H). ^{13}C NMR (151 MHz, CDCl_3) δ 69.9, 75.5, 94.0, 97.4, 112.1, 114.7, 125.3, 129.2, 135.2, 137.9, 166.8, 176.3, 197.5. APCI-HRMS m/z : calcd for $\text{C}_{15}\text{H}_{12}\text{IO}_3$ (MH^+), 366.9826, found 366.9805. Purity (HPLC): 100%.

^1H NMR	^{13}C NMR
<ul style="list-style-type: none"> The singlet at 5.05 ppm (2H) corresponds to the benzylic CH_2 protons at C1'. The singlet at 4.60 ppm (2H) corresponds to the coumaranone CH_2 protons at C2. The doublet at 7.15 ppm (2H) and the doublet at 7.72 ppm (2H) correspond to the phenyl protons at C3' and C4'. The doublet at 7.56 ppm (1H) corresponds to the coumaranone CH proton at C4. The small coupling constant indicates that the doublet at 6.56 ppm (1H) corresponds to the coumaranone CH proton at C7. The doublet of doublets at 6.68 ppm (1H) corresponds to the coumaranone CH proton at C5. 	<ul style="list-style-type: none"> The signals at 69.9 ppm and 75.5 ppm represent the aliphatic carbons C1' and C2, respectively. The signal at 197.5 ppm represents the carbonyl carbon C3. The signals at 166.8 ppm and 176.3 ppm most likely represent the carbons C6 and C7a. The other aromatic carbons are represented by the signals at 97.4, 112.1, 114.7, 125.3, 129.2, 135.2, 137.9 ppm.

1i: 6-(3-Iodobenzyloxy)-2H-1-benzofuran-3-one

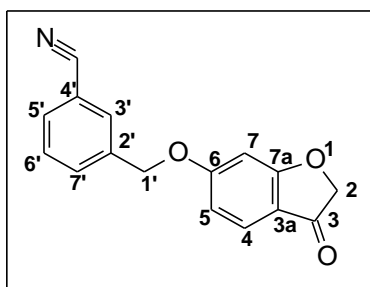
The title compound was prepared in a yield of 51%. mp 161.2–164.5°C. ^1H NMR (600 MHz, CDCl_3) δ 7.77 (s, 1H), 7.68 (d, $J = 8.0$ Hz, 1H), 7.57 (d, $J = 8.6$ Hz, 1H), 7.36 (d, $J = 8.1$ Hz, 1H), 7.12 (t, $J = 7.8$ Hz, 1H), 6.70 (dd, $J = 8.6, 2.1$ Hz, 1H), 6.57 (d, $J = 2.0$ Hz, 1H), 5.05 (s, 2H), 4.61 (s, 2H). ^{13}C NMR (151 MHz, CDCl_3) δ 69.5, 75.6, 94.5, 97.4, 112.0, 114.8, 125.3, 126.5, 130.4, 136.3, 137.5, 137.8, 166.8, 176.3, 197.5. APCI-HRMS m/z : calcd for $\text{C}_{15}\text{H}_{12}\text{IO}_3$ (MH^+), 366.9826, found 366.9809. Purity (HPLC): 100%.

^1H NMR	^{13}C NMR
<ul style="list-style-type: none"> The singlet at 5.05 ppm (2H) corresponds to the benzylic CH_2 protons at C1'. The singlet at 4.61 ppm (2H) corresponds to the coumaranone CH_2 protons at C2. The signals at 7.77 ppm (1H), 7.68 ppm (1H), 7.36 ppm (1H), and 7.12 ppm (1H) correspond to the phenyl protons at C3', C5', C6' and C7'. The doublet at 7.57 ppm (1H) corresponds to the coumaranone CH proton at C4. The small coupling constant indicates that the doublet at 6.57 ppm (1H) corresponds to the coumaranone CH proton at C7. The doublet of doublets at 6.70 ppm (1H) corresponds to the coumaranone CH proton at C5. 	<ul style="list-style-type: none"> The signals at 69.5 ppm and 75.6 ppm represent the aliphatic carbons C1' and C2, respectively. The signal at 197.5 ppm represents the carbonyl carbon C3. The signals at 166.8 ppm and 176.3 ppm most likely represent the carbons C6 and C7a. The other aromatic carbons are represented by the signals at, 97.4, 112.0, 114.8, 125.3, 126.5, 130.4, 136.3, 137.5, 137.8 ppm.

1j: 6-(4-Cyanobenzyloxy)-2H-1-benzofuran-3-one

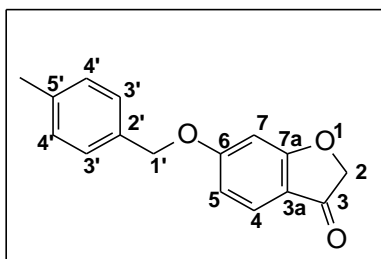
The title compound was prepared in a yield of 59%. mp 185.8–187.2 °C. ^1H NMR (600 MHz, CDCl_3) δ 7.68 (d, J = 8.2 Hz, 2H), 7.57 (d, J = 8.6 Hz, 1H), 7.52 (d, J = 8.3 Hz, 2H), 6.70 (dd, J = 8.6, 2.1 Hz, 1H), 6.56 (d, J = 2.0 Hz, 1H), 5.17 (s, 2H), 4.60 (s, 2H). ^{13}C NMR (151 MHz, CDCl_3) δ 69.3, 75.5, 97.5, 111.8, 112.2, 115.0, 118.4, 125.4, 127.5, 132.5, 140.9, 166.4, 176.2, 197.4. APCI-HRMS m/z : calcd for $\text{C}_{16}\text{H}_{12}\text{NO}_3$ (MH^+), 266.0812, found 266.0812. Purity (HPLC): 100%.

^1H NMR	^{13}C NMR
<ul style="list-style-type: none"> The singlet at 5.17 ppm (2H) corresponds to the benzylic CH_2 protons at C1'. The singlet at 4.60 ppm (2H) corresponds to the coumaranone CH_2 protons at C2. The doublet at 7.52 ppm (2H) and the doublet at 7.68 ppm (2H) correspond to the phenyl protons at C3' and C4'. The doublet at 7.57 ppm (1H) corresponds to the coumaranone CH proton at C4. The small coupling constant indicates that the doublet at 6.56 ppm (1H) corresponds to the coumaranone CH proton at C7. The doublet of doublets at 6.70 ppm (1H) corresponds to the coumaranone CH proton at C5. 	<ul style="list-style-type: none"> The signals at 69.3 ppm and 75.5 ppm represent the aliphatic carbons C1' and C2, respectively. The signal at 197.4 ppm represents the carbonyl carbon C3. The signals at 166.4 ppm and 176.2 ppm most likely represent the carbons C6 and C7a. The other aromatic carbons and the nitrile carbon are represented by the signals at 97.5, 111.8, 112.2, 115.0, 118.4, 125.4, 127.5, 132.5, 140.9 ppm.

1k: 6-(3-Cyanobenzoyloxy)-2H-1-benzofuran-3-one

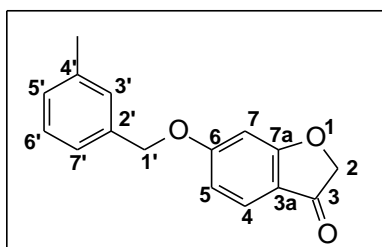
The title compound was prepared in a yield of 59%. mp 148.4-155.9 °C. ^1H NMR (600 MHz, CDCl_3) δ 7.72 (s, 1H), 7.67–7.61 (m, 2H), 7.58 (d, J = 8.6 Hz, 1H), 7.51 (t, J = 7.8 Hz, 1H), 6.71 (dd, J = 8.6, 2.1 Hz, 1H), 6.58 (d, J = 2.1 Hz, 1H), 5.14 (s, 2H), 4.61 (s, 2H). ^{13}C NMR (151 MHz, CDCl_3) δ 69.1, 75.6, 97.5, 111.9, 113.0, 115.0, 118.4, 125.4, 129.6, 130.7, 131.5, 132.0, 137.2, 166.4, 176.2, 197.5. APCI- HRMS m/z : calcd for $\text{C}_{16}\text{H}_{12}\text{NO}_3$ (MH^+), 266.0812, found 266.0797. Purity (HPLC): 100%.

^1H NMR	^{13}C NMR
<ul style="list-style-type: none"> The singlet at 5.14 ppm (2H) corresponds to the benzylic CH_2 protons at C1'. The singlet at 4.61 ppm (2H) corresponds to the coumaranone CH_2 protons at C2. The signals at 7.72 ppm (1H), 7.61 ppm - 7.81 ppm (2H), and 7.51 ppm (1H) correspond to the phenyl protons at C3', C5', C6' and C7'. The doublet at 7.58 ppm (1H) corresponds to the coumaranone CH proton at C4. The small coupling constant indicates that the doublet at 6.58 ppm (1H) corresponds to the coumaranone CH proton at C7. The doublet of doublets at 6.71 ppm (1H) corresponds to the coumaranone CH proton at C5. 	<ul style="list-style-type: none"> The signals at 69.1 ppm and 75.6 ppm represent the aliphatic carbons C1' and C2, respectively. The signal at 197.5 ppm represents the carbonyl carbon C3. The signals at 166.4 ppm and 176.2 ppm most likely represent the carbons C6 and C7a. The other aromatic carbons and nitrate carbons are represented by the signals at 97.5, 111.9, 113.0, 115.0, 118.4, 125.4, 129.6, 130.7, 131.5, 132.0, 137.2 ppm.

11: 6-(4-Methylbenzyloxy)-2H-1-benzofuran-3-one

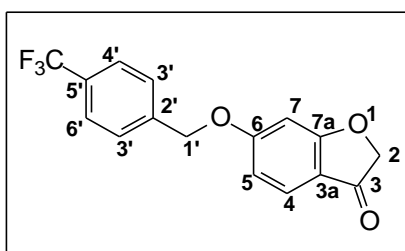
The title compound was prepared in a yield of 52%. mp 104.9–109.2 °C. ^1H NMR (600 MHz, CDCl_3) δ 7.55 (d, J = 8.6 Hz, 1H), 7.29 (d, J = 8.0 Hz, 2H), 7.20 (d, J = 7.8 Hz, 2H), 6.69 (dd, J = 8.6, 2.1 Hz, 1H), 6.59 (d, J = 2.1 Hz, 1H), 5.06 (s, 2H), 4.59 (s, 2H), 2.35 (s, 3H). ^{13}C NMR (151 MHz, CDCl_3) δ 21.2, 70.6, 75.5, 97.3, 112.2, 114.4, 125.1, 127.7, 129.4, 132.4, 138.3, 167.3, 176.4, 197.5. APCI-HRMS m/z : calcd for $\text{C}_{16}\text{H}_{15}\text{O}_3$ (MH^+), 255.1016, found 255.1003. Purity (HPLC): 58%.

^1H NMR	^{13}C NMR
<ul style="list-style-type: none"> The singlet at 5.06 ppm (2H) corresponds to the benzylic CH_2 protons at C1'. The singlet at 4.59 ppm (2H) corresponds to the coumaranone CH_2 protons at C2. The doublet at 7.29 ppm (2H) and the doublet at 7.20 ppm (2H) correspond to the phenyl protons at C3' and C4'. The doublet at 7.55 ppm (1H) corresponds to the coumaranone CH proton at C4. The small coupling constant indicates that the doublet at 6.59 ppm (1H) corresponds to the coumaranone CH proton at C7. The doublet of doublets at 6.69 ppm (1H) corresponds to the coumaranone CH proton at C5. The singlet at 2.35 ppm (3H) represents the methyl protons. 	<ul style="list-style-type: none"> The signals at 70.6 ppm and 75.5 ppm represent the aliphatic carbons C1' and C2, respectively. The signal at 197.5 ppm represents the carbonyl carbon C3. The signals at 167.3 ppm and 176.4 ppm most likely represent the carbons C6 and C7a. The other aromatic carbons are represented by the signals at 97.3, 112.2, 114.4, 125.1, 127.7, 129.4, 132.4, 138.3 ppm. The signal at 21.2 ppm represents the methyl carbon.

1m: 6-(3-Methylbenzyloxy)-2H-1-benzofuran-3-one

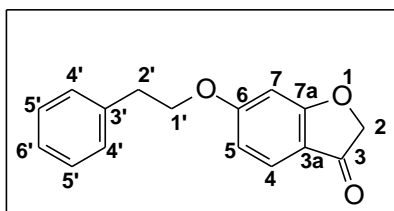
The title compound was prepared in a yield of 54%. mp 158.4–161.7 °C. ^1H NMR (600 MHz CDCl_3) δ 7.56 (d, J = 8.6 Hz, 1H), 7.15 (d, J = 7.5 Hz, 1H), 7.23 – 7.19 (m, 2H), 7.28 (t, J = 7.5 Hz, 1H), 6.71 (dd, J = 8.6, 2.1 Hz, 1H), 6.60 (d, J = 2.0 Hz, 1H), 5.07 (s, 2H), 4.60 (s, 2H), 2.36 (s, 3H). ^{13}C NMR (151 MHz, CDCl_3) δ 21.4, 70.7, 75.5, 97.4, 112.2, 114.5, 124.6, 125.1, 128.2, 128.6, 129.2, 135.4, 138.5, 167.3, 176.4, 197.6. APCI-HRMS m/z : calcd for $\text{C}_{16}\text{H}_{15}\text{O}_3$ (MH^+), 255.1016, found 255.1020. Purity (HPLC): 72%.

^1H NMR	^{13}C NMR
<ul style="list-style-type: none"> The singlet at 5.07 ppm (2H) corresponds to the benzylic CH_2 protons at C1'. The singlet at 4.60 ppm (2H) corresponds to the coumaranone CH_2 protons at C2. The signals at 7.15 ppm (1H), 7.23 ppm - 7.19 ppm (2H), and 7.28 ppm (1H) correspond to the phenyl protons at C3', C5', and C6'. The doublet at 7.56 ppm (1H) corresponds to the coumaranone CH proton at C4. The small coupling constant indicates that the doublet at 6.60 ppm (1H) corresponds to the coumaranone CH proton at C7. The doublet of doublets at 6.71 ppm (1H) corresponds to the coumaranone CH proton at C5. The singlet at 2.36 ppm (3H) represents the methyl protons. 	<ul style="list-style-type: none"> The signals at 70.7 ppm and 75.5 ppm represent the aliphatic carbons C1' and C2, respectively. The signal at 197.6 ppm represents the carbonyl carbon C3. The signals at 167.3 ppm and 176.4 ppm most likely represent the carbons C6 and C7a. The other aromatic carbons are represented by the signals at 97.4, 112.2, 114.5, 124.6, 125.1, 128.2, 128.6, 129.2, 135.4, 138.5 ppm. The signal at 21.4 ppm represents the methyl carbon.

1n: 6-[4-(Trifluoromethyl)benzyloxy]-2H-1-benzofuran-3-one

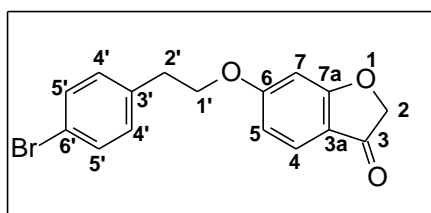
The title compound was prepared in a yield of 45%. mp 137.5–143.8 °C. ^1H NMR (600 MHz, CDCl_3) δ 7.65 (d, J = 8.1 Hz, 2H), 7.57 (d, J = 8.6 Hz, 1H), 7.53 (d, J = 8.0 Hz, 2H), 6.71 (dd, J = 8.6, 2.1 Hz, 1H), 6.58 (d, J = 2.1 Hz, 1H), 5.17 (s, 2H), 4.61 (s, 2H). ^{13}C NMR (151 MHz, CDCl_3) δ 69.6, 75.5, 97.5, 112.0, 114.9, 123.0, 124.8, 125.3, 125.7 (q), 127.4, 130.5 (q), 139.5, 166.7, 176.3, 197.5. APCI-HRMS m/z : calcd for $\text{C}_{16}\text{H}_{12}\text{F}_3\text{O}_3$ (MH^+), 309.0733, found 309.0720. Purity (HPLC): 82%.

^1H NMR	^{13}C NMR
<ul style="list-style-type: none"> The singlet at 5.17 ppm (2H) corresponds to the benzylic CH_2 protons at C1'. The singlet at 4.61 ppm (2H) corresponds to the coumaranone CH_2 protons at C2. The doublet at 7.53 ppm (2H) and the doublet at 7.65 ppm (2H) correspond to the phenyl protons at C3' and C4'. The doublet at 7.57 ppm (1H) corresponds to the coumaranone CH proton at C4. The small coupling constant indicates that the doublet at 6.58 ppm (1H) corresponds to the coumaranone CH proton at C7. The doublet of doublets at 6.71 ppm (1H) corresponds to the coumaranone CH proton at C5. 	<ul style="list-style-type: none"> The signals at 69.6 and 75.5 ppm represent the aliphatic carbons C1' and C2, respectively. The signal at 197.5 ppm represents the carbonyl carbon C3. The signals at 166.7 ppm and 176.3 ppm most likely represent the carbons C6 and C7a. The other aromatic carbons and CF_3 are represented by the signals at, 97.5, 112.0, 114.9, 123.0, 124.8, 125.3, 125.7 (q), 127.4, 130.5 (q), 139.5 ppm.

1o: 6-(2-Phenylethoxy)-2H-1-benzofuran-3-one

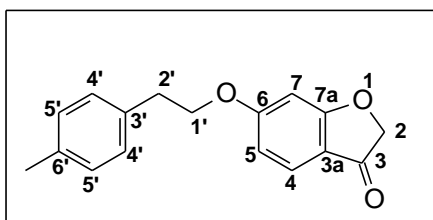
The title compound was prepared in a yield of 50%. mp 77.1–84.8 °C. ^1H NMR (600 MHz, CDCl_3) δ 7.53 (d, J = 8.6 Hz, 1H), 7.33 – 7.30 (m, 2H), 7.27 – 7.23 (m, 3H), 6.62 (dd, J = 8.6, 2.0 Hz, 1H), 6.51 (d, J = 2.0 Hz, 1H), 4.59 (s, 2H), 4.22 (t, J = 7.0 Hz, 2H), 3.11 (t, J = 7.0 Hz, 2H). ^{13}C NMR (151 MHz, CDCl_3) δ 35.4, 69.3, 75.5, 96.9, 112.0, 114.3, 125.1, 126.8, 128.6, 128.9, 137.5, 167.4, 176.5, 197.6. APCI- HRMS m/z : calcd for $\text{C}_{16}\text{H}_{15}\text{O}_3$ (MH^+), 255.1016, found 255.1011. Purity (HPLC): 100%.

^1H NMR	^{13}C NMR
<ul style="list-style-type: none"> The triplets at 4.22 ppm (2H) and 3.11 ppm (2H) corresponds to the CH_2 - CH_2 protons at C1' and C2'. The singlet at 4.59 ppm (2H) corresponds to the coumaranone CH_2 protons at C2. The multiplet at 7.33 ppm - 7.30 ppm (2H), and 7.27 ppm - 7.23 ppm (3H) correspond to the phenyl protons at C4', C5', and C6'. The doublet at 7.53 (1H) corresponds to the coumaranone CH proton at C4. The small coupling constant indicates that the doublet at 6.51 (1H) corresponds to the coumaranone CH proton at C7. The doublet of doublets at 6.62 (1H) corresponds to the coumaranone CH proton at C5. 	<ul style="list-style-type: none"> The signals at 35.4 ppm, 69.3 ppm, and 75.5 ppm represent the aliphatic carbons C2', C1' and C2, respectively. The signal at 197.5 ppm represents the carbonyl carbon C3. The signals at 167.4 ppm and 176.3 ppm most likely represent the carbons C6 and C7a. The other aromatic carbons are represented by the signals at 96.9, 112.0, 114.3, 125.1, 126.8, 128.6, 128.9, 137.5 ppm.

1p: 6-[2-(4-Bromophenyl)ethoxy]-2H-1-benzofuran-3-one

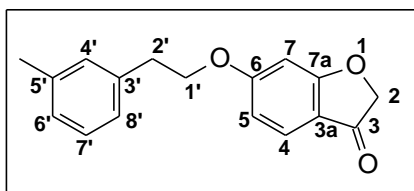
The title compound was prepared in a yield of 45%. mp 40.7–40.8 °C. ^1H NMR (600 MHz, CDCl_3) δ 7.53 (d, J = 8.6 Hz, 1H), 7.43 (d, J = 8.4 Hz, 2H), 7.14 (d, J = 8.4 Hz, 2H), 6.60 (dd, J = 8.6, 2.1 Hz, 1H), 6.49 (d, J = 2.0 Hz, 1H), 4.59 (s, 2H), 4.19 (t, J = 6.7 Hz, 2H), 3.06 (t, J = 6.7 Hz, 2H). ^{13}C NMR (151 MHz, CDCl_3) δ 34.8, 68.9, 75.5, 96.9, 111.9, 114.5, 120.6, 125.1, 130.7, 131.7, 136.6, 167.2, 176.4, 197.5. APCI-HRMS m/z : calcd for $\text{C}_{16}\text{H}_{14}\text{BrO}_3$ (MH^+), 333.0121, found 333.0129. Purity (HPLC): 100%.

^1H NMR	^{13}C NMR
<ul style="list-style-type: none"> The triplets at 4.19 ppm (2H) and 3.06 ppm (2H) corresponds to the $\text{CH}_2\text{-CH}_2$ protons at C1' and C2'. The singlet at 4.59 ppm (2H) corresponds to the coumaranone CH_2 protons at C2. The doublet at 7.14 ppm (2H) and the doublet at 7.43 ppm (2H) correspond to the phenyl protons at C4', and C5'. The doublet at 7.53 ppm (1H) corresponds to the coumaranone CH proton at C4. The small coupling constant indicates that the doublet at 6.49 ppm (1H) corresponds to the coumaranone CH proton at C7. The doublet of doublets at 6.60 ppm (1H) corresponds to the coumaranone CH proton at C5. 	<ul style="list-style-type: none"> The signals at 34.8 ppm, 68.9 ppm, and 75.5 ppm represent the aliphatic carbons C2', C1' and C2, respectively. The signal at 197.5 ppm represents the carbonyl carbon C3. The signals at 167.2 ppm and 176.4 ppm most likely represent the carbons C6 and C7a. The other aromatic carbons are represented by the signals at 96.9, 111.9, 114.5, 120.6, 125.1, 130.7, 131.7, 136.6 ppm.

1q: 6-[2-(4-Methylphenyl)ethoxy]-2H-1-benzofuran-3-one

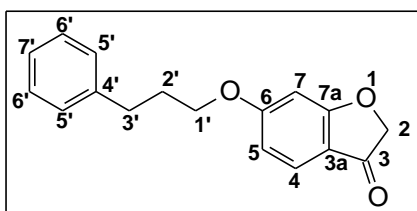
The title compound was prepared in a yield of 56%. mp 98.6–104.2 °C. ^1H NMR (600 MHz, CDCl_3) δ 7.53 (d, J = 8.6 Hz, 1H), 7.15 (d, J = 8.1 Hz, 2H), 7.12 (d, J = 8.0 Hz, 2H), 6.62 (dd, J = 8.6, 2.1 Hz, 1H), 6.50 (d, J = 2.0 Hz, 1H), 4.59 (s, 2H), 4.19 (t, J = 7.1 Hz, 2H), 3.07 (t, J = 7.0 Hz, 2H), 2.32 (s, 3H). ^{13}C NMR (151 MHz, CDCl_3) δ 21.0, 35.0, 69.5, 75.5, 96.8, 112.0, 114.3, 125.1, 128.8, 129.3, 134.3, 136.3, 167.4, 176.5, 197.6. APCI-HRMS m/z : calcd for $\text{C}_{17}\text{H}_{17}\text{O}_3$ (MH^+), 269.1172, found 269.1159. Purity (HPLC): 85%.

^1H NMR	^{13}C NMR
<ul style="list-style-type: none"> The triplets at 4.19 ppm (2H) and 3.07 ppm (2H) corresponds to the CH_2- CH_2 protons at C1' and C2'. The singlet at 4.59 ppm (2H) corresponds to the coumaranone CH_2 protons at C2. The doublet at 7.15 ppm (2H) and the doublet at 7.12 ppm (2H) correspond to the phenyl protons at C4' and C5'. The doublet at 7.53 ppm (1H) corresponds to the coumaranone CH proton at C4. The small coupling constant indicates that the doublet at 6.50 ppm (1H) corresponds to the coumaranone CH proton at C7. The doublet of doublets at 6.62 ppm (1H) corresponds to the coumaranone CH proton at C5. 	<ul style="list-style-type: none"> The signals at 35.0 ppm, 69.5 ppm, and 75.5 ppm represent the aliphatic carbons C2', C1' and C2, respectively. The signal at 197.6 ppm represents the carbonyl carbon C3. The signals at 167.4 ppm and 176.5 ppm most likely represent the carbons C6 and C7a. The other aromatic carbons are represented by the signals at 96.8, 112.0, 114.3, 125.1, 128.8, 129.3, 134.3, 136.3 ppm. The signal 21.0 ppm corresponds to the methyl carbon.

1r: 6-[2-(3-Methylphenyl)ethoxy]-2H-1-benzofuran-3-one

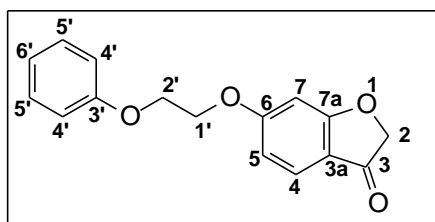
The title compound was prepared in a yield of 66%. mp 209.3–212.2 °C. ^1H NMR (600 MHz, CDCl_3) δ 7.54 (d, J = 8.6 Hz, 1H), 7.20 (t, J = 7.5 Hz, 1H), 7.09–7.04 (m, 3H), 6.63 (dd, J = 8.6, 2.0 Hz, 1H), 6.51 (d, J = 2.0 Hz, 1H), 4.60 (s, 2H), 4.20 (t, J = 7.1 Hz, 2H), 3.07 (t, J = 7.1 Hz, 2H), 2.33 (s, 3H). ^{13}C NMR (151 MHz, CDCl_3) δ 21.4, 35.3, 69.4, 75.5, 96.9, 112.0, 114.3, 125.1, 125.9, 127.5, 128.5, 129.7, 137.3, 138.2, 167.4, 176.5, 197.6. APCI-HRMS m/z : calcd for $\text{C}_{17}\text{H}_{17}\text{O}_3$ (MH^+), 269.1172, found 269.1159. Purity (HPLC): 91%.

^1H NMR	^{13}C NMR
<ul style="list-style-type: none"> The triplets at 4.20 ppm (2H) and 3.07 ppm (2H) corresponds to the CH_2 - CH_2 protons at C1' and C2'. The singlet at 4.60 ppm (2H) corresponds to the coumaranone CH_2 protons at C2. The triplet at 7.20 ppm (1H) and the multiplet at 7.04 – 7.09 ppm (3H) correspond to the phenyl protons at C4', C6' and C7'. The doublet at 7.54 (1H) corresponds to the coumaranone CH proton at C4. The small coupling constant indicates that the doublet at 6.51 (1H) corresponds to the coumaranone CH proton at C7. The doublet of doublets at 6.63 (1H) corresponds to the coumaranone CH proton at C5. 	<ul style="list-style-type: none"> The signals at 69.4 ppm, 35.3 ppm and 75.5 ppm represent the aliphatic carbons C1', C2' and C2, respectively. The signal at 197.6 ppm represents the carbonyl carbon C3. The signals at 167.4 ppm and 176.5 ppm most likely represent the carbons C6 and C7a. The other aromatic carbons are represented by the signals at 96.9, 112.0, 114.3, 125.1, 125.9, 127.5, 128.5, 129.7, 137.3, 138.2 ppm. The signal at 21.4 ppm corresponds to the methyl carbon.

1s: 6-(3-Phenylpropoxy)-2H-1-benzofuran-3-one

The title compound was prepared in a yield of 53%. mp 84.4–96.7 °C. ^1H NMR (600 MHz CDCl_3) δ 7.54 (d, J = 8.6 Hz, 1H), 7.30–7.27 (m, 2H), 7.21–7.18 (m, 3H), 6.63 (dd, J = 8.6, 2.1 Hz, 1H), 6.48 (d, J = 2.0 Hz, 1H), 4.59 (s, 2H), 3.99 (t, J = 6.3 Hz, 2H), 2.80 (t, J = 7.6 Hz, 2H), 2.16–2.09 (m, 2H). ^{13}C NMR (151 MHz, CDCl_3) δ 30.3, 31.9, 67.6, 75.5, 96.8, 112.0, 114.2, 125.0, 126.1, 128.4, 128.5, 140.9, 167.6, 176.5, 197.5. APCI-HRMS m/z : calcd for $\text{C}_{17}\text{H}_{17}\text{O}_3$ (MH^+), 269.1172, found 269.1180. Purity (HPLC): 76%.

^1H NMR	^{13}C NMR
<ul style="list-style-type: none"> The triplets at 3.99 ppm (2H) and 2.80 ppm (2H) and the multiplet at 2.09 ppm - 2.16 ppm corresponds to the $(\text{CH}_2)_3$ protons at C1', C2' and C3'. The singlet at 4.59 ppm (2H) corresponds to the coumaranone CH_2 protons at C2. The triplet at 7.21 ppm - 7.18 ppm (3H) and the multiplet at 7.27 ppm - 7.30 ppm (2H) correspond to the phenyl protons at C5', C6' and C7'. The doublet at 7.54 ppm (1H) corresponds to the coumaranone CH proton at C4. The small coupling constant indicates that the doublet at 6.48 ppm (1H) corresponds to the coumaranone CH proton at C7. The doublet of doublets at 6.63 ppm (1H) corresponds to the coumaranone CH proton at C5. 	<ul style="list-style-type: none"> The signals at 30.3 ppm, 31.9 ppm, 67.6 ppm and 75.5 ppm represent the aliphatic carbons C3', C2', C1' and C2, respectively. The signal at 197.5 ppm represents the carbonyl carbon C3. The signals at 167.6 ppm and 176.5 ppm most likely represent the carbons C6 and C7a. The other aromatic carbons are represented by the signals at 96.8, 112.0, 114.2, 125.0, 126.1, 128.4, 128.5, 140.9 ppm.

1t: 6-(2-Phenoxyethoxy)-2H-1-benzofuran-3-one

The title compound was prepared in a yield of 53%. mp 156.2–158.2 °C. ^1H NMR (600 MHz, CDCl_3) δ 7.56 (d, J = 8.6 Hz, 1H), 7.30 (td, J = 7.4, 2.0 Hz, 2H), 6.97 (t, J = 7.4 Hz, 1H), 6.94 (d, J = 7.9 Hz, 2H), 6.68 (dd, J = 8.6, 2.1 Hz, 1H), 6.58 (d, J = 2.0 Hz, 1H), 4.62 (s, 2H), 4.39–4.36 (m, 2H), 4.35–4.33 (m, 2H). ^{13}C NMR (151 MHz, CDCl_3) δ 65.9, 67.2, 75.5, 97.1, 112.0, 114.6, 114.6, 121.3, 125.2, 129.6, 158.3, 167.1, 176.4, 197.6. APCI-HRMS m/z : calcd for $\text{C}_{16}\text{H}_{15}\text{O}_4$ (MH^+), 271.0965, found 271.0953. Purity (HPLC): 100%.

^1H NMR	^{13}C NMR
<ul style="list-style-type: none"> The multiplets at 4.35 ppm – 4.33 ppm (2H) and 4.39 ppm – 4.36 ppm (2H) corresponds to the CH_2- CH_2 protons at C1' and C2'. The singlet at 4.62 ppm (2H) corresponds to the coumaranone CH_2 protons at C2. The signals at 7.30 ppm (2H), 6.97 ppm (1H), and 6.94 ppm (2H) correspond to the phenyl protons at C4', C5' and C6'. The doublet at 7.56 ppm (1H) corresponds to the coumaranone CH proton at C4. The small coupling constant indicates that the doublet at 6.59 ppm (1H) corresponds to the coumaranone CH proton at C7. The doublet of doublets at 6.68 ppm (1H) corresponds to the coumaranone CH proton at C5. 	<ul style="list-style-type: none"> The signals at 67.2 ppm, 65.9 ppm and 75.5 ppm represent the aliphatic carbons C1', C2' and C2, respectively. The signal at 197.6 ppm represents the carbonyl carbon C3. The signals at 158.3 ppm, 167.1 ppm and 176.4 ppm most likely represent the carbons C3', C6 and C7a. The other aromatic carbons are represented by the signals at 97.1, 112.0, 114.6, 114.6, 121.3, 125.2, 129.6 ppm.

3.6 Mass spectrometry

The 3-coumaranone derivatives that were synthesised in this study were also characterised by mass spectrometry. The calculated and experimental molecular masses were determined and are given in the table below. The small differences between the calculated and experimental masses indicate that the structures correspond to those given in table 3.1. To illustrate the difference between the calculated and experimental molecular masses, the variation in parts per million (ppm) are given in the table 3.2. The ppm values were determined as follows:

$$\text{ppm} = \left[\frac{\text{found} - \text{calculated}}{\text{calculated}} \right] \times 1000000$$

The mass spectra were recorded in APCI mode with positive ionization. The masses thus recorded are those of the parent ion, carrying a positive charge as a result of protonation. The masses provided in Table 3.2 are thus $[M+1]^+$. In general, a ppm difference smaller than 5 is considered to be good agreement.

Table 3.2 The mass spectrometric data for the 3-coumaranone derivatives, **1a-t**.

COMPOUND	CALCULATED	FOUND	FORMULA [M+1] ⁺	ppm
1a	241.0859	241.0852	C ₁₅ H ₁₃ O ₃	-2.904
1b	259.0765	259.0764	C ₁₅ H ₁₂ FO ₃	-0.386
1c	259.0765	259.0752	C ₁₅ H ₁₂ FO ₃	-5.018
1d	275.0469	275.0452	C ₁₅ H ₁₂ ClO ₃	-3.999
1e	275.0469	275.0453	C ₁₅ H ₁₂ ClO ₃	-5.817
1f	318.9964	318.9963	C ₁₅ H ₁₂ BrO ₃	-0.314
1g	318.9964	318.9955	C ₁₅ H ₁₂ BrO ₃	-2.821
1h	366.9826	366.9805	C ₁₅ H ₁₂ IO ₃	-5.722
1i	366.9826	366.9809	C ₁₅ H ₁₂ IO ₃	-1.907
1j	266.0812	266.0812	C ₁₆ H ₁₂ NO ₃	0.000
1k	266.0812	266.0797	C ₁₆ H ₁₂ NO ₃	-5.637
1l	255.1016	255.1003	C ₁₆ H ₁₅ O ₃	-5.096
1m	255.1016	255.1020	C ₁₆ H ₁₅ O ₃	1.586
1n	309.0733	309.0720	C ₁₆ H ₁₂ F ₃ O ₃	-4.206
1o	255.1016	255.1011	C ₁₆ H ₁₅ O ₃	-1.960
1p	333.0121	333.0129	C ₁₆ H ₁₄ BrO ₃	-2.402
1q	269.1172	269.1159	C ₁₇ H ₁₇ O ₃	-4.831
1r	269.1172	269.1159	C ₁₇ H ₁₇ O ₃	-4.831
1s	269.1172	269.1180	C ₁₇ H ₁₇ O ₃	-1.858
1t	271.0965	271.0953	C ₁₆ H ₁₅ O ₄	-4.427

3.7 Interpretation of HPLC analysis

The chromatograms obtained for the synthesised compounds are given in the addendum. HPLC analysis was used to determine the purity of the synthesised compounds. Under strong eluting conditions most of compounds present in the samples are expected to elute. Furthermore, at a wavelength of 254 nm and 210 nm, most of the compounds are expected to absorb and therefore detectable. Most of the analysed compounds showed a high degree of purity with a single major peak for each compound. If additional peaks occurred, the percentage purities were calculated based on the integrated areas of the analyte and impurity peaks. The purities of the 3-coumaranone derivatives, **1a-t**, were thus estimated to be 57-100%. The only two compounds that may have relatively low purities are **1l** and **1s**. Since the NMR spectra of these compounds appeared to be free of contaminating compounds, the origin of these impurities in the HPLC traces is unknown.

3.8 Conclusion

This chapter describes the successful synthesis of twenty 3-coumaranone derivatives. The structures of the synthesised compounds were characterised and confirmed by NMR and MS analyses. The structures of these compounds correlate to the ^1H NMR and ^{13}C NMR spectra, and their experimentally determined masses correspond with the calculated masses. HPLC analyses were used to determine the purity of the compounds and a single major peak was observed for most compounds analysed. The only two compounds that may have relatively low purities are **1l** and **1s**. Therefore it can be concluded that at least 18 of the twenty synthesised compounds are of an acceptable degree of purity. In the next chapter, the MAO inhibition properties of the 3-coumaranone derivatives will be investigated.

CHAPTER 4

ENZYMOLGY

4.1 Introduction

In this chapter, the series of 3-coumaronone derivatives (**1a-t**) synthesised in chapter 3, will be investigated as inhibitors of human MAO-A and MAO-B. As discussed in chapter 2, there are several methods for measuring MAO activity *in vitro*. In this study, fluorescence spectrophotometry was used to determine the IC₅₀ values of the newly synthesised compounds. The inhibition assay uses kynuramine as substrate, and MAO-A and MAO-B oxidise kynuramine to yield 4-hydroxyquinoline. 4-Hydroxyquinoline is a metabolite, which fluoresces at an excitation wavelength of 310 nm and an emission wavelength of 400 nm. The formation of 4-hydroxyquinoline can be measured in the presence of the test inhibitors since it was established that the 3-coumaronone derivatives do not fluoresce under these assay conditions. The MAO activity measurements in the presence of the test inhibitors were used to construct sigmoidal dose-response curves from which the inhibition potencies, the corresponding IC₅₀ values, were calculated.

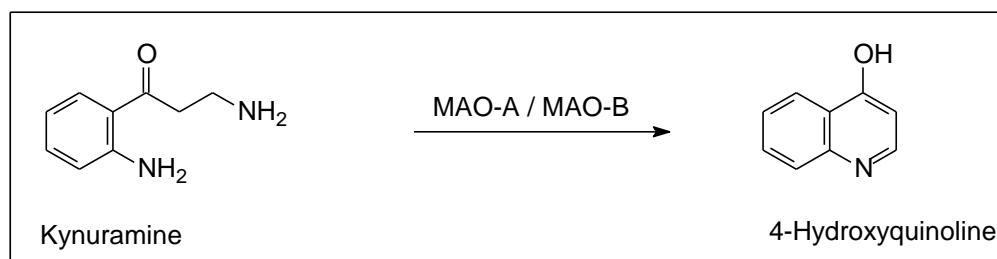


Figure 4.1. Oxidative deamination of kynuramine by MAO-A and MAO-B to yield 4-hydroxyquinoline.

4.2 MAO activity measurements

4.2.1 General background

In this study kynuramine was used as enzyme substrate. Kynuramine is a non-specific substrate of both MAO-A and MAO-B. Kynuramine has a characteristic ultraviolet light absorption spectrum with a maximum at 366 nm. Through enzymatic degradation an aldehyde is produced, which subsequently undergoes ring-closure to form 4-hydroxyquinoline. 4-Hydroxyquinoline exhibits no absorption at 366 nm, but absorbs light at a wavelength of 310 nm. In contrast to kynuramine, 4-hydroxyquinoline also is fluorescent in alkaline media. MAO activity may thus be monitored spectrophotometrically by the disappearance of kynuramine (366 nm) or the appearance of 4-hydroxyquinoline (310 nm).

Rapid and reliable assays have been developed according to these findings, which will be used in this study to determine whether the synthesised derivatives exhibit any MAO-A and MAO-B inhibition activities (Weissbach *et al.*, 1960).

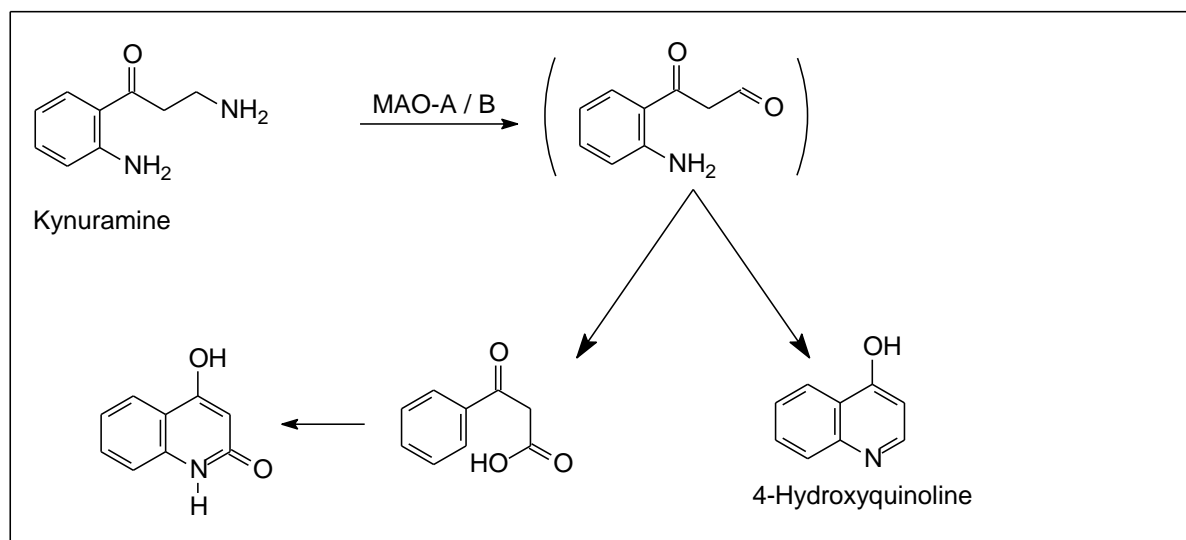


Figure 4.2. Kynuramine is oxidatively deaminated by MAO to yield 4-hydroxyquinoline (Nicotra & Parvez, 1999).

The first step of the oxidative deamination catalysed by MAO, is the formation of an aldehyde. The aldehyde can then either condense to yield the 4-hydroxyquinoline or it can generate an acid or 2,4-dihydroxyquinoline by undergoing further oxidation (Figure 4.2). Evidence show that the non-enzymatic condensation of the aldehyde occurs faster than the further oxidation to the acid or 2,4-dihydroxyquinoline (Weissbach *et al.*, 1960).

4.2.2 Chemicals and instrumentation

In this study a Varian Eclipse fluorescence spectrophotometer was employed for the fluorometric measurements. Kynuramine.2HBr as well as insect cell microsomes containing recombinant human MAO-A and MAO-B (5 mg/ml) were obtained from Sigma-Aldrich. The Graphpad Prism 5 software package was used to create sigmoidal dose-response curves and to establish the IC_{50} values of the test inhibitors.

4.2.3 Experimental method for determining IC_{50} values

The IC_{50} values were determined for the inhibition of MAO-A and MAO-B by the 3-coumaronone derivatives (**1a–t**). The IC_{50} values are measures of the MAO-A/B inhibition potencies of the test compounds. To determine the MAO-A and MAO-B inhibition potency of each compound, sigmoidal dose-response curves were constructed, and the IC_{50} values were calculated using the Prism software package. The lowest IC_{50} value indicates the most potent inhibitor.

Preparation of inhibitors	<ul style="list-style-type: none"> • Prepare 10 mM concentrations of various compounds in DMSO • Dilute the 10 mM solutions to 1 μM using DMSO • Prepare test inhibitors from the 1 μM concentration (0-100 μM) using DMSO
K₂HPO₄ / KH₂PO₄ Buffer	<ul style="list-style-type: none"> • 92 μl Potassium phosphate buffer 100 mM, pH 7.4, made isotonic with KCl 20.2 mM
Enzyme and Substrate concentration	<ul style="list-style-type: none"> • MAO-A 0.03 mg/ml and 200 μM kynuramine • MAO-B 0.06mg/ml and 200 μM kynuramine
Preparation of incubations	<ul style="list-style-type: none"> • To the 92 μl K₂HPO₄/KH₂PO₄ buffer add: • 8 μl of various test inhibitors to yield concentrations of 0–100 μM • 50 μl kynuramine (200 μM)
Incubation	<ul style="list-style-type: none"> • Incubate for 30 min at 37 °C
Enzyme addition and termination of reaction	<ul style="list-style-type: none"> • Add 50 μl of MAO-A (0.03 mg/ml) or MAO-B (0.06 mg/ml) • Incubate for 20 min at 37 °C • Terminate by adding 80 μl NaOH (2N)
Fluorescence measurements	<ul style="list-style-type: none"> • Measure MAO-generated 4-hydroxyquinoline concentrations • At excitation wavelength of 310 nm and emission wavelength of 400 nm
Quantative estimations	<ul style="list-style-type: none"> • Construct a linear calibration curve containing the following: 0.047–1.560 μM 4-hydroxyquinoline in K₂PO₄ buffer • Add 80 μl NaOH to each calibration.
Calculate IC₅₀ values	<ul style="list-style-type: none"> • Plot initial rate of kynuramine oxidation vs. the logarithm of inhibitor concentration • Determine IC₅₀ values in triplicate and express as mean \pm SD

Figure 4.3. Flow-diagram summarizing the experimental method for IC₅₀ determination.

All enzymatic reactions were carried out in polypropylene 96-well microtiter plates. The enzymatic reactions contained the following:

- 92 μl potassium phosphate buffer (100 mM, pH 7.4, and KCl 20.2 mM)
- 50 μl kynuramine as substrate with a final concentration of 50 μM for both MAO-A/B.
- 8 μl of the test inhibitors with a final concentration of 0–100 μM .
- The stock solutions of the inhibitors were prepared in 4% DMSO.

The reactions were prepared and incubated for 30 min at 37 °C. After incubation, the enzyme (50 μl) was added. The final concentration of MAO-A was 0.0075 mg/ml, and of MAO-B was 0.015 mg/ml. A second incubation of 20 min occurred after the 50 μl of enzyme were added. The reactions were terminated with the addition of 80 μl of NaOH (2 N). The concentration measurements of 4-hydroxyquinoline were carried out spectrofluorometrically at an excitation wavelength of 310 nm and an emission wavelength of 400 nm.

Quantitative estimations of 4-hydroxyquinoline in the various enzymatic reactions were made with a linear calibration curve. The curve was constructed from known concentrations of 4-hydroxyquinoline (0.047–1.50 μM) dissolved in potassium phosphate buffer to a final volume of 200 μl . To each calibration standard, 80 μl of NaOH (2 N) was added. To provide confirmation that the test inhibitors do not fluoresce, control samples were included. The control samples contained 1.50 μM of 4-hydroxyquinoline and 100 μM of the test inhibitor. 80 μl NaOH was added to each control sample. The calibration curve values that were obtained should bracket the obtained fluorescence values for the inhibition studies and it should also display linearity.

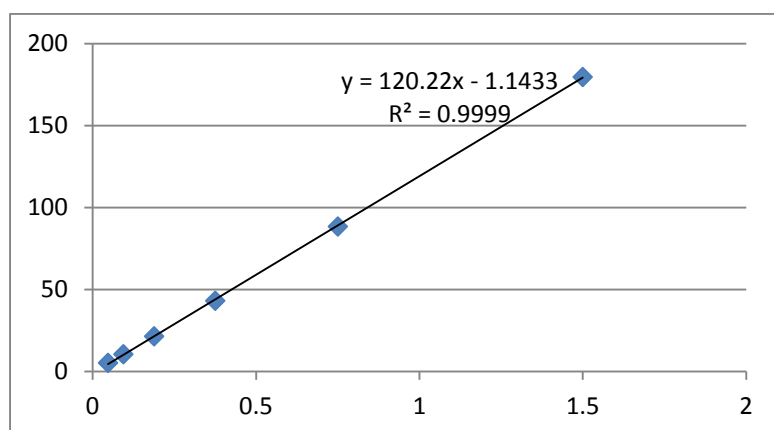


Figure 4.4 An example of a calibration curve routinely constructed in this study. The graph is that of fluorescence intensity (FL) of 4-hydroxyquinoline versus the concentration of authentic 4-hydroxyquinoline (4-HQ), expressed in micromolar.

4.2.4 Results - IC₅₀ values

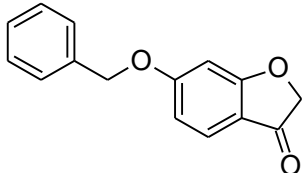
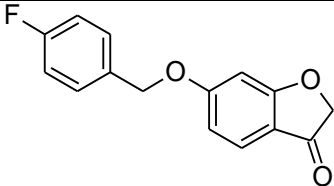
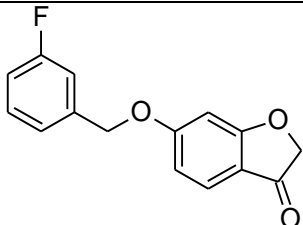
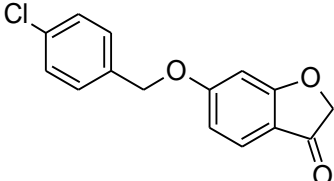
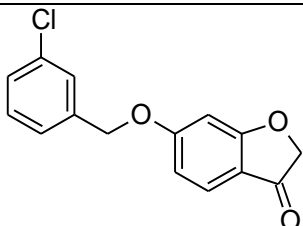
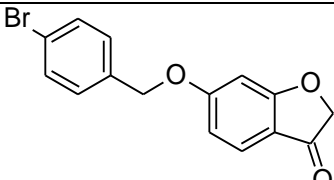
The results of the MAO inhibition studies are given in Table 4.1. From the inhibition data the following observations may be made:

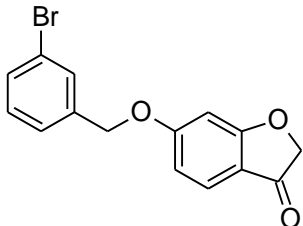
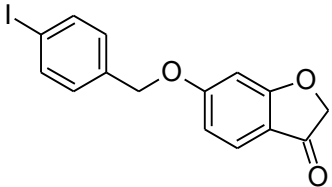
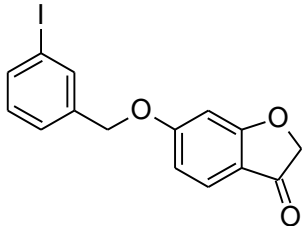
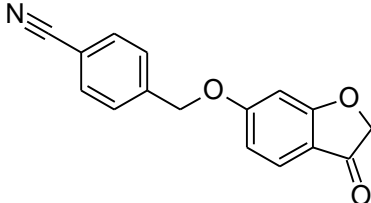
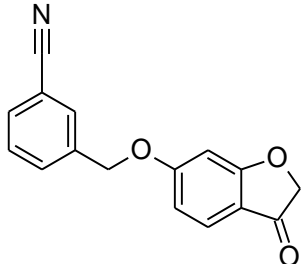
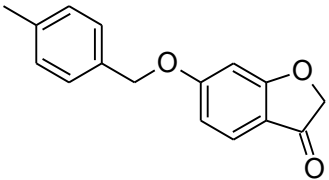
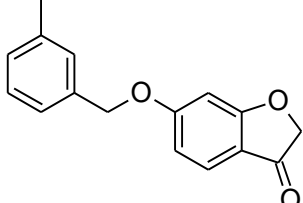
- *The 3-coumaronone derivatives are selective for MAO-B over the MAO-A isoform.* In all instances, the 3-coumaronone derivatives are more potent MAO-B inhibitors than MAO-A inhibitors. The most selective inhibitors are compounds **1h**, **1l**, **1n** and **1t**, which did not inhibit MAO-A, even at a maximal concentration of 100 μ M.
- *Potent MAO-A inhibitors have been discovered.* Although the 3-coumaronone derivatives are selective for the MAO-B isoform, potent MAO-A inhibitors have been discovered. For example, compound **1k** inhibits MAO-A with an IC₅₀ value of 0.586 μ M. This value is in the submicromolar range and may thus be viewed as potent inhibition. For comparison, tolloxatone, a clinically used MAO-A inhibitor exhibits a reported IC₅₀ value of 3.92 μ M under identical conditions (Petzer *et al.*, 2013). Compound **1k** is thus a more potent MAO-A inhibitor than tolloxatone.
- *The 3-coumaronone derivatives are highly potent MAO-B inhibitors.* Based on the IC₅₀ values of the 3-coumaronone derivatives that are in the submicromolar range, this class of compounds is potent MAO-B inhibitors. For the 3-coumaronone derivatives, the IC₅₀ values for the inhibition of MAO-B ranged from 0.004–0.564 μ M. The most potent MAO-B inhibitor discovered is compound **1g**, with an IC₅₀ value of 0.004 μ M. For comparison, lazabemide, a reference MAO-B inhibitor exhibits a reported IC₅₀ value of 0.091 μ M under identical conditions (Petzer *et al.*, 2013). Compound **1g** is thus a more potent MAO-B inhibitor than lazabemide. Other highly potent MAO-B inhibitors with IC₅₀ values < 0.020 μ M were also discovered, and are **1d-f** and **1i**. Even the weakest 3-coumaronone MAO-B inhibitor, compound **1k** with an IC₅₀ value of 0.564 μ M, may be viewed as a potent inhibitor.
- *Structure-activity relationships for the benzyloxy-substituted derivatives.* Since all of the 3-coumaronone derivatives are potent MAO-B inhibitors, few clear SARs are apparent. For the benzyloxy-substituted derivatives (**1a-n**), no clear correlation between the position (*meta* or *para*) of the substituent on the benzyloxy ring and MAO-B inhibition potency is apparent, and high potency inhibitors are represented by compounds substituted on both the *meta* and *para* positions of the benzyloxy ring. Definitive correlations between the nature (alkyl and halogen) of the substituent and MAO-B inhibition potency also are not apparent, and high potency inhibitors are represented by compounds substituted with halogens (F, Cl, Br, I) and alkyl groups (CH₃, CN, CF₃) on the benzyloxy ring. It is, however, noticeable that among the 5 most potent MAO-B inhibitors, the four compounds containing chlorine or bromine as substituents are

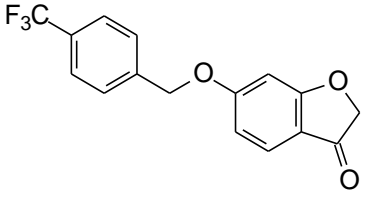
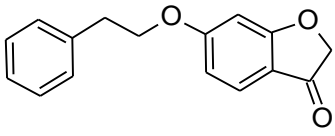
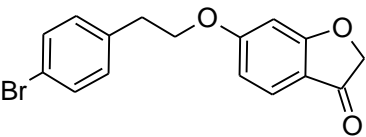
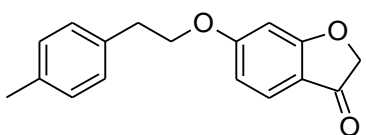
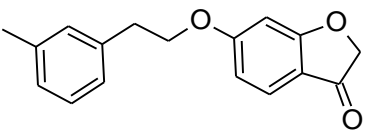
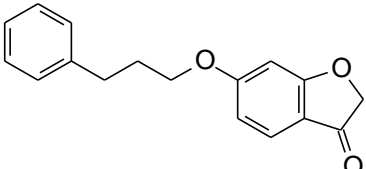
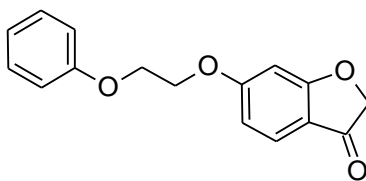
included. As for MAO-B, no clear correlation between the position (*meta* or *para*) or nature (alkyl and halogen) of the substituent and MAO-A inhibition potency is apparent. Since only one of the 20 derivatives, compound **1k**, inhibited MAO-A with an IC_{50} value in the submicromolar range, this particular substitute pattern (the 3-CN group) on the benzyloxy ring is more appropriate for MAO-A inhibition than the others considered in this study.

- *Structure-activity relationships for the phenylethoxy-substituted derivatives.* It is interesting that the phenylethoxy-substituted 3-coumaronone derivatives, compounds **1o-r**, exhibit reduced MAO-B inhibition potency compared to the benzyloxy-substituted compounds. In this respect, bromine in *para* position and methyl substitution on the *meta* position reduce MAO-B inhibition potency (compared to **1o**). The unsubstituted homologue, compound **1o** and the methyl (*para*) substituted homologue, **1q**, exhibit the most potent MAO-B inhibition of the series. Although clear SARs for the inhibition of MAO-A are not apparent, it is noteworthy that the bromine substituted homologue is the most potent MAO-A inhibitor among the phenylethoxy-substituted 3-coumaronone derivative.
- *Effect of the length of the C5 substituent.* Increasing the length of the C5 substituent from benzyloxy (**1a**) to phenylethoxy (**1o**) to phenylpropoxy (**1s**) enhances MAO-A inhibition potency. This suggests that for 3-coumaronone derivatives, a larger C5 side chain is more appropriate for MAO-A inhibition, at least with respect to chain length. For MAO-B inhibition, a clear trend is not apparent, since the benzyloxy- and phenylpropoxy-substituted derivatives are more potent than the phenylethoxy-substituted derivative. Among these three homologues, the phenylpropoxy-substituted derivative is the most potent MAO-B inhibitor with an IC_{50} value of 0.055 μ M.
- *Effect of the phenoxyethoxy substituent.* For the inhibition of MAO-B, the phenoxyethoxy-substituted derivative, **1t** (IC_{50} = 0.050 μ M), may be viewed as equipotent to the phenylpropoxy-substituted derivative **1s** (IC_{50} = 0.055 μ M). For the inhibition of MAO-B, the phenoxy oxygen may thus be viewed as isosteric with the CH_2 of the phenylpropoxy substituent. The phenoxyethoxy-substituted derivative, in contrast, is not an inhibitor of MAO-A, up to a maximal tested concentration of 100 μ M. Since the phenylpropoxy-substituted derivative **1s** is a MAO-A inhibitor with an IC_{50} value of 11.8 μ M, it may thus be concluded that the phenoxy oxygen reduces MAO-A inhibition activity.

Table 4.1. The IC₅₀ values (provided in μM) for the inhibition of human MAO-A and MAO-B by the 3-coumaronone derivatives **1a-t**.

Compound	Structure	IC ₅₀ (mean \pm SD), μM^a		
		MAO-A	MAO-B	SI
1a		26.7 \pm 0.351	0.062 \pm 0.011	430
1b		11.4 \pm 2.54	0.022 \pm 0.003	518
1c		80.7 \pm 9.22	0.136 \pm 0.030	593
1d		2.19 \pm 0.135	0.019 \pm 0.007	115
1e		18.7 \pm 7.82	0.012 \pm 0.003	1561
1f		2.80 \pm 0.079	0.016 \pm 0.003	172

1g		3.92 ± 0.827	0.004 ± 0.001	981
1h		$>100^b$	0.028 ± 0.006	
1i		7.57 ± 1.82	0.007 ± 0.001	1082
1j		5.01 ± 0.919	0.079 ± 0.019	63.39
1k		0.586 ± 0.133	0.166 ± 0.015	3.5
1l		$>100^b$	0.054 ± 0.011	
1m		62.0 ± 16.9	0.096 ± 0.003	646

1n		>100 ^b	0.039 ± 0.005	
1o		13.8 ± 2.11	0.107 ± 0.010	128
1p		2.65 ± 0.629	0.564 ± 0.049	4
1q		11.3 ± 0.683	1.05 ± 0.147	11
1r		25.9 ± 8.72	0.181 ± 0.021	143
1s		11.8 ± 0.930	0.055 ± 0.008	214
1t		>100 ^b	0.050 ± 0.006	

All values expressed as the mean ± SD of triplicate determinations.

^a Selectivity index (SI) = IC₅₀(MAO-A)/IC₅₀(MAO-B), which is indicative of the extent to which the inhibitor is more selective for MAO-B compared to MAO-A.

^b No inhibition observed at maximum tested concentration of 100 μM.

4.2.5 Experimental method for the determination of the reversibility of inhibition

To evaluate the reversibility of inhibition, the recovery of enzyme activities after dialysis of the enzyme-inhibitor complexes was examined (Petzer *et al.*, 2012). For the purpose of this study, MAO-B and a selected test inhibitor, compound **1g** was pre-incubated for 15 min at 37 °C. The inhibitor concentration was equal to $4 \times IC_{50}$ value. The reactions were subsequently placed into hydrated dialysis cassettes and dialysed for 20–25 h at 4 °C in 80 ml sucrose buffer. After dialysis, the residual MAO-B activities were measured by adding kynuramine to the dialysed mixtures. After 20 min of incubation, the 4-hydroxyquinoline generated from the MAO-B-catalysed oxidation of kynuramine was quantified by fluorescence spectrophotometry. The MAO-B activities in the dialysed and non-dialysed enzyme inhibitor complexes were recorded and compared to determine whether the selected compound **1g** is a reversible MAO-B inhibitor. For comparison, similar experiments with the irreversible MAO-B inhibitors were also carried out.

The reversibility of MAO inhibition by **1g** was examined by dialysis. Slide-A-Lyzer dialysis cassettes (Thermo Scientific) with a molecular weight cut-off of 10 000 and a sample volume capacity of 0.5–3 ml were used. The test inhibitor, at a concentration equal to fourfold the IC_{50} value for the inhibition of MAO-B ($4 \times 0.004 \mu\text{M}$), and MAO-B (0.3 mg/ml) were combined. These mixtures with a final volume of 0.8 mL was prepared in a potassium phosphate buffer (100 mM, pH 7.4, 5% sucrose), and contained 4% DMSO as co-solvent. The enzyme reactions were pre-incubated for 15 min at 37 °C. As controls, MAO-B was similarly pre-incubated in the presence of an irreversible inhibitor, (R)-deprenyl, as well as in the absence of the inhibitor. The concentration of (R)-deprenyl [$IC_{50}(\text{MAO-B}) = 0.079 \mu\text{M}$] employed was equal to fourfold its reported IC_{50} value for the inhibition of MAO-B. The enzyme-inhibitor mixtures were subsequently dialysed in 80 ml of dialysis buffer (100 mM potassium phosphate, pH 7.4, 5% sucrose) at 4 °C. After the start of dialysis, the dialysis buffer was replaced every 3 h and 7 h. At 24 h after the start of the dialysis, the reactions were diluted twofold with the addition of kynuramine (dissolved in potassium phosphate buffer, 100 mM, pH 7.4, made isotonic with KCl). The final inhibitor concentration in these reactions was equal to twofold its IC_{50} value, and the final kynuramine concentration was 50 μM . These reactions were incubated for 20 min at 37 °C and were subsequently terminated by the addition of 400 μl NaOH. Distilled water (1000 μl) was added to each reaction to make up the final volume. Concentration measurements of 4-hydroxyquinoline in each incubation were carried out spectrofluorometrically by measuring the fluorescence of the supernatant at an excitation wavelength of 310 nm and an emission wavelength of 400 nm. For comparison, undialysed mixtures of MAO-B and the test inhibitor were maintained at 4 °C over the same time period.

Quantitative estimations were made with a linear calibration curve. This linear calibration curve was constructed with known amounts (0.047–1.56 μM) of 4-hydroxyquinoline dissolved in 500 μl potassium phosphate buffer (100 mM, pH 7.4, made isotonic with KCl 20.2 mM). To each calibration standard, volumes of 400 μl NaOH (2 N) and 1000 μl water were added. All reactions were carried out in triplicate and the residual enzyme catalytic rates were expressed as mean \pm SD.

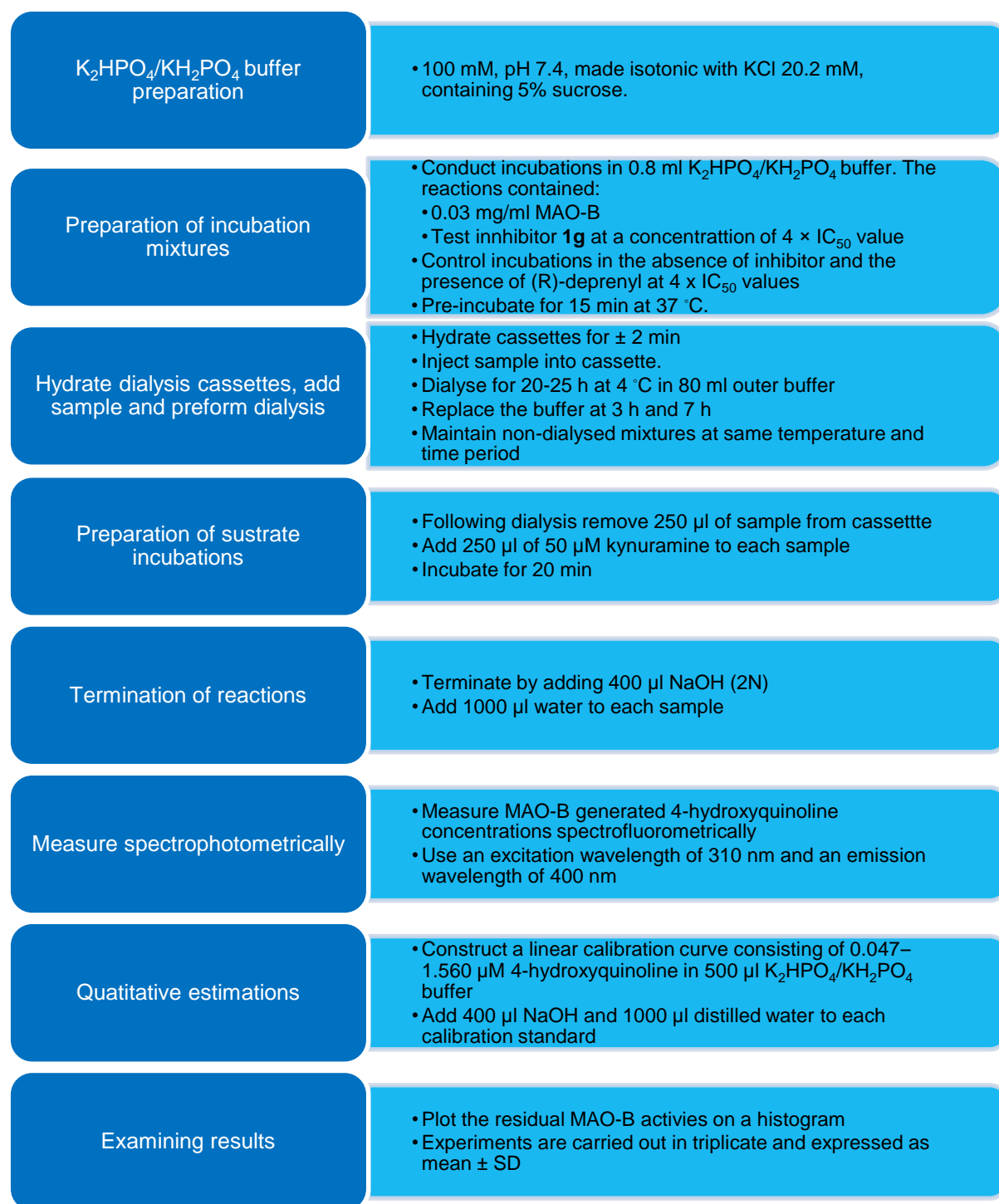


Figure 4.5 Flow-diagram summarizing the experimental method for the determination of the reversibility of inhibition by dialysis.

4.2.6 Results - reversibility of inhibition

The reversibility of MAO-B inhibition by the 3-coumaronone derivatives was examined by employing compound **1g**. As mentioned above, to evaluate the reversibility of inhibition the recovery of enzyme activities after dialysis of the enzyme-inhibitor complexes was examined (Petzer *et al.*, 2012). For this purpose, MAO-B and the selected test inhibitor, compound **1g**,

was pre-incubated for 15 min. The inhibitor concentration for this study was equal to $4 \times \text{IC}_{50}$. The reactions were subsequently dialysed for 24 h. After dialysis, the residual MAO-B activities were measured by adding kynuramine to the dialysed mixtures. After 20 min incubation, 4-hydroxyquinoline, generated from the MAO-B-catalysed oxidation of kynuramine was quantified by fluorescence spectrophotometry. The MAO-B activities in dialysed and non-dialysed enzyme-inhibitor complexes were recorded and compared to determine whether the selected compound (**1g**) is a reversible MAO-B inhibitor.

As shown in figure 4.6, MAO-B inhibition by **1g** is completely reversed after 24 h of dialysis, with MAO-B catalytic activity recovering to a level of 87% of the control value (recorded in the absence of inhibitor). In contrast, the MAO-B activity of undialysed mixtures of MAO-B and **1g** is 42% of the control value. These data suggest that **1g** is a reversible MAO-B inhibitor. After similar treatment and dialysis of mixtures of MAO-B and the irreversible inhibitor, (R)-deprenyl, the enzyme activity is not recovered, with the residual enzyme activity at a level of only 3% of the control value. It may therefore be concluded that compound **1g**, and most likely all synthesised 3-coumarone derivatives are reversible inhibitors of human MAO-B.

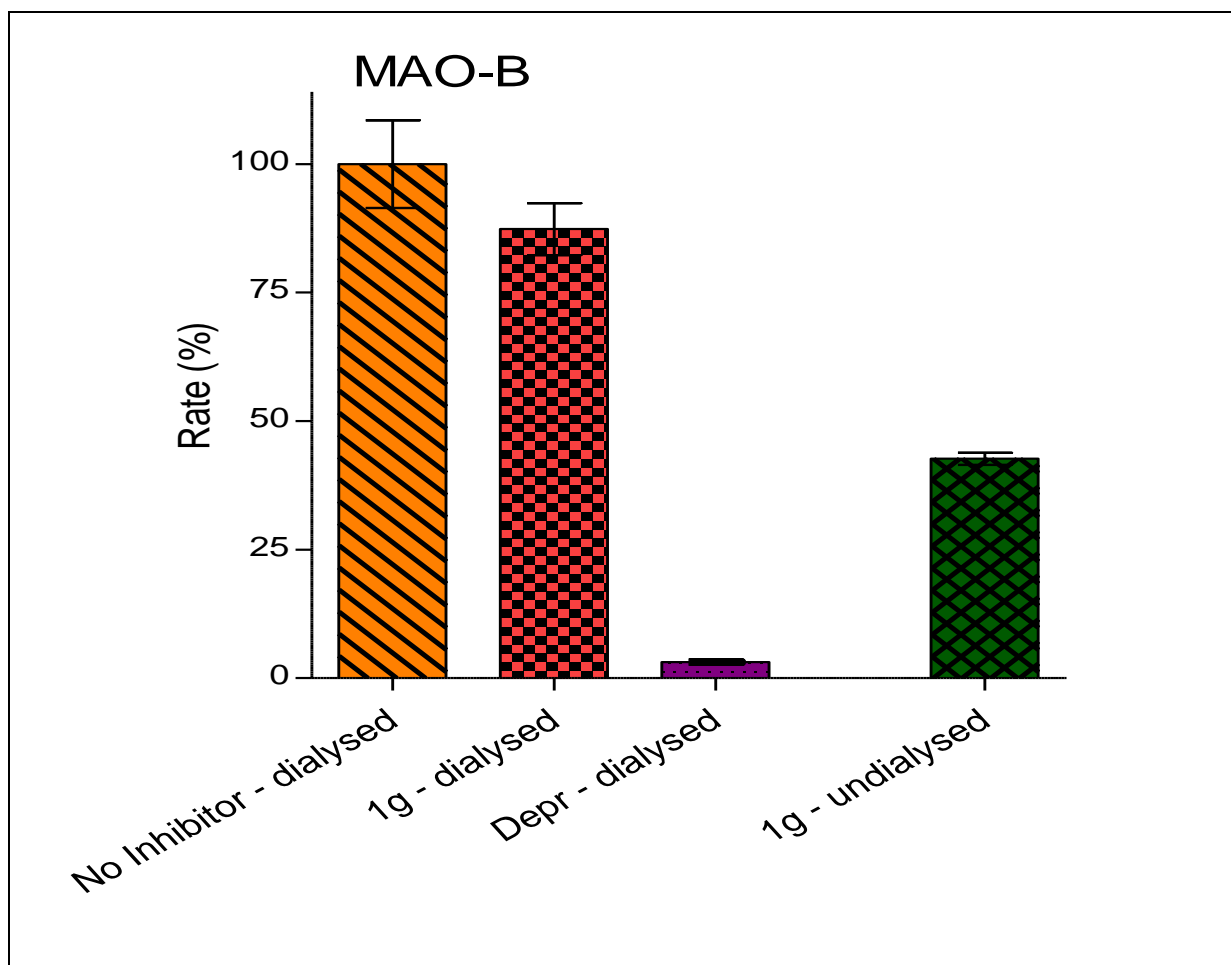


Figure 4.6 Histogram of the reversibility of MAO-B inhibition by compound **1g**.

4.2.7 Experimental method for the construction of Lineweaver-Burk plots

Lineweaver-Burk plots were constructed for the selected representative inhibitor, compound **1g**, in this study. The mode of inhibition of test inhibitors is determined by Lineweaver-Burk plots. In this study Lineweaver-Burk plots were constructed for compound **1g** to establish whether this compound exhibits a competitive or non-competitive mode of inhibition. For the purpose of this study the MAO-B catalytic rates were recorded at eight different kynuramine concentrations (15–250 μM) in the absence of inhibitor, and presence of four different inhibitor concentrations (0.002–0.005 μM) of **1g**.

Recombinant human MAO-B (5 mg/ml) was obtained from Sigma-Aldrich, and was pre-aliquoted and stored at $-70\text{ }^{\circ}\text{C}$. All enzymatic reactions were conducted in KH_2PO_4 buffer (100 mM, pH 7.4, made isotonic with KCl 20.2 mM) to a final volume of 500 μl . All the reactions contained kynuramine as substrate (15–250 μM final concentration), MAO-B (0.015 mg/ml

final concentration), compound **1g** (at four different concentrations, 0.002–0.005 μM) and 4% DMSO. A Lineweaver-Burk plot in the absence of inhibitor was also constructed. All the reactions were incubated for 20 min at 37 °C and terminated with the addition of 400 μl NaOH and 1000 μl distilled water. The initial rates by which MAO-B catalyses the oxidation of kynuramine were determined spectrofluorometrically as described in the previous section (reversibility of inhibition). The concentrations of the MAO-B-generated 4-hydroxyquinoline was determined by measuring the fluorescence of the samples at an excitation wavelength of 310 nm and an emission wavelength of 400 nm. Thereafter a calibration curve was constructed with the known amounts (0.047–1.560 μM) of 4-hydroxyquinoline dissolved in 500 μl KH_2PO_4 buffer (100 mM, pH 7.4, made isotonic with KCl 20.2 mM). To each calibration curve was added 400 μl NaOH and 1000 μl water. From the data obtained Lineweaver-Burk plots were constructed.

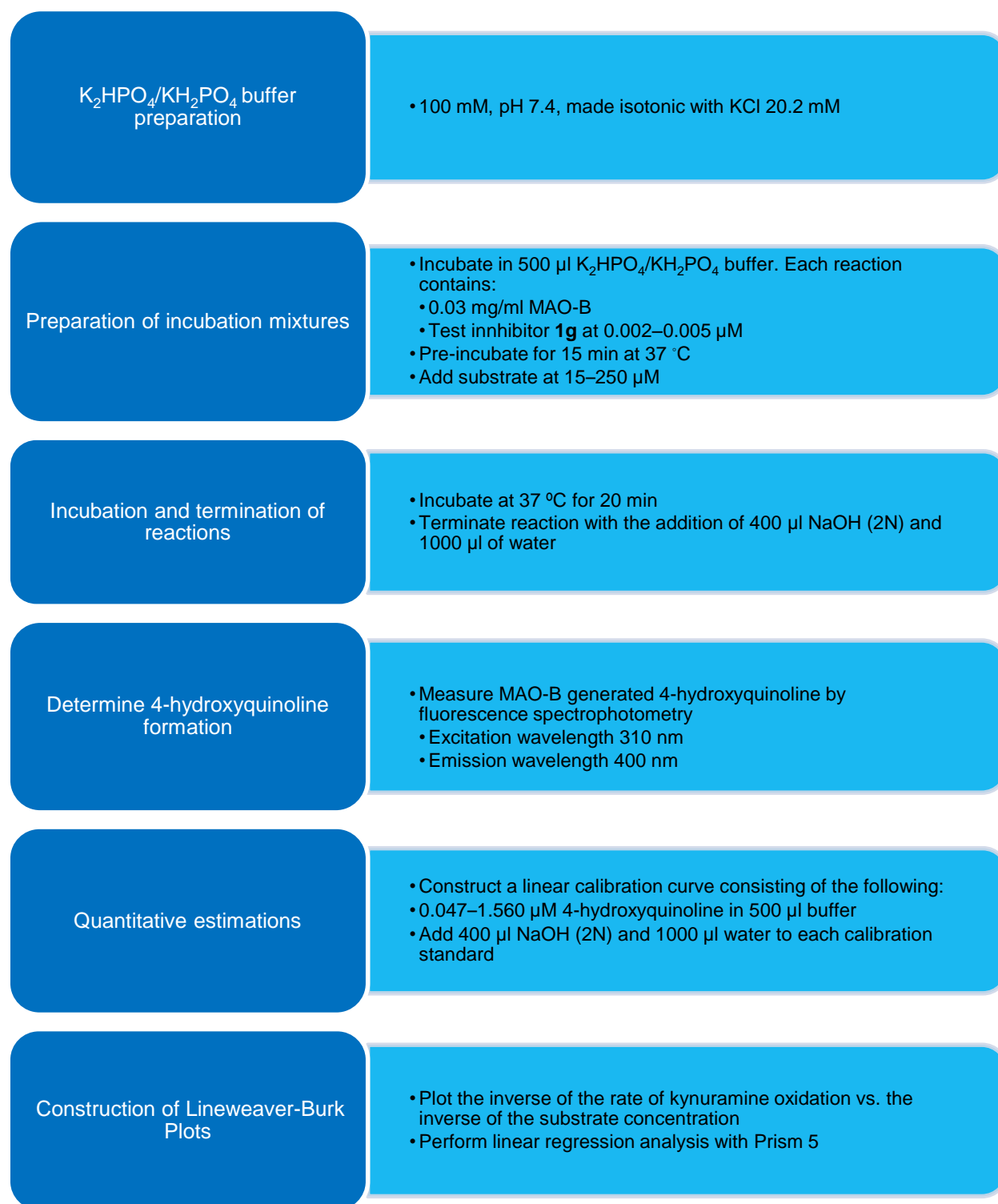


Figure 4.7. Flow-diagram summarizing the experimental method of constructing Lineweaver-Burk plots.

4.2.8 Results - Lineweaver-Burk plots

Since the selective representative inhibitor **1g** exhibited the most potent MAO-B inhibitory activity it was selected for the construction of Lineweaver-Burk plots in this study. The inverse of the measured rates of kynuramine oxidation (4-hydroxyquinoline formation) were plotted against the inverse of the substrate concentrations used. Plots were constructed from data obtained with the four inhibitor concentrations (0.002–0.005 μM) and from data recorded in the absence of the selected inhibitor.

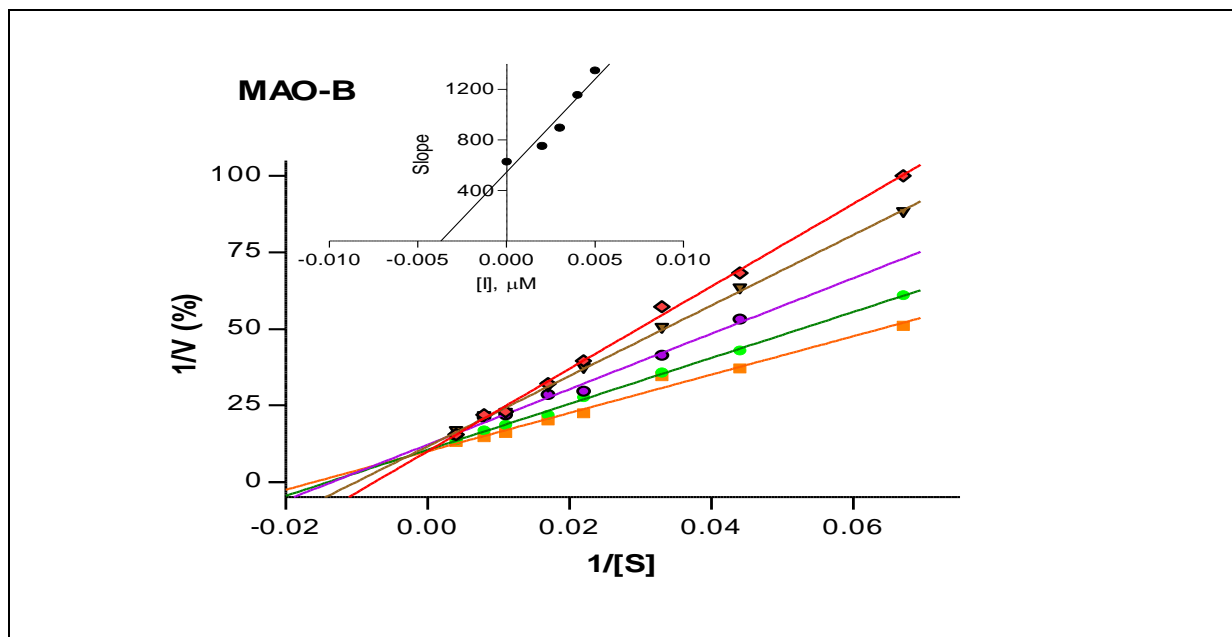


Figure 4.8. Lineweaver-Burk plots for the oxidation of kynuramine by MAO-B in the absence (filled squares) and the presence of five concentrations of compound **1g** (0.002–0.005 μM). The inset graph displays the slopes of the Lineweaver-Burk plots vs. the inhibitor concentration ($K_i = 0.0037 \mu\text{M}$).

Typical competitive inhibition is displayed by this set of Lineweaver-Burk plots for the inhibition of MAO-B by compound **1g**. This is evident from the fact that the Lineweaver-Burk plots intersect on a point on the y-axis. Thus, it may be concluded that compound **1g** most likely act as a competitive inhibitor of human MAO-B.

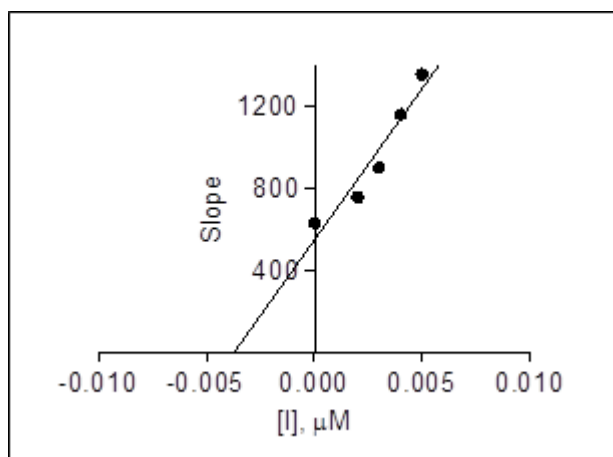


Figure 4.9. Graph of the slopes of the Lineweaver-Burk plots versus the concentration of the inhibitor **1g**.

Lineweaver-Burk plots are not only used to distinguish between competitive and non-competitive inhibitors, but it may also be used to calculate the dissociation constant (K_i), which allows the comparison of inhibition potencies between inhibitors for the same enzyme and for different enzymes. Similar to the IC_{50} values, the lower the K_i value the more potent the inhibitor. The dissociation constant, K_i , may be determined by replotting the slopes of the Lineweaver-Burk plots against the inhibitor concentration (Figure 4.9). Using then this graph, the negative of the x-axis intercept is equal to the K_i value. Compound **1g** thus exhibits a K_i of $0.0037 \mu\text{M}$. Based on the above findings it may be proposed that all the synthesised 3-coumaranone derivatives in this study most likely exhibit competitive inhibition of human MAO-B.

4.3 Summary

In this chapter it is shown that the 3-coumaranone derivatives are selective inhibitors of MAO-B over the MAO-A isoform. For all compounds evaluated the 3-coumaranone derivatives are more potent MAO-B inhibitors than MAO-A inhibitors. Based on the IC_{50} values, the 3-coumaranone derivatives are highly potent MAO-B inhibitors with the most potent MAO-B inhibitor discovered being compound **1g** ($\text{IC}_{50} = 0.004 \mu\text{M}$). For comparison, lazabemide, a reference MAO-B inhibitor exhibits a reported IC_{50} value of $0.091 \mu\text{M}$ under identical conditions (Petzer et al., 2003). Although the 3-coumaranone derivatives are selective for the MAO-B isoform, potent MAO-A inhibitors were also discovered. In this respect, compound **1k** inhibits MAO-A with an IC_{50} value of $0.586 \mu\text{M}$. It was further shown for a representative 3-coumaranone derivative, compound **1g**, that this compound is a reversible MAO-B inhibitor, with a competitive mode of inhibition. Compound **1g** exhibits a K_i value of $0.0037 \mu\text{M}$ for the

inhibition of MAO-B. It may thus be concluded that 3-coumaranones are good lead compounds for the design of MAO-B inhibitors. Such compounds may find application in the treatment of neurodegenerative disorders such as PD. In addition, 3-coumaranones that are also potent MAO-A inhibitors, such as compound **1k**, may serve as leads for the design of drugs for the treatment of depression. Dual-target-directed MAO-A/B inhibitors (such as compound **1k**), in turn, have potential application in the therapy to treat PD patients with depressive illness.

CHAPTER 5

CONCLUSION

As discussed in Chapter 2, PD is an incurable progressive, neurodegenerative disorder. Neurodegenerative disorders are characterised by progressive and irreversible loss of neurons from specific regions of the brain. PD is thus characterised by the loss of dopaminergic innervation in the striatum as a result of neurodegeneration of dopaminergic cells in the ventral midbrain (Romero-Ramos *et al.*, 2004; Hardman *et al.*, 2001). The pathological hallmark of PD is the loss of the pigmented dopaminergic neurons of the SNpc with the appearance of intracellular inclusions known as Lewy bodies. The loss of dopaminergic neurons is a feature of normal aging, a risk factor for the development of PD. PD symptoms only appear after the loss of 70–80% of dopaminergic neurons (Gibb, 1992; Fearnley & Lees, 1994). The aetiology of PD is complex and not well understood. It likely involves both genetic and environmental factors (Wirdefeldt *et al.*, 2011). Genetic contribution seems to be highly dependent on age of onset.

Monoamine oxidase (MAO) are flavin adenine dinucleotide (FAD) containing enzymes within the outer mitochondrial membrane. MAO plays a major role in the oxidation of monoamine neurotransmitters such as dopamine, and xenobiotic amines such as dietary tyramine (Youdim & Bakhle, 2006; Inoue *et al.*, 1999). MAO consists of two isoenzymes, MAO-A and MAO-B. The MAOs are considered to be drug targets for the treatment of various psychiatric and neurological disorders (Strydom *et al.*, 2013). Therapeutically, MAO-A inhibitors are used as antidepressant agents, while MAO-B inhibitors are used in the treatment of PD (Youdim & Bakhle, 2006; Youdim *et al.*, 2006). A significant proportion of PD patients exhibit signs of depression, and the antidepressant action of MAO-A inhibitors may thus be of value to these patients. MAO-B inhibitors, in turn, are used to reduce the MAO-B-catalysed metabolism of dopamine in the brain thus conserving depleted dopamine stores and prolonging the action of dopamine in the striatum. MAO-B inhibitors are also frequently combined with levodopa in PD therapy since MAO-B inhibitors, by reducing the oxidative metabolism of dopamine, may further enhance dopamine levels derived from levodopa (Youdim & Bakhle, 2006).

Various treatment options exist, which include non-pharmacological and pharmacological treatment. Progressive loss of dopaminergic neurons is the main cause of the motor symptoms of PD, and the focus of current PD therapy is on the replacement of dopamine in the nigrostriatal pathway (Yacoubian & Standaert, 2009; Dauer & Przedborski, 2003). None of the treatment options available today halt or retard the disease progression and dopaminergic neuron degeneration. As stated in Chapter 1, the aim of this study was to design new potent, reversible MAO inhibitors with selectivity towards MAO-B for symptomatic treatment of PD.

The lead compound for this study was phthalide. Previously, phthalide has been used as a scaffold in the design of MAO inhibitors, but this compound proved to be a weak MAO-B inhibitor ($IC_{50} = 28.6 \mu M$). However, substitution on the C5 position of phthalide yielded highly potent reversible MAO-B inhibitors. For example, 5-benzyloxyphthalide was found to inhibit human MAO-B with an IC_{50} value of $0.024 \mu M$ (Strydom *et al.*, 2013). Substituted phthalides were also found to be potent inhibitors of human MAO-A. For example, 5-(3-phenylpropoxy)phthalide was found to inhibit human MAO-A with an IC_{50} value of $0.096 \mu M$ (Strydom *et al.*, 2012). In all cases, phthalide derivatives are, however, selective for MAO-B over the MAO-A isoform. Based on these observations it was decided to further explore the MAO inhibition properties by focusing on the 3-coumaranone scaffold. The structural similarity between phthalide and 3-coumaranone is the principal reason to explore the possibility that 3-coumarone may be a useful scaffold for the design of reversible MAO-B inhibitors. In the present study 3-coumaranone derivatives were synthesised and evaluated as potential MAO-A and MAO-B inhibitors.

A series of twenty 3-coumaranone derivatives was thus synthesised and investigated as potential MAO-A and MAO-B inhibitors. The target compounds were synthesised by reacting 6-hydroxycoumaranone with an appropriate alkyl bromide in the presence of anhydrous potassium carbonate in DMF. The structures and purities of the target 3-coumaranone derivatives were verified by NMR, MS and HPLC analyses.

These 3-coumaranone derivatives were evaluated as inhibitors of human MAO-A and MAO-B. The MAO activity measurements were based on the oxidative deamination of kynuramine by the MAOs to yield 4-hydroxyquinoline. For each compound, the IC_{50} value for the inhibition of MAO-A and MAO-B was measured. For this purpose, sigmoidal dose-response curves were constructed. The results showed that, in all instances, the 3-coumaranone derivatives are more potent MAO-B inhibitors than MAO-A inhibitors. The most selective inhibitors are compounds **1h**, **1l**, **1n** and **1t**, which did not inhibit MAO-A, even at a maximal concentration of $100 \mu M$. The most potent MAO-A inhibitor is compound **1k**, which inhibits MAO-A with an IC_{50} value of $0.586 \mu M$. This value is in the submicromolar range and may thus be viewed as potent inhibition. For comparison, toloxatone, a clinically used MAO-A inhibitor exhibits a reported IC_{50} value of $3.92 \mu M$ under identical conditions (Petzer *et al.*, 2012). In addition to its potency towards MAO-B, compound **1k** exhibits inhibitory action against MAO-B ($IC_{50} = 0.166 \mu M$), which indicate its dual MAO-A/B activity. The dual-target-directed MAO-A/B inhibitors (such as compound **1k**), may have potential application in the therapy of both PD and depressive illness. Selective MAO-B inhibitors, in turn, are appropriate for the treatment of PD

The most potent MAO-B inhibitor discovered is compound **1g**, with an IC_{50} value of 0.004 μ M. For comparison, lazabemide, a reference MAO-B inhibitor exhibits a reported IC_{50} value of 0.091 μ M under identical conditions (Petzer *et al.*, 2012).

To evaluate the reversibility of inhibition, the recovery of enzyme activity after the dialysis of enzyme-inhibitor complexes was examined (Petzer *et al.*, 2012). Compound **1g** was the selected analogue for this study, since it was the most potent MAO-B inhibitor discovered in this study. The data suggest that **1g** is a reversible MAO-B inhibitor since the inhibition of MAO-B by **1g** may be reversed by dialysis. To determine the mode of inhibition, a set of Lineweaver-Burk plots were constructed. The selected compound for this study, compound **1g**, was selected to establish whether 3-coumaranone derivatives exhibit competitive or non-competitive modes of inhibition. It is evident from the results, that compound **1g** displays typical competitive inhibition of MAO-B since the lines of the Lineweaver-Burk plots were linear and intersected on the y-axis.

This study has shown that the 3-coumaranone derivatives are selective inhibitors of MAO-B over the MAO-A isoform. Although the 3-coumaranone derivatives are selective for the MAO-B isoform, potent MAO-A inhibitors have also been discovered. It was further shown, by a representative inhibitor, that 3-coumaranone derivatives are reversible MAO-B inhibitors, with a competitive mode of inhibition. It may thus be concluded that 3-coumaranones are good lead compounds for the design of MAO-A and -B inhibitors.

BIBLIOGRAPHY

- Ballard, P.A., Tetrud, J.W. and Lanston, J.W. 1985. Permanent human parkinsonism due to N-methyl-4-phenyl-1,2,3,6-tetrahydropyridine (MPTP): seven cases. *Neurology*, 35:949-956.
- Bara-Jimenez, W., Sherzaim A., Dimetrova, T., Favit, A., Babbiani, F. and Gillespie, M. 2003. Adenosine A_{2A} receptor antagonist treatment of Parkinson's disease. *Neurology*, 61:293-296.
- Betarbet, R., Sherer., T.B., Di Monte, D.A. and Greenamyre, J.T. 2002. Mechanistic approaches to Parkinson's disease. *Brain pathology*, 12:499-510.
- Bové, J., Prou, D., Perier, C. and Przedborski, S. 2005. Toxin-induced models of Parkinson's disease. *The journal of the American society for experimental neurotherapeutics*, 2:484-494.
- Bonnet, U. 2003. Moclobemide: therapeutic use and clinical studies. *CNS drug reviews*, 9:97-140.
- Binda, C., Newton-Vinson, P., Hubálek, F., Edmondson, D.E. & Mattevi, A. 2002. Structure of human monoamine oxidase B, a drug target for the treatment of neurological disorders. *Nature structural biology*, 9:22-26.
- Bretler, A. and Rossengren, E. 1959. Occurrence and distribution of catecholamines in brain. *Acta physiologica Scandinavica*, 47:350-361.
- Carlsson, A., Lindqvist, M., Magnusson, T. and Waldeck, B. 1958. On the presence of 3-hydroxytyramine in brain. *Science*, 127:471-472.
- Chao, J., Leung, Y., Wang, M., Chang, R. 2012. Nutraceuticals and their preventative or potential therapeutic value in Parkinson's disease. *Nutr Rev*, 7: 373-386.
- Chen, J.J. and Swope, D.M. 2007. Pharmacotherapy for Parkinson's disease. *Pharmacotherapy*, 27:161S-173S.
- Cranwell-Bruce, L.A. 2010. Drugs for Parkinson's disease. *Nursing Pharmacology*, 10:347-349.
- Cummings, J.L., Vinters, H.V., Cole, G.M. and Khachaturian, Z.S. 1998. Alzheimer's disease: etiologies, pathophysiology, cognitive reserve and treatment opportunities. *Neurology*, 51:S2-S17.
- Cunha, R.A. 2005. Neuroprotection by adenosine in the brain: from A₁ receptor activation to A_{2A} receptor blockade. *Purnergic signalling*, 1:111-134.
- Dauer, W. and Przedborski, S. 2003. Parkinson's disease: mechanisms and Models. *Neuron*, 39:889-909.
- Deleu, D., Northway, M.G. and Hanssens, Y. 2002. Clinical pharmacokinetic and pharmacodynamics properties of drugs used in the treatment of Parkinson's disease. *Clinical pharmacokinetics*, 41:261-309.
- Edmondson, D.E., Binda, C. and Mattevi, A. 2007. Structural insights into the mechanism of amine oxidation by monoamine oxidases A and B. *Archives of biochemistry and biophysics*, 464:269-276.

BIBLIOGRAPHY

Edmondson, D.E., Binda, C. and Mattevi, A. 2004a. The FAD binding sites of human monoamine oxidase A and B. *Neurotoxicology*, 25:63-72.

Edmondson, D.E., Binda, C., Mattevi, A. and Hubalek, F. 2004b. Structure and mechanism of monoamine oxidase. *Current medicinal chemistry*, 11:1983-1993.

Edmondson, D.E., Binda, C., Wang, J., Upadhyay, A.K. & Mattevi, A. 2009. Molecular and mechanistic properties of the membrane-bound mitochondrial monoamine oxidases. *Biochemistry*, 48:4220-4230.

Factor, S.A. 2008. Current status of symptomatic medicinal therapy in Parkinson's disease. *Neurotherapeutics*, 5:164-180.

Fearnley, J. and Lees, A. 1994. Pathology of Parkinson's disease. In *Neurodegenerative Disease*(Calne,D.B., ed.) Saunders, Philadelphia, 545-554.

Fernandez, H.H. and Chen, J.J. 2007. Monoamine oxidase B inhibition in the treatment of Parkinson's disease. *Pharmacotherapy*, 27:174S-185S.

Finberg, J.P. and Tenne, M. 1982. Relationship between tyramine potentiation and selective inhibition of monoamine oxidase type A and B in rat vas deferens. *British journal of pharmacology*, 77:13-21.

Fowler, J.S., Volkow, N.D., Wang, G., Pappas, N., Logan, J., Shea, C., Alexoff, D., MacGregor, R.R. 1997. Age related increases in brain monoamine oxidase B in living healthy human subjects. *Neurobiology of aging*, 18:431-435.

Gibb, W.R. 1992. Neuropathology of Parkinson's disease and related syndromes. *Neurologic clinics*, 10:361-376.

Grimsby, J., Lan, N.C., Neve, R., Chen, K. and Shih, J.C. 1990. Identification of a region important for human monoamine oxidase A and B. *Journal of neurochemistry*, 55:1166-1169.

Hardman, J.G., L.E. Limbird, P.B., A.G. Gilman. 2001. Goodman and Gilman's *The Pharmacological Basis of Therapeutics*. 10th ed. New York, NY: McGraw-Hill, p. 557

Heister, D. 2011. Parkinson's disease: symptoms, treatments and research. *British journal of nursing*, 20:548-554.

Hoy, S.M. and Keating, G.M. 2012. Rasaglyline: a review of its use in the treatment of idiopathic Parkinson's disease. *Drugs*, 72:643-669.

Heister, D. and Bains, J. 2012. Side effects of treatment for Parkinson's disease. *Nursing and residential care*, 14:2330-2332

Hisahara, S. and Shimohama, S. 2010. Toxin-induced and genetic animal models of Parkinson's disease. *Parkinson's disease*, 951709.

Inoue, H., Castagnoli, K., Van der Schyf, C., Mabic, S., Igarashi, K. and Castanoli, N., Jr. 1999. Species-dependent differences in monoamine oxidase A and B-catalyzed oxidation of various C4 substituted 1-methyl-4-phenyl-1,2,3,6-tetrahydropyridinyl derivatives. *Journal of pharmacology and experimental therapeutics*, 291:856-864.

BIBLIOGRAPHY

- Jalkanen, S. and Salmi, M. 2001. Cell surface monoamine oxidases: enzymes in search of a function. *The EMBO journal*, 20:3896-3901.
- Karunapuzha, C.A., Shilpa, M.D. and Dewey, R.B. 2010. Monoamine oxidase type B inhibitors in the treatment of early Parkinson's disease. *US Neurology*, 6:36-40.
- Knoll, J. 1992. (-)-Deprenyl medication: a strategy to modulate the age related decline of the striatal dopaminergic system. *Journal of the American geriatric society*, 40:839-847.
- Laczkowski, K.Z., Pakulski, M.M., Krzeminski, M.P., Jaisankar, P. and Zaidlewicz, M. 2008. *Tetrahedron asymmetry*, 19:788-795.
- Lantos, I., Flisak, J., Liu, L., Matsuoka, R., Mendelson, W., Stevenson, D., Tubman, K., Tucker, L., Zhang, W., Adams, J., Sorenson, M., Garigipati, R., Erhardt, K. and Ross, S. 1997. Enantioselective synthesis of 5-LO inhibitor hydroxyureas. Tandem nucleophilic addition-intramolecular cyclization of chiral nitrones. *Journal of organic chemistry*, 62:5385-5391.
- Lees, A. 2005. Alternatives to levodopa in the initial treatment of early Parkinson's disease. *Drugs & aging*, 22:731-770.
- Lees, A.J., Hardy, J. and Revesz, T. 2009. Parkinson's disease. *The Lancet*, 373:2055-2066.
- LeWitt, P.A. and Taylor, D.C. 2008. Protection against Parkinson's disease progression: clinical experience. *Neurotherapeutics*, 5:210-225.
- Nagatsu, T. 2004. Progress in monoamine oxidase (MAO) research in relation to genetic engineering. *Neurotoxicology*, 25:11-20.
- Nicotra, A. and Parvez, S.H. 1999. Methods for assaying monoamine oxidase A and B activities: recent developments. *Biogenic amines*, 15:307-320.
- Pahwa, R., Factor, S.A. and Lyons, K.E. 2006. Practice parameter: treatment of Parkinson's disease with motor fluctuations and dyskinesia (an evidence-based review). *Neurology*, 66:983-995.
- Pedrosa, D.J. and Timmerman, L. 2013. Review: management of Parkinson's disease. *Neuropsychiatric disease and treatment*, 9:321-340.
- Petzer, J.P., Steyn, S., Castagnoli, K.P., Chen, J., Schwarzschild, M.A., Van der Schyf, C.J. and Castagnoli, N., 2003. Inhibition of monoamine oxidase B by selective adenosine A_{2A} receptor antagonists. *Bioorganic & medicinal chemistry*, 11:1299-1310.
- Petzer, A., Harvey, B.H., Wegener, G. and Petzer, J.P. 2012. Azure B, a metabolite of methylene blue, is a high-potency, reversible inhibitor of monoamine oxidase. *Toxicology and applied pharmacology*, 258:403-409.
- Petzer, A., Pienaar, A., Petzer, J.P. 2013. The inhibition of monoamine oxidase by esomeprazole. *Drug Research*, 63 (9), 462-467.

BIBLIOGRAPHY

- Riederer, P., Youdim, M.B.H. 1986. Monoamine oxidase activity and monoamine metabolism in brains of Parkinson's patients treated with L-deprenyl. *Journal of neurochemistry*, 46:1359-1365.
- Riederer, P., Youdim, M.B.H., Sofic, E., Rausch, W.D., Schmidt, B., Reynolds, G.P. and Jellinger, K. 1989. Transition metals, ferritin, glutathione, and ascorbic acid in parkinsonian brains. *Journal of neurochemistry*, 52:515-520.
- Romero-Ramos, M., Maingay, M. and Kirik, D. 2004. Parkinson's Disease, in *Neuroprotection: Models, Mechanisms and Therapies* (ed M. Bähr), Wiley-VCH Verlag GmbH & Co. KGaA, Weinheim, FRG. doi: 10.1002/3527603867.ch2
- Schnaitman, C., Erwin, V.G. and Greenawalt, J.W. 1967. The submitochondrial localization of monoamine oxidase. An enzymatic marker for the outer membrane of rat liver mitochondria. *Journal of cell biology*, 32:719-735.
- Schwarzschild, M.A., Agnati, L., Fuxe, K., Chen, J. and Morelli, M., 2006. Targeting adenosine A_{2A} receptors in Parkinson's disease. *Trends in neurosciences*, 29:647-654.
- Silverman, R.B., Hoffman, S.J. and Catus, W.B. 1980. A mechanism for mitochondrial monoamine oxidase catalyzed amine oxidation. *Journal of the American chemical society*, 102:7126-7128.
- Snyder, C.H. and Adler, C.H. 2007. The patient with Parkinson's disease: Part 1-treating the motor symptoms; Part II-treating the nonmotor symptoms. *Journal of the American academy of nurse practitioners*, 19:179-197.
- Strydom, B., Bergh, J.J. and Petzer, J.P. 2011. 8-Aryl- and alkyloxycaffeine analogues as inhibitors of monoamine oxidase. *European journal of medicinal chemistry*, 46:3474-3485.
- Strydom, B., Malan, S.F., Castagnoli, N., Jr., Bergh, J.J. and Petzer, J.P. 2010. Inhibition of monoamine oxidase by 8-benzoyloxycaffeine analogues. *Bioorganic & medicinal chemistry*, 18:1018-1028.
- Strydom, B., Bergh, J.J. and Petzer, J.P. 2013. Inhibition of monoamine oxidase by phthalide analogues. *Bioorganic & medicinal chemistry*. 23:1269-1273.
- Tipton, K.F., Boyce, S., O'Sullivan, J., Davey, G.P. and Healy, J. 2004. Monoamine oxidase: certainties and uncertainties. *Current medicinal chemistry*, 11:1965-1982.
- Weissbach, H., Smith, T.E., Daly, J.W., Witkop, B. and Udenfriend, S. 1960. A rapid spectrophotometric assay of monoamine oxidase based on the rate of disappearance of kynuramine. *The journal of biological chemistry*, 235:1160-1163.
- Wirdefeldt, K., Adami, H.O., Cole, P., Trichopoulos, D. and Mandel, J. 2011. Epidemiology and etiology of Parkinson's disease: a review of the evidence. *European journal of epidemiology*, 26:S1-S58.
- Yacoubian, T.A. and Standaert, D.G. 2009. Targets for neuroprotection in Parkinson's disease. *Biochimica et biophysica acta (BBA) - molecular basis of disease*, 1792:676-687.

BIBLIOGRAPHY

Youdim, M.B.H. and Bakhle, Y.S. 2006. Monoamine oxidase: isoforms and inhibitors in Parkinson's disease and depressive illness. *British journal of pharmacology*, 147:S287-S296.

Youdim, M.B.H., Edmondson, D. and Tipton, K.F. 2006. The therapeutic potential of monoamine oxidase inhibitors. *Nature reviews neuroscience*, 7:295-309.

Youdim, M.B.H. and Weinstock, M. 2004. Therapeutic applications of selective and non-selective inhibitors of monoamine oxidase A and B that do not cause significant tyramine potentiation. *Neurotoxicology*, 25:243-250.

Youdim, M.B.H., Finberg, J.P.M. and Tipton K.F. 1988. Catecholamines I. *Handbook of experimental Pharmacology*. Trendelenburg U and Weiner N. (eds) *Handbook of experimental Pharmacology*. Berlin: Springer-Verlag, 119–192.

Yu, J.1998. Synthesis and mechanistic studies on the monoamine oxidase (MAO) catalyzed oxidation of 1,4-disubstituted-1,2,3,6-tetrahydropyridines. Ph.D thesis. Virginia Polytechnic Institute and State University.

APPENDIX

SECTION 1:

LIST OF ¹H NMR AND ¹³C NMR SPECTRA OF THE FOLLOWING COMPOUNDS

- 1a:** 6-(Benzyloxy)-2H-1-benzofuran-3-one
1b: 6-(4-Fluorobenzyloxy)-2H-1-benzofuran-3-one
1c: 6-(3-Fluorobenzyloxy)-2H-1-benzofuran-3-one
1d: 6-(4-Chlorobenzyloxy)-2H-1-benzofuran-3-one
1e: 6-(3-Chlorobenzyloxy)-2H-1-benzofuran-3-one
1f: 6-(4-Bromobenzyloxy)-2H-1-benzofuran-3-one
1g: 6-(3-Bromobenzyloxy)-2H-1-benzofuran-3-one
1h: 6-(4-Iodobenzyloxy)-2H-1-benzofuran-3-one
1i: 6-(3-Iodobenzyloxy)-2H-1-benzofuran-3-one
1j: 6-(4-Cyanobenzyloxy)-2H-1-benzofuran-3-one
1k: 6-(3-Cyanobenzyloxy)-2H-1-benzofuran-3-one
1l: 6-(4-Methylbenzyloxy)-2H-1-benzofuran-3-one
1m: 6-(3-Methylbenzyloxy)-2H-1-benzofuran-3-one
1n: 6-[4-(Trifluoromethyl)benzyloxy]-2H-1-benzofuran-3-one
1o: 6-(2-Phenylethoxy)-2H-1-benzofuran-3-one
1p: 6-[2-(4-Bromophenyl)ethoxy]-2H-1-benzofuran-3-one
1q: 6-[2-(4-Methylphenyl)ethoxy]-2H-1-benzofuran-3-one
1r: 6-[2-(3-Methylphenyl)ethoxy]-2H-1-benzofuran-3-one
1s: 6-(3-Phenylpropoxy)-2H-1-benzofuran-3-one
1t: 6-(2-Phenoxyethoxy)-2H-1-benzofuran-3-one

APPENDIX

SECTION 2:

LIST OF MASS SPECTRA OF THE FOLLOWING COMPOUNDS

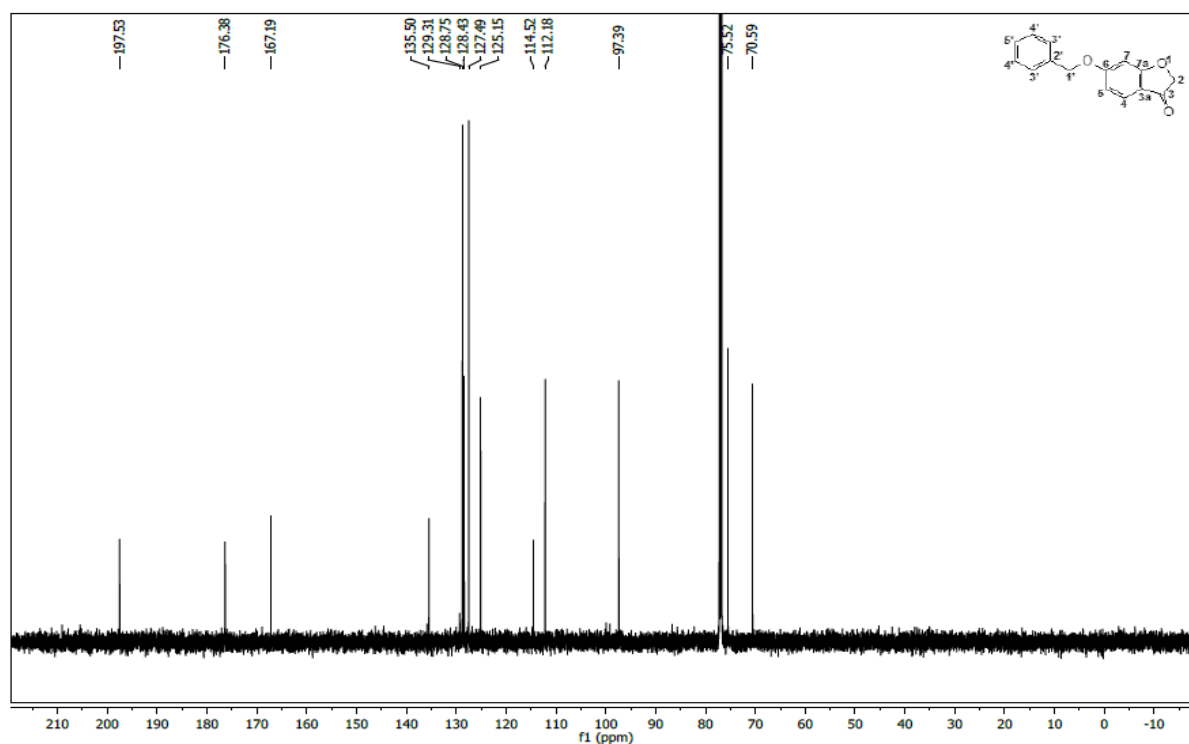
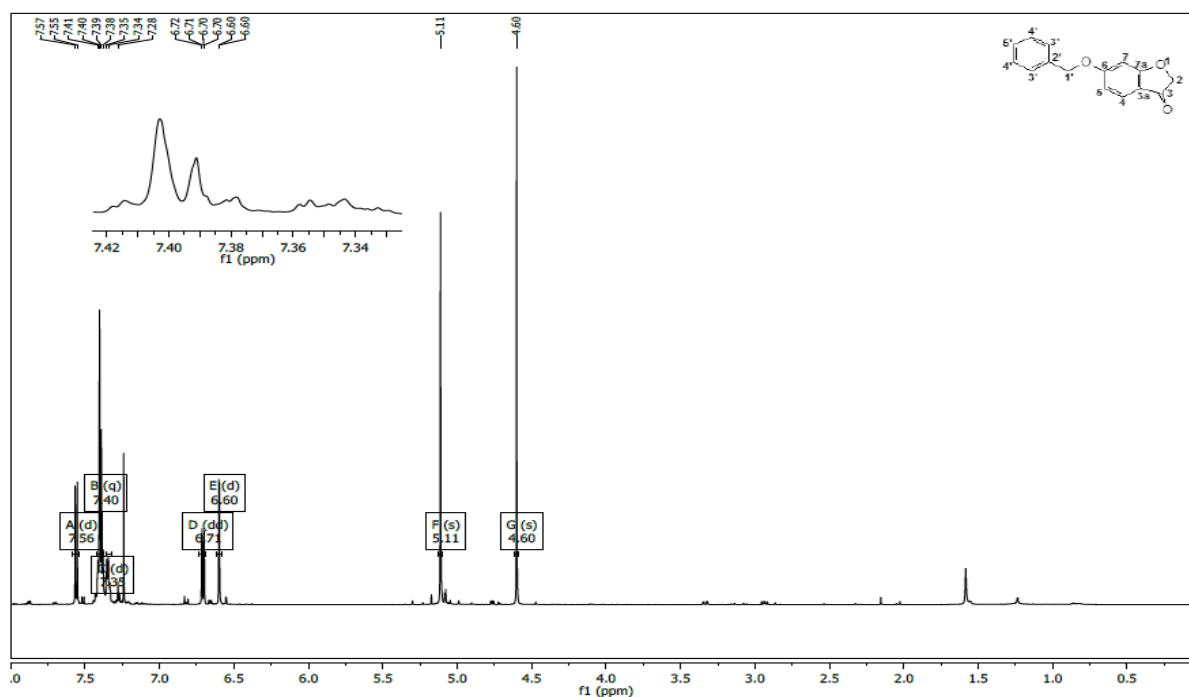
- 1a:** 6-(Benzyloxy)-2H-1-benzofuran-3-one
- 1b:** 6-(4-Fluorobenzyloxy)-2H-1-benzofuran-3-one
- 1c:** 6-(3-Fluorobenzyloxy)-2H-1-benzofuran-3-one
- 1d:** 6-(4-Chlorobenzyloxy)-2H-1-benzofuran-3-one
- 1e:** 6-(3-Chlorobenzyloxy)-2H-1-benzofuran-3-one
- 1f:** 6-(4-Bromobenzyloxy)-2H-1-benzofuran-3-one
- 1g:** 6-(3-Bromobenzyloxy)-2H-1-benzofuran-3-one
- 1h:** 6-(4-Iodobenzyloxy)-2H-1-benzofuran-3-one
- 1i:** 6-(3-Iodobenzyloxy)-2H-1-benzofuran-3-one
- 1j:** 6-(4-Cyanobenzyloxy)-2H-1-benzofuran-3-one
- 1k:** 6-(3-Cyanobenzyloxy)-2H-1-benzofuran-3-one
- 1l:** 6-(4-Methylbenzyloxy)-2H-1-benzofuran-3-one
- 1m:** 6-(3-Methylbenzyloxy)-2H-1-benzofuran-3-one
- 1n:** 6-[4-(Trifluoromethyl)benzyloxy]-2H-1-benzofuran-3-one
- 1o:** 6-(2-Phenylethoxy)-2H-1-benzofuran-3-one
- 1p:** 6-[2-(4-Bromophenyl)ethoxy]-2H-1-benzofuran-3-one
- 1q:** 6-[2-(4-Methylphenyl)ethoxy]-2H-1-benzofuran-3-one
- 1r:** 6-[2-(3-Methylphenyl)ethoxy]-2H-1-benzofuran-3-one
- 1s:** 6-(3-Phenylpropoxy)-2H-1-benzofuran-3-one
- 1t:** 6-(2-Phenoxyethoxy)-2H-1-benzofuran-3-one

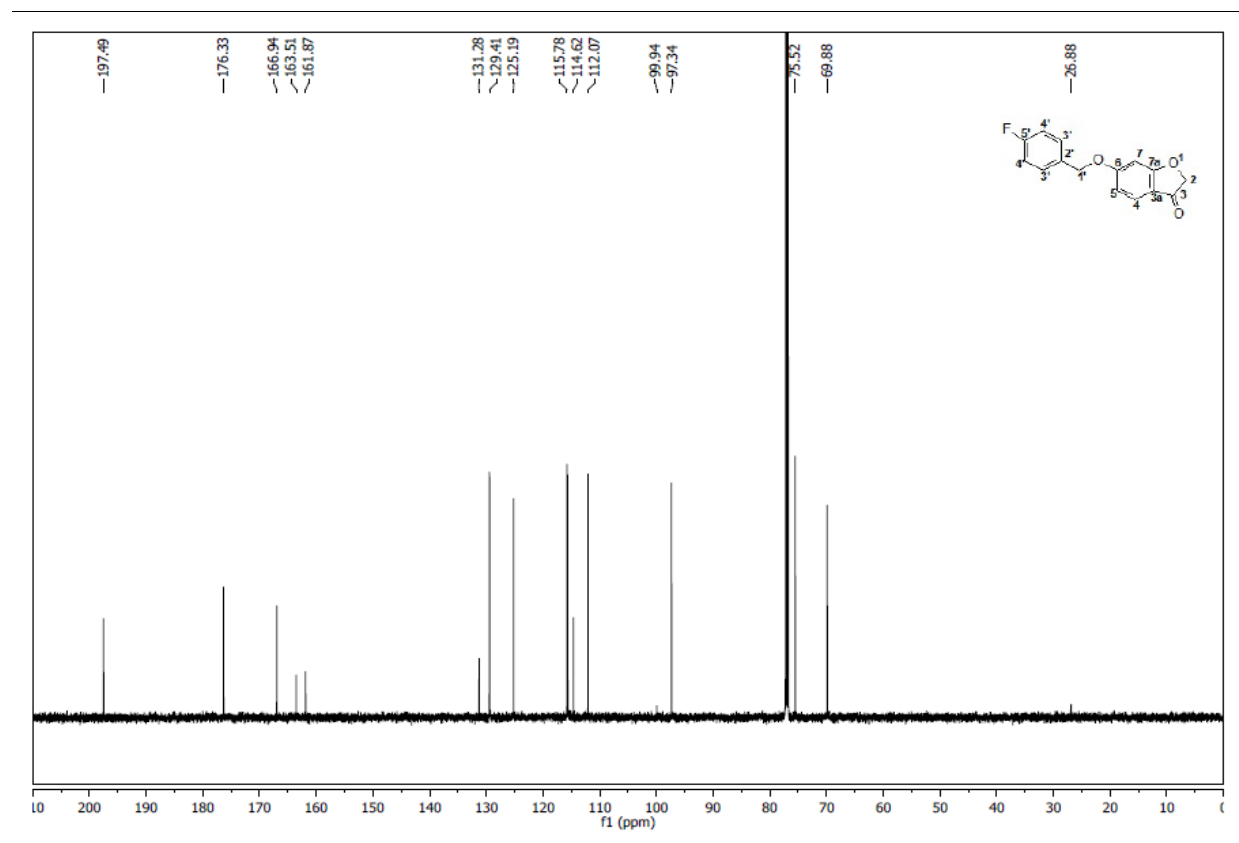
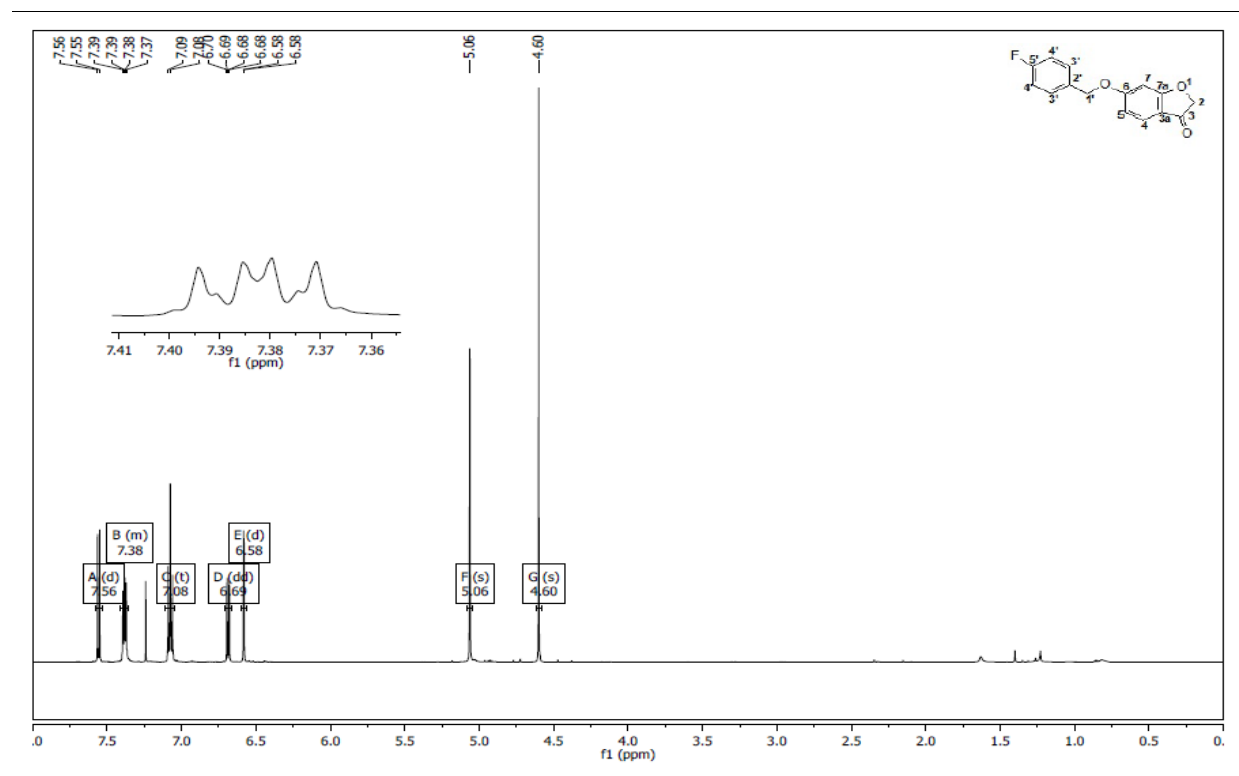
APPENDIX

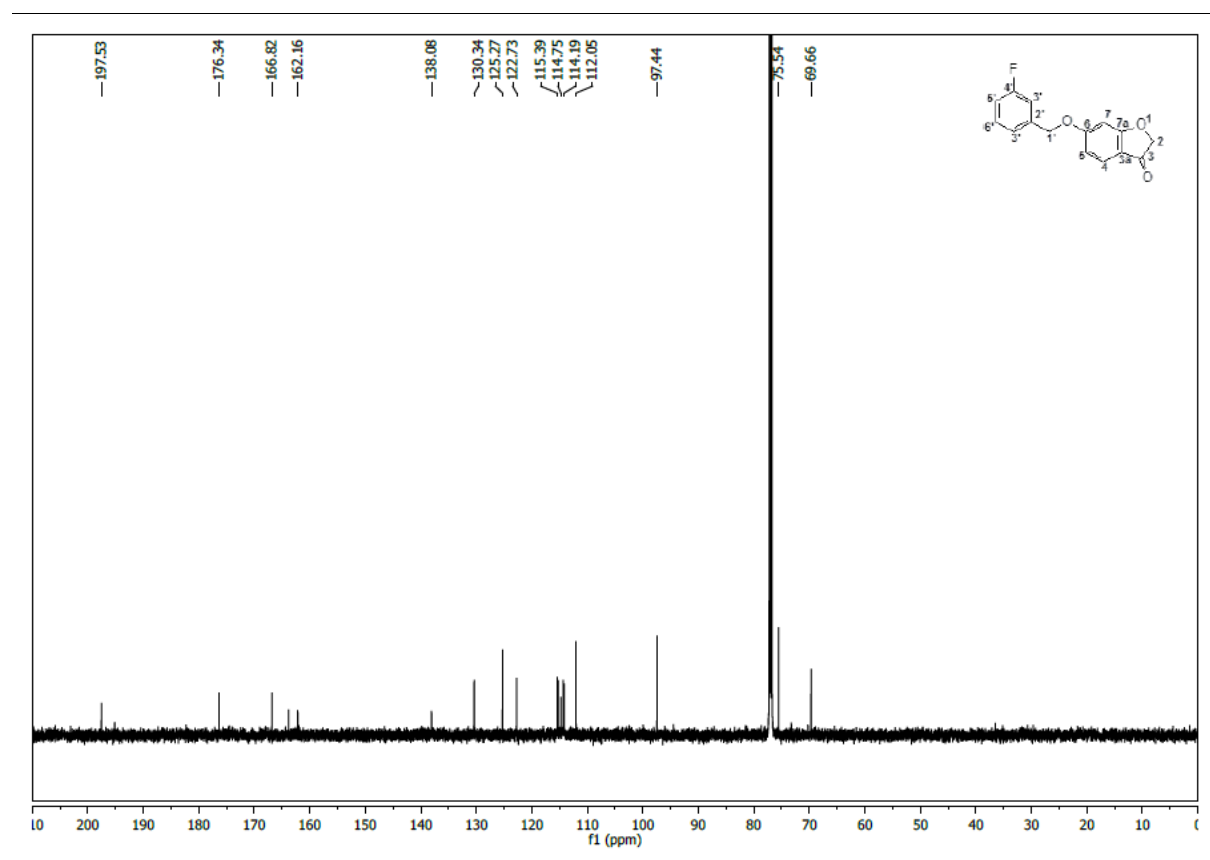
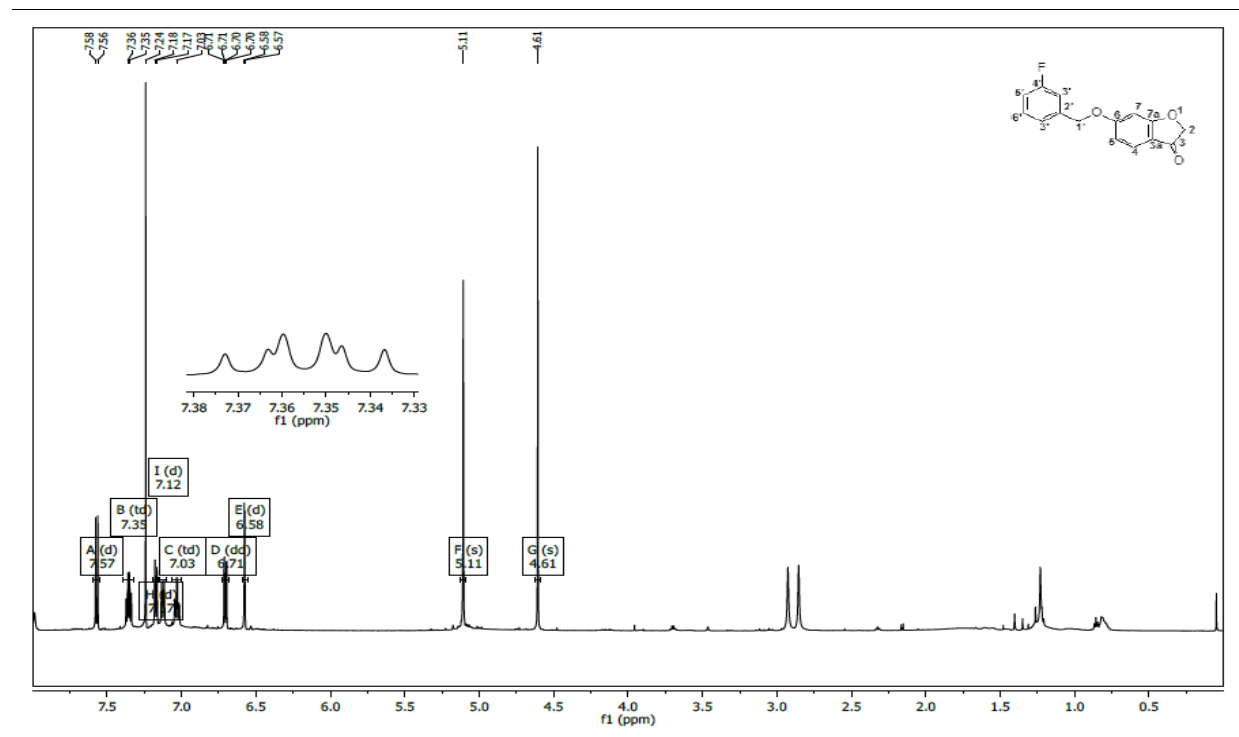
SECTION 3:

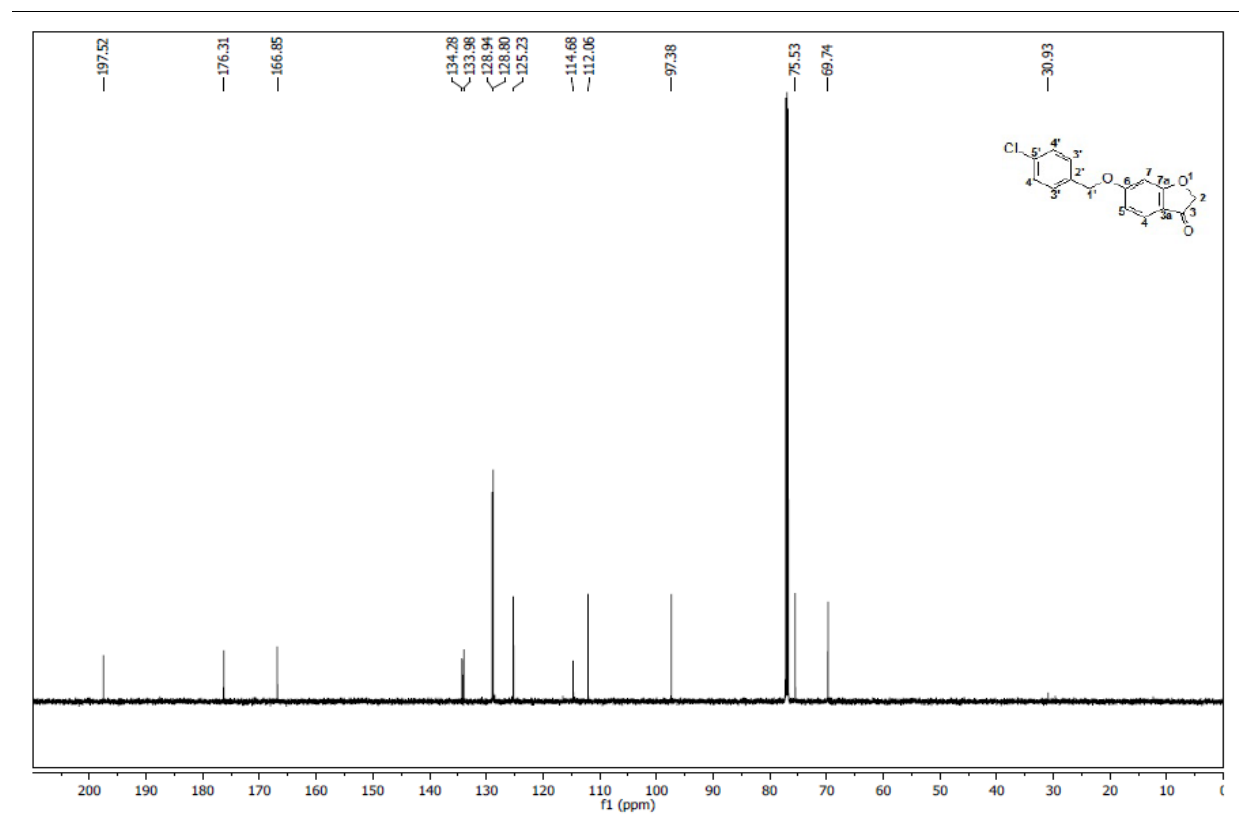
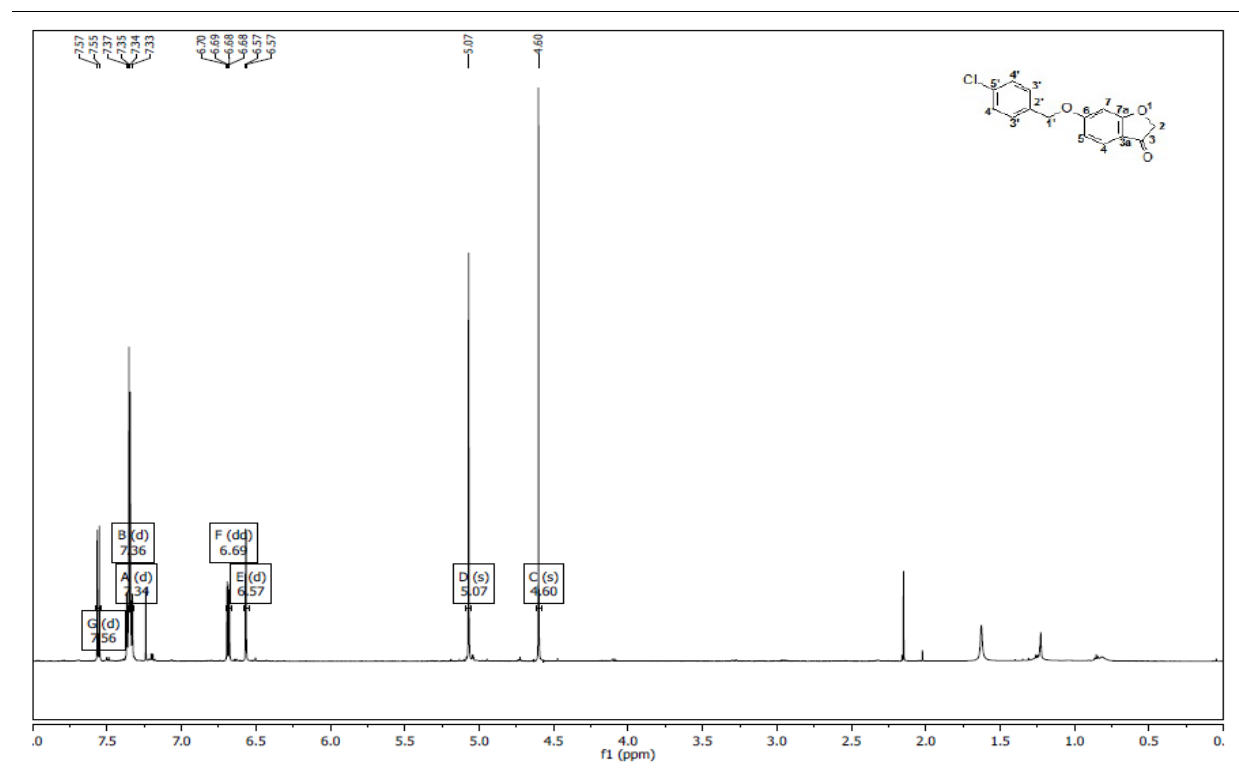
LIST OF HPLC TRACES OF THE FOLLOWING COMPOUNDS

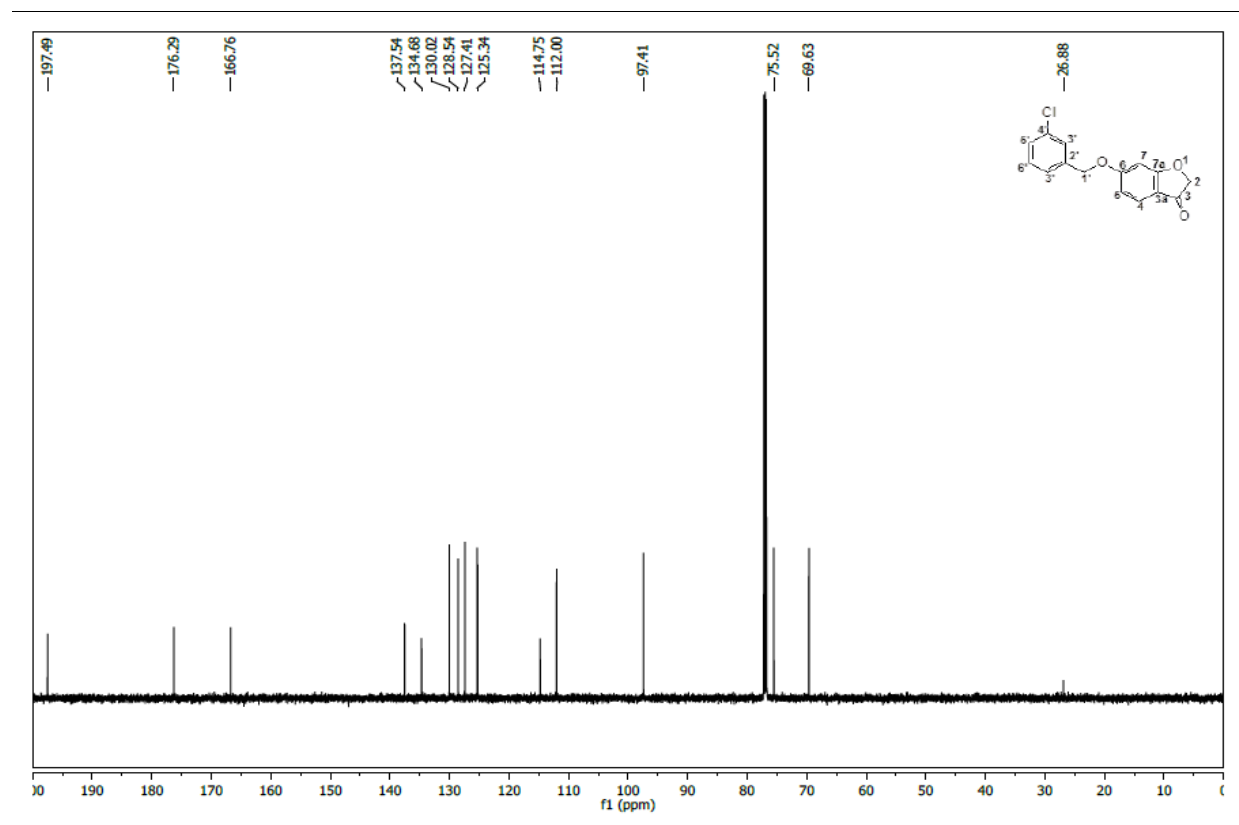
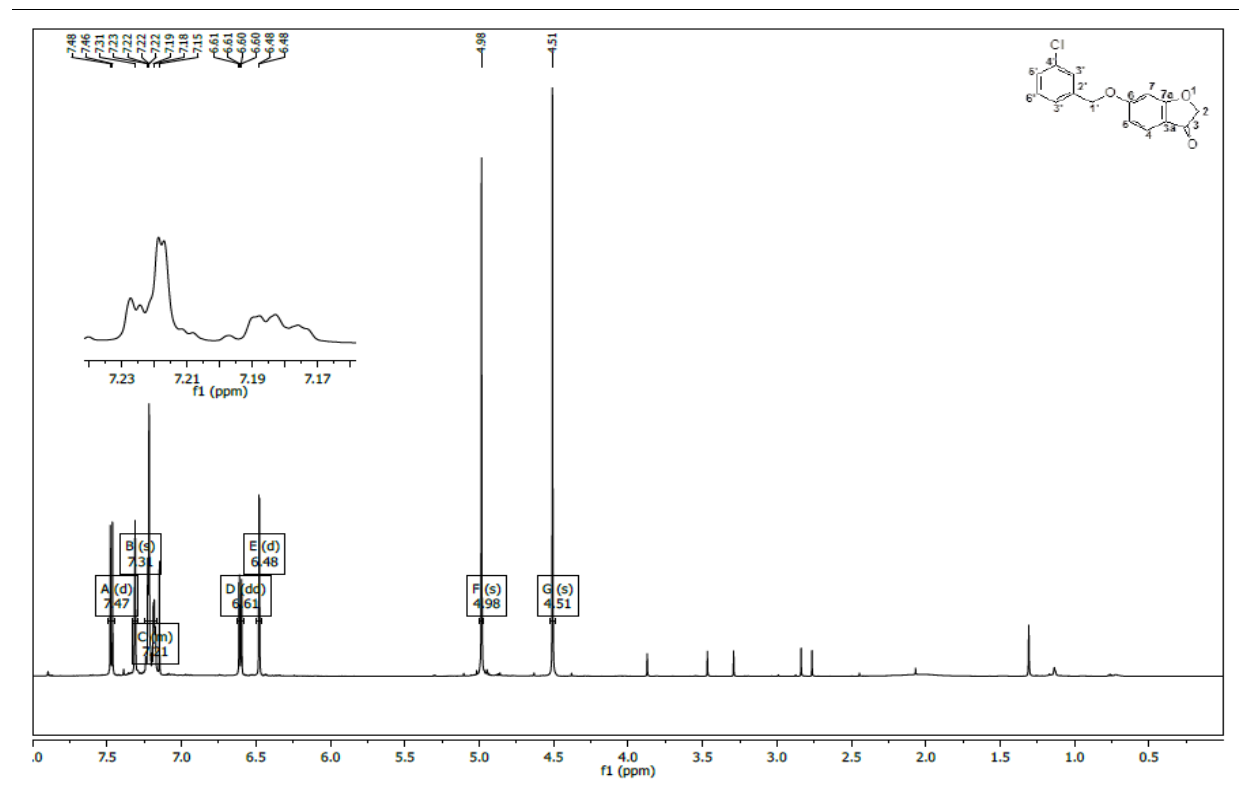
- 1a:** 6-(Benzyloxy)-2H-1-benzofuran-3-one
- 1b:** 6-(4-Fluorobenzyloxy)-2H-1-benzofuran-3-one
- 1c:** 6-(3-Fluorobenzyloxy)-2H-1-benzofuran-3-one
- 1d:** 6-(4-Chlorobenzyloxy)-2H-1-benzofuran-3-one
- 1e:** 6-(3-Chlorobenzyloxy)-2H-1-benzofuran-3-one
- 1f:** 6-(4-Bromobenzyloxy)-2H-1-benzofuran-3-one
- 1g:** 6-(3-Bromobenzyloxy)-2H-1-benzofuran-3-one
- 1h:** 6-(4-Iodobenzyloxy)-2H-1-benzofuran-3-one
- 1i:** 6-(3-Iodobenzyloxy)-2H-1-benzofuran-3-one
- 1j:** 6-(4-Cyanobenzyloxy)-2H-1-benzofuran-3-one
- 1k:** 6-(3-Cyanobenzyloxy)-2H-1-benzofuran-3-one
- 1l:** 6-(4-Methylbenzyloxy)-2H-1-benzofuran-3-one
- 1m:** 6-(3-Methylbenzyloxy)-2H-1-benzofuran-3-one
- 1n:** 6-[4-(Trifluoromethyl)benzyloxy]-2H-1-benzofuran-3-one
- 1o:** 6-(2-Phenylethoxy)-2H-1-benzofuran-3-one
- 1p:** 6-[2-(4-Bromophenyl)ethoxy]-2H-1-benzofuran-3-one
- 1q:** 6-[2-(4-Methylphenyl)ethoxy]-2H-1-benzofuran-3-one
- 1r:** 6-[2-(3-Methylphenyl)ethoxy]-2H-1-benzofuran-3-one
- 1s:** 6-(3-Phenylpropoxy)-2H-1-benzofuran-3-one
- 1t:** 6-(2-Phenoxyethoxy)-2H-1-benzofuran-3-one

^1H NMR AND ^{13}C NMR SPECTRA OF THE SYNTHESISED COMPOUNDS**1a:** 6-(Benzyloxy)-2H-1-benzofuran-3-one

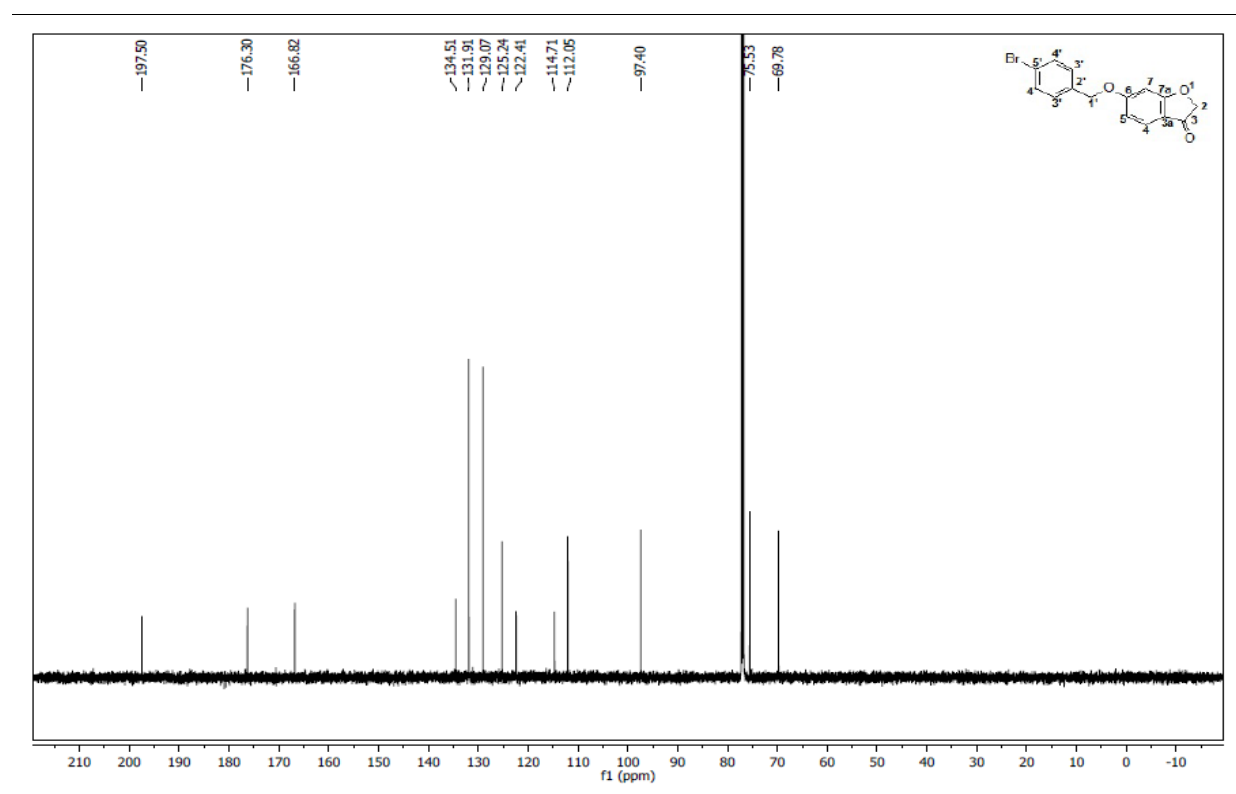
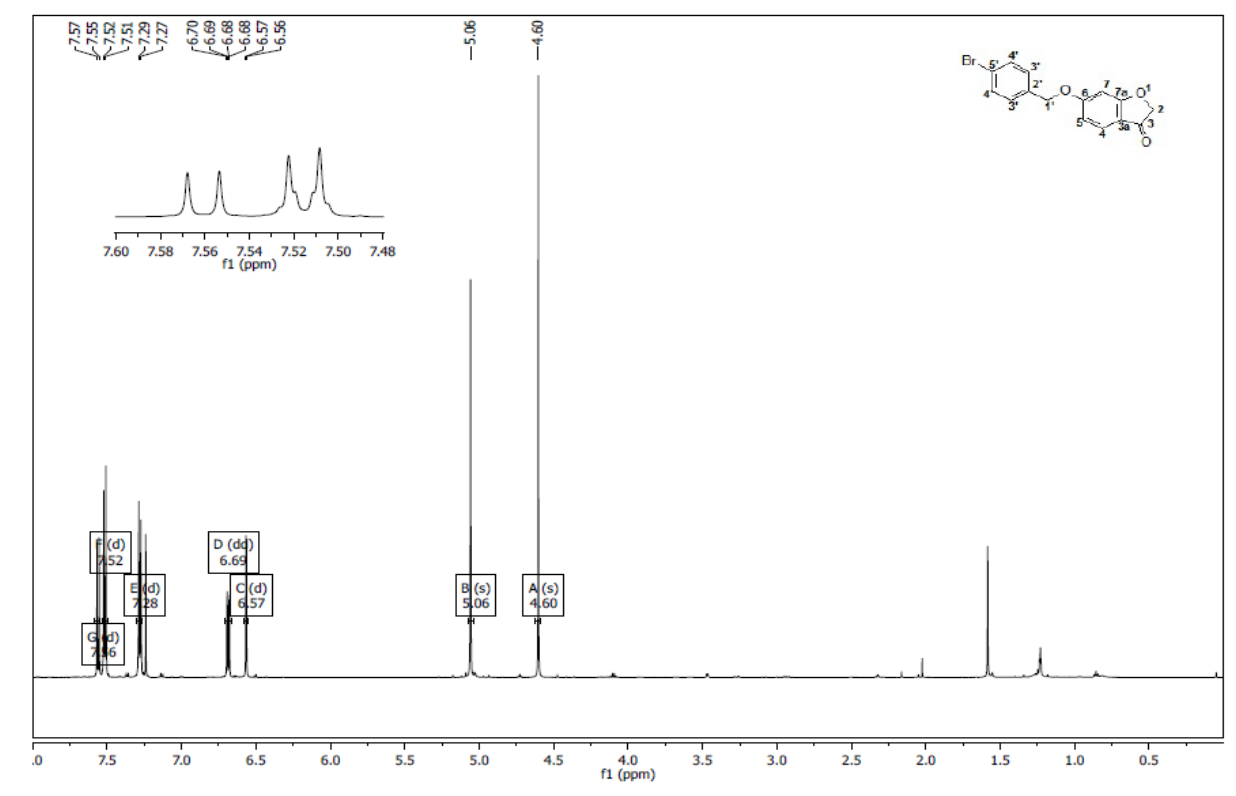
1b: 6-(4-Fluorobenzyloxy)-2H-1-benzofuran-3-one

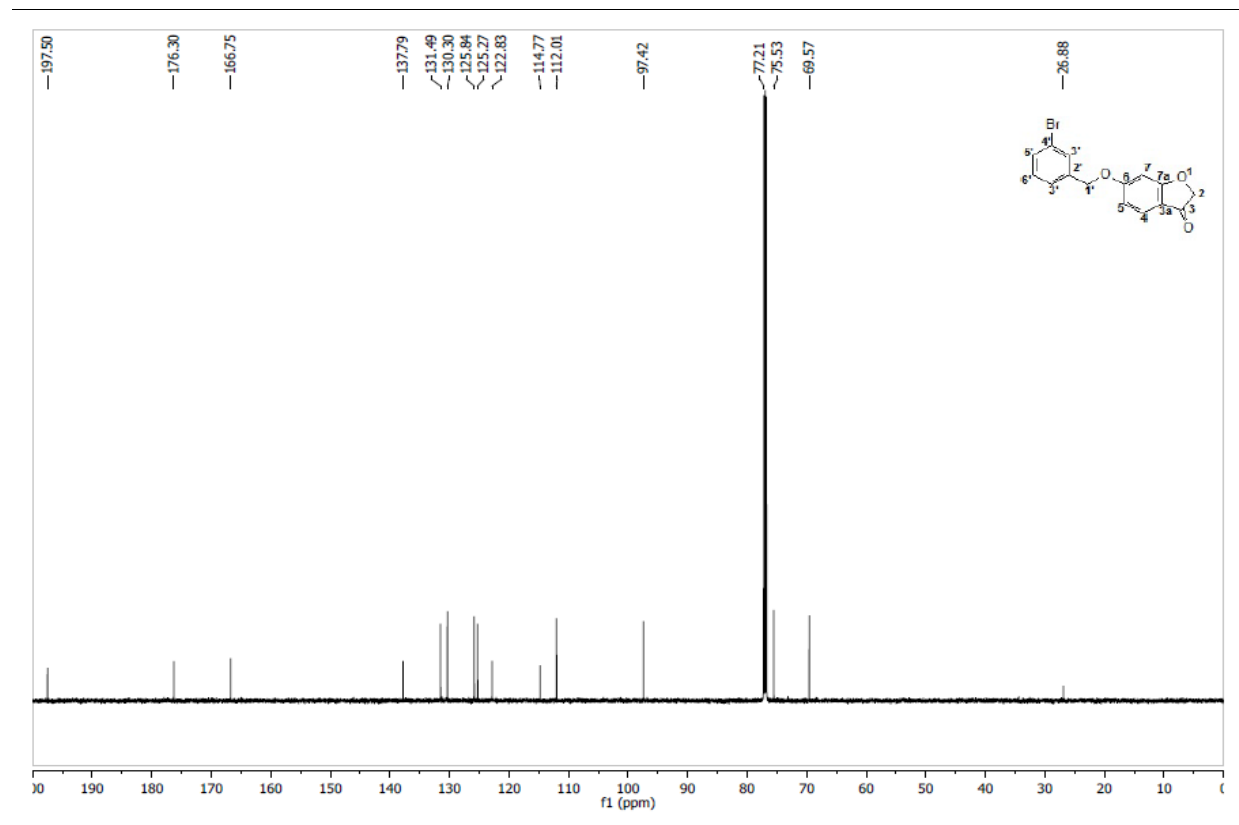
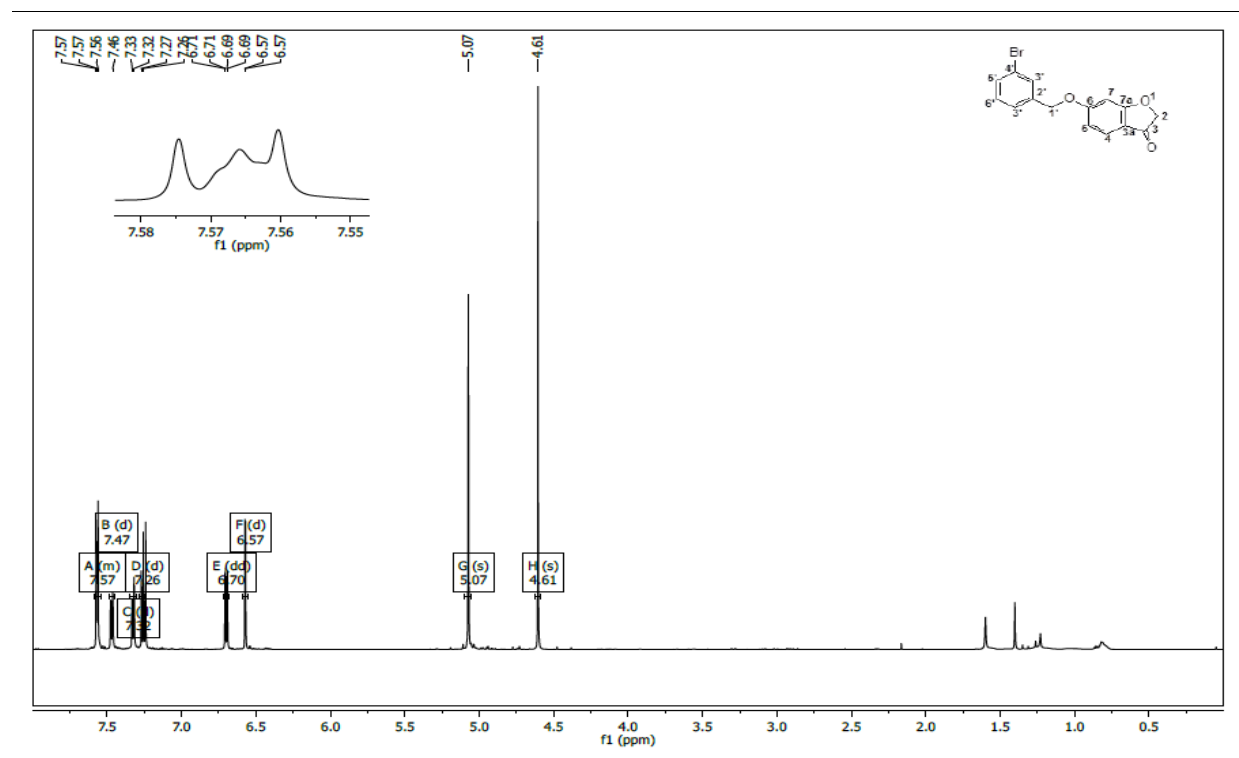
1c: 6-(3-Fluorobenzoyloxy)-2H-1-benzofuran-3-one

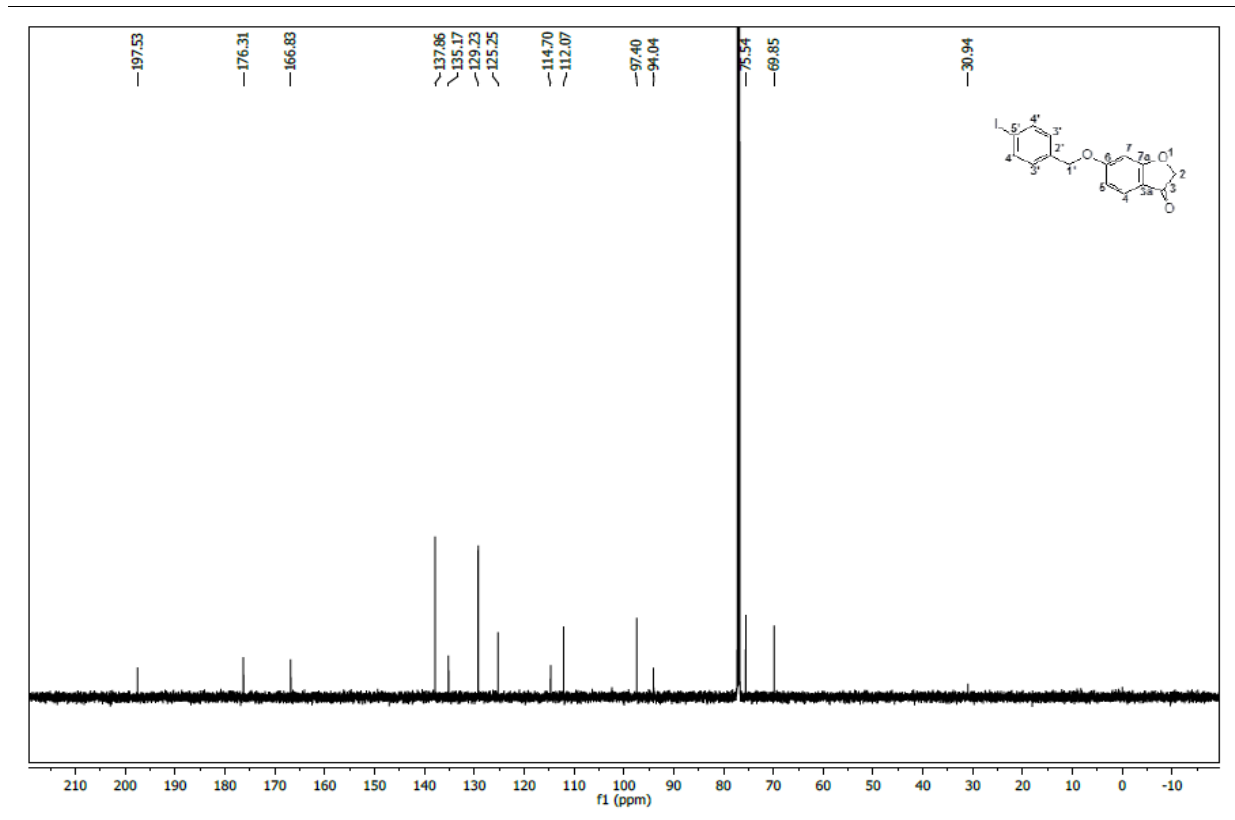
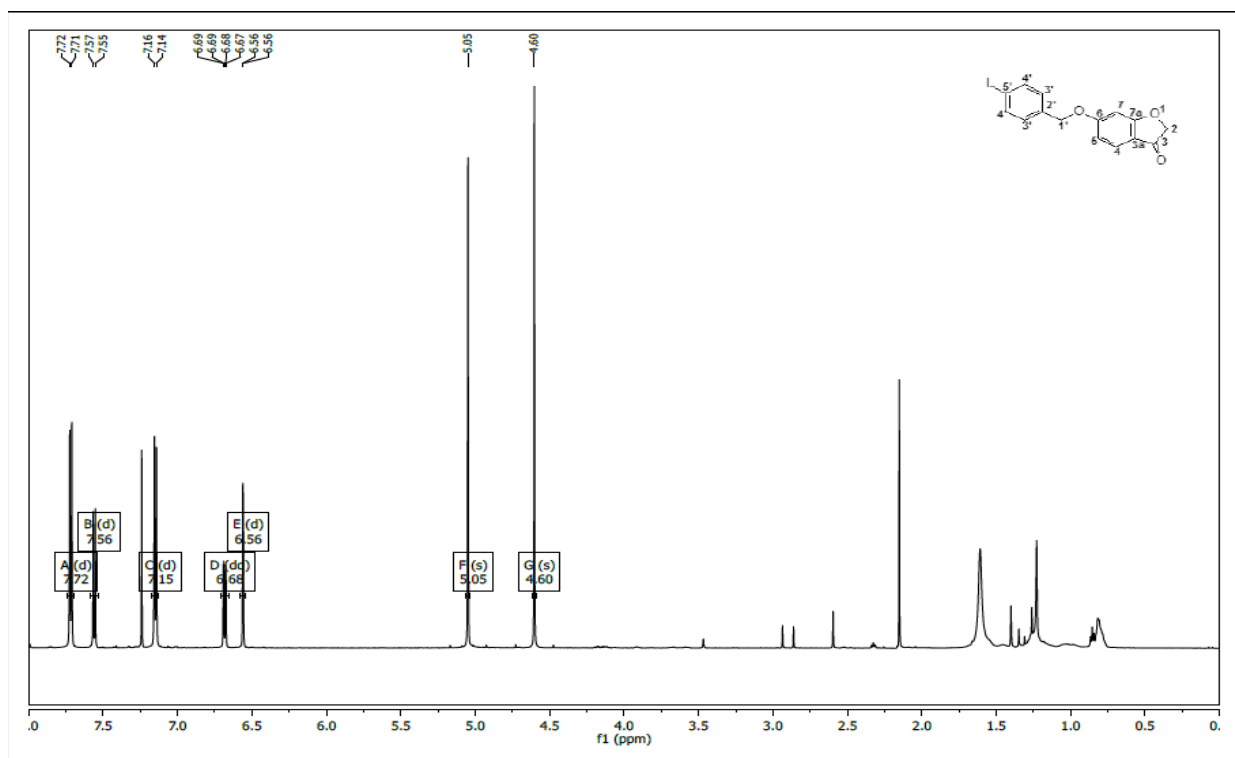
1d: 6-(4-Chlorobenzoyloxy)-2H-1-benzofuran-3-one

1e: 6-(3-Chlorobenzoyloxy)-2H-1-benzofuran-3-one

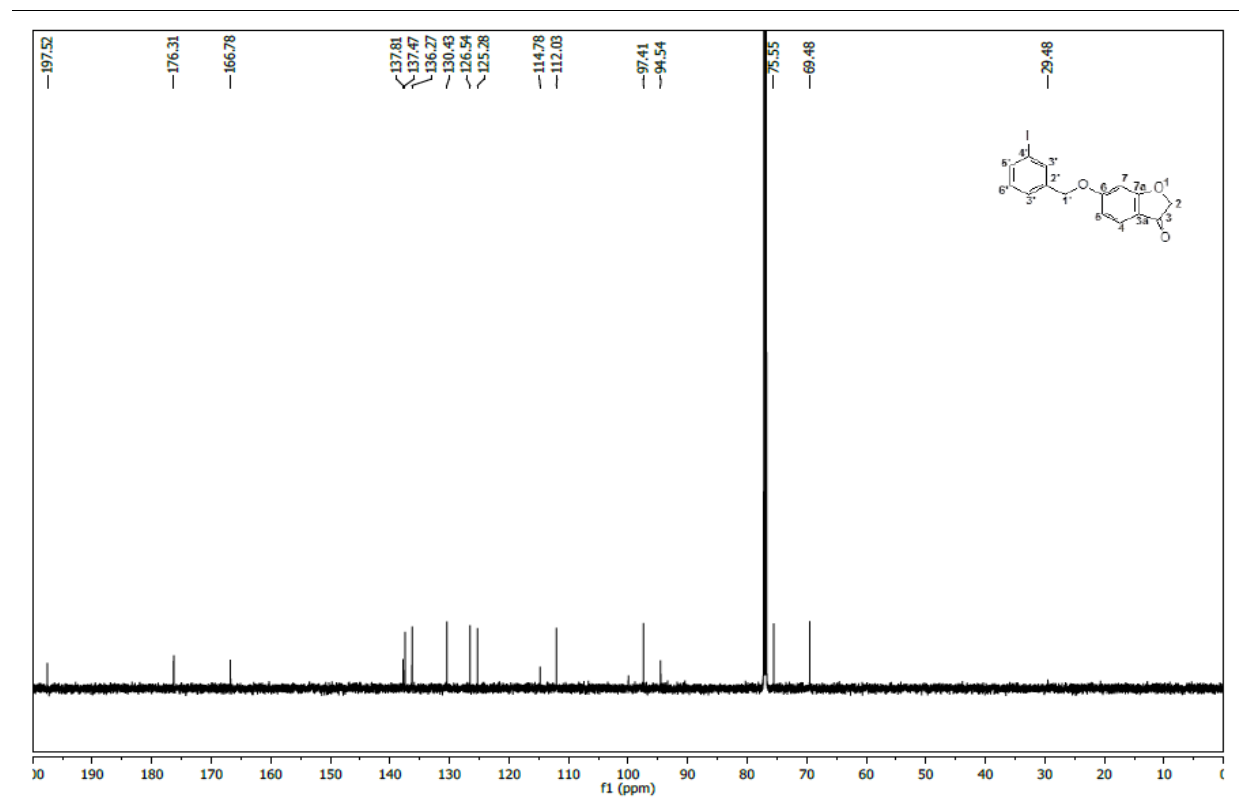
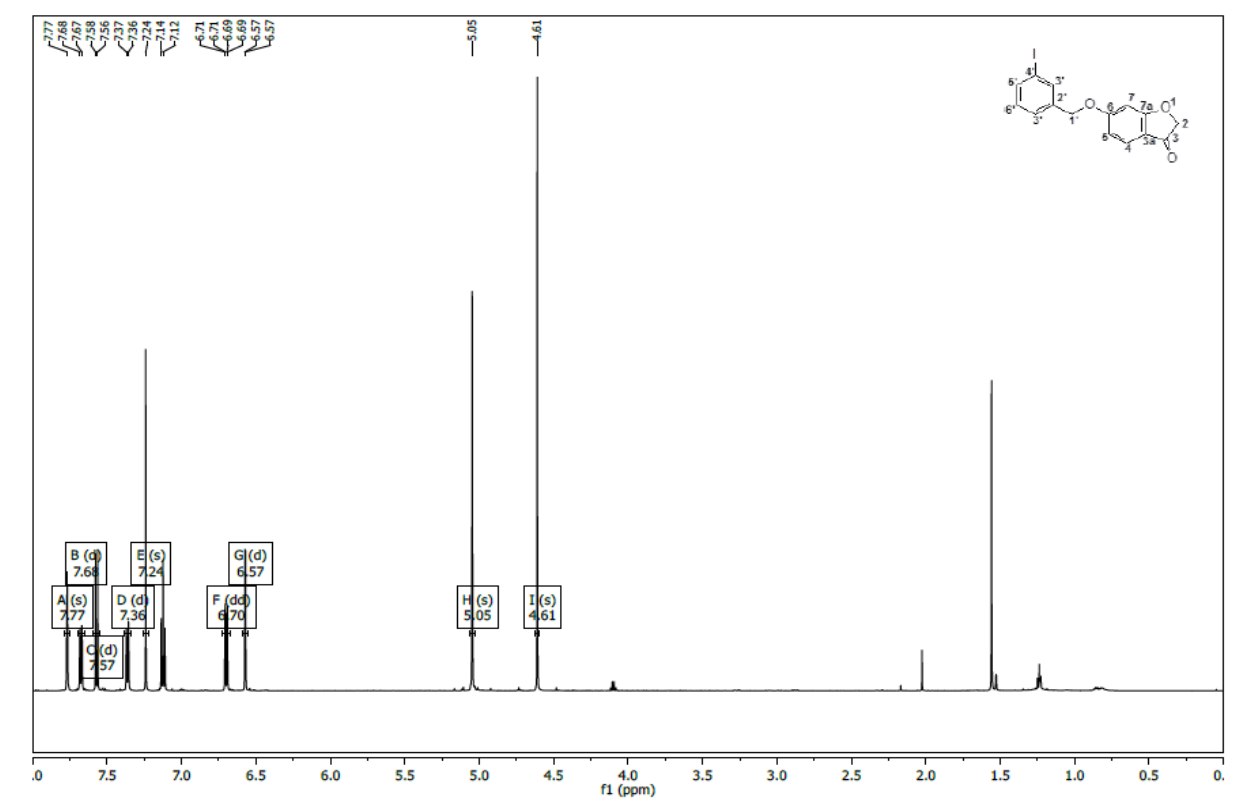
1f: 6-(4-Bromobenzyloxy)-2H-1-benzofuran-3-one



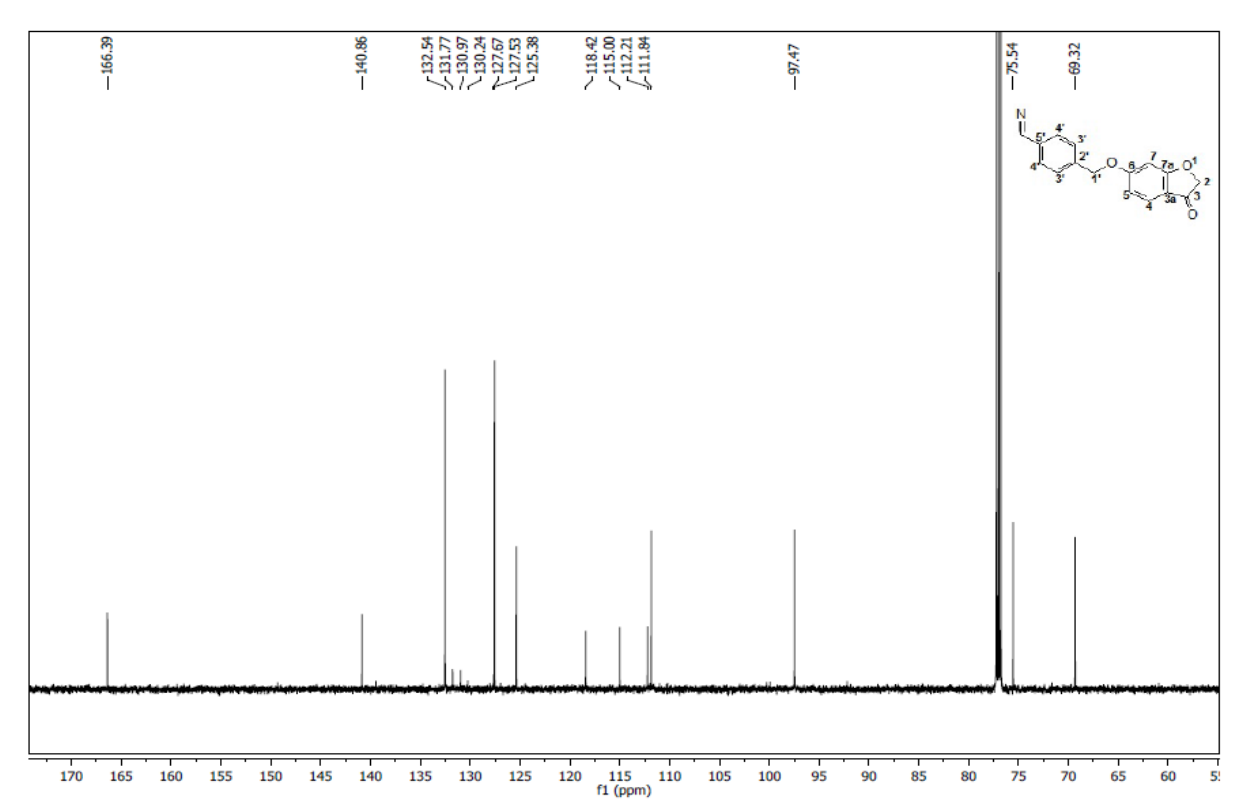
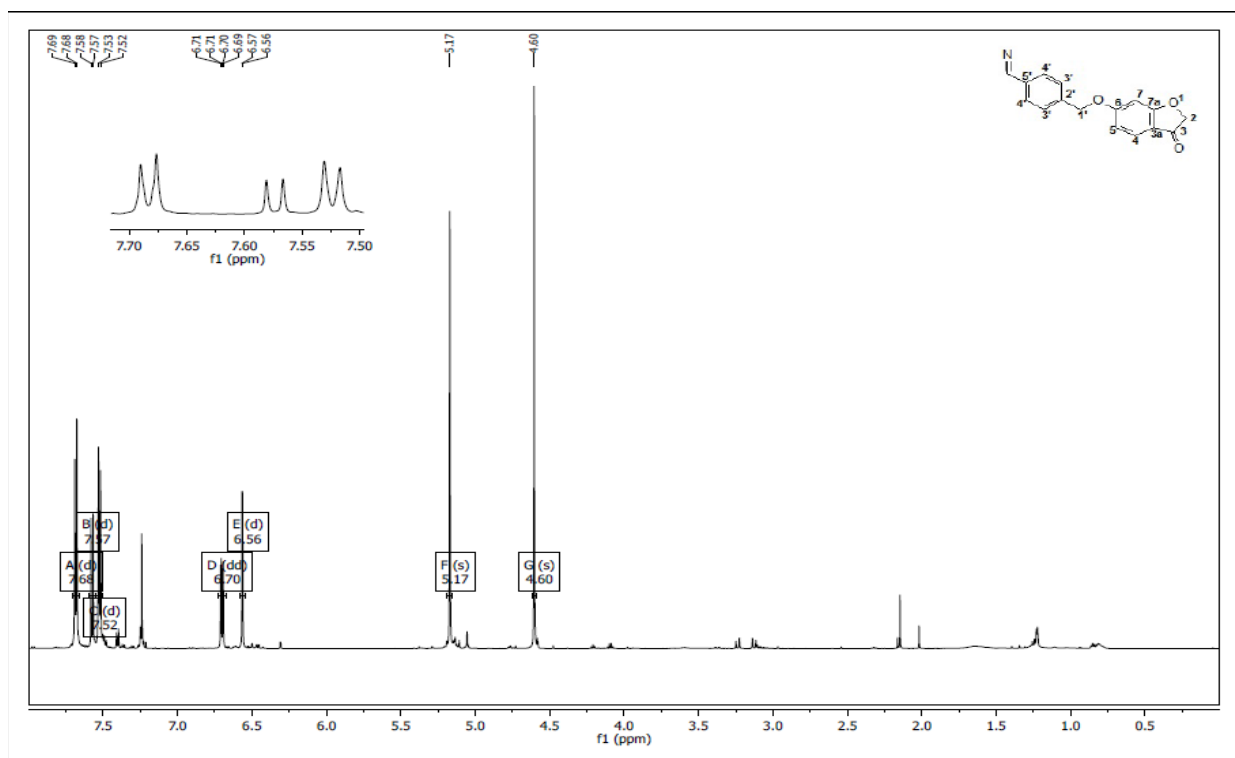
1g: 6-(3-Bromobenzoyloxy)-2H-1-benzofuran-3-one

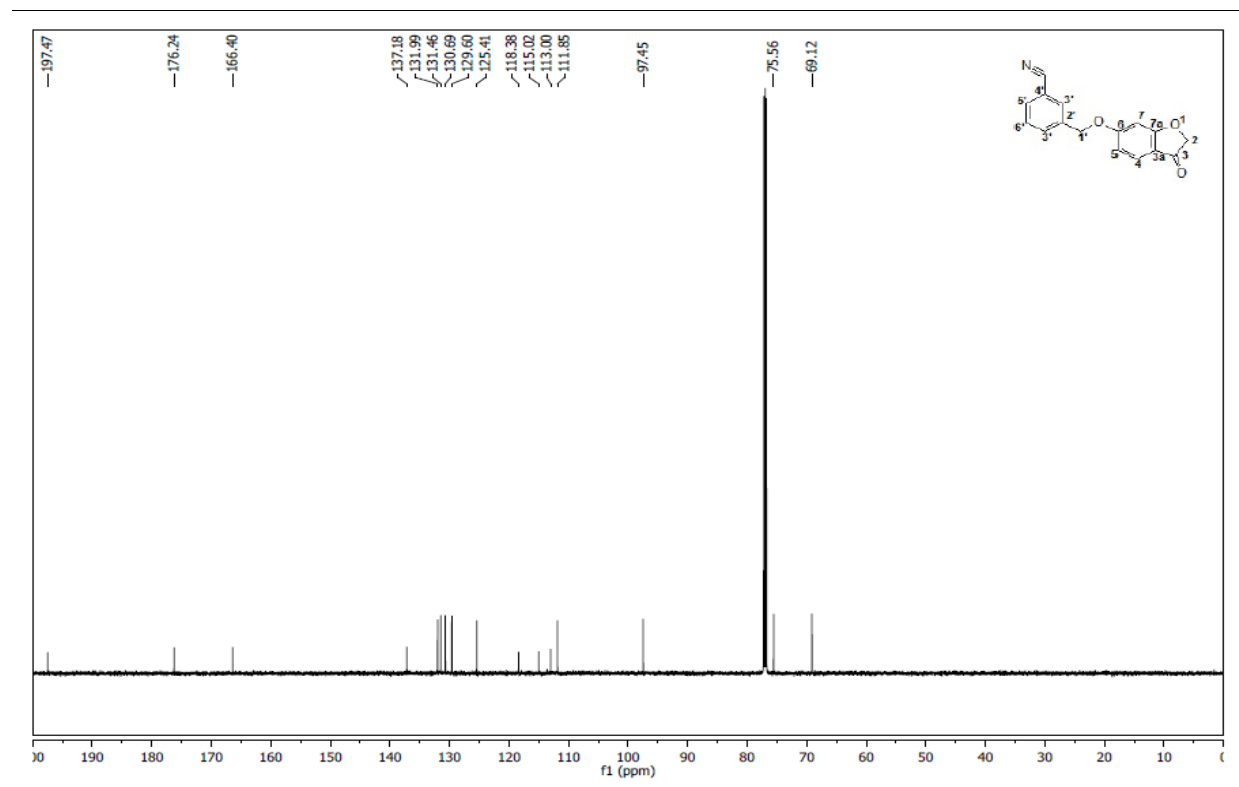
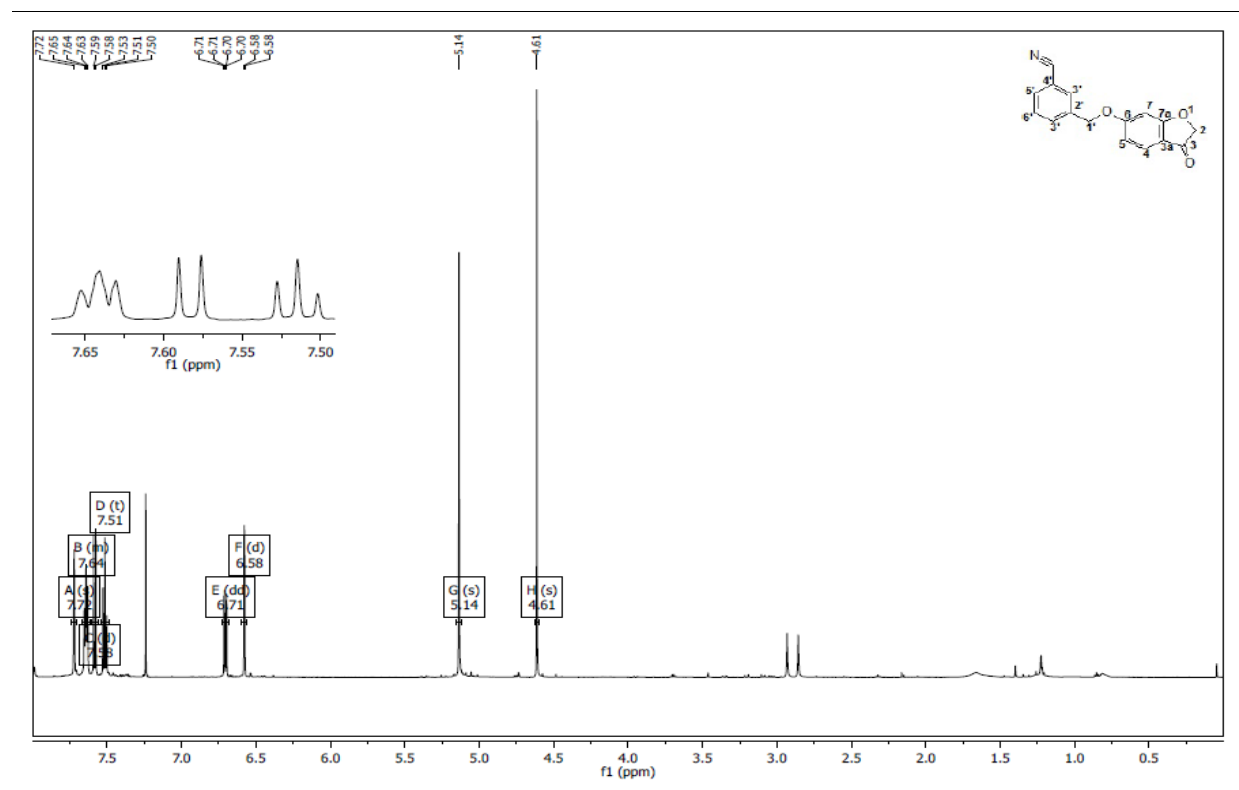
1h: 6-(4-Iodobenzyloxy)-2H-1-benzofuran-3-one

1i: 6-(3-Iodobenzyloxy)-2H-1-benzofuran-3-one

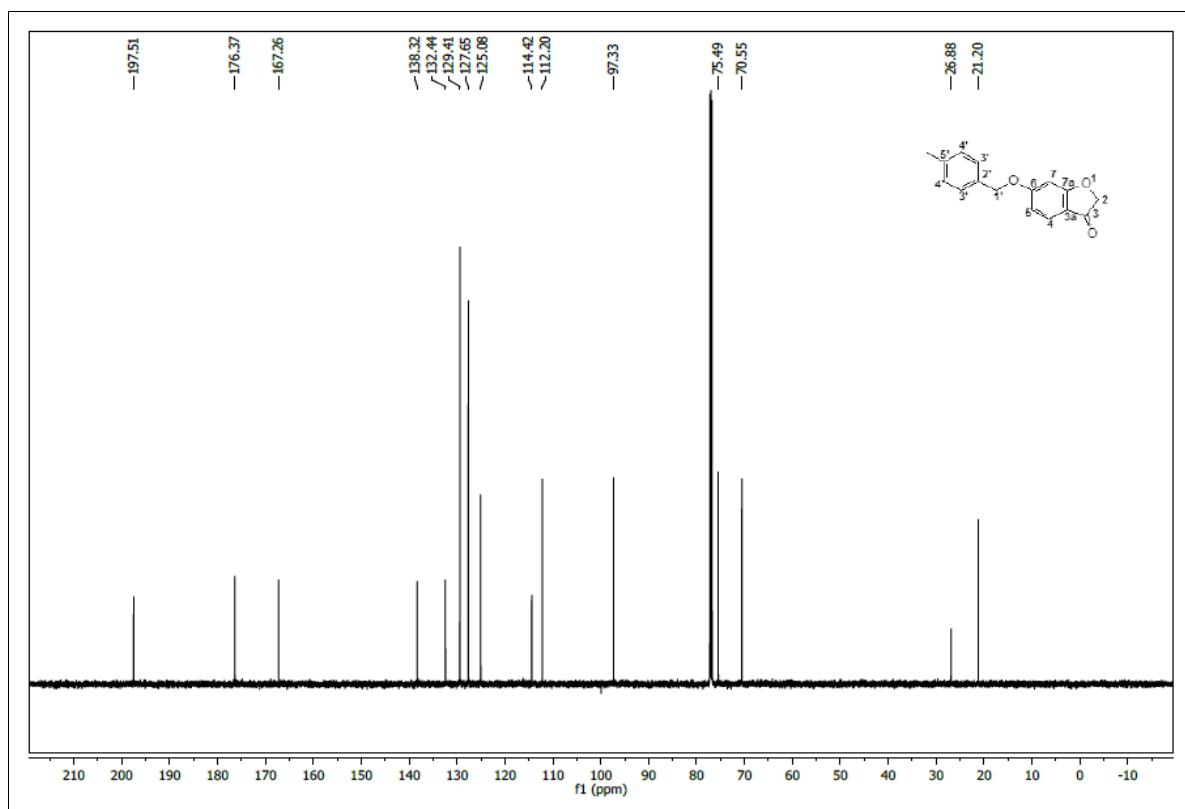
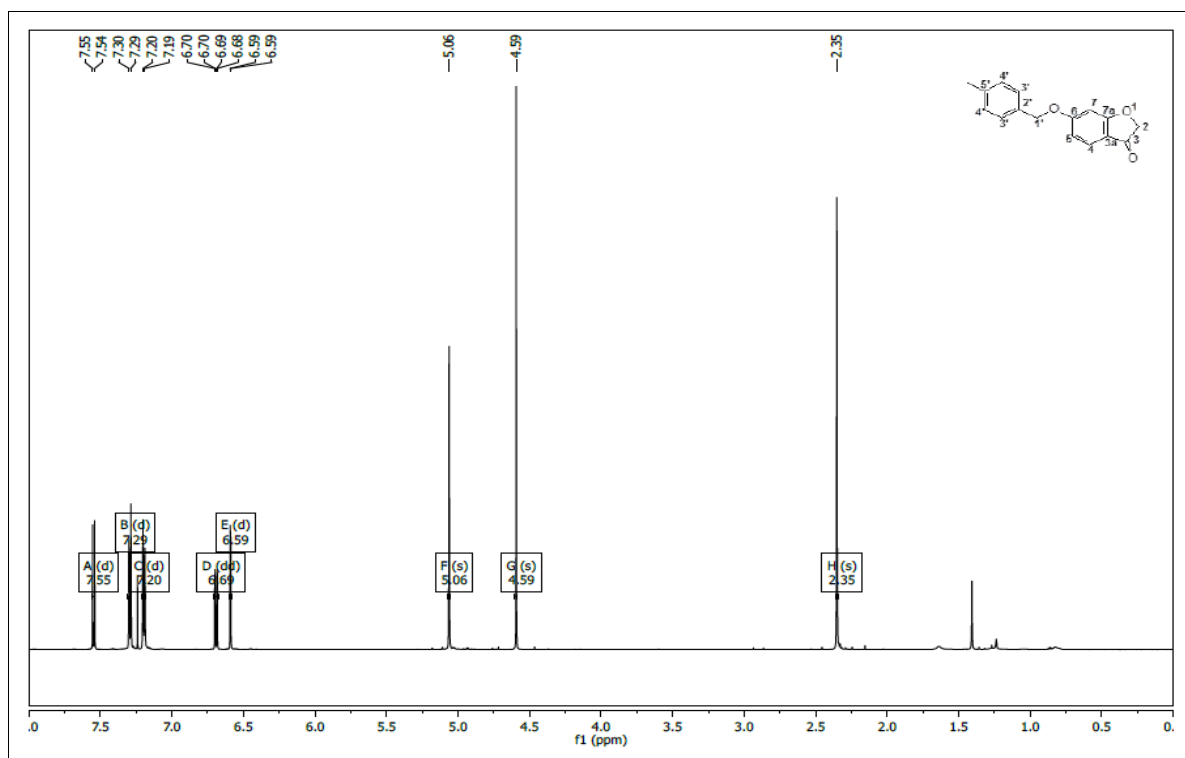


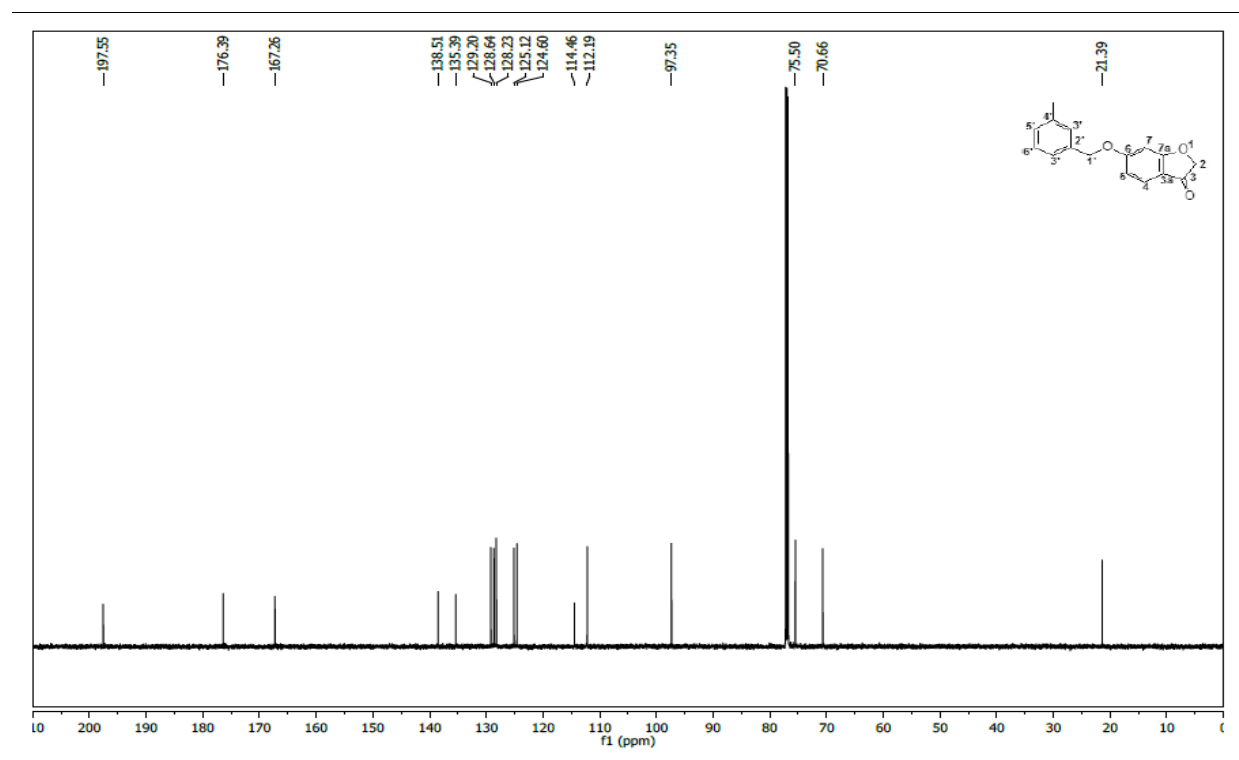
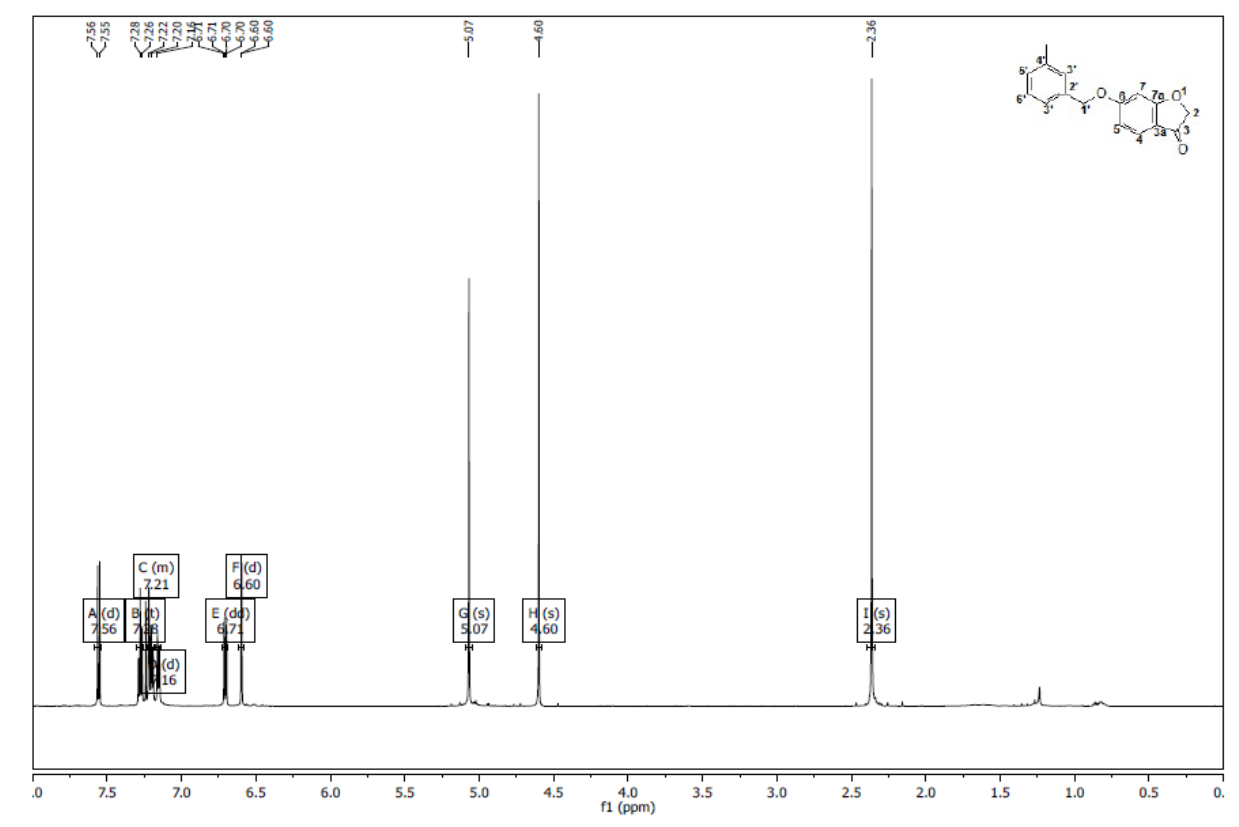
1j: 6-(4-Cyanobenzoyloxy)-2H-1-benzofuran-3-one

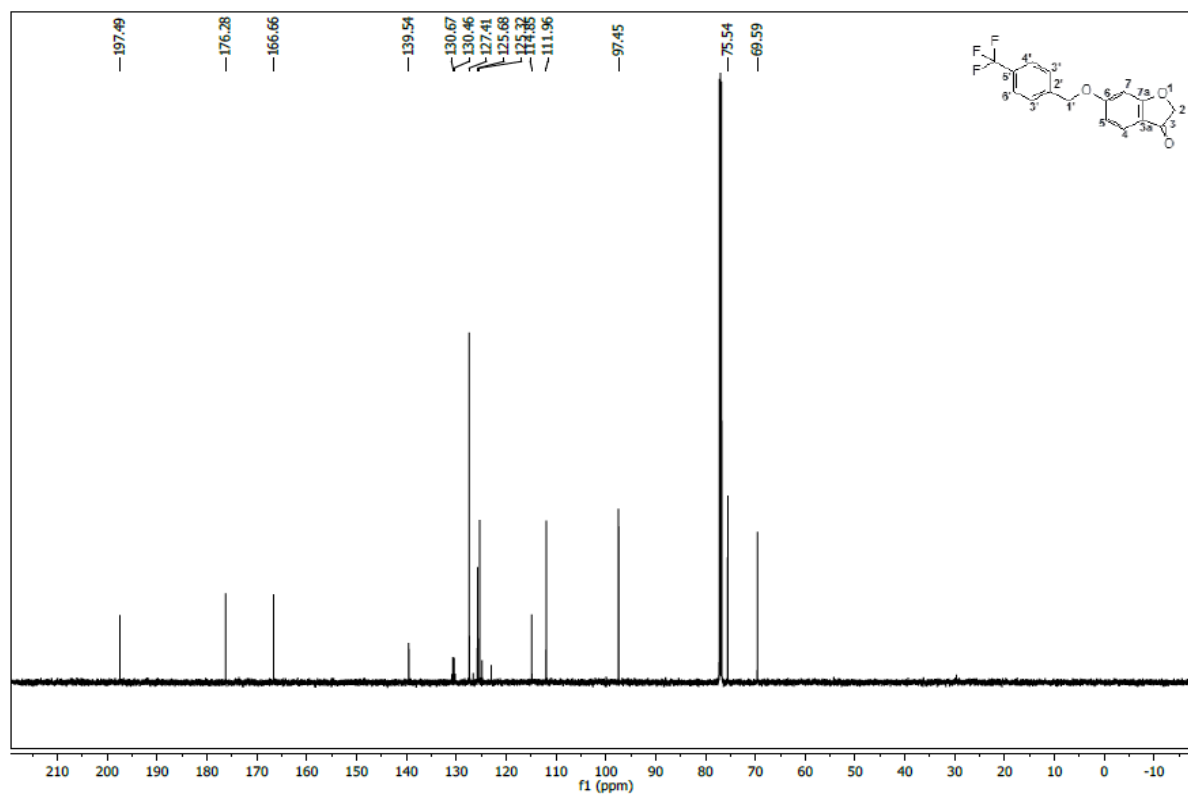
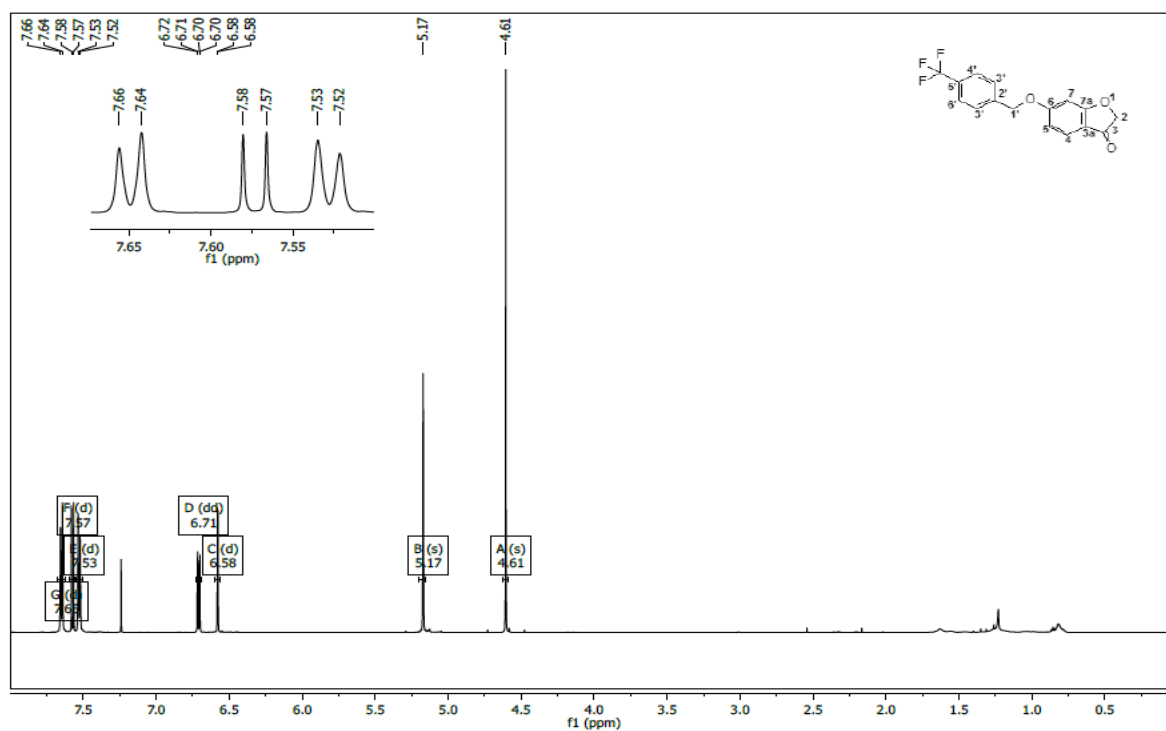


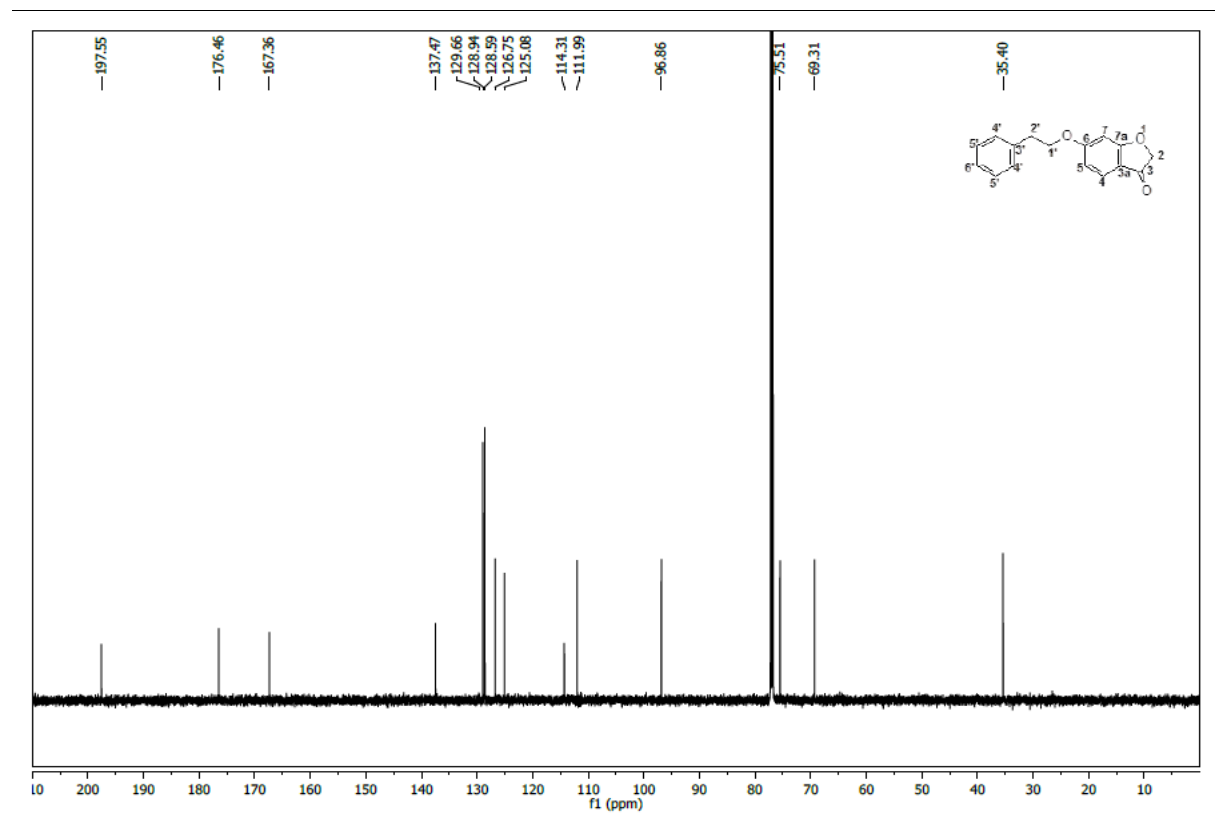
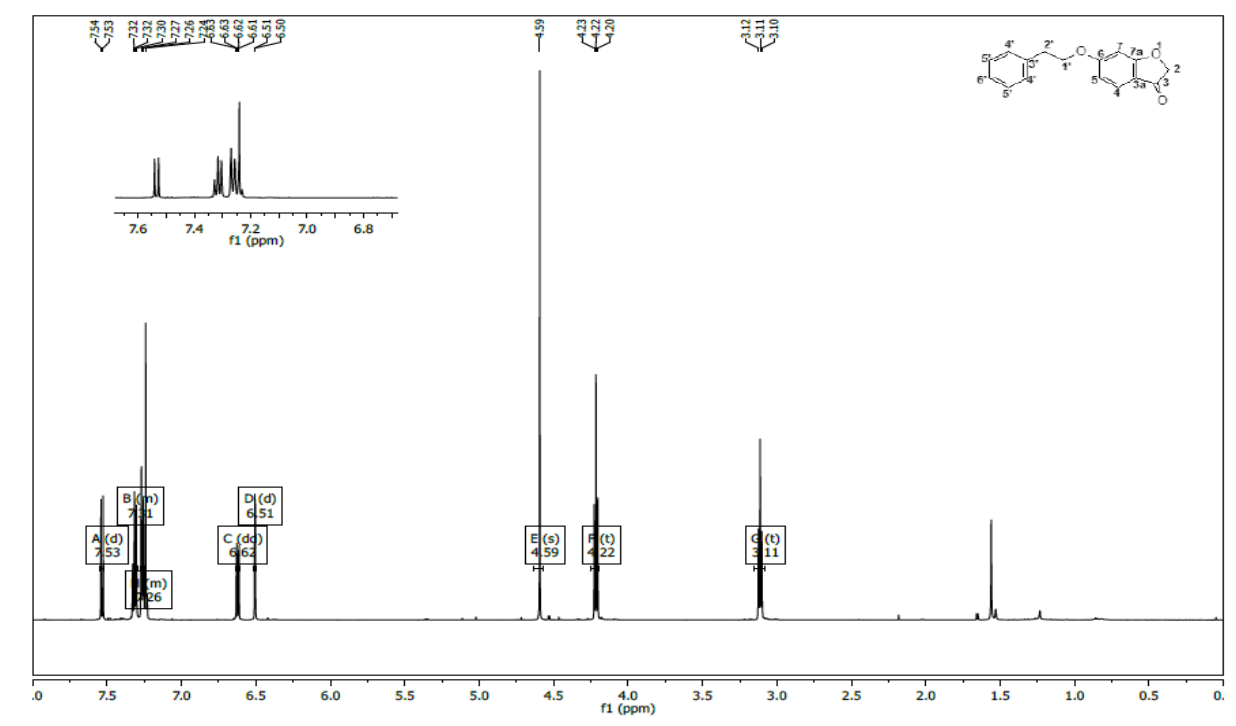
1k: 6-(3-Cyanobenzoyloxy)-2H-1-benzofuran-3-one

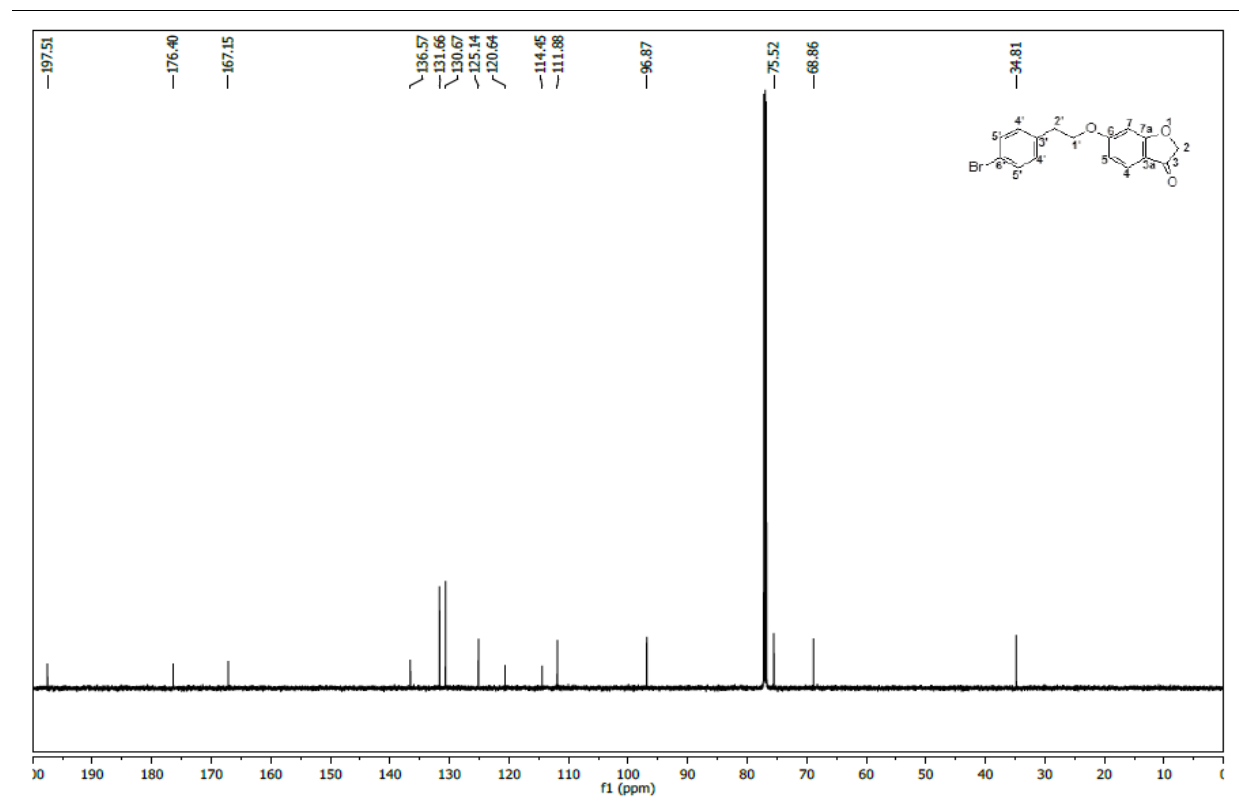
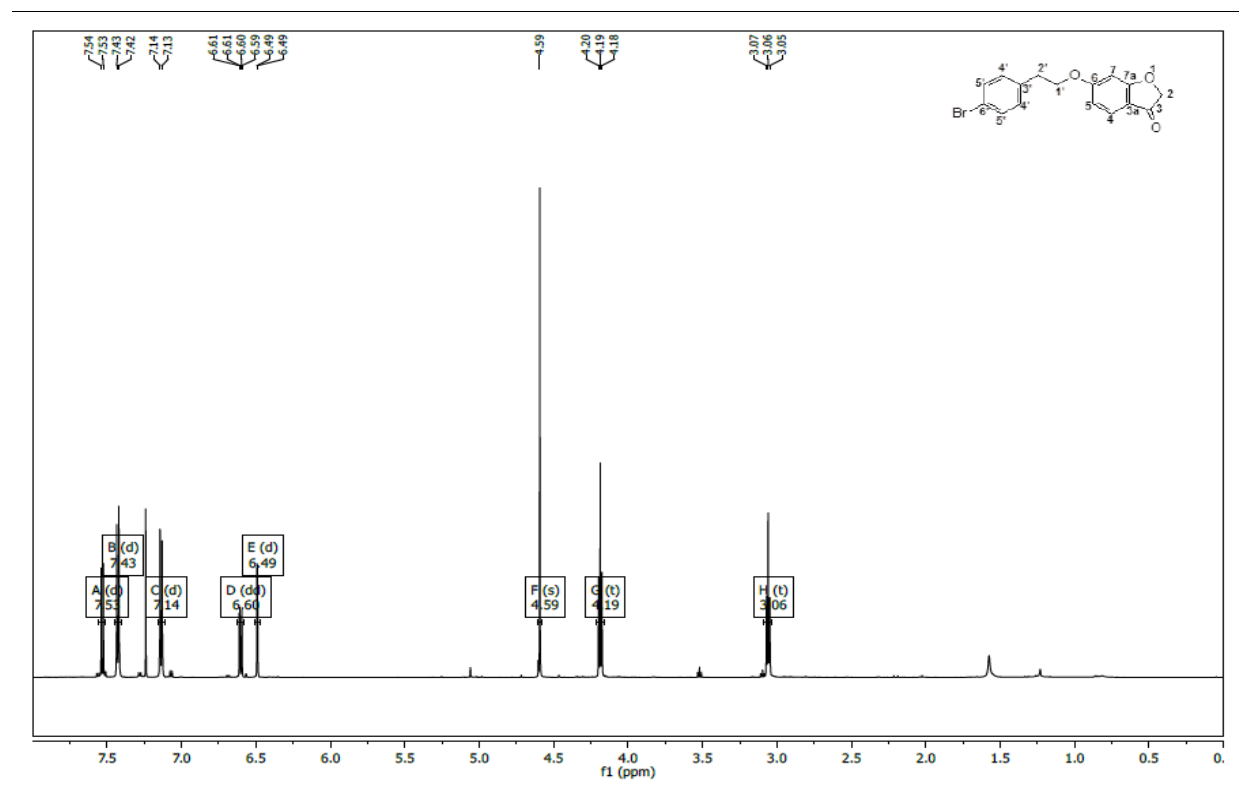
11: 6-(4-Methylbenzyloxy)-2H-1-benzofuran-3-one

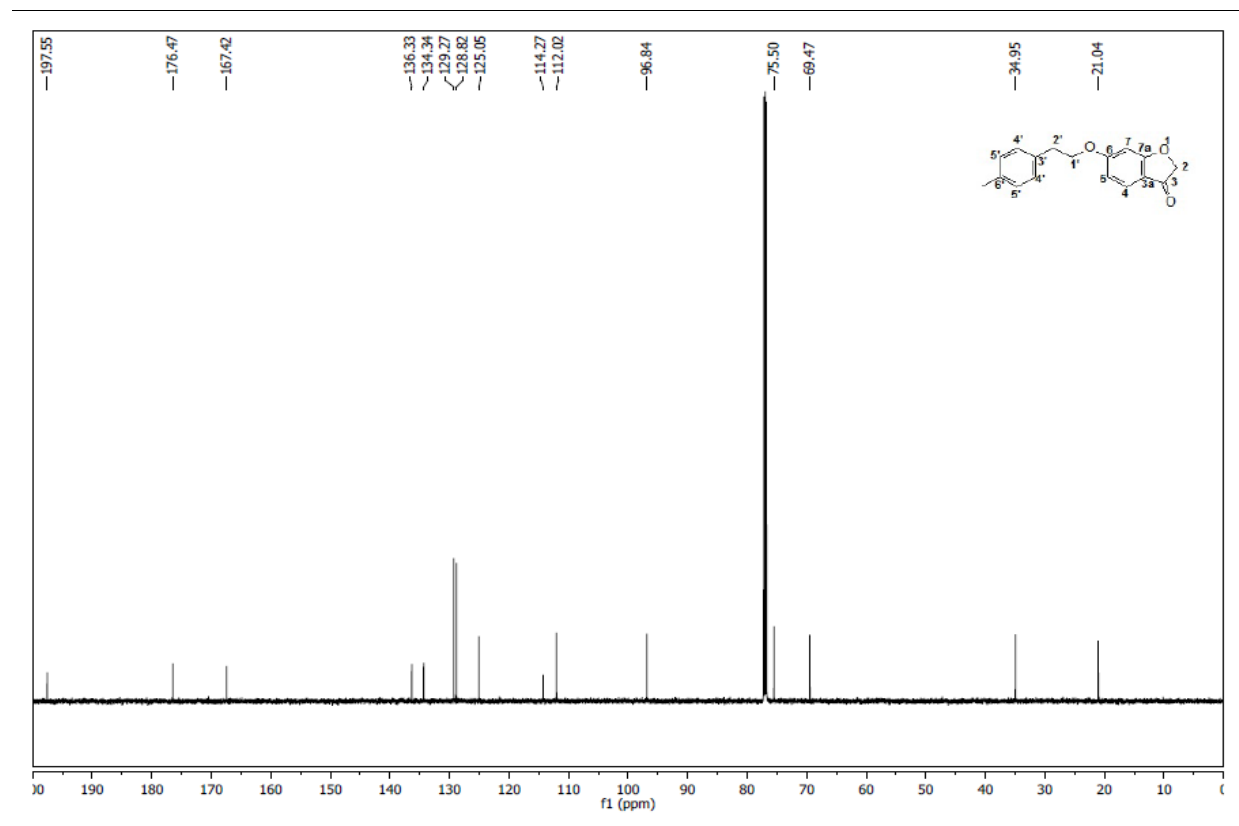
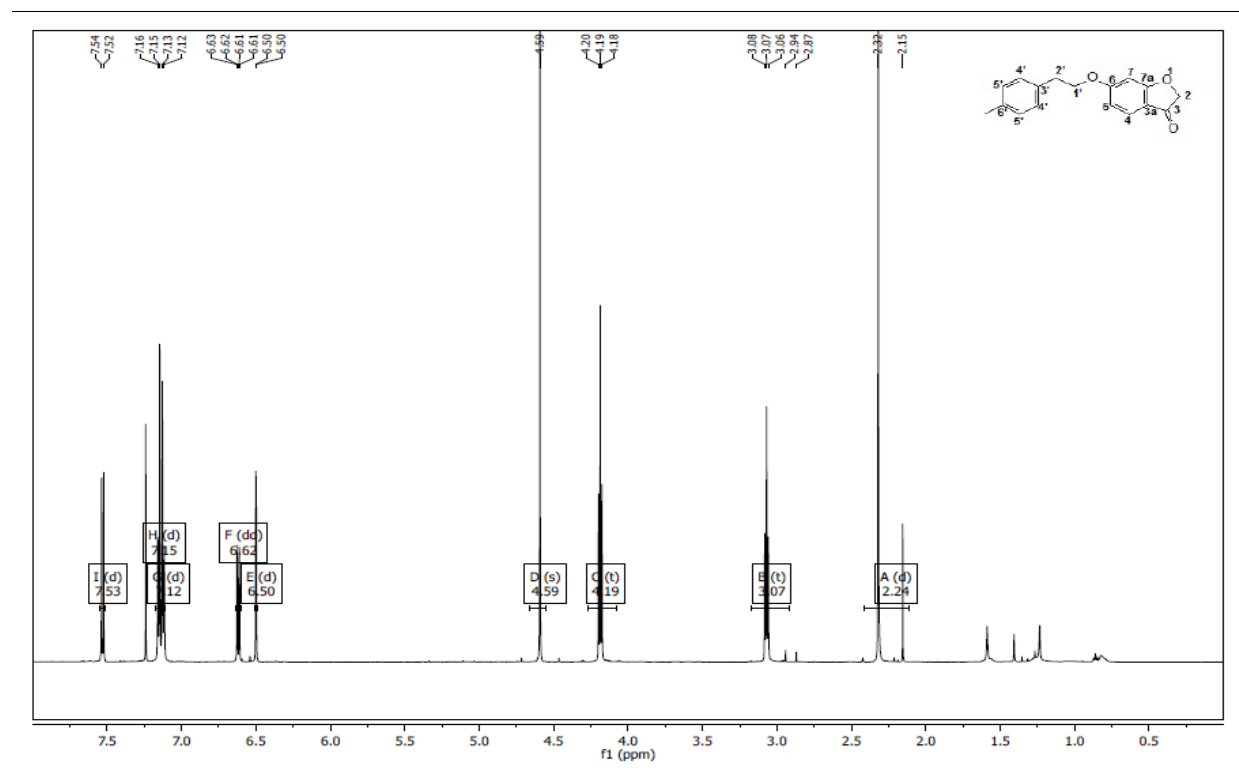


1m: 6-(3-Methylbenzyloxy)-2H-1-benzofuran-3-one

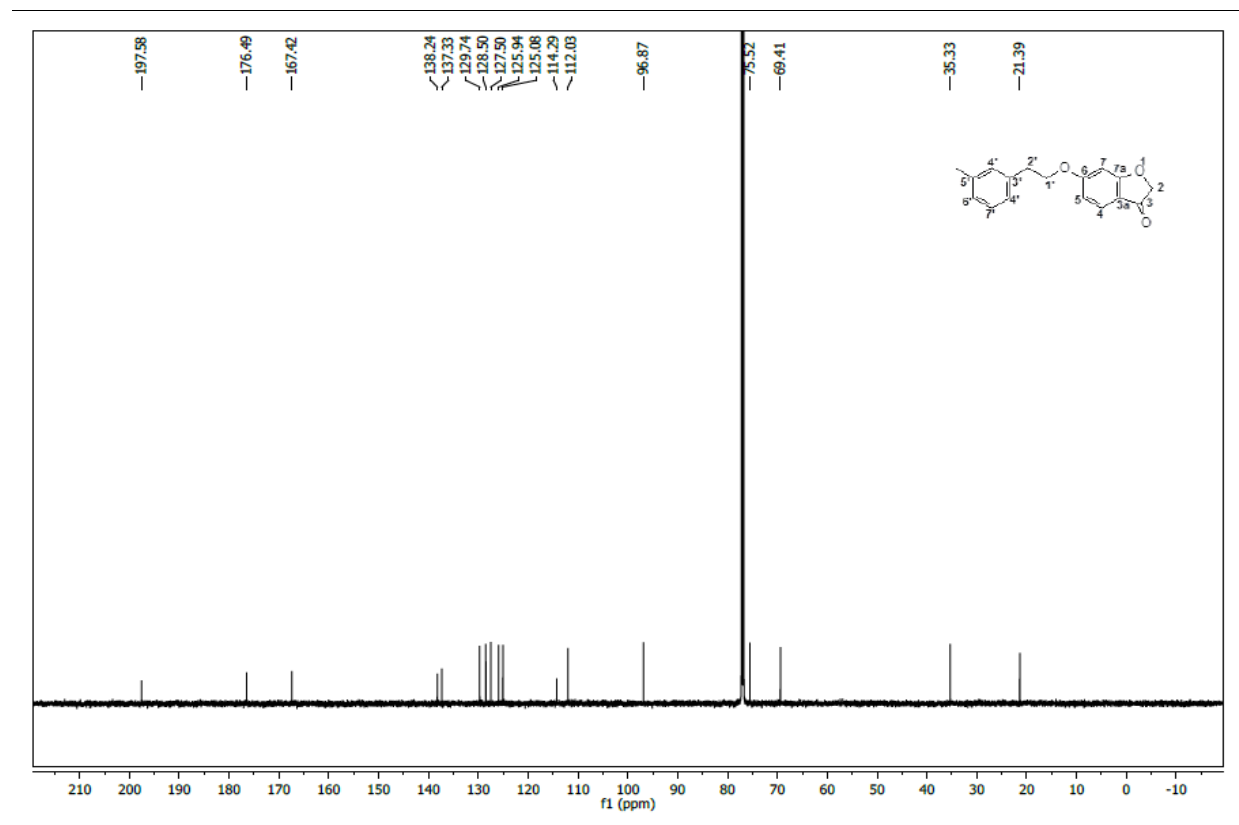
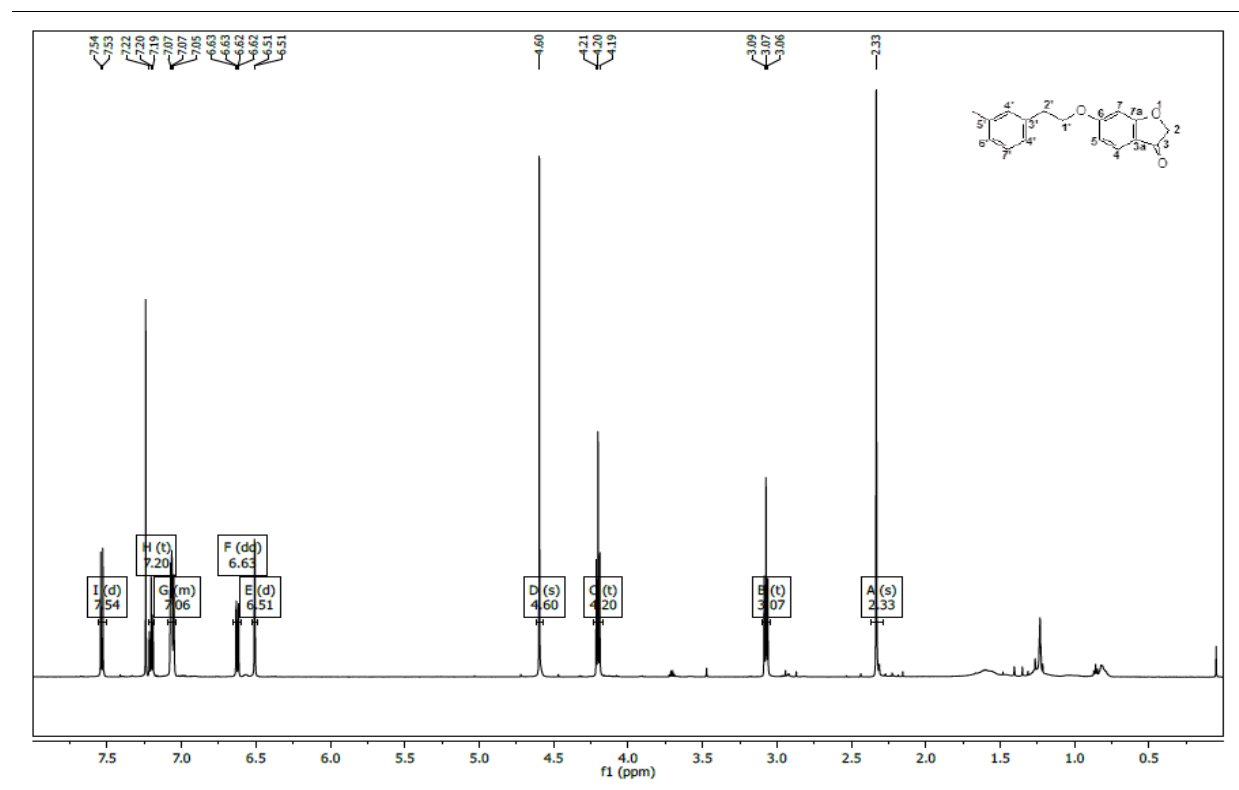
1n: 6-[4-(Trifluoromethyl)benzyloxy]-2H-1-benzofuran-3-one

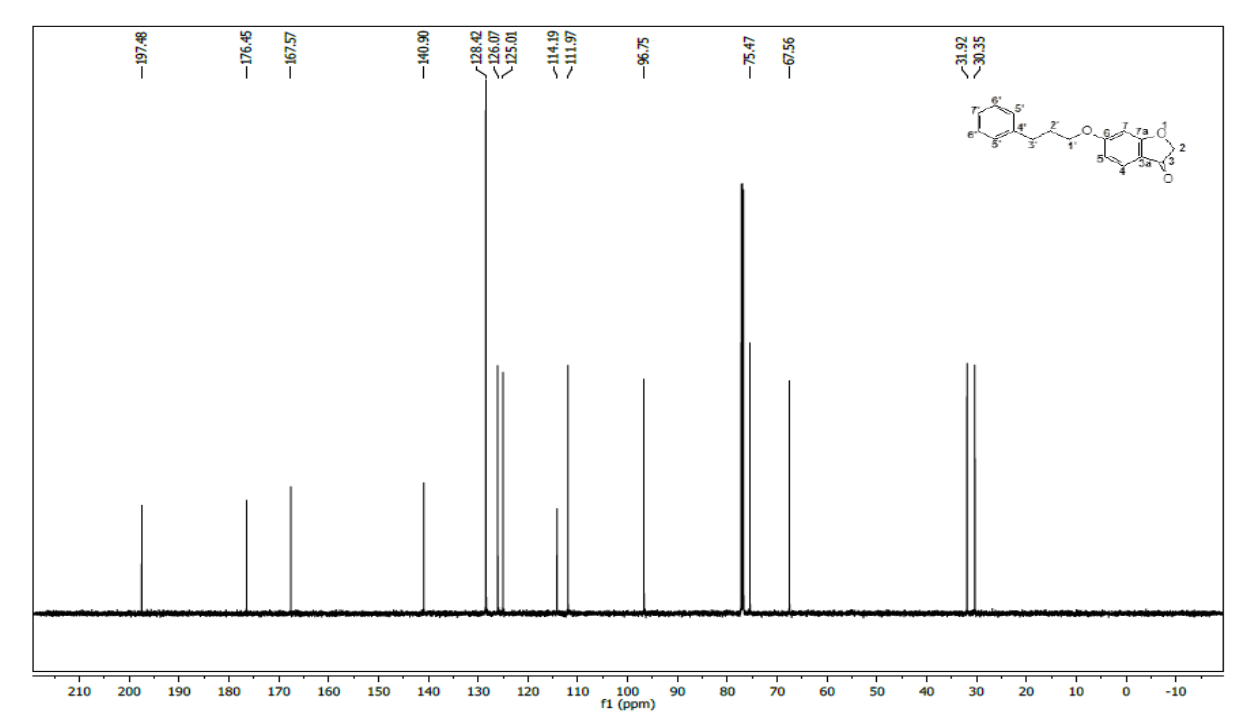
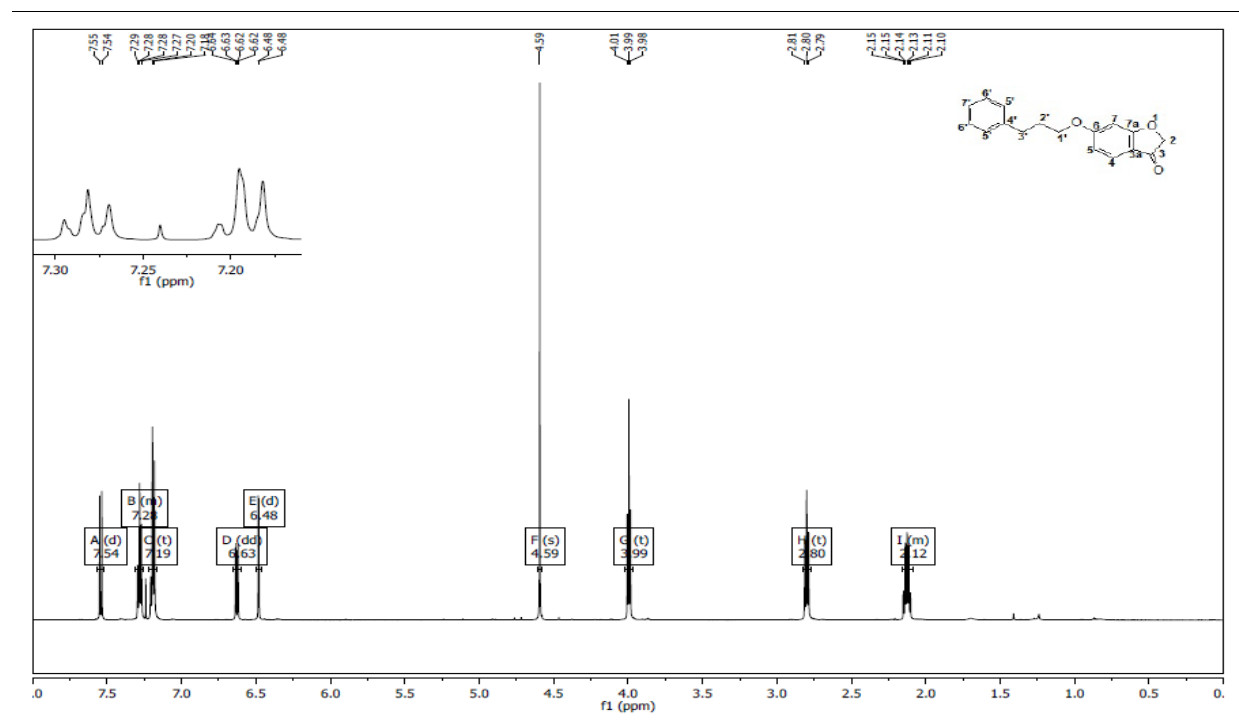
1o: 6-(2-Phenylethoxy)-2H-1-benzofuran-3-one

1p: 6-[2-(4-Bromophenyl)ethoxy]-2H-1-benzofuran-3-one

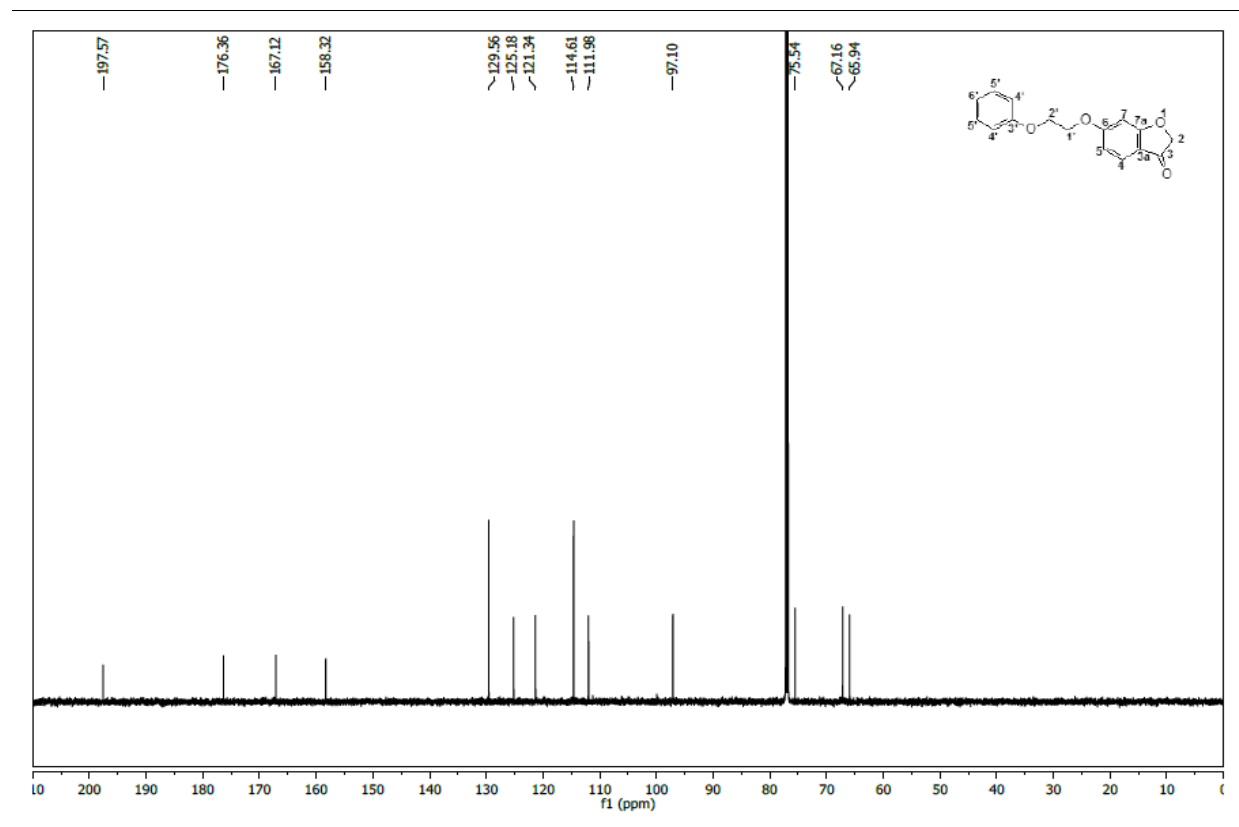
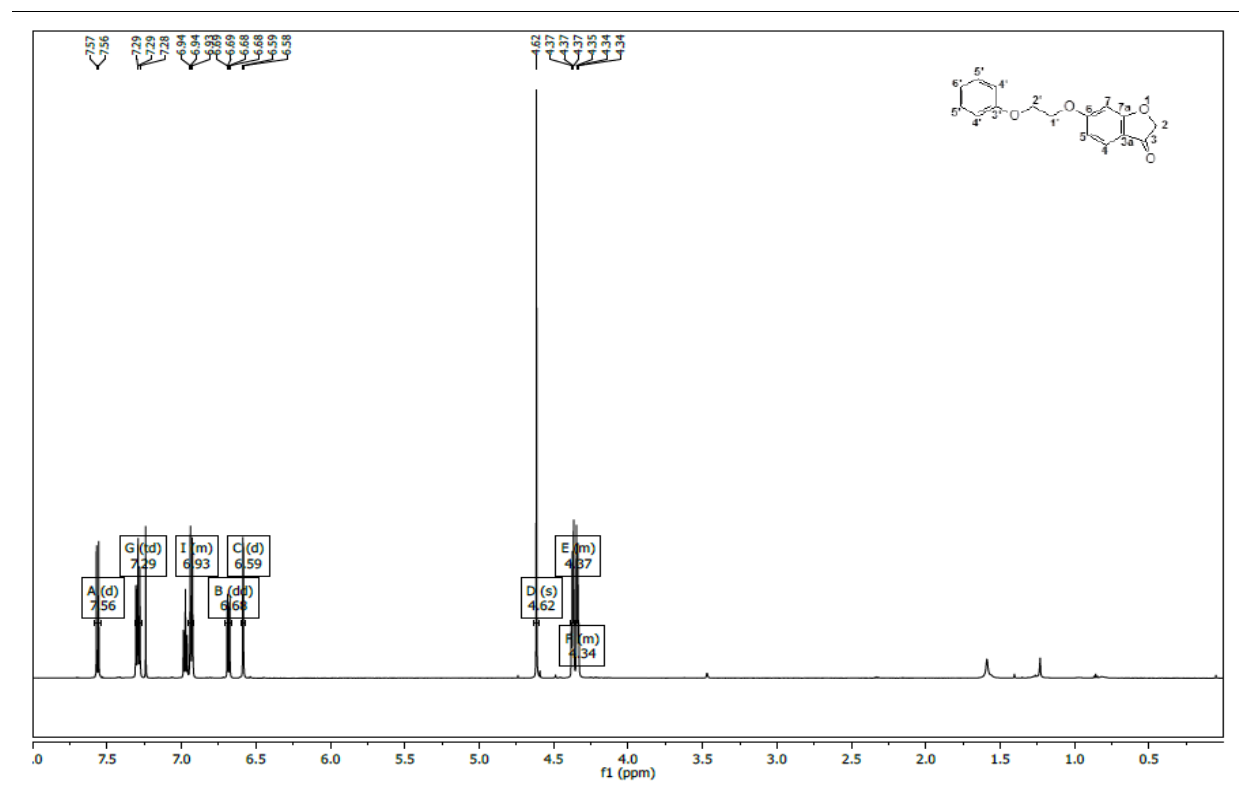
1q: 6-[2-(4-Methylphenyl)ethoxy]-2H-1-benzofuran-3-one

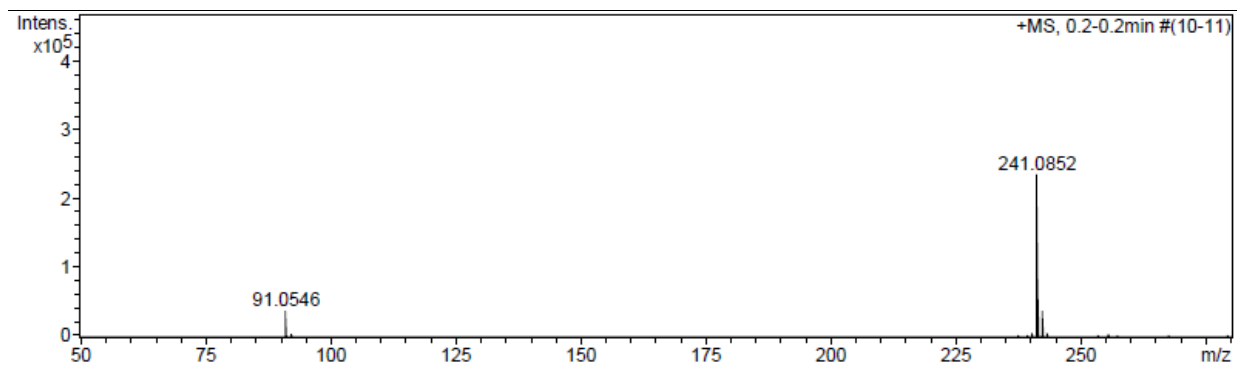
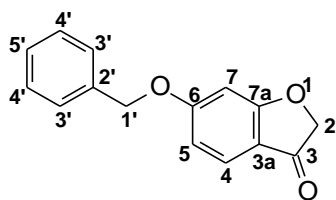
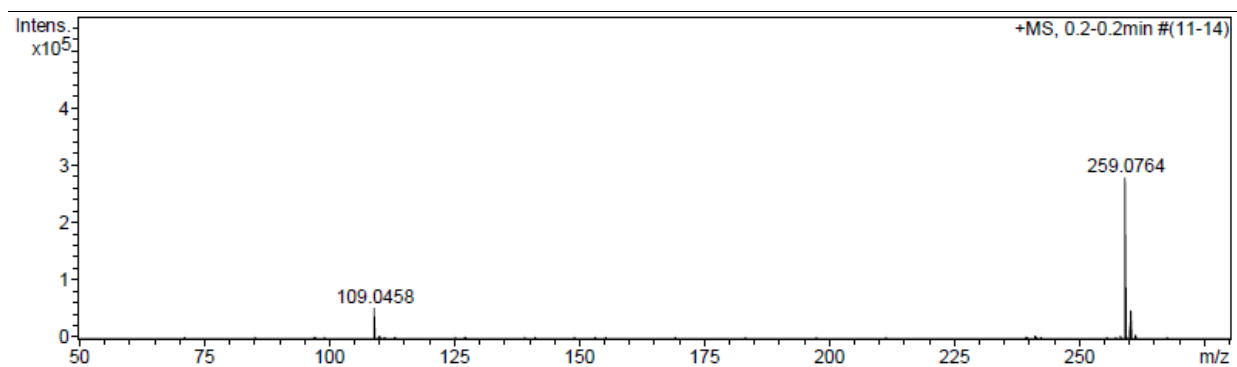
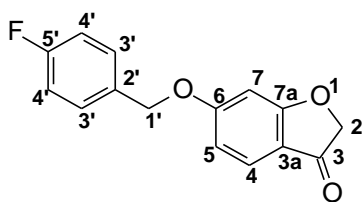
1r: 6-[2-(3-Methylphenyl)ethoxy]-2H-1-benzofuran-3-one

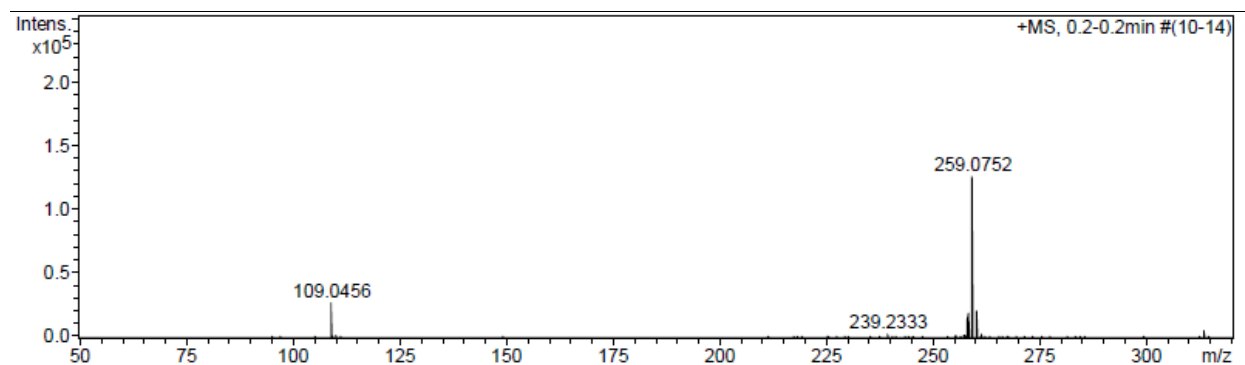
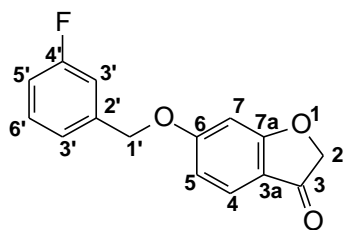
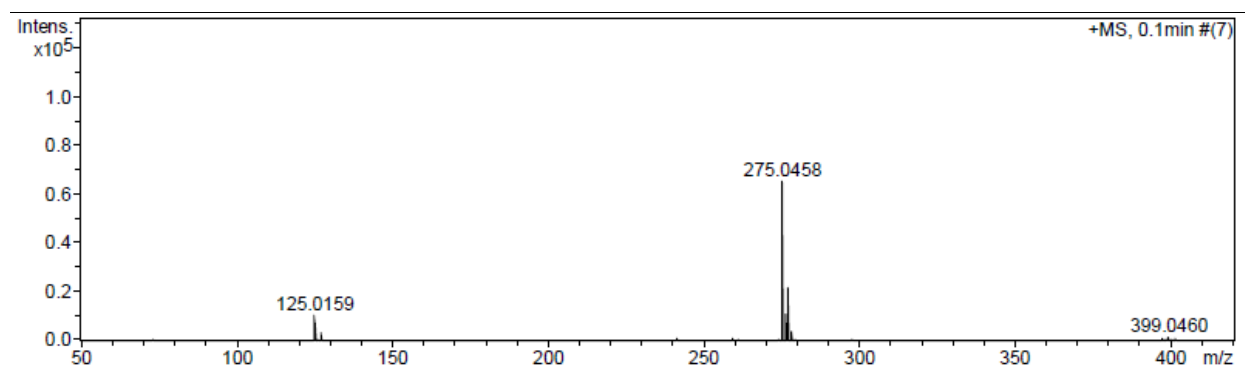
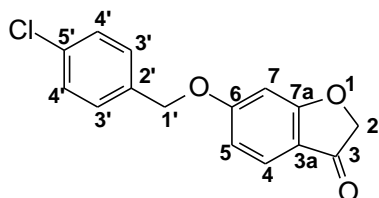


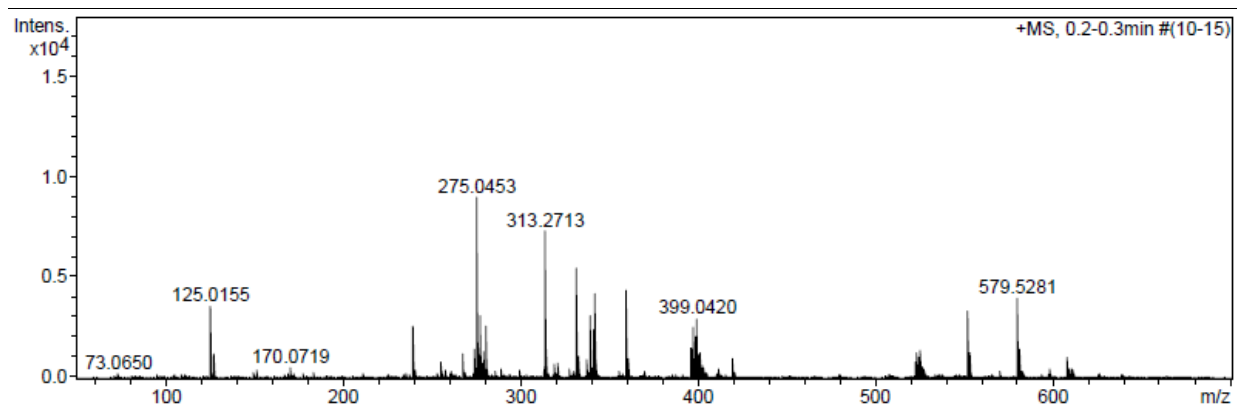
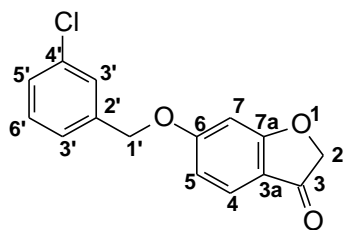
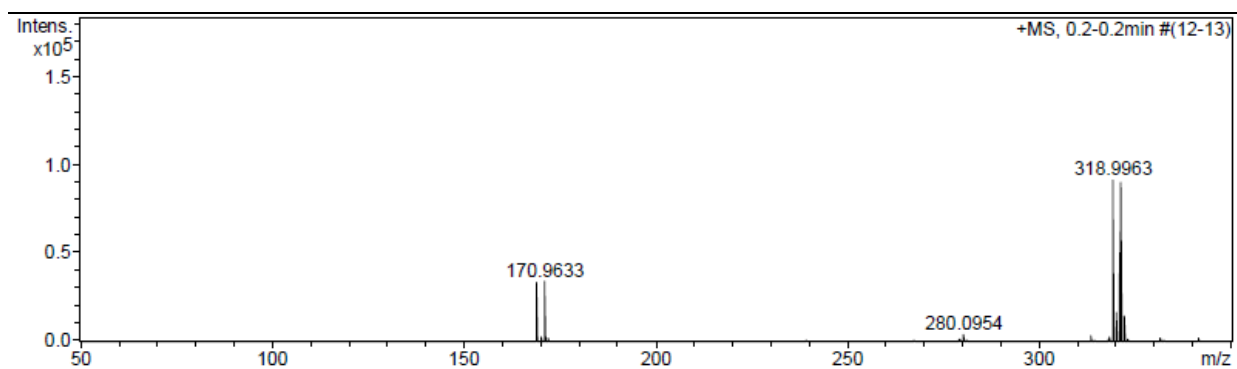
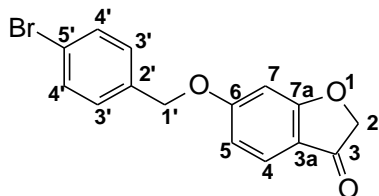
1s: 6-(3-Phenylpropoxy)-2H-1-benzofuran-3-one

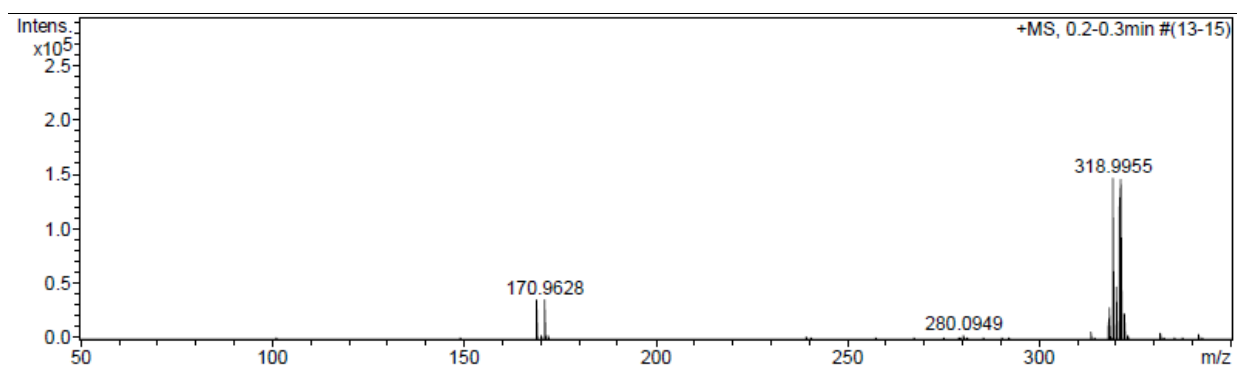
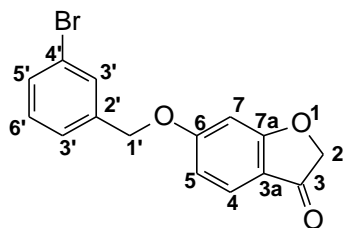
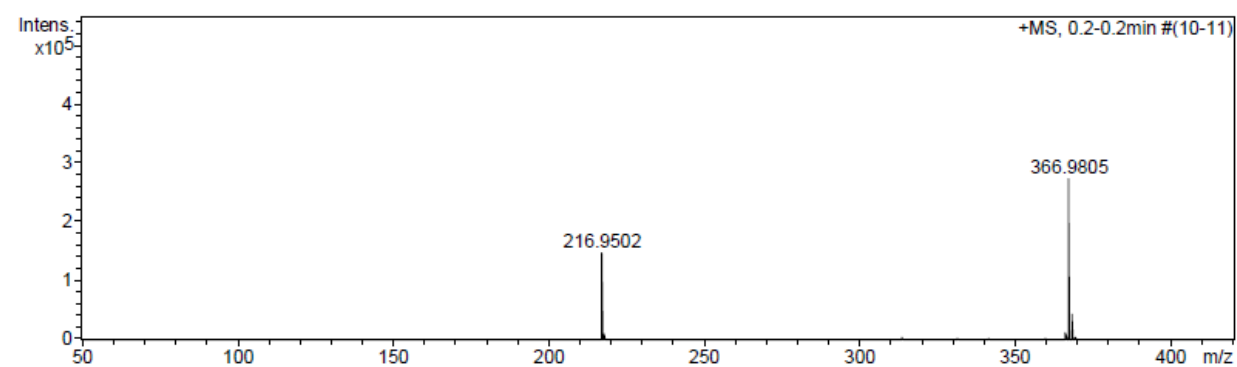
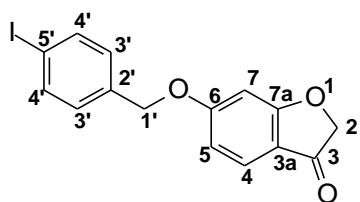
1t: 6-(2-Phenoxyethoxy)-2H-1-benzofuran-3-one

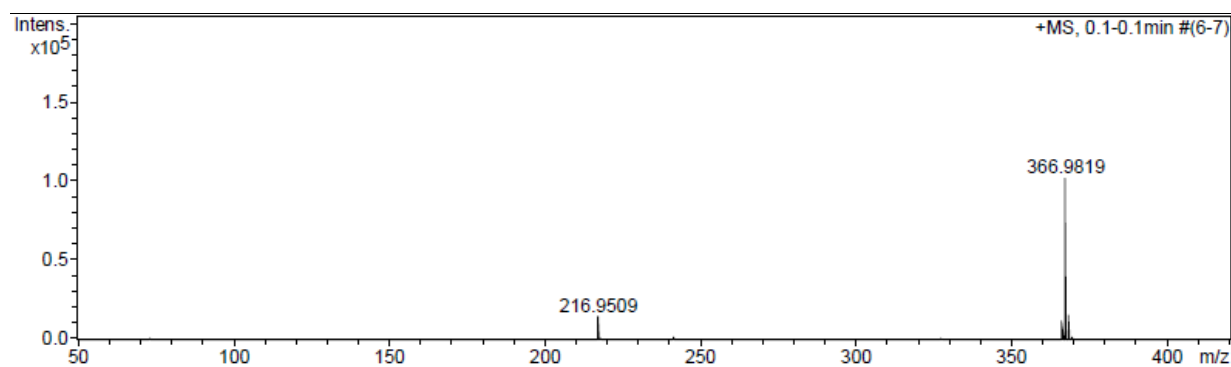
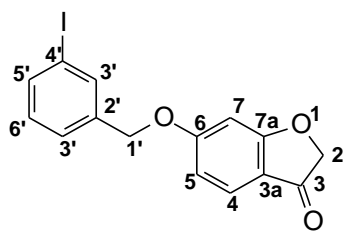
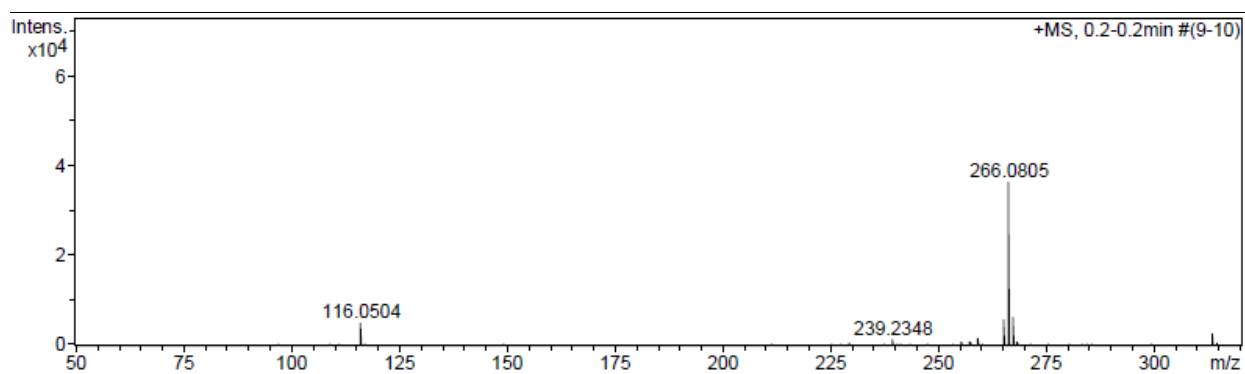
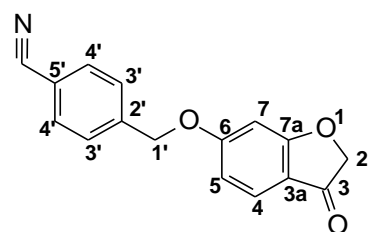


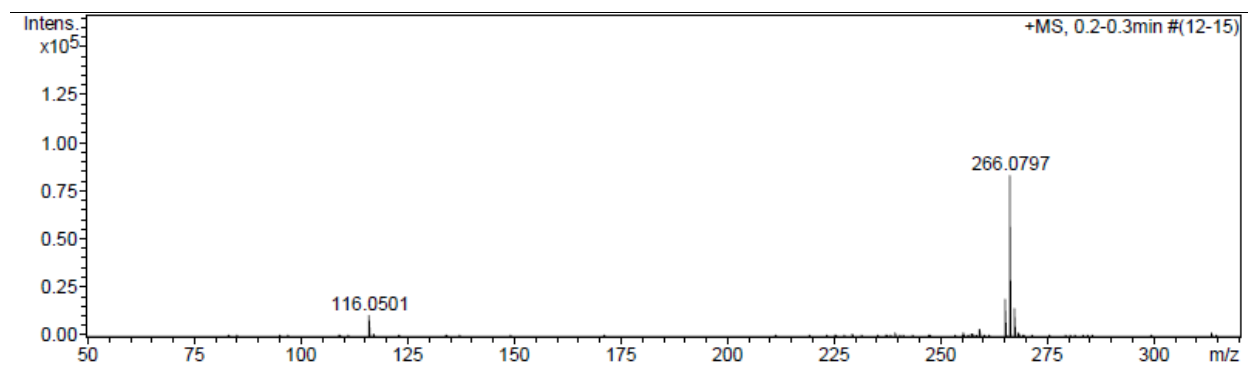
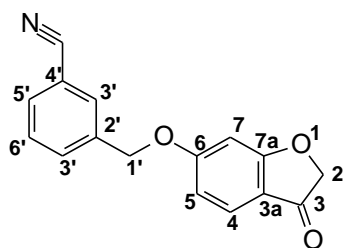
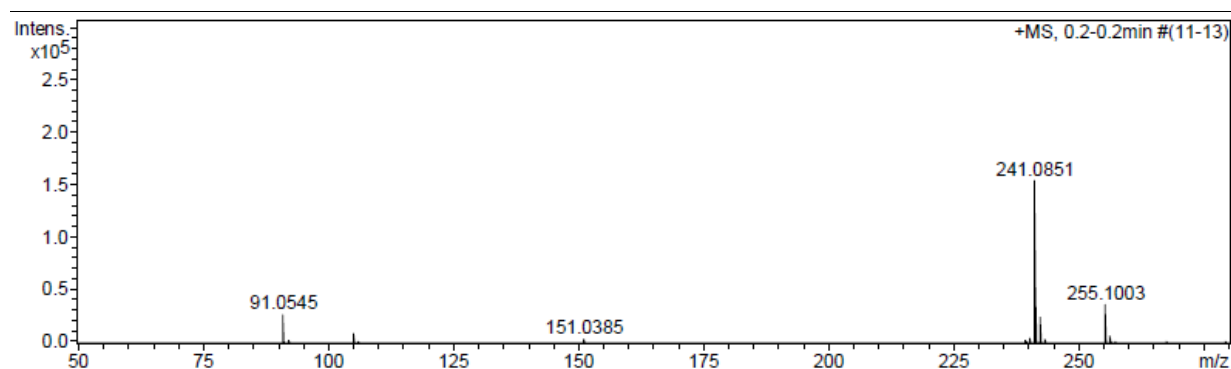
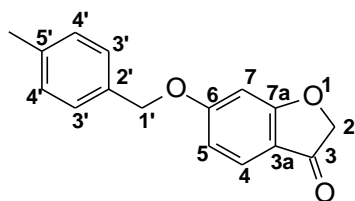
MASS SPECTRA OF THE SYNTHESISED COMPOUNDS**1a:** 6-(Benzyloxy)-2H-1-benzofuran-3-one**1b:** 6-(4-Fluorobenzyloxy)-2H-1-benzofuran-3-one

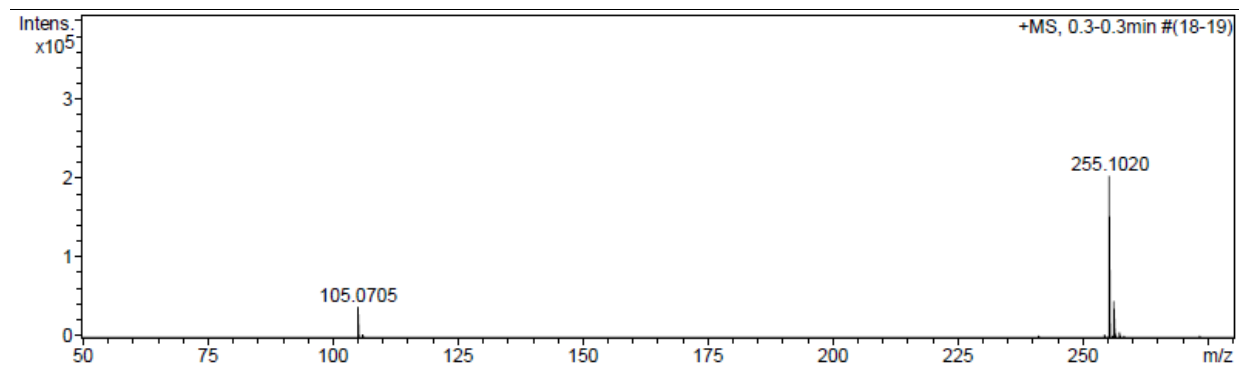
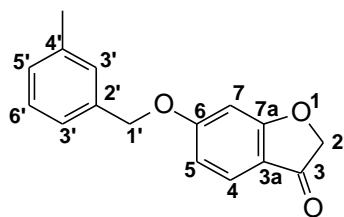
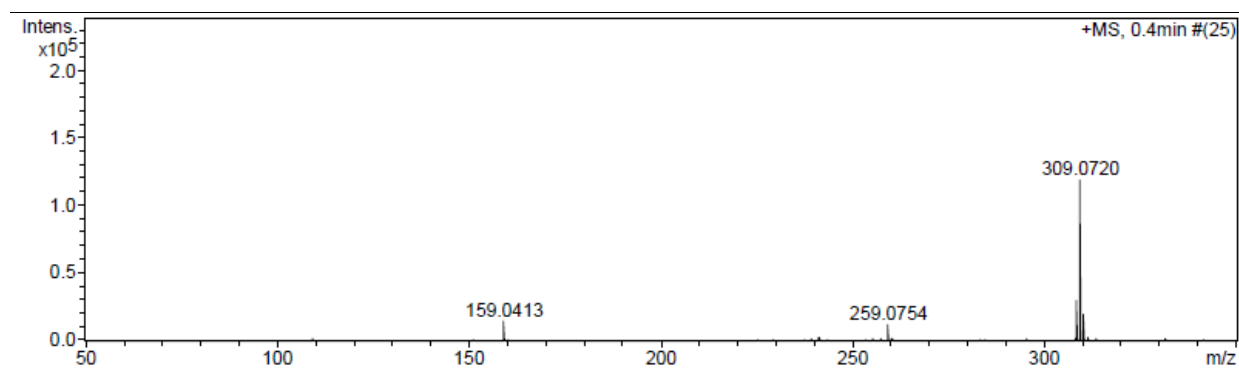
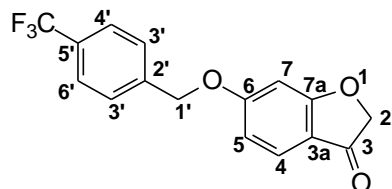
1c: 6-(3-Fluorobenzoyloxy)-2H-1-benzofuran-3-one**1d:** 6-(4-Chlorobenzoyloxy)-2H-1-benzofuran-3-one

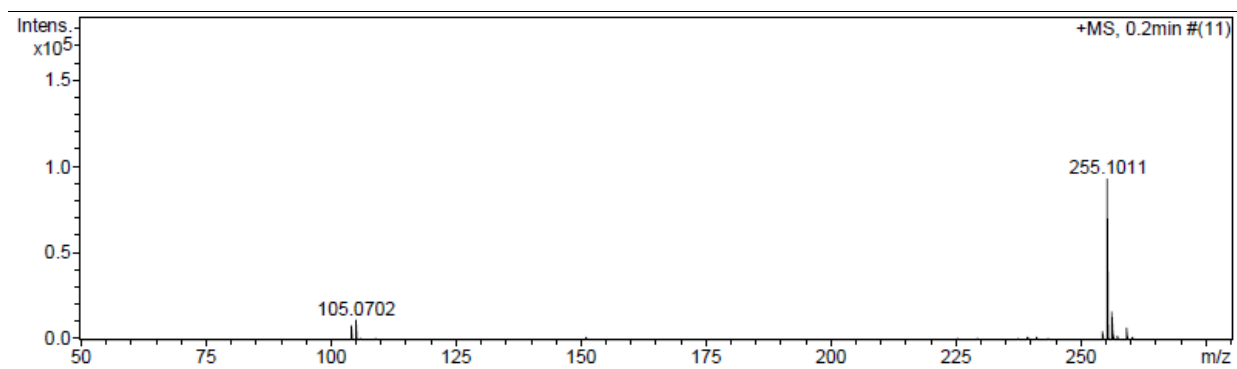
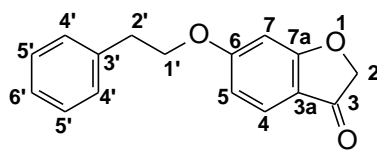
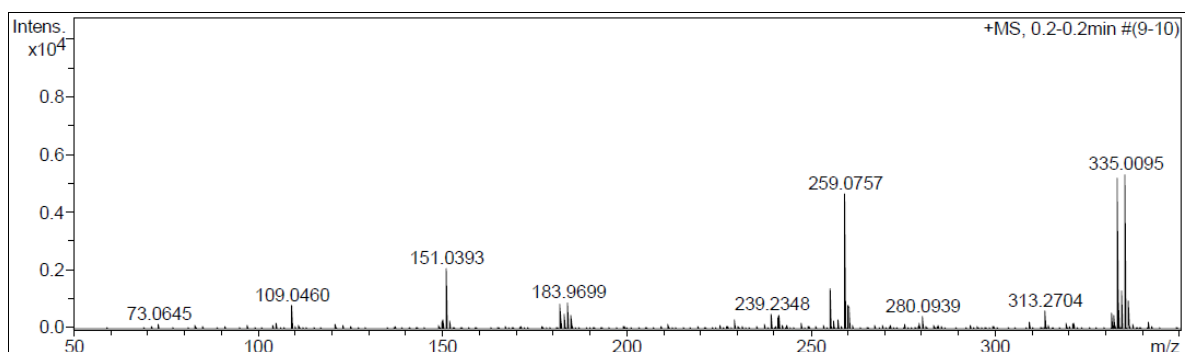
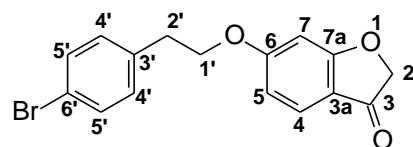
1e: 6-(3-Chlorobenzoyloxy)-2H-1-benzofuran-3-one**1f:** 6-(4-Bromobenzoyloxy)-2H-1-benzofuran-3-one

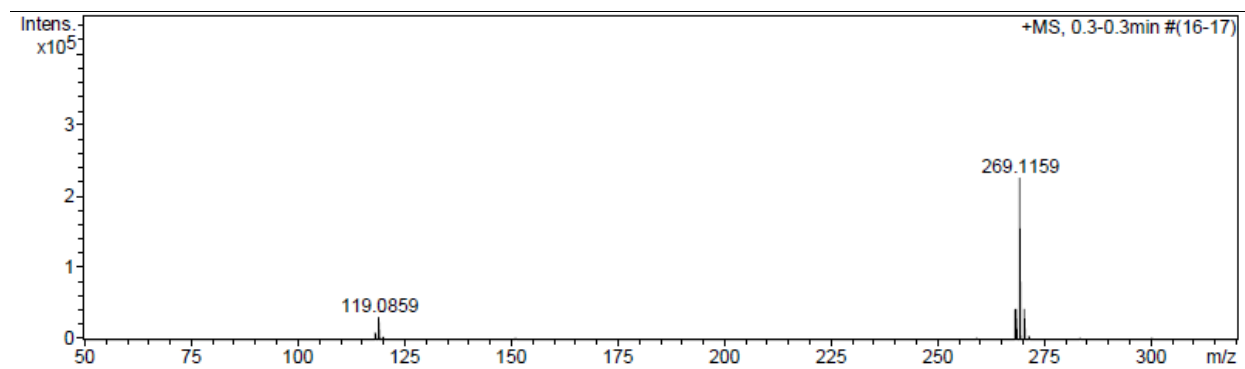
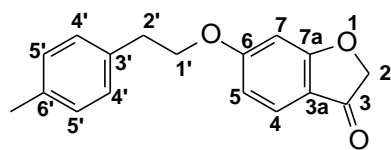
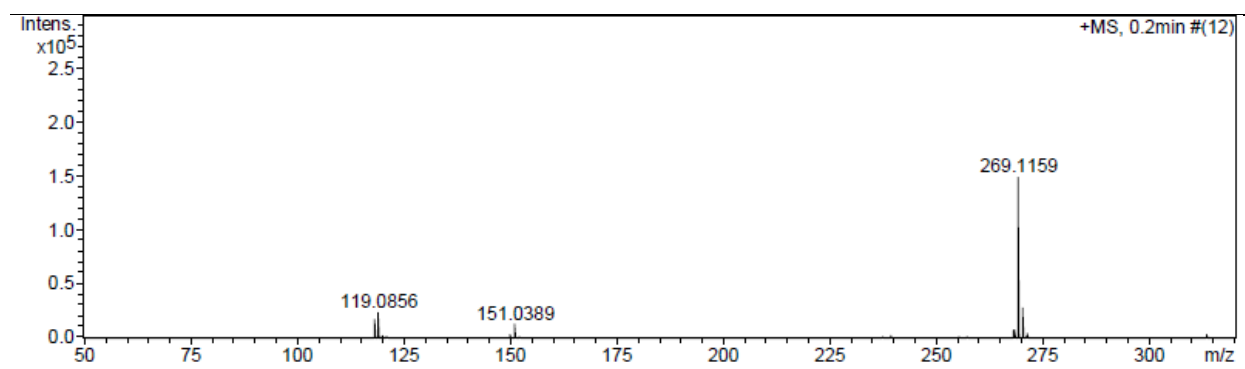
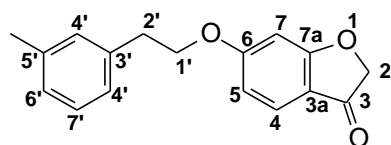
1g: 6-(3-Bromobenzyloxy)-2H-1-benzofuran-3-one**1h:** 6-(4-Iodobenzyloxy)-2H-1-benzofuran-3-one

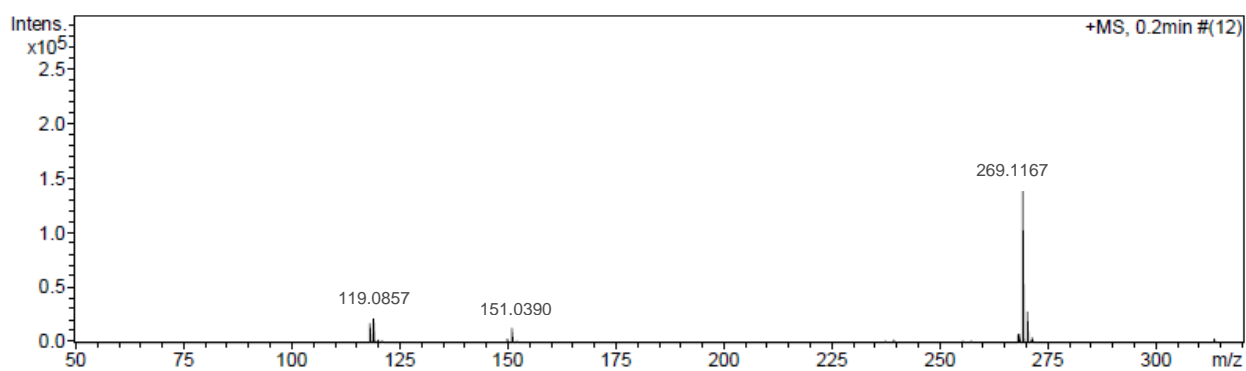
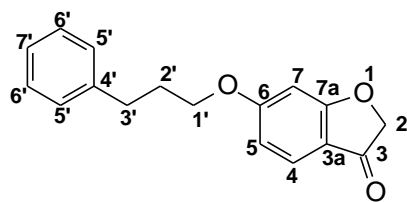
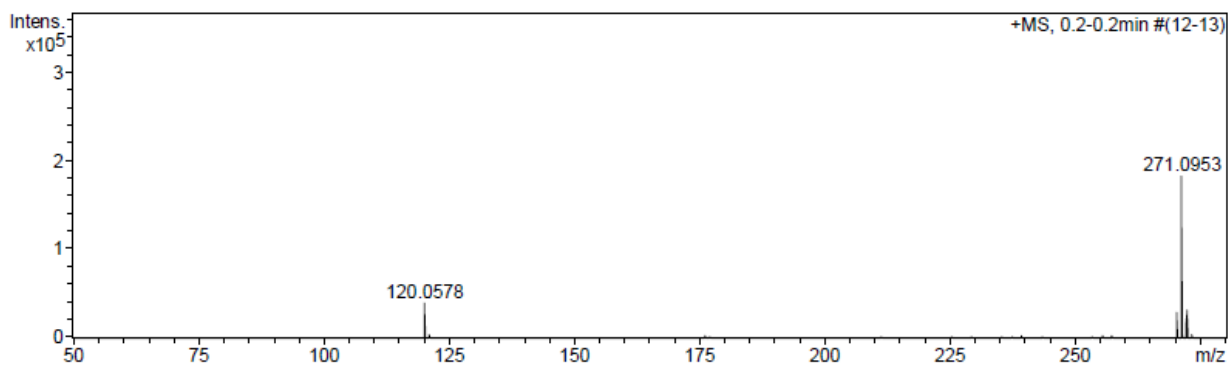
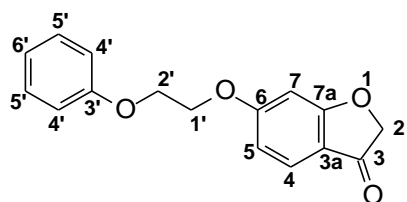
1i: 6-(3-Iodobenzyloxy)-2H-1-benzofuran-3-one**1j:** 6-(4-Cyanobenzyloxy)-2H-1-benzofuran-3-one

1k: 6-(3-Cyanobenzoyloxy)-2H-1-benzofuran-3-one**1l:** 6-(4-Methylbenzyloxy)-2H-1-benzofuran-3-one

1m: 6-(3-Methylbenzyloxy)-2H-1-benzofuran-3-one**1n:** 6-[4-(Trifluoromethyl)benzyloxy]-2H-1-benzofuran-3-one

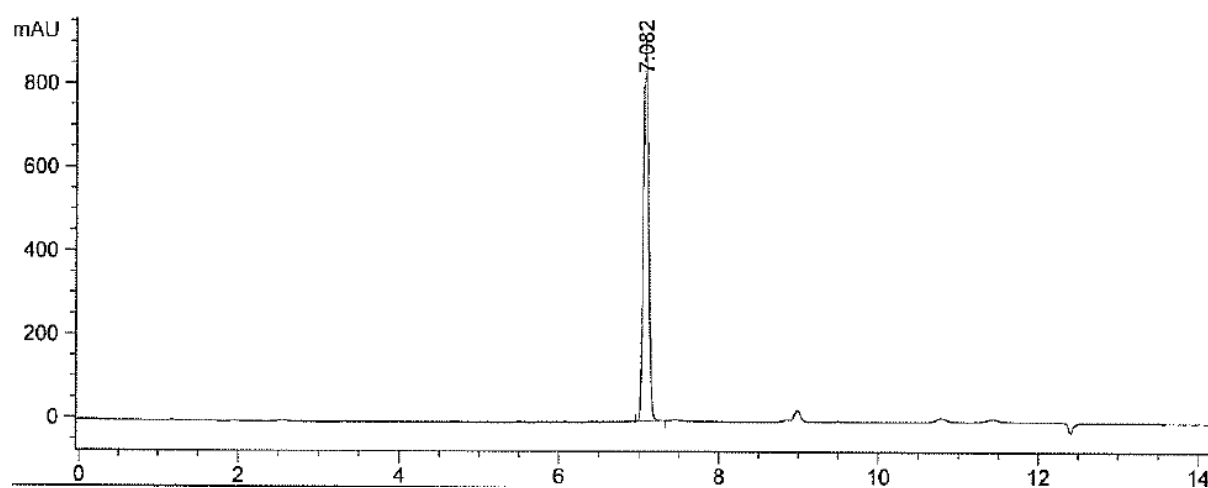
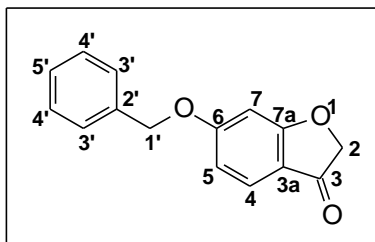
1o: 6-(2-Phenylethoxy)-2H-1-benzofuran-3-one**1p:** 6-[2-(4-Bromophenyl)ethoxy]-2H-1-benzofuran-3-one

1q: 6-[2-(4-Methylphenyl)ethoxy]-2H-1-benzofuran-3-one**1r:** 6-[2-(3-Methylphenyl)ethoxy]-2H-1-benzofuran-3-one

1s: 6-(3-Phenylpropoxy)-2H-1-benzofuran-3-one**1t:** 6-(2-Phenoxyethoxy)-2H-1-benzofuran-3-one

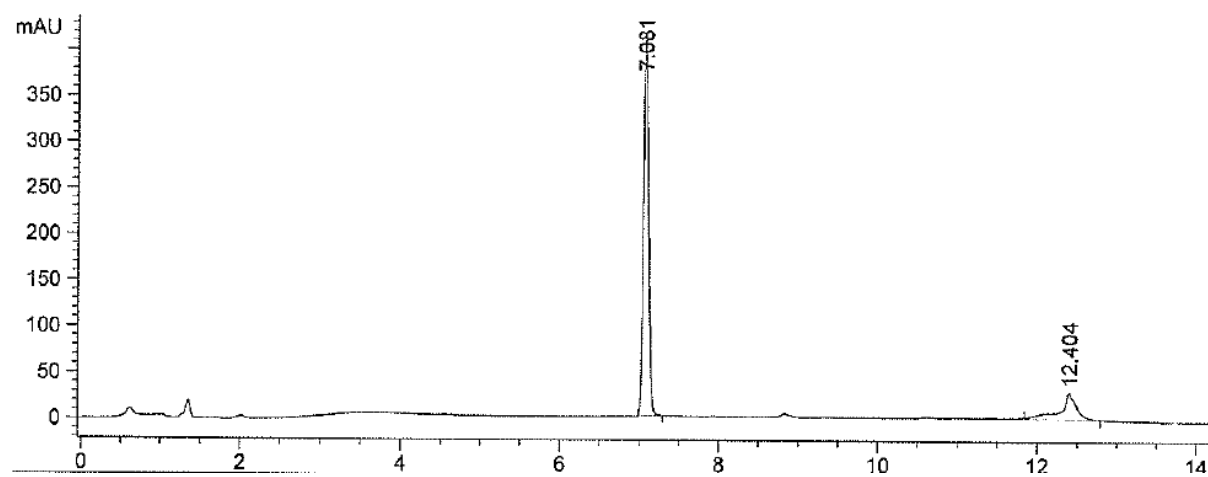
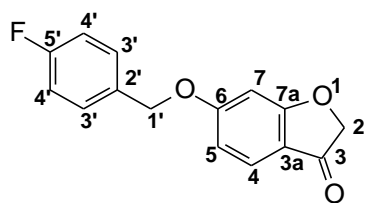
HPLC TRACES OF SYNTHESISED COMPOUNDS

1a: 6-(Benzyloxy)-2H-1-benzofuran-3-one



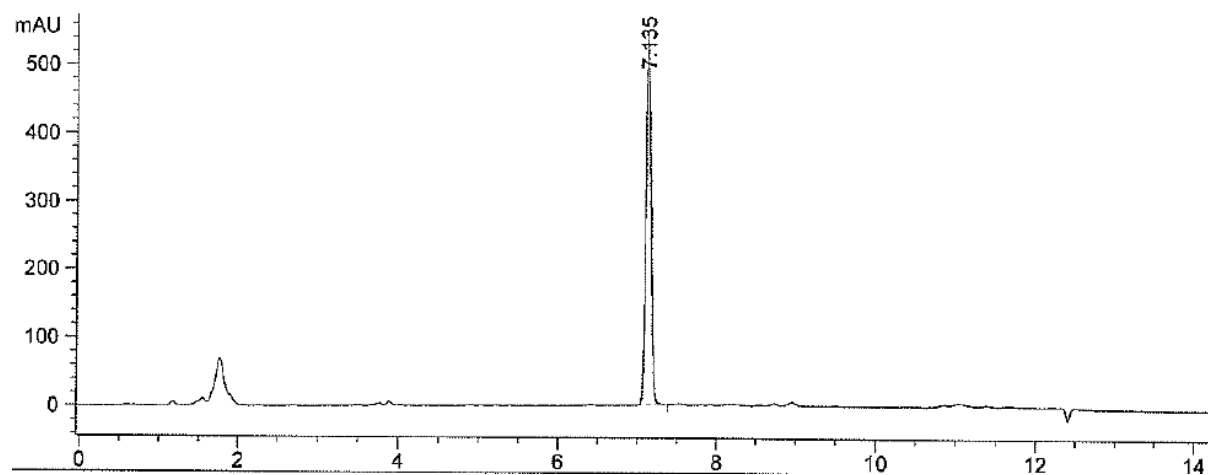
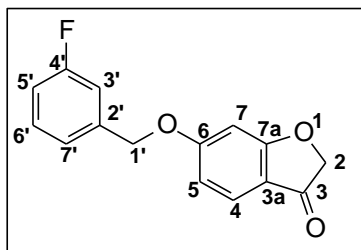
Peak #	RetTime [min]	Type	Width [min]	Area [mAU*s]	Height [mAU]	Area %
1	7.082	BBA	0.0716	4207.74072	915.24841	100.0000

1b: 6-(4-Fluorobenzoyloxy)-2H-1-benzofuran-3-one



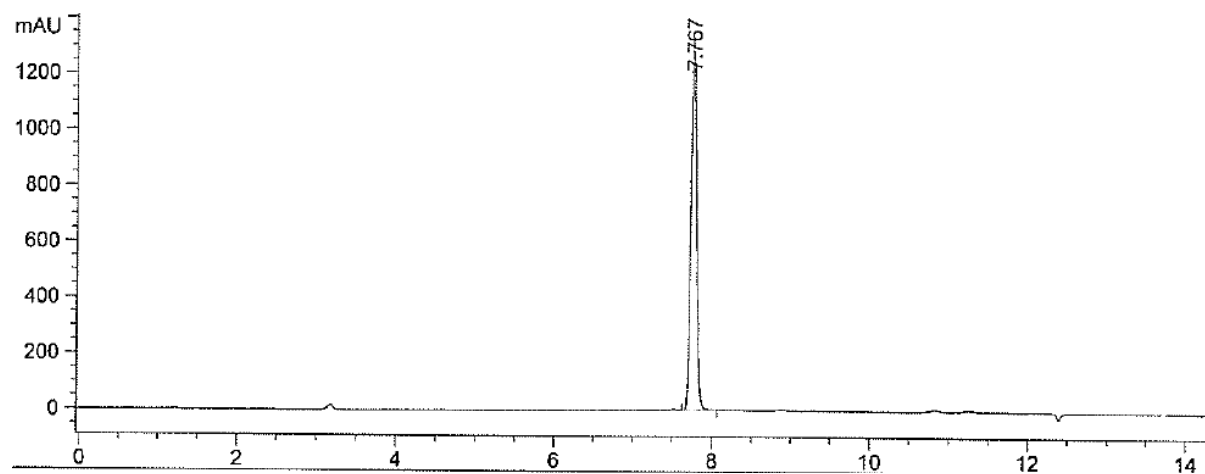
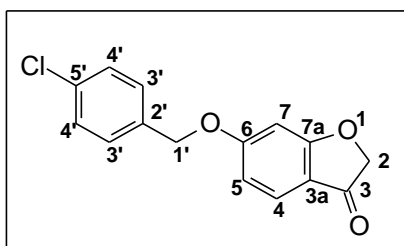
Peak #	RetTime [min]	Type	Width [min]	Area [mAU*s]	Height [mAU]	Area %
1	7.081	BBA	0.0710	1871.02954	411.70969	81.9802

1c: 6-(3-Fluorobenzoyloxy)-2H-1-benzofuran-3-one



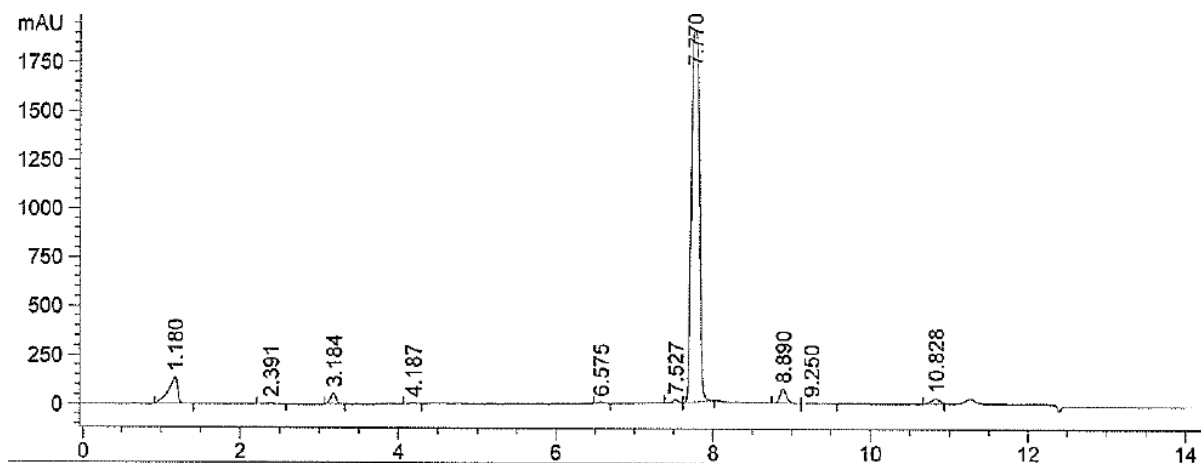
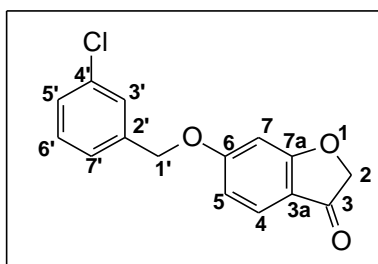
Peak #	RetTime [min]	Type	Width [min]	Area [mAU*s]	Height [mAU]	Area %
1	7.135	PBA	0.0709	2455.92749	541.41968	100.0000

1d: 6-(4-Chlorobenzoyloxy)-2H-1-benzofuran-3-one



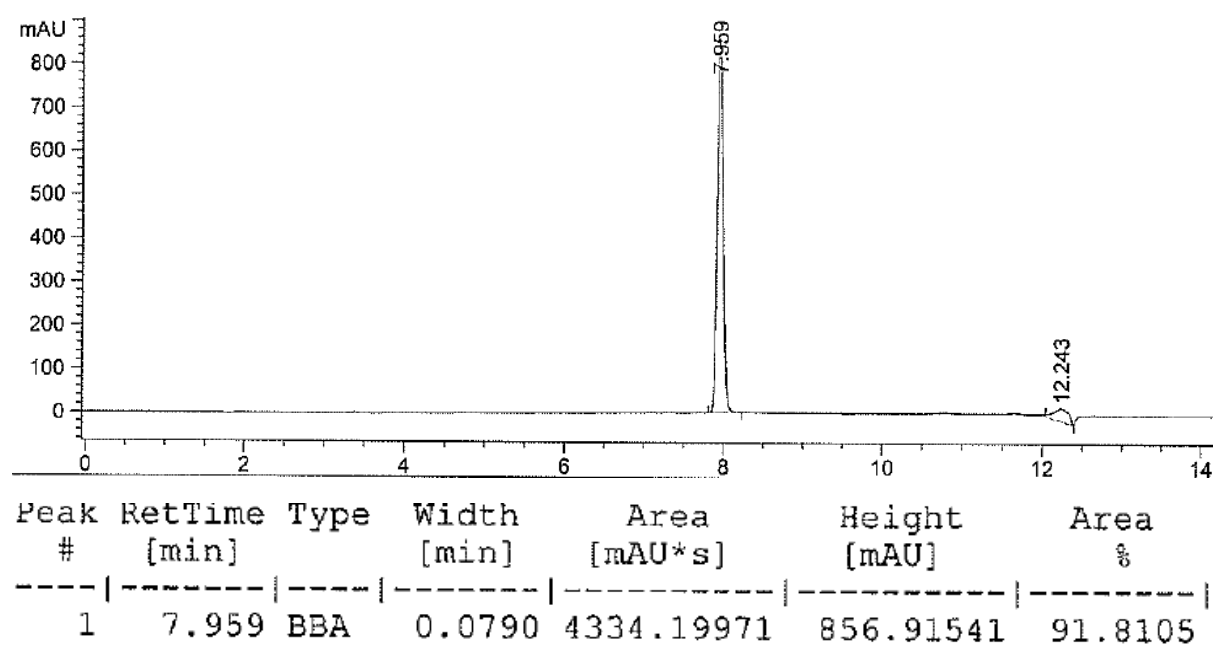
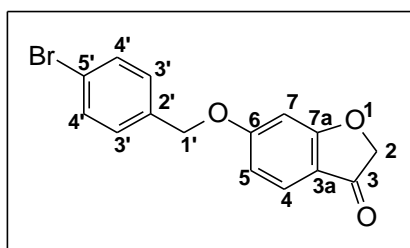
Peak #	RetTime [min]	Type	Width [min]	Area [mAU*s]	Height [mAU]	Area %
1	7.767	BBA	0.0780	6651.84424	1338.11401	100.0000

1e: 6-(3-Chlorobenzoyloxy)-2H-1-benzofuran-3-one

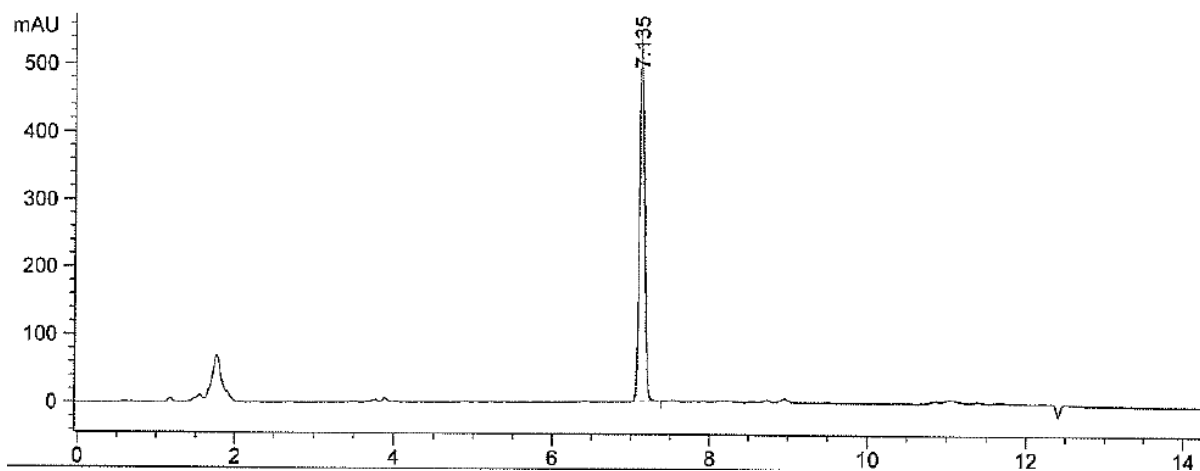
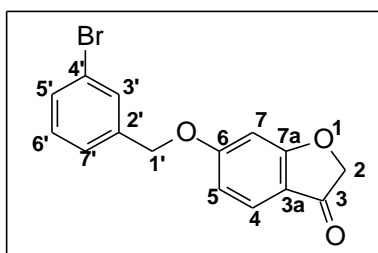


Peak #	RetTime [min]	Type	Width [min]	Area [mAU*s]	Height [mAU]	Area %
7	7.770	BB	0.1152	1.31732e4	1893.09912	85.0151

1f: 6-(4-Bromobenzyloxy)-2H-1-benzofuran-3-one

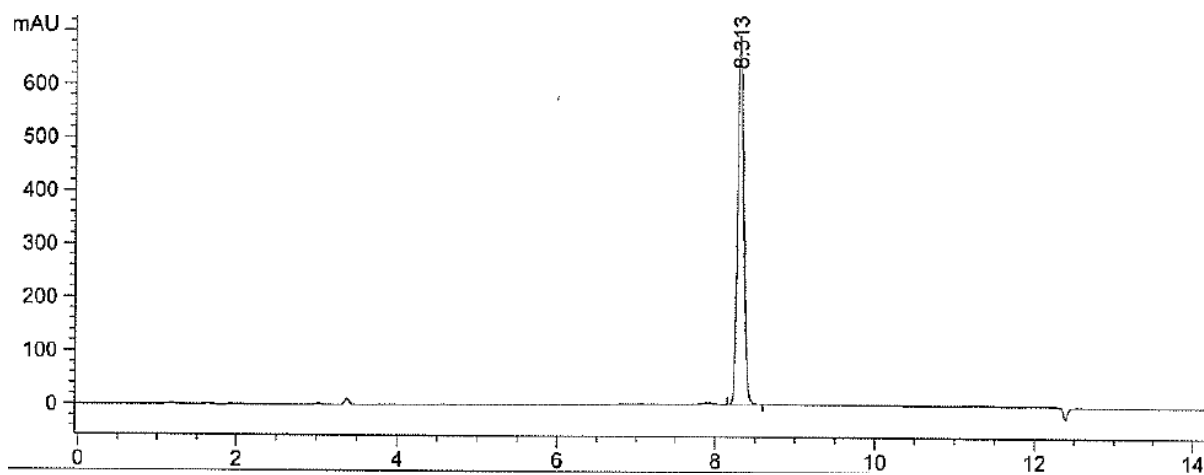
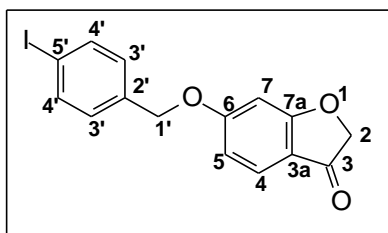


1g: 6-(3-Bromobenzyloxy)-2H-1-benzofuran-3-one



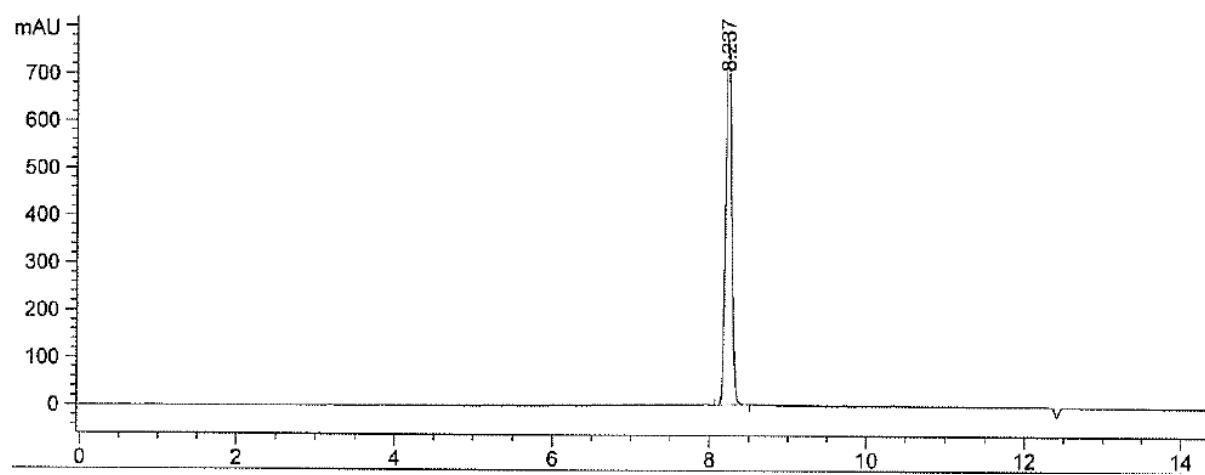
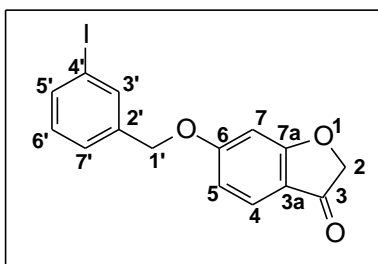
Peak #	RetTime [min]	Type	Width [min]	Area [mAU*s]	Height [mAU]	Area %
1	7.135	PBA	0.0709	2455.92749	541.41968	100.0000

1h: 6-(4-Iodobenzyloxy)-2H-1-benzofuran-3-one



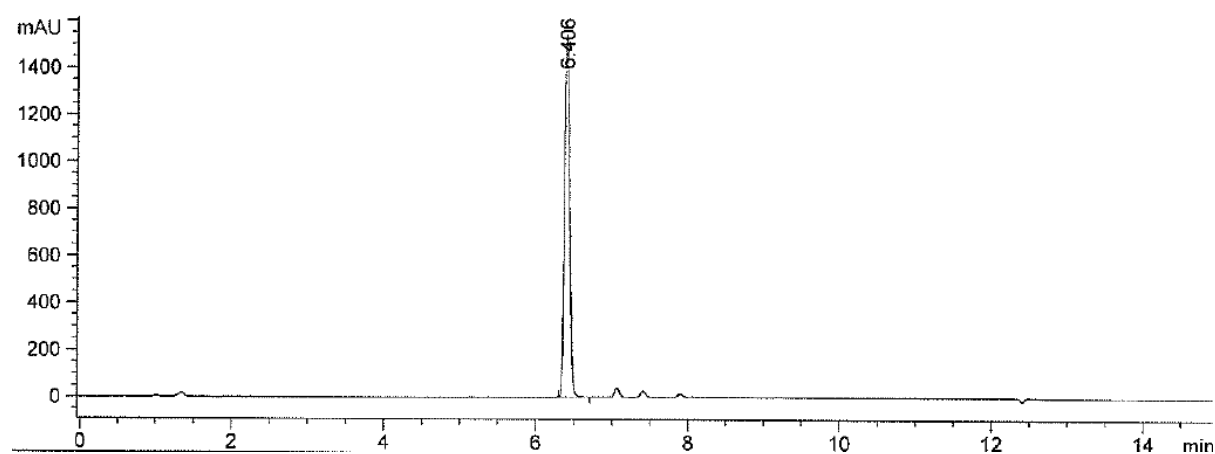
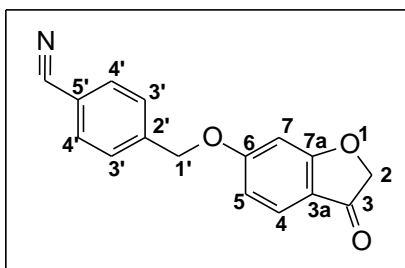
Peak #	RetTime [min]	Type	Width [min]	Area [mAU*s]	Height [mAU]	Area %
1	8.313	BBA	0.0851	3754.55396	693.71301	100.0000

1i: 6-(3-Iodobenzyloxy)-2H-1-benzofuran-3-one

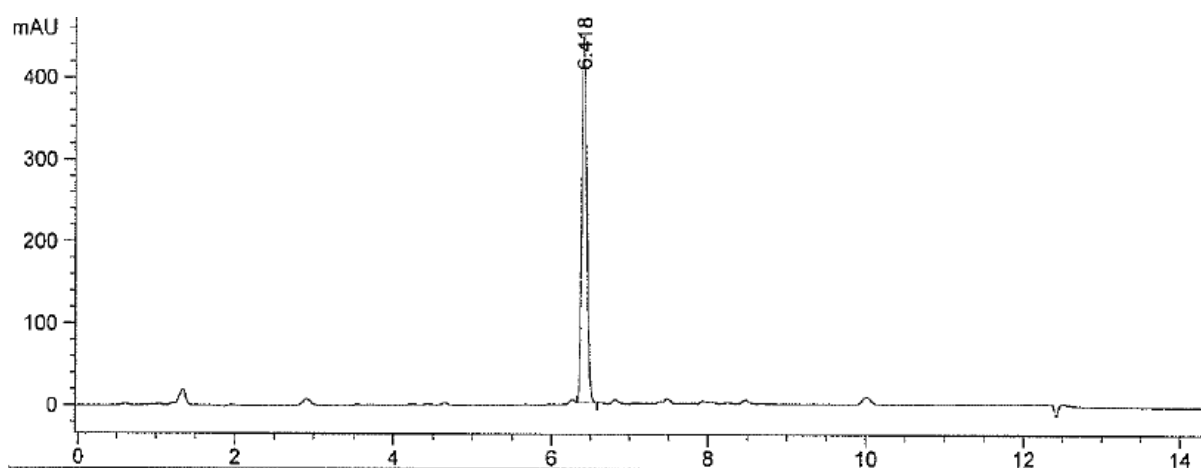
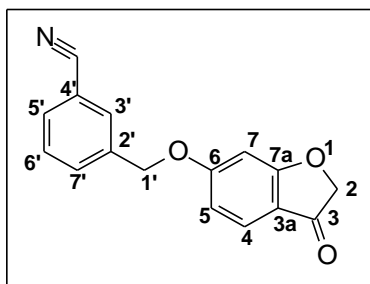


Peak #	RetTime [min]	Type	Width [min]	Area [mAU*s]	Height [mAU]	Area %
1	8.237	BBA	0.0845	4155.49512	776.28455	100.0000

1j: 6-(4-Cyanobenzoyloxy)-2H-1-benzofuran-3-one

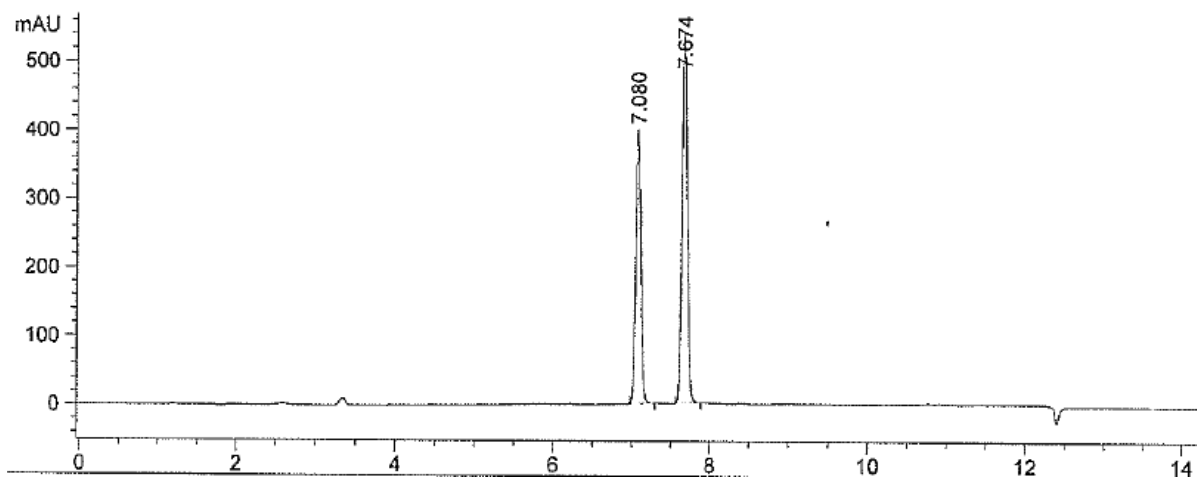
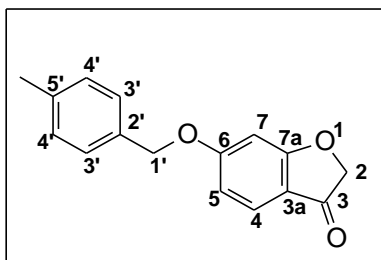


Peak #	RetTime [min]	Type	Width [min]	Area [mAU*s]	Height [mAU]	Area %
1	6.406	PBA	0.0717	7076.79883	1538.42664	100.0000

1k: 6-(3-Cyanobenzoyloxy)-2H-1-benzofuran-3-one

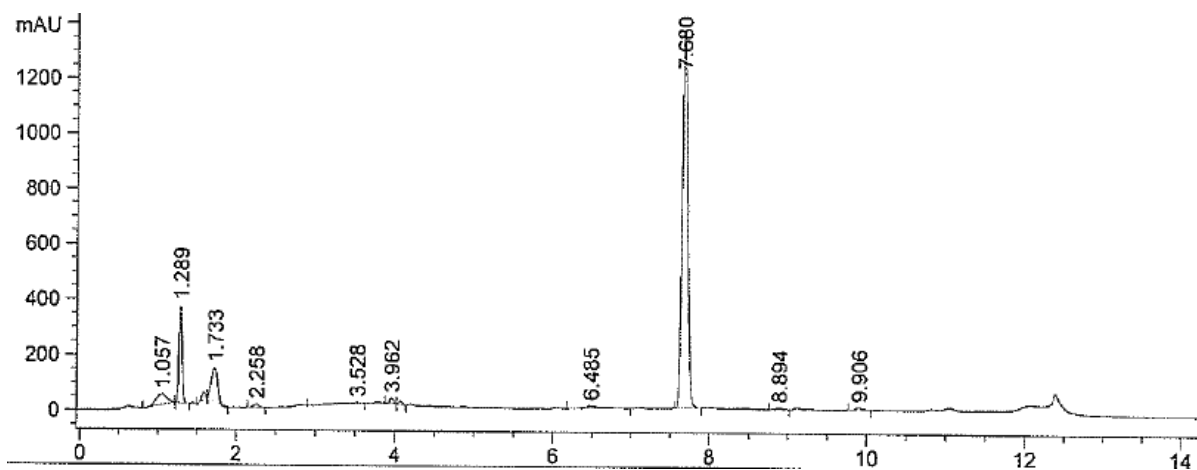
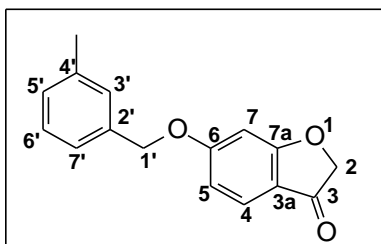
Peak #	RetTime [min]	Type	Width [min]	Area [mAU*s]	Height [mAU]	Area %
1	6.418	BBA	0.0699	1997.65308	448.99377	100.0000

11: 6-(4-Methylbenzyloxy)-2H-1-benzofuran-3-one



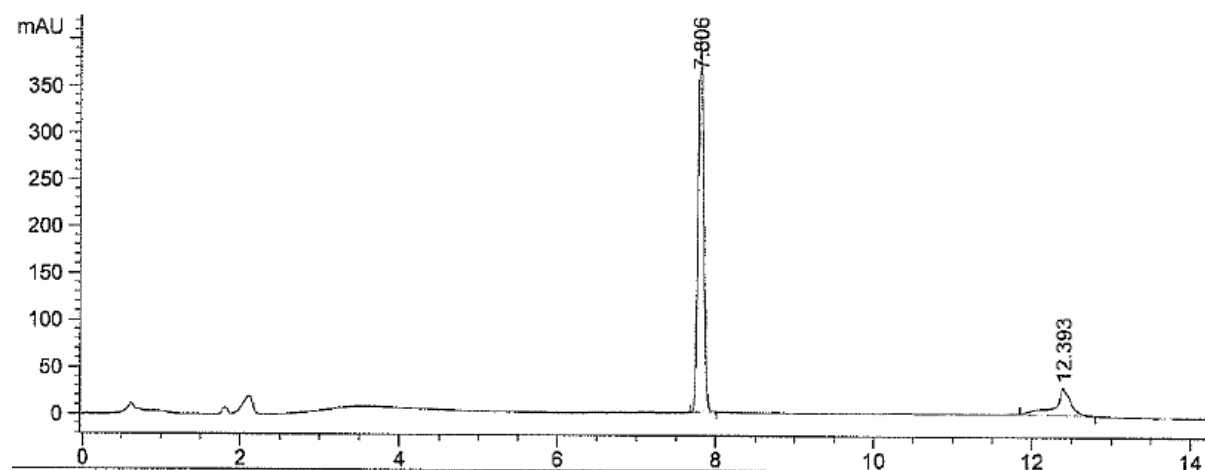
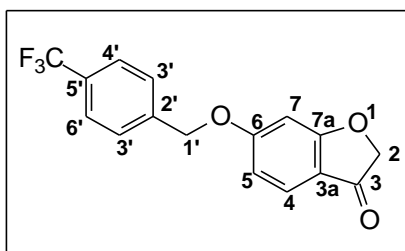
Peak #	RetTime [min]	Type	Width [min]	Area [mAU*s]	Height [mAU]	Area %
2	7.674	PBA	0.0735	2552.16162	536.44983	58.4213

1m: 6-(3-Methylbenzyloxy)-2H-1-benzofuran-3-one



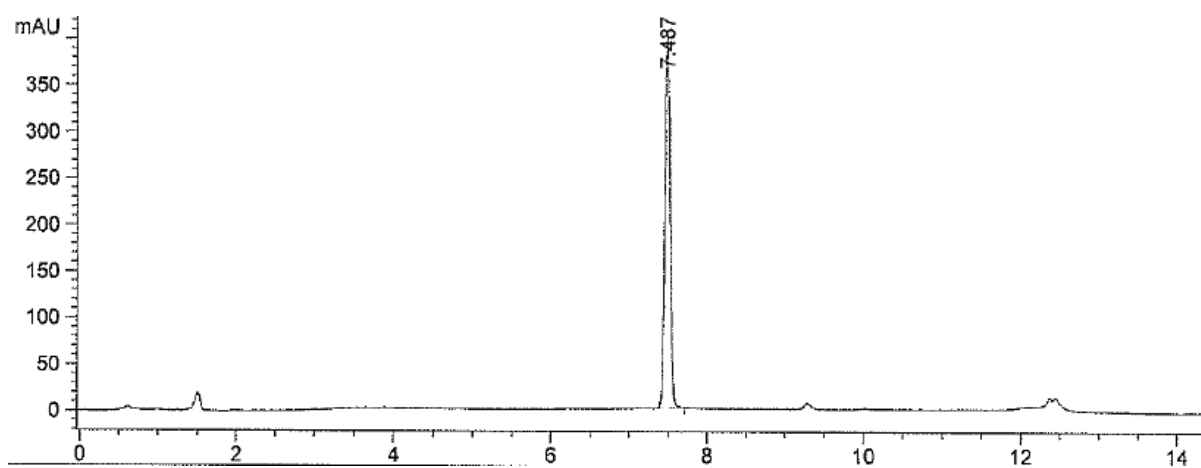
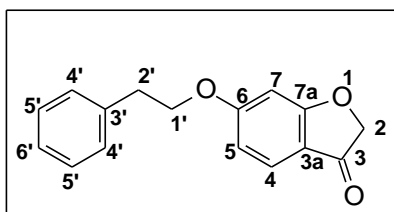
Peak #	RetTime [min]	Type	Width [min]	Area [mAU*s]	Height [mAU]	Area %
10	7.680	BB	0.0796	6635.50195	1344.89600	72.4065

1n: 6-[4-(Trifluoromethyl)benzyloxy]-2H-1-benzofuran-3-one



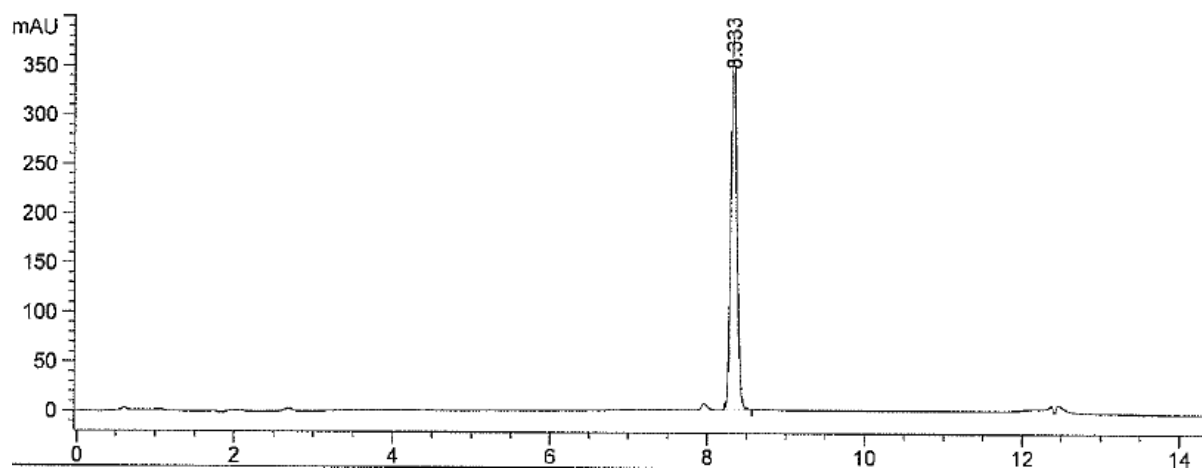
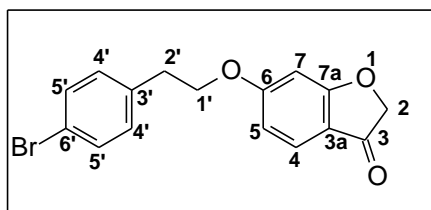
Peak #	RetTime [min]	Type	Width [min]	Area [mAU*s]	Height [mAU]	Area %
1	7.806	PBA	0.0752	1908.50574	403.14240	81.6802

1o: 6-(2-Phenylethoxy)-2H-1-benzofuran-3-one



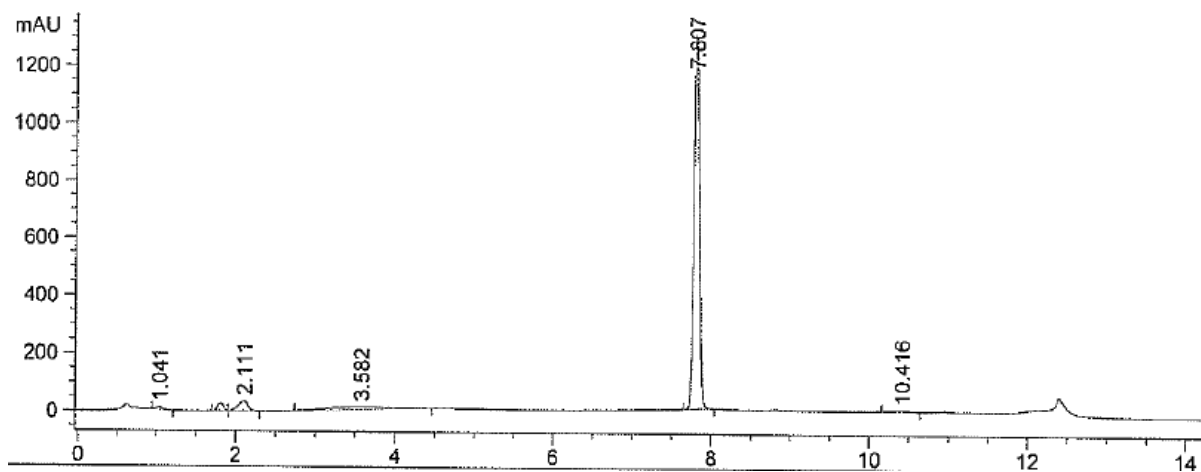
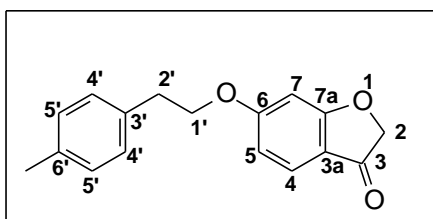
Peak #	RetTime [min]	Type	Width [min]	Area [mAU*s]	Height [mAU]	Area %
1	7.487	BBA	0.0727	1876.78577	400.48337	100.0000

1p: 6-[2-(4-Bromophenyl)ethoxy]-2H-1-benzofuran-3-one



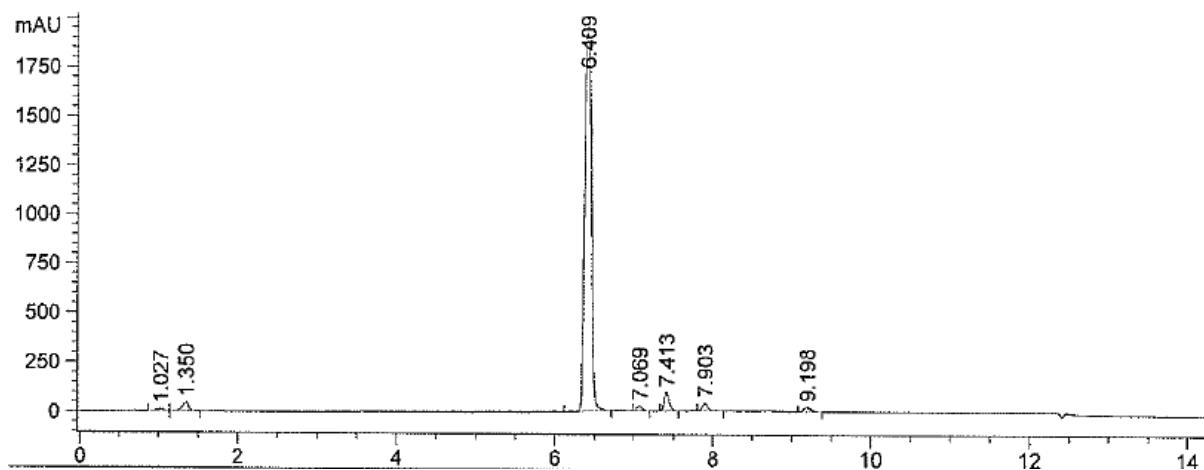
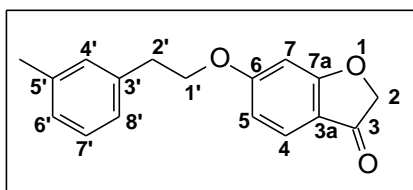
Peak #	RetTime [min]	Type	Width [min]	Area [mAU*s]	Height [mAU]	Area %
1	8.333	BBA	0.0827	2037.04651	378.81955	100.0000

1q: 6-[2-(4-Methylphenyl)ethoxy]-2H-1-benzofuran-3-one



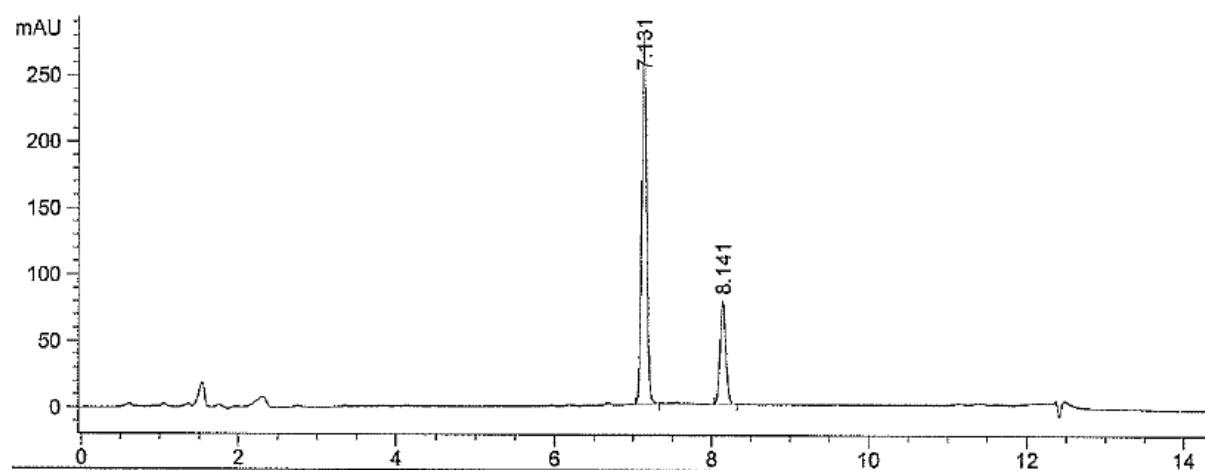
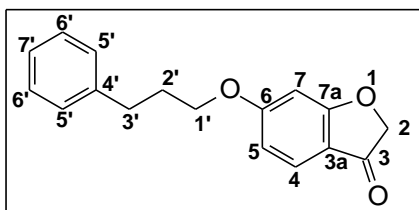
Peak #	RetTime [min]	Type	Width [min]	Area [mAU*s]	Height [mAU]	Area %
5	7.807	PBA	0.0769	6337.39990	1299.06055	85.0193

1r: 6-[2-(3-Methylphenyl)ethoxy]-2H-1-benzofuran-3-one



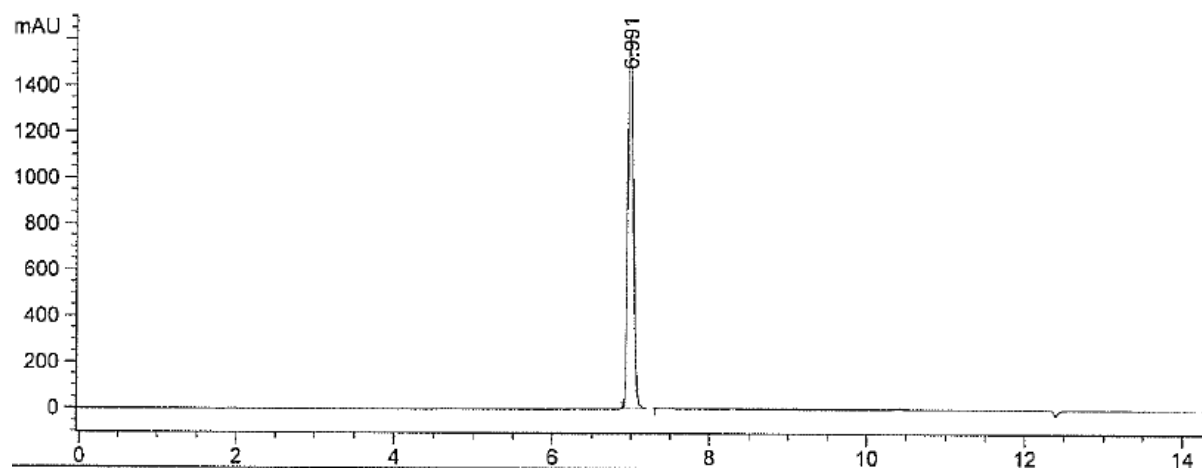
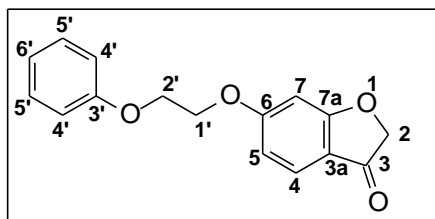
Peak #	RetTime [min]	Type	Width [min]	Area [mAU*s]	Height [mAU]	Area %
3	6.409	BB	0.0990	1.16283e4	1911.06055	90.9274

1s: 6-(3-Phenylpropoxy)-2H-1-benzofuran-3-one



Peak #	RetTime [min]	Type	Width [min]	Area [mAU*s]	Height [mAU]	Area %
1	7.131	BBA	0.0712	1259.57080	276.41095	76.0068

1t: 6-(2-Phenoxyethoxy)-2H-1-benzofuran-3-one



Peak #	RetTime [min]	Type	Width [min]	Area [mAU*s]	Height [mAU]	Area %
1	6.991	PBA	0.0755	7711.66113	1621.72388	100.0000

ACKNOWLEDGEMENTS

During the two years of this study much required advice and support were necessary to reach and accomplish this goal. I would like to take this opportunity to thank the following.

- First and foremost I want to give praise and thanks to my Heavenly Father Jesus Christ, for giving me a healthy and sound mind and body to complete this task.
- Dr. Lesetja Legoabe, thank you for being a invaluable mentor, and advisor, thank you for your inputs and unwavering willingness in assisting me to complete this task. Your support and knowledge are irreplaceable. Thank you for the pep talks.
- Prof. J.P Petzer, thank you for your guidance, advice and support your knowledge and guidance is exceptional.
- Dr. A. Petzer, thank you for all your time and support , and untiring willingness for the essays.
- To my parents thank you for all your support, and love during my life especially the last two years, without your love and support I would have been lost. Thank you for the example you set for me.
- My family, thank you for the support and love: Heleen & Johan (and kids), Dawie (in the USA), Marthie & Lafras (and kids) thanks for the late night messages of support and love from you guys. Marthie thank you for all the help and assistance you provided with MS Word.
- Yolandi Malan thank you for keeping up with me the last two years, thank you for your never ending love, support, and sacrifices you've made. I love you.
- Ida, Ruan, and Renier thank you for your friendship and support.
- Samantha and Daleen thank you for all the guidance, and help.

I would also like to thank the following institutions for their assistance during the study:

- Northwest University for granting me the opportunity to study at their institution.
- Andre Joubert at the SASOL Centre for Chemistry, for the numerous NMR spectra.
- The NRF and MRC for their financial contribution.